ISSN 0021-9673

VOL. 644 NO. 1 JULY 30, 1993

JOURNAL OF CHROMATOGRAPHY

INCLUDING ELECTROPHORESIS AND OTHER SEPARATION METHODS

ELSEVIER

JOURNAL OF CHROMATOGRAPHY

INCLUDING ELECTROPHORESIS AND OTHER SEPARATION METHODS

Scope. The *Journal of Chromatography* publishes papers on all aspects of **chromatography, electrophoresis** and related methods. Contributions consist mainly of research papers dealing with chromatographic theory, instrumental developments and their applications. The section *Biomedical Applications*, which is under separate editorship, deals with the following aspects: developments in and applications of chromatographic and electrophoretic techniques related to clinical diagnosis or alterations during medical treatment; screening and profiling of body fluids or tissues related to the analysis of active substances and to metabolic disorders; drug level monitoring and pharmacokinetic studies; clinical toxicology; forensic medicine; veterinary medicine; occupational medicine; results from basic medical research with direct consequences in clinical practice. In *Symposium volumes*, which are under separate editorship, proceedings of symposia on chromatography, electrophoresis and related methods are published.

Submission of Papers. The preferred medium of submission is on disk with accompanying manuscript (see *Electronic manuscripts* in the Instructions to Authors, which can be obtained from the publisher, Elsevier Science Publishers B.V., P.O. Box 330, 1000 AH Amsterdam, Netherlands). Manuscripts (in English; *four* copies are required) should be submitted to: Editorial Office of *Journal of Chromatography*, P.O. Box 681, 1000 AR Amsterdam, Netherlands, Telefax (+31-20) 5862 304, or to: The Editor of *Journal of Chromatography, Biomedical Applications*, P.O. Box 681, 1000 AR Amsterdam, Netherlands. Review articles are invited or proposed in writing to the Editors who welcome suggestions for subjects. An outline of the proposed review should first be forwarded to the Editors for preliminary discussion prior to preparation. Submission of an article is understood to imply that the article is original and unpublished and is not being considered for publication elsewhere. For copyright regulations, see below.

Publication. The *Journal of Chromatography* (incl. *Biomedical Applications*) has 40 volumes in 1993. The subscription prices for 1993 are:

J. Chromatogr. (incl. *Cum. Indexes, Vols. 601–650*) + *Biomed. Appl.* (Vols. 612–651):
Dfl. 8520.00 plus Dfl. 1320.00 (p.p.h.) (total *ca.* US$ 5466.75)

J. Chromatogr. (incl. *Cum Indexes, Vols. 601–650*) only (Vols. 623–651):
Dfl. 7047.00 plus Dfl. 957.00 (p.p.h.) (total *ca.* US$ 4446.75)

Biomed. Appl. only (Vols. 612–622):
Dfl. 2783.00 plus Dfl. 363.00 (p.p.h.) (total *ca.* US$ 1747.75).

Subscription Orders. The Dutch guilder price is definitive. The US$ price is subject to exchange-rate fluctuations and is given as a guide. Subscriptions are accepted on a prepaid basis only, unless different terms have been previously agreed upon. Subscriptions orders can be entered only by calender year (Jan.–Dec.) and should be sent to Elsevier Science Publishers, Journal Department, P.O. Box 211, 1000 AE Amsterdam, Netherlands, Tel. (+31-20) 5803 642, Telefax (+31-20) 5803 598, or to your usual subscription agent. Postage and handling charges include surface delivery except to the following countries where air delivery via SAL (Surface Air Lift) mail is ensured: Argentina, Australia, Brazil, Canada, China, Hong Kong, India, Israel, Japan*, Malaysia, Mexico, New Zealand, Pakistan, Singapore, South Africa, South Korea, Taiwan, Thailand, USA. *For Japan air delivery (SAL) requires 25% additional charge of the normal postage and handling charge. For all other countries airmail rates are available upon request. Claims for missing issues must be made within six months of our publication (mailing) date, otherwise such claims cannot be honoured free of charge. Back volumes of the *Journal of Chromatography* (Vols. 1–611) are available at Dfl. 230.00 (plus postage). Customers in the USA and Canada wishing information on this and other Elsevier journals, please contact Journal Information Center, Elsevier Science Publishing Co. Inc., 655 Avenue of the Americas, New York, NY 10010, USA, Tel. (+1-212) 633 3750, Telefax (+1-212) 633 3764.

Abstracts/Contents Lists published in Analytical Abstracts, Biochemical Abstracts, Biological Abstracts, Chemical Abstracts, Chemical Titles, Chromatography Abstracts, Current Awareness in Biological Sciences (CABS), Current Contents/Life Sciences, Current Contents/Physical, Chemical & Earth Sciences, Deep-Sea Research/Part B: Oceanographic Literature Review, Excerpta Medica, Index Medicus, Mass Spectrometry Bulletin, PASCAL-CNRS, Referativnyi Zhurnal, Research Alert and Science Citation Index.

US Mailing Notice. *Journal of Chromatography* (ISSN 0021-9673) is published weekly (total 52 issues) by Elsevier Science Publishers (Sara Burgerhartstraat 25, P.O. Box 211, 1000 AE Amsterdam, Netherlands). Annual subscription price in the USA US$ 4446.75 (subject to change), including air speed delivery. Second class postage paid at Jamaica, NY 11431. **USA POSTMASTERS**: Send address changes to *Journal of Chromatography*, Publications Expediting, Inc., 200 Meacham Avenue, Elmont, NY 11003. Airfreight and mailing in the USA by Publications Expediting.

See inside back cover for Publication Schedule, Information for Authors and information on Advertisements.

0021-9673/93/$06.00

This issue is printed on acid-free paper.

Printed in the Netherlands

VOL. 644, NO. 1 JOURNAL OF CHROMATOGRAPHY JULY 30, 1993

CONTENTS

(Abstracts/Contents Lists published in Analytical Abstracts, Biochemical Abstracts, Biological Abstracts, Chemical Abstracts, Chemical Titles, Chromatography Abstracts, Current Awareness in Biological Sciences (CABS), Current Contents/Life Sciences, Current Contents/Physical, Chemical & Earth Sciences, Deep-Sea Research/Part B: Oceanographic Literature Review, Excerpta Medica, Index Medicus, Mass Spectrometry Bulletin, PASCAL-CNRS, Referativnyi Zhurnal, Research Alert and Science Citation Index)

REGULAR PAPERS

Column Liquid Chromatography

Applications of mathematical modelling to the simulation of binary perfusion chromatography
by M.A. McCoy and A.I. Liapis (Rolla, MO, USA) and K.K. Unger (Mainz, Germany) (Received April 5th, 1993) 1

Salt-induced immobilization of proteins on a high-performance liquid chromatographic epoxide affinity support
by J.B. Wheatley and D.E. Schmidt, Jr. (South San Francisco, CA, USA) (Received April 6th, 1993) 11

Molecular mass determination of low-molecular-mass heparins. Application of wide collection angle measurements of light scattering using a high-performance gel permeation chromatographic system equipped with a low-angle laser light-scattering photometer
by H. Komatsu, K. Yoshii, S. Ishimitsu and S. Okada (Osaka, Japan) and T. Takahata (Matsubara, Japan) (Received March 2nd, 1993) 17

Recognition and separation of isoenzymes by metal chelates. Immobilized metal ion affinity partitioning of lactate dehydrogenase isoenzymes
by A. Otto and G. Birkenmeier (Leipzig, Germany) (Received March 8th, 1993) 25

Isolation of chitin deacetylase from *Mucor rouxii* by immunoaffinity chromatography
by A. Martinou, D. Kafetzopoulos and V. Bouriotis (Heraklion, Greece) (Received March 29th, 1993) 35

Determination and quantitative analysis of *Aconitum* alkaloids in plants by liquid chromatography–atmospheric pressure chemical ionization mass spectrometry
by K. Wada, H. Bando and N. Kawahara (Otaru, Japan) (Received March 30th, 1993) 43

Automated high-performance liquid chromatographic method for the determination of organophosphorus pesticides in waters with dual electrochemical (reductive–oxidative) detection
by R. Carabias Martínez, E. Rodríguez Gonzalo, F. Garay García and J. Hernández Méndez (Salamanca, Spain) (Received March 16th, 1993) 49

Reversed-phase high-performance liquid chromatographic determination of linear alkylbenzene sulphonates, nonylphenol polyethoxylates and their carboxylic biotransformation products
by A. Marcomini (Venice, Italy) and A. Di Corcia, R. Samperi and S. Capri (Rome, Italy) (Received March 3rd, 1993) 59

Rapid and continuous ion chromatographic determination of trace heavy metal impurities in noble metals
by Y. Liu and Q. Wang (Gansu, China) (Received March 19th, 1993) 73

Fast Flow Fractionation

Use of thermal field flow fractionation for the fractionation of polybutadiene in various organic solvents
by A.C. van Asten, E. Venema, W.Th. Kok and H. Poppe (Amsterdam, Netherlands) (Received March 19th, 1993 83

Gas Chromatography

Hydrogen bonding. XXVII. Solvation parameters for functionally substituted aromatic compounds and heterocyclic compounds, from gas–liquid chromatographic data
by M.H. Abraham (London, UK) (Received January 22nd, 1993) 95

Determination of anthropogenic and biogenic organic compounds on airborne particles: flash chromatographic fractionation and capillary gas chromatographic analysis
by E.G. Stephanou and N.E. Stratigakis (Heraklion, Greece) (Received February 25th, 1993) 141

(Continued overleaf)

Alkyltin speciation in sea water with on-line hydride conversion and gas chromatography–atomic emission detection
by T.M. Dowling and P.C. Uden (Amherst, MA, USA) (Received April 6th, 1993) 153

Electrophoresis

Axial temperature effects in electromigration
by B. Gaš (Prague, Czech Republic) (Received March 12th, 1993) 161

Influence of column temperature and physico-chemical properties on the electrophoretic behaviour of polyglycine peptides in free-solution capillary electrophoresis
by N. Chen, L. Wang and Y. Zhang (Dalian, China) (Received March 24th, 1993) 175

SHORT COMMUNICATION

Column Liquid Chromatography

Adsorption isotherm of undissociated eluent acid and its relation to the retention of system peaks in non-suppressed ion chromatography
by A. Yamamoto, A. Matsunaga and E. Mizukami (Toyama, Japan) and K. Hayakawa and M. Miyazaki (Kanazawa, Japan) (Received March 9th, 1993) 183

Preparative separation of higher fullerenes by high-performance liquid chromatography on a tetrachlorophthalimidopropyl-modified silica column
by D. Herren (Berne, Switzerland), C. Thilgen (Zurich, Switzerland), G. Calzaferri (Berne, Switzerland) and F. Diederich (Zurich, Switzerland) (Received April 20th, 1993) 188

Simultaneous analysis of *l*-hyoscyamine, *l*-scopolamine and *dl*-tropic acid in plant material by reversed-phase high-performance liquid chromatography
by M.-A. Fliniaux, F. Manceau and A. Jacquin-Dubreuil (Amiens, France) (Received April 20th, 1993) 193

Anion-exchange selectivity of cyclic phosphate oligomers
by G. Kura (Fukuoka, Japan) (Received February 23rd, 1993) 198

Gas Chromatography

Improved enantiomeric separation with a 2,6-di-O-pentyl-3-O-trifluoroacetylated β-cyclodextrin and OV-7 mixed stationary phase chiral capillary column
by H. Wan, Y. Wang, Q. Ou and W. Yu (Lanzhou, China) (Received March 1st, 1993) 202

Electrophoresis

Capillary electrophoresis with amperometric detection using a porous cellulose acetate joint
by I.-C. Chen and C.-W. Whang (Taichung, Taiwan) (Received April 6th, 1993) 208

SOFTWARE REVIEW

Savant computer-based instruction series in HPLC: Troubleshooting high performance liquid chromatography (by D. Saunders), reviewed by J.W. Dolan (Amity, OR, USA) 213

JOURNAL OF CHROMATOGRAPHY

VOL. 644 (1993)

JOURNAL of CHROMATOGRAPHY

INCLUDING ELECTROPHORESIS AND OTHER SEPARATION METHODS

ELSEVIER

AMSTERDAM — LONDON — NEW YORK — TOKYO

0021-9673/93/$06.00

Printed in the Netherlands

Journal of Chromatography, 644 (1993) 1–9
Elsevier Science Publishers B.V., Amsterdam

CHROM. 25 190

Applications of mathematical modelling to the simulation of binary perfusion chromatography

M.A. McCoy and A.I. Liapis*

Department of Chemical Engineering and Biochemical Processing Institute, University of Missouri-Rolla, Rolla, MO 65401-0249 (USA)

K.K. Unger

Institute für Anorganische Chemie und Analytische Chemie, Johannes Gutenberg-Universität Mainz, W-6500 Mainz (Germany)

(First received January 20th, 1993; revised manuscript received April 5th, 1993)

ABSTRACT

A mathematical model of binary (competitive adsorption involving two components) perfusion chromatography is used to simulate and study the behavior of a binary adsorption system. The dynamic behavior of column systems (frontal analysis) is examined for different particles sizes, column fluid superficial velocities, V_f, and intraparticle fluid velocities, v_p. Column systems with perfusive ($v_p > 0$) and purely diffusive ($v_p = 0$) adsorbent particles are studied. The results obtained from the binary system studied in this work suggest that the times at which breakthrough begins for components 1 and 2, and the dynamic (unsteady state) relative separation between components 1 and 2 obtained from the column with perfusive particles, are higher than those obtained from the column having purely diffusive particles, especially as the particle size, z_0, and the column fluid superficial velocity, V_f, increase. The improved separation efficiency obtained from the chromatographic columns with perfusive adsorbent particles studied in this work, is mainly due to the intraparticle fluid flow which enhances intraparticle mass transport.

INTRODUCTION

Perfusion chromatography represents the separation process that involves the flow of a mobile phase (*i.e.* liquid phase) through porous chromatographic particles [1–5]. In perfusive adsorbent particles the intraparticle convective fluid velocity, v_p, is non-zero [3], while in purely diffusive adsorbent particles the value of v_p is considered to be equal to zero. Liapis and McCoy [3] constructed a theory of perfusion chromatography, and their mathematical models could describe the dynamic behavior of single and multicomponent adsorption in columns having perfusive ($v_p > 0$) adsorbent particles, as well as in columns having purely diffusive ($v_p = 0$) adsorbent particles. The model expressions [3] for the adsorbent particles include the intraparticle mass transfer mechanisms of convection and diffusion, as well as the mass transfer step involving the interaction between the adsorbate molecules and the active sites on the surface of the porous adsorbent particles. The perfusion chromatography model was solved and used to study the dynamic behavior of single-component adsorption systems [3] for different column lengths, particle sizes, column fluid superficial velocities, intraparticle fluid velocities, as well as for different values of the effective pore diffusivity and of the total number of active sites per volume of adsorbent. The dynamics of the interaction mechanisms of the adsorption step of the single component adsorption systems studied by

* Corresponding author.

0021-9673/93/$06.00

Liapis and McCoy [3] were (a) relatively not fast, (b) relatively fast and (c) infinitely fast. The values of certain variables which could be used to evaluate column performance, as well as the breakthrough curves obtained from columns having perfusive adsorbent particles, were compared [3] with those obtained from columns having purely diffusive adsorbent particles. The results from the single-component adsorption systems [3] suggest that for single-component adsorption systems having relatively fast or infinitely fast interaction kinetics (that is, the dynamics of the interaction step between the adsorbate molecules and the active sites are relatively fast or infinitely fast), the use of perfusive particles could have the potential to provide improved column performance. The results obtained from single component adsorption systems suggest [3,6] that the dynamic behavior of columns with perfusive adsorbent particles could be more effective than the dynamic behavior of columns with purely diffusive particles when both the intraparticle Peclet number [6-8] and the Porath parameter [6–8] are large. The intraparticle Peclet number [6] is a general measure of the importance of intraparticle convection —as a means of mass transfer— compared to pore diffusion. The Porath parameter may be considered [6–8] to provide a measure of the speed of the adsorbate-active site (adsorbate–ligand) association step relative to the pore diffusion of the adsorbate in the pores of the adsorbent particle. It should be emphasized that the intraparticle Peclet number alone is inadequate to fully describe intraparticle mass transfer when adsorption occurs [3,6]. In adsorption systems, a second quantity, the Porath parameter [6–8] comes also into play.

In this work, one of the theoretical mathematical models constructed by Liapis and McCoy [3] for multicomponent adsorption in columns is solved and used to study the dynamic behavior of binary (competitive adsorption involving two components) perfusion chromatography.

MATHEMATICAL MODEL

Adsorption is considered to take place from a flowing liquid stream in a fixed bed of perfusive adsorbent particles under isothermal conditions. Two of the components in the feed solution to the bed are considered to be the adsorbates which compete for the available active sites for adsorption. One of the adsorbates is taken to be component 1 ($i = 1$ in ref. 3) and the second adsorbate is taken to be component 2 ($i = 2$ in ref. 3). The differential mass balance for each adsorbate i ($i = 1, 2$) in the flowing fluid stream is given by eqn. 1 in ref. 3 and equations 2, 4 and 5 in ref. 3 are considered to provide the initial and boundary conditions for these differential mass balance equations. Eqn. 8 in ref. 3 is taken to represent the differential mass balance for each adsorbate i ($i = 1, 2$) in a perfusive adsorbent particle, and its initial and boundary conditions are given by eqns. 12–14 in ref. 3. The term $\partial \bar{C}_{psi}/\partial t$ ($i = 1, 2$) of eqn. 1 in ref. [3] is obtained from eqn. 19 in ref. 3, while the intraparticle velocity, v_p, could be estimated from eqn. 20 in ref. 3.

Eqn. 8 in ref. 3 can be solved if mathematical expressions for the terms $\partial C_{s1}/\partial t$ and $\partial C_{s2}/\partial t$ are available. These terms represent the accumulation of components 1 and 2 in the adsorbed phase, which is on the internal surface of the perfusive adsorbent particle. For isothermal adsorption systems, the term $\partial C_{si}/\partial t$ ($i = 1, 2$) could be of the form given by eqn. 9 in ref. 3, which is as follows:

$$\frac{\partial C_{si}}{\partial t} = f_i(\mathbf{C}_p, \mathbf{C}_s, \mathbf{k}), \quad i = 1, 2 \tag{1}$$

In eqn. 1, f_i represents the functional form of the dynamic adsorption mechanism for adsorbate i; $\mathbf{C}_p$ represents the concentration vector of the adsorbates in the pore fluid, $\mathbf{C}_p = (C_{p1}, C_{p2})$; $\mathbf{C}_s$ denotes the concentration vector of the adsorbates in the adsorbed phase, $\mathbf{C}_s = (C_{s1}, C_{s2})$, and $\mathbf{k}$ represents the vector of the rate constants that characterize the interaction kinetics between the adsorbates and the active sites. For certain multicomponent adsorption systems, adsorption models of the form given in eqn. 1 have been constructed and presented in the literature [3,6–11]. In this work, the expressions for $\partial C_{s1}/\partial t$ and $\partial C_{s2}/\partial t$ are taken to be as follows:

$$\frac{\partial C_{s1}}{\partial t} = k_{11} C_{p1}\left(C_{T1} - \sum_{j=1}^{2} C_{sj}\right) - k_{21} C_{s1} \tag{2}$$

$$\frac{\partial C_{s2}}{\partial t} = k_{12}C_{p2}\left(C_{T2} - \sum_{j=1}^{2} C_{sj}\right) - k_{22}C_{s2} \qquad (3)$$

Eqns. 2 and 3 represent one model of a dynamic adsorption mechanism of the form given in equation 1, for the competitive adsorption of components 1 and 2 [8–11]. The initial conditions of eqns. 2 and 3 are given by eqn. 15 in ref. 3. In this study, the mathematical model of binary perfusion chromatography is then represented by eqn. 1 (eqns. 2 and 3 provide one possible dynamic adsorption mechanism of the form given in eqn. 1) of this work and by equations 1, 2, 4, 5, 8 and 12–15 of ref. 3.

The dynamic behavior of a binary adsorption system involving perfusive adsorbent particles packed in a column, could be obtained by solving eqns. 2 and 3 of this work simultaneously with equations 1, 2, 4, 5, 8 and 12–15 of ref. 3. The solution of the equations of this mathematical model of binary perfusion chromatography, was obtained [6] by employing the method of orthogonal collocation [12,13] on the space variable of the perfusive particle and the method of orthogonal collocation on finite elements [6] on the space variable along the axis of the column. The resulting ordinary non-linear differential equations were integrated [6] by using Gear's method [13] which is employed in the LSODES component of the ODEPACK [14] software package. It should be mentioned at this point that if the intraparticle velocity, v_p, is set equal to zero in eqn. 8 of ref. 3, then the solution of the above mentioned equations would provide the dynamic behavior of a binary adsorption system in a column having purely diffusive adsorbent particles.

RESULTS AND DISCUSSION

The mathematical model of binary perfusion chromatography presented in this work, was used to study the dynamic behavior of a binary adsorption system whose parameter values are presented in Table I. The values of the parameters in Table I are in the range of the values of such parameters measured and/or estimated from experiments involving affinity adsorption of biologically active macromolecules [7,8,15–20]. Two different values for the particle size, z_0, have been considered: (i) $z_0 = 8.06 \cdot 10^{-6}$ m, and (ii) $z_0 = 16.12 \cdot 10^{-6}$ m. The values of other parameters of the binary perfusion model are reported in the captions of the figures. In the simulations of this study, the dynamic behavior of the binary perfusion chromatography system was examined for the following intraparticle velocities (for a given column fluid superficial velocity, V_f): $v_p = 0$, $v_p = 0.02V_f$, $v_p = 0.03V_f$ and $v_p = 0.05V_f$. The range of the values of V_f examined in this work is similar to the range of the experimental values of V_f considered by Afeyan *et al.* [1]. Furthermore, the resulting range of the non-zero values of the intraparticle velocity, v_p, examined in this study, is in the range suggested by the data of Afeyan *et al.* [1] and by calculations performed [6] with eqn. 20 in ref. 3. It is worth noting again that the adsorbent particles are considered to be purely diffusive when $v_p = 0$. For the binary system studied in this work, adsorbate 1 represents the most preferentially adsorbed component while adsorbate 2 is the least strongly adsorbed component. Furthermore, in the figures of this paper the results for component 1 are represented by solid curves while those of component 2 are denoted by dashed curves.

In Figs. 1–3, the breakthrough curves of components 1 and 2 are shown for different values of V_f, v_p and z_0. The results in Fig. 1 indicate that there are no large differences between the breakthrough curves of purely diffusive ($v_p = 0$) and perfusive ($v_p > 0$) particles when $V_f = 0.138 \cdot 10^{-3}$ m/s, especially with par-

TABLE I

PARAMETER VALUES OF THE BINARY PERFUSION CHROMATOGRAPHY SYSTEM

$C_{d1,in} = 0.1$ kg/m^3; $C_{d2,in} = 0.1$ kg/m^3; $C_{T1} = 2.2$ kg/m^3;
$C_{T2} = 2.2$ kg/m^3; $D_{p1} = 6.9 \cdot 10^{-12}$ m^2/s;
$D_{p2} = 17.885 \cdot 10^{-12}$ m^2/s;
$k_{11} = 2.35 \cdot 10^{-1}$ m^3/(kg) (s); $k_{21} = 5.17 \cdot 10^{-5}$ s^{-1};
$K_{a1} = k_{11}/k_{21} = 4545.45$ m^3/kg; $k_{12} = 4.108 \cdot 10^{-1}$ m^3/(kg) (s);
$k_{22} = 2.222 \cdot 10^{-2}$ s^{-1}; $K_{a2} = k_{12}/k_{22} = 18.488$ m^3/kg;
$K_I = K_{a1}/K_{a2} = 245.859$; $\varepsilon = 0.35$; $\varepsilon_p = 0.50$

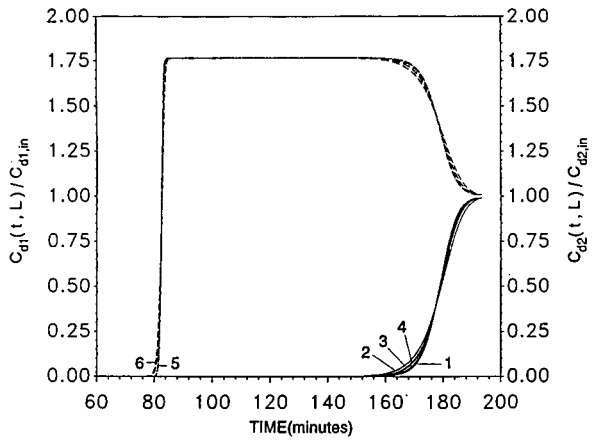

Fig. 1. Breakthrough curves of components 1 and 2 of the binary system (the solid curves are for component 1 and the dashed curves are for component 2). $V_f = 0.138 \cdot 10^{-3}$ m/s; $L = 0.1$ m; $1 \equiv z_0 = 8.06 \cdot 10^{-6}$ m, $v_p = (0.00, 0.02, 0.03, 0.05)V_f$; $2 \equiv z_0 = 16.12 \cdot 10^{-6}$ m, $v_p = 0$; $3 \equiv z_0 = 16.12 \cdot 10^{-6}$ m, $v_p = 0.02V_f$; $4 \equiv z_0 = 16.12 \cdot 10^{-6}$ m, $v_p = (0.03, 0.05)V_f$; $5 \equiv z_0 = 8.06 \cdot 10^{-6}$ m, $v_p = (0.00, 0.02, 0.03, 0.05)V_f$; $6 \equiv z_0 = 16.12 \cdot 10^{-6}$ m, $v_p = (0.00, 0.02, 0.03, 0.05)V_f$.

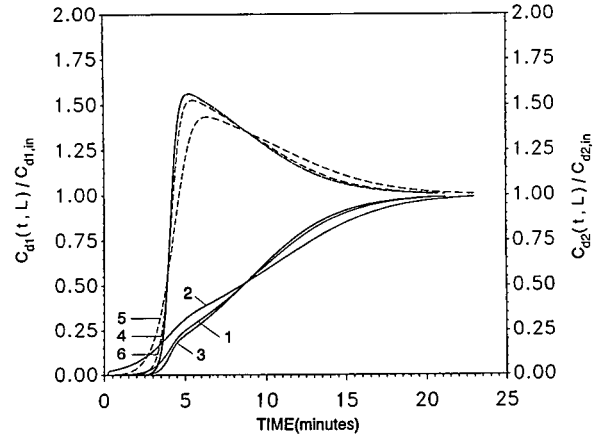

Fig. 3. Breakthrough curves for components 1 and 2 of the binary system (the solid curves are for component 1 and the dashed curves are for component 2). $V_f = 5.556 \cdot 10^{-3}$ m/s; $L = 0.2$ m; $1 \equiv z_0 = 8.06 \cdot 10^{-6}$ m, $v_p = 0$; $2 \equiv z_0 = 16.12 \cdot 10^{-6}$ m, $v_p = 0$; $3 \equiv z_0 = 8.06 \cdot 10^{-6}$ and $16.12 \cdot 10^{-6}$ m, $v_p = (0.02, 0.03, 0.05)V_f$; $4 \equiv z_0 = 8.06 \cdot 10^{-6}$ m, $v_p = 0$; $5 \equiv z_0 = 16.12 \cdot 10^{-6}$ m, $v_p = 0$; $6 \equiv z_0 = 8.06 \cdot 10^{-6}$ m and $16.12 \cdot 10^{-6}$ m, $v_p = (0.02, 0.03, 0.05)V_f$.

ticles of size $z_0 = 8.06 \cdot 10^{-6}$ m. It can be observed in Fig. 1 that when $z_0 = 16.12 \cdot 10^{-6}$ m, the breakthrough of component 1 for the systems having perfusive particles, begins to occur slightly later than that obtained from the system involving purely diffusive particles. Also, the results in Fig. 1 indicate that as the particle size is increased the time at which breakthrough begins is decreased, and this decrease is smaller for the systems using perfusive particles.

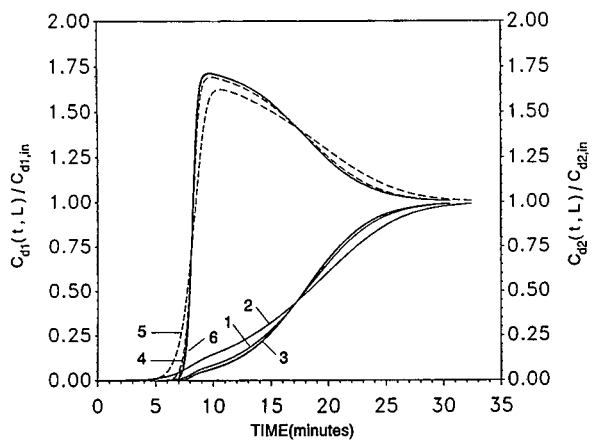

Fig. 2. Breakthrough curves for components 1 and 2 of the binary system (the solid curves are for component 1 and the dashed curves are for component 2). $V_f = 2.778 \cdot 10^{-3}$ m/s; $L = 0.2$ m; $1 \equiv z_0 = 8.06 \cdot 10^{-6}$ m, $v_p = 0$; $2 \equiv z_0 = 16.12 \cdot 10^{-6}$ m, $v_p = 0$; $3 \equiv z_0 = 8.06 \cdot 10^{-6}$ and $16.12 \cdot 10^{-6}$ m, $v_p = (0.02, 0.03, 0.05)V_f$; $4 \equiv z_0 = 8.06 \cdot 10^{-6}$ m, $v_p = 0$; $5 \equiv z_0 = 16.12 \cdot 10^{-6}$ m, $v_p = 0$; $6 \equiv z_0 = 8.06 \cdot 10^{-6}$ m and $16.12 \cdot 10^{-6}$ m, $v_p = (0.02, 0.03, 0.05)V_f$.

When the superficial velocity, V_f, in the column is increased to $2.778 \cdot 10^{-3}$ m/s and $5.556 \cdot 10^{-3}$ m/s, then the results in Figs. 2 and 3 indicate that when perfusive adsorbent particles are used, the times at which breakthrough begins for components 1 and 2 are larger than the corresponding times obtained when purely diffusive particles are employed. The results in Figs. 2 and 3 show that the differences in the initial breakthrough times obtained from perfusive and purely diffusive particles increase as the particle size increases, and the breakthrough curves obtained from the column having perfusive particles are steeper and their shape is not significantly affected when the particle size, z_0, and the column fluid superficial velocity, V_f, are increased. On the contrary, in Figs. 2 and 3 it can be observed that the shape of the breakthrough curves obtained from the column having purely diffusive particles, is influenced significantly when the particle size and the column fluid superficial velocity are increased. Furthermore,

the steepness of the breakthrough curves obtained from columns having perfusive particles, as well as the times at which breakthrough begins for components 1 and 2, increase [6] with increasing intraparticle velocity, v_p, and the effect of the magnitude of the intraparticle velocity becomes more important as the particle size increases. It should be noted at this point that the differences in the breakthrough curves obtained from $v_p = 0.02V_f$, $v_p = 0.03V_f$, and $v_p = 0.05V_f$, for the system studied in this work, are not large; in fact, for the systems with $V_f = 2.778 \cdot 10^{-3}$ m/s and $V_f = 5.556 \cdot 10^{-3}$ m/s (Figs. 2 and 3), the differences in the breakthrough curves cannot be shown graphically because of the graphical scale that was used in the presentation of the results.

The results in Figs. 2 and 3 also show that the magnitude of the maximum outlet concentration of component 2 (component 2 is the least preferentially adsorbed component) obtained from the systems with perfusive particles, is higher than that obtained from the systems using purely diffusive particles. Also, it can be observed that the magnitude of the maximum outlet concentration of component 2 decreases as the superficial fluid velocity, V_f, increases. Furthermore, the differences in the magnitudes of the maximum outlet concentrations of component 2 obtained from the systems with perfusive and purely diffusive particles, increase as the superficial fluid velocity, V_f, increases. It is also observed that the magnitude of the maximum outlet concentration of component 2 obtained from systems with purely diffusive particles, decreases as the particle size, z_0, increases (see Figs. 2 and 3). The results obtained from the systems with perfusive particles indicate that the effect of particle size on the magnitude of the maximum outlet concentration of component 2 is not significant; of course, it is worth mentioning that the magnitude of the maximum outlet concentration of component 2 is slightly higher when the smaller size of perfusive particles is used, but the difference is so small that it is considered to be insignificant. Component 2 attains its maximum outlet concentration faster in the systems with the perfusive adsorbent particles, and furthermore, the time period required for the outlet concentration of component 2 to return to its feed concentration is shorter than that required in the systems with purely diffusive particles (see Figs. 2 and 3).

The results in Figs. 1–3 discussed above and additional results reported in ref. 6, suggest that the dynamic (unsteady state) relative separation between components 1 and 2 obtained from the systems with perfusive particles, is higher than that obtained from the systems with purely diffusive particles. This occurs because the intraparticle fluid flow enhances intraparticle mass transfer and causes the overall intraparticle mass transfer resistance of the perfusive particles, for a given particle size, to become smaller [3,6] than the overall intraparticle mass transfer resistance of the purely diffusive particles, when practical values for the column fluid superficial velocity, V_f, are employed. Furthermore, the results reported in ref. 6 indicate that complete separation of the two adsorption fronts (one adsorption front is for component 1 and the second adsorption front is for component 2) always occurred in the columns with the perfusive adsorbent particles; also, McCoy [6] found that the location in the column with purely diffusive particles at which complete separation of the two adsorption fronts occurs, is longer than the corresponding location in the column with perfusive particles. The findings reported in ref. 6 and the results in Figs. 1–3, suggest that in systems having perfusive particles the most preferentially adsorbed component 1 could utilize the capacity of the active sites on the adsorbent particles more effectively than in systems with purely diffusive particles. This could lead to a higher dynamic relative separation between components 1 and 2 in columns having perfusive particles than the dynamic relative separation that could be obtained in columns with purely diffusive particles.

In Fig. 4, the dimensionless concentration profiles of components 1 and 2 in the pore fluid of a single particle are shown, while in Fig. 5 the dimensionless concentration profiles of components 1 and 2 in the adsorbed phase of the same particle are presented. The results in Figs. 4 and 5 have been obtained when $V_f = 2.778 \cdot 10^{-3}$ m/s, $L = 0.5$ m, $z_0 = 16.12 \cdot 10^{-6}$ m, and represent the

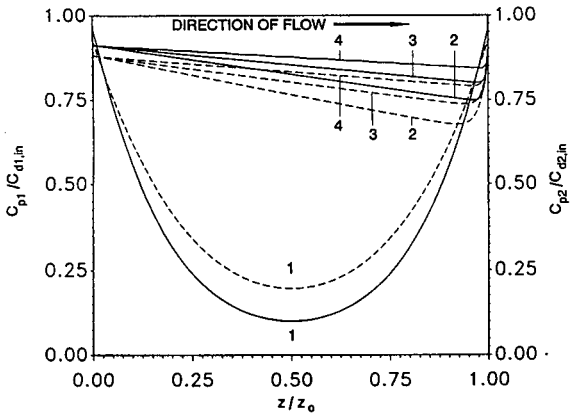

Fig. 4. Dimensionless concentration profiles of components 1 and 2 of the binary system in the pore fluid of the porous adsorbent particle at time $t = 0.15$ min and at location $x = 1.2723 \cdot 10^{-3}$ m in the column (the solid curves are for component 1 and the dashed curves are for component 2). $V_f = 2.778 \cdot 10^{-3}$ m/s; $L = 0.5$ m; $z_0 = 16.12 \cdot 10^{-6}$ m; $1 \equiv v_p = 0$; $2 \equiv v_p = 0.02V_f$; $3 \equiv v_p = 0.03V_f$; $4 \equiv v_p = 0.05V_f$.

dynamic behavior of the concentration profiles at time $t = 0.15$ min at the column location of $x = 1.2723 \cdot 10^{-3}$ m. It can be clearly observed that for the purely diffusive ($v_p = 0$) particle the concentrations of components 1 and 2 in the pore fluid and in the adsorbed phase are substantially lower than the corresponding concentrations in the perfusive ($v_p > 0$) particle for a significant portion of the particle. This difference

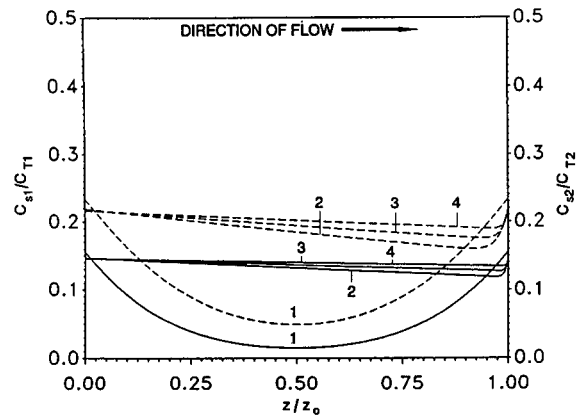

Fig. 5. Dimensionless concentration profiles of components 1 and 2 of the binary system in the adsorbed phase of the porous adsorbent particle at time $t = 0.15$ min and at location $x = 1.2723 \cdot 10^{-3}$ m in the column (the solid curves are for component 1 and the dashed curves are for component 2). $V_f = 2.778 \cdot 10^{-3}$ m/s; $L = 0.5$ m; $z_0 = 16.12 \cdot 10^{-6}$ m; $1 \equiv v_p = 0$; $2 \equiv v_p = 0.02V_f$; $3 \equiv v_p = 0.03V_f$; $4 \equiv v_p = 0.05V_f$.

is due to the fact that the intraparticle fluid flow in the perfusive particle provides within the particle additional amounts of components 1 and 2, and thus, the total contents of components 1 and 2 provided by intraparticle fluid flow and pore diffusion in a perfusive particle could be higher than those provided only by pore diffusion in a purely diffusive particle. Furthermore, the concentration profiles of the purely diffusive particle are symmetric, as expected, and the point of symmetry is located at the center of the particle where $z/z_0 = 0.5$. For the perfusive particle, the results in Figs. 4 and 5 show that as the intraparticle velocity, v_p, increases, the concentration minima for components 1 and 2 in the pore fluid and in the adsorbed phase move downstream while the overall contents of components 1 and 2 increase within the particle.

In Fig. 5, the values of C_{s2}/C_{T2} for a given v_p are higher than the values of C_{s1}/C_{T1}. The reason for this is that for short operational times the magnitudes of the forward rate constants k_{11} and k_{12} (see Table I) play a very significant role in determining the relative amounts of components 1 and 2 in the adsorbed phase. For the system in Figs. 4 and 5 the forward rate constant of component 2 is higher than the forward rate constant of component 1 ($k_{12} > k_{11}$), but the reverse rate constant of component 1, k_{21}, is significantly smaller than the reverse rate constant of component 2, k_{22} ($k_{22} > k_{21}$). Therefore, since $K_{a1} > K_{a2}$ (see Table I), component 1 is the most preferentially adsorbed component and displaces previously adsorbed component 2 as the operational time increases and the adsorption front of component 1 proceeds downstream (as shown in Figs. 1–3 that they were discussed above). Thus, at larger operational times the values of C_{s1}/C_{T1} for a given v_p become higher than the values of C_{s2}/C_{T2} in the adsorbent particle.

CONCLUSIONS AND REMARKS

A mathematical model of binary perfusion chromatography was presented, solved, and used to study the dynamic behavior of a binary adsorption system. The equations of the model for the adsorbent particles include the intrapar-

ticle mass transfer mechanisms of convection (intraparticle fluid flow) and pore diffusion, as well as the mass transfer steps involving the dynamic interactions of components 1 and 2 (the dynamics of the adsorption steps are finite) with the active sites on the surface of the porous adsorbent particles. The values of the parameters that characterize the mass transfer and interaction mechanisms of the binary system studied in the simulations of this work, are in the range of the values of such parameters measured and/or estimated from experiments involving affinity adsorption of biologically active macromolecules [7,8,15–20]. The dynamic behavior of column systems (frontal analysis) was examined for different particle sizes (z_0), column fluid superficial velocities (V_f) and intraparticle fluid velocities (v_p). The studies in this work examined column systems having perfusive ($v_p > 0$) and purely diffusive ($v_p = 0$) adsorbent particles.

It was found that for the binary system studied in this work, the breakthrough curves obtained from the column having perfusive particles are not significantly different from the breakthrough curves obtained from the column with purely diffusive particles when the column fluid superficial velocity is low (Fig. 1). When the column fluid superficial velocity is high (Figs. 2 and 3), then the breakthrough curves obtained from the column involving perfusive particles are different from those obtained from the column with purely diffusive particles, and their differences become larger as the particle size and the column fluid superficial velocity increase. The steepness of the breakthrough curves of components 1 and 2 obtained from the column with perfusive particles, as well as the times at which breakthrough begins for components 1 and 2, were found to increase with increasing intraparticle fluid velocity, v_p; in general, the breakthrough curves from the column with perfusive particles were less disperse than those obtained from the column with purely diffusive particles. As the particle size was increased, the increase in the value of the intraparticle fluid velocity had a more significant effect on the shape of the breakthrough curves and on the time at which breakthrough begins. It was also found that the magnitude of the maximum outlet concentration of the least preferentially adsorbed component 2 obtained from the systems with perfusive particles, is higher than that obtained from the corresponding systems having purely diffusive particles, and the difference increases as the column fluid superficial velocity increases. Component 2 attains its maximum outlet concentration faster in the systems having perfusive particles, and furthermore, it appears that the time period required for the outlet concentration of component 2 to return to its feed concentration in the systems with perfusive particles, is shorter than that required in the systems having purely diffusive particles.

The results obtained from the binary adsorption system studied in this work suggest that the times at which breakthrough begins for components 1 and 2, and the dynamic (unsteady state) relative separation between components 1 and 2 obtained from the column with perfusive particles, are higher than those obtained from the column having purely diffusive particles, especially as the particle size and the column fluid superficial velocity increase. These results occur because the overall intraparticle mass transfer resistance of the perfusive particles, for a given particle size, is smaller [3,6] than the overall intraparticle mass transfer resistance of the purely diffusive particles, when practical values for the column fluid superficial velocity, V_f, are employed. In systems having perfusive particles, the most preferentially adsorbed component 1 could utilize the capacity of the active sites on the adsorbent particles more effectively than in systems with purely diffusive particles, and this could lead to a higher dynamic relative separation between components 1 and 2. The results of this study also suggest that when the column fluid superficial velocity is increased, the effect on the dynamic relative separation between components 1 and 2, is substantially smaller in columns with perfusive particles than in columns having purely diffusive particles. These findings suggest that for a given overall operational time, a larger number of binary adsorption cycles having high dynamic relative separations between components 1 and 2, could be realized, when columns with perfusive particles and high values of V_f are employed.

In conclusion, the improved separation efficiency obtained from the chromatographic columns with perfusive adsorbent particles studied in this work, is mainly due to the intraparticle fluid flow which enhances intraparticle mass transport. The intraparticle fluid flow causes the overall intraparticle mass transfer resistance of the perfusive particles to become smaller than the overall intraparticle mass transfer resistance of the purely diffusive particles.

SYMBOLS

C_{di}	concentration of component i (i = 1, 2) in the flowing fluid stream of the column, kg/m^3
$C_{di,in}$	concentration of component i (i = 1, 2) at $x = 0$, kg/m^3
$\mathbf{C}_p$	vector of concentration variables defined after eqn. 1
C_{pi}	concentration of component i (i = 1, 2) in pore fluid, kg/m^3
$\mathbf{C}_s$	vector of concentration variables defined after eqn. 1
C_{si}	concentration of component i (i = 1, 2) in adsorbed phase, kg/m^3 particle
C_{T1}	saturation value (limiting value) of C_{s1}, kg/m^3 particle
C_{T2}	saturation value (limiting value) of C_{s2}, kg/m^3 particle
D_{pi}	effective pore diffusion coefficient of component i (i = 1, 2), m^2/s
$f_i(\mathbf{C}_p, \mathbf{C}_s, \mathbf{k})$	functional form defined after eqn. 1
K_{a1}	$K_{a1} = k_{11}/k_{21}$ (see Table I), m^3/kg
K_{a2}	$K_{a2} = k_{12}/k_{22}$ (see Table I), m^3/kg
K_I	parameter defined in Table I
$\mathbf{k}$	vector of adsorption rate constants defined after eqn. 1
k_{11}	adsorption rate constant for component 1 in eqn. 2, m^3/(kg) (s)
k_{12}	adsorption rate constant for component 2 in eqn. 3, m^3/(kg) (s)
k_{21}	adsorption rate constant for component 1 in eqn. 2, s^{-1}
k_{22}	adsorption rate constant for component 2 in eqn. 3, s^{-1}
L	column length, m
t	time, s
V_f	column fluid superficial velocity, m/s
v_p	intraparticle fluid velocity (intraparticle convective velocity), m/s
x	axial distance along column, m
z	space coordinate of adsorbent, m
z_0	size of adsorbent particle, m

Greek letters

ε	void fraction in column
ε_p	void fraction in porous adsorbent particle

ACKNOWLEDGEMENTS

The authors gratefully acknowledge that this work was supported by the Monsanto Company and the NATO Scientific Affairs Division under Grant No. 880770.

REFERENCES

1 N.B. Afeyan, N.F. Gordon, I. Mazsaroff, L. Varady, S.P. Fulton, Y.B. Yang and F.E. Regnier, *J. Chromatogr.*, 519 (1990) 1.
2 N.B. Afeyan, S.P. Fulton and F.E. Regnier, *J. Chromatogr.*, 544 (1991) 267.
3 A.I. Liapis and M.A. McCoy, *J. Chromatogr.*, 599 (1992) 87.
4 L. Lloyd and F. Warner, *J. Chromatogr.*, 512 (1990) 365.
5 A.E. Rodrigues, J.C. Lopes, Z.P. Lu, J.M. Loureiro and M.M. Dias, *J. Chromatogr.*, 590 (1992) 93.
6 M.A. McCoy, *Ph.D. Dissertation*, Department of Chemical Engineering, University of Missouri-Rolla, Rolla, MO, 1992.
7 A.I. Liapis, *Sep. Purif. Methods*, 19 (1990) 133.
8 B.H. Arve and A.I. Liapis, *AIChE J.*, 33 (1987) 179.
9 R.L. Beissinger and E.F. Leonard, *J. Colloid Interface Sci.*, 85 (1982) 521.
10 E.C. Moreno, M. Kresak, J.J. Kane and D.I. Hay, *Langmuir*, 3 (1987) 511.
11 D.M. Ruthven, *Principles of Adsorption and Adsorption Processes*, Wiley, New York, 1984.
12 J. Villadsen and M.L. Michelsen, *Solution of Differential Equation Models by Polynomial Approximation*, Prentice-Hall, Englewood Cliffs, NJ, 1978.
13 C.D. Holland and A.I. Liapis, *Computer Methods for Solving Dynamic Separation Problems*, McGraw-Hill, New York, 1983.
14 T. Wicks, *Scientific Computing and Analysis Library Report, SCA-LR-52*, Boeing Computer Services, Seattle, WA, October 1988.
15 A. Johnston and M.T.W. Hearn, *J. Chromatogr.*, 512 (1990) 101.

16 A.I. Liapis, A.B. Anspach, M.E. Findley, J. Davies, M.T.W. Hearn and K.K. Unger, *Biotechnol. Bioeng.*, 34 (1989) 467.
17 A.B. Anspach, A. Johnston, H.-J. Wirth, K.K. Unger and M.T.W. Hearn, *J. Chromatogr.*, 476 (1989) 205.
18 F.H. Arnold, H.W. Blanch and C.R. Wilke, *Chem. Eng. J.*, 30 (1985) B9.
19 F.H. Arnold, H.W. Blanch and C.R. Wilke, *Chem. Eng. J.*, 30 (1985) B25.
20 M.A. McCoy, B.J. Hearn and A.I. Liapis, *Chem. Eng. Commun.*, 108 (1991) 225.

Journal of Chromatography, 644 (1993) 11–16
Elsevier Science Publishers B.V., Amsterdam

CHROM. 25 169

Salt-induced immobilization of proteins on a high-performance liquid chromatographic epoxide affinity support

Jeffrey B. Wheatley* and Donald E. Schmidt, Jr.

Terrapin Technologies, Incorporated, 750-H Gateway Boulevard, South San Francisco, CA 94080 (USA)

(First received August 4th, 1992; revised manuscript received April 6th, 1993)

ABSTRACT

The immobilization of thirteen proteins on a high-performance liquid chromatography epoxy affinity support was studied as a function of ammonium sulfate concentration. Without exception the fraction of protein immobilized at 20 h increased with increasing salt concentration at higher salt concentrations. Ten of the proteins were 95–100% immobilized in 20 h at ammonium sulfate concentrations ranging from 0.4 to 2.5 *M*. At lower salt concentrations the affinity support exhibited lower reactivity with all proteins. A kinetic model is proposed in which protein in solution is at equilibrium with a noncovalent protein–affinity support complex. The nucleophiles on the protein of the complex then react in a slow step with epoxy groups on the affinity phase. The dependence of immobilization on salt concentration is interpreted as a salt induced hydrophobic interaction on the equilibrium formation of the noncovalent protein–affinity matrix complex.

INTRODUCTION

We reported previously [1] that in studies of protein coupling to an epoxide-type, silica-based HPLC affinity support, the presence of relatively high concentrations of salt results in highly efficient protein immobilization at neutral pH. In that study the bound proteins, comprised of individual immobilizations of human albumin, α_1-acid glycoprotein and IgG immunoglobulin, retained good activity in the purification of their antibodies from antisera. The extent of coupling for two proteins (goat IgG and human α_1-acid glycoprotein) was examined and found to increase with salt concentration, and there was a large difference in the concentration of salt required to attain a given coupling efficiency for the two proteins. It was suggested that the increased coupling reactivity results from a salt-induced association between the protein and the surface of the affinity support thereby increasing the effective concentration of protein near the epoxide reactive sites. The variation in coupling observed for different proteins at a given concentration of salt could result from differences in the susceptibilities of individual proteins to salt-induced partitioning along the surface of the support, combined with variations due to differences in the inherent reactivities of the proteins.

A close analogy has been drawn between the salt-induced solute–stationary phase interactions responsible for retention in hydrophobic interaction chromatography (HIC) and solute–solute interactions associated with precipitation in the salting-out effect. An underlying explanation for these phenomena and their close similarities has been reported [2–5]. This theory describes salt induced interfacial interactions as representing a balance between electrostatic contributions, which tend to support solvation of the solute, and hydrophobic interactions which favor solute–solute or solute–stationary phase interac-

* Corresponding author.

0021-9673/93/$06.00

tions. The theory may be extended to describe the salt induced protein–affinity phase complex formation postulated above.

Other investigators [6,7] have used conditions at high salt concentrations for the efficient coupling of proteins to silica-based epoxide affinity phases with the retention of biological activity as evidenced by the affinities of the bound moieties for mobile phase components. Dependence of protein immobilization on salt concentration has also been described for coupling to polymer-based epoxide and azyl-lactone activated supports [5,8,9]. In this investigation the extent of coupling for a collection of proteins was measured on an epoxide affinity support over a wide range of salt concentrations. Using a general first-order kinetics model to describe the relationship between soluble and immobilized protein, an expression was derived for this reaction.

EXPERIMENTAL

Materials

The proteins used in this study were obtained from Sigma (St. Louis, MO, USA). The salts and reagents used for pH adjustments are products of J.T. Baker (VWR, Brisbane, CA, USA) and were reagent grade or better. The epoxy activated affinity phase, Hydropore-EP (12 mm, 300 Å), is a product of Rainin Instrument Company (Woburn, MA, USA).

Immobilization of proteins on the affinity support

Protein immobilization was performed as previously described [1]. The protein was dissolved in 0.010 *M* potassium phosphate, pH 7.0, and to this solution was added varying amounts of 3.0 *M* ammonium sulfate in 0.010 *M* potassium phosphate, pH 7.0, resulting in protein solutions containing increasing concentrations of salt. Typically, 6 to 8 concentrations were examined for each protein, ranging at regular intervals from 0 to 1.0–2.8 *M* ammonium sulfate, depending on the protein. A 500-μl volume of the above solutions was then combined with 50 mg of the affinity support in a 1.5-ml capped vial. Each sample contained 500 μg of protein with the exception of avidin and IgG_1k monoclonal antibody which contained 400 and 167 μg, respectively. In all cases the protein solution was observed to ensure that the solubility had not been exceeded at a particular ammonium sulfate concentration.

The mixture was turned overnight by orbital rotation at room temperature and at an angle and speed which effected thorough mixing. This was achieved in the following way. A common 500-ml polyethylene bottle was attached to an overhead stirring motor, co-axial with the stirring shaft. The vials containing the coupling mixtures were attached to the surface of the bottle, vertical with respect to the bottle and motor shaft. The motor was then tilted about 45° from the horizontal. The result was that as the motor turned the bottle, the vials were rotated such that the contents turned continuously over the course of the reaction. Best mixing was achieved at low motor speeds. The reactions were carried out for 20 h except in the case of lysozyme and albumin which reacted for 25 h. The derivatized supports were then centrifuged, twice washed in 500 μl of 0.010 *M* potassium phosphate, pH 7.0, and in 1000 μl of 0.10 *M* sodium acetate, pH 4.5, containing 0.3 *M* sodium chloride. The supernatant from the washes was combined with that recovered following the reaction.

The amount of protein bound to the support in the immobilization was calculated from the difference between the amount of protein initially added and that recovered in the post-coupling wash. This was deduced from the spectrophotometric absorbance (Hitachi Model U-2000, San Jose, CA, USA) at 230 nm, except in the cases of α-chymotrypsinogen A, α-chymotrypsin, myoglobin and ribonuclease A which were measured at 280 nm. For these calculations it was assumed that variations in the extinction coefficient with salt concentration were small for the range of concentrations in the study. Most measurements were made at final salt concentrations (after dilution in the wash step) of less than 0.5 *M*, with a few measurements made at up to 0.7 *M*. Also, in nearly all cases the data set for each protein was obtained in one sitting. This eliminates the possibility of error within a data set arising from inconsisten-

cies in the wavelength setting. Determined on separate days were the two data points corresponding to the highest concentration of salt in the measurements for ribonuclease A, avidin and lysozyme.

RESULTS AND DISCUSSION

In this study we examined the efficiency with which proteins react with an epoxide affinity support in the presence of increasing concentrations of ammonium sulfate. Thirteen proteins were studied and the results obtained for percent immobilization as a function of ammonium sulfate concentration are shown in Figs. 1 and 2. Table I shows the approximate concentration of ammonium sulfate required for 90% immobilization in 20 h. All but three of the proteins exhibited 95–100% immobilization within 20 h, and the salt concentration at which this occurred depended on the individual protein examined. Of those that failed to react completely, ribonuclease A attained 85–90% immobilization while α-chymotrypsinogen A reached 60–65% and lysozyme attained only about 50% immobilization.

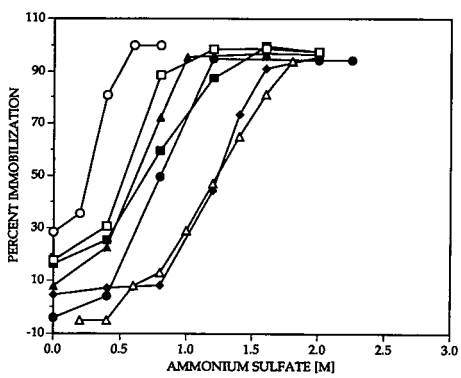

Fig. 1. Percent immobilization of proteins on an epoxy affinity support *vs.* ammonium sulfate concentration for proteins exhibiting elevated immobilization at zero salt concentration. Protein was dissolved in solutions containing varying amounts of ammonium sulfate. The protein solution was reacted with the epoxy affinity phase and after reaction the remaining protein was removed from the particles by washing. The amount of protein bound to the support was determined spectrophotometrically by the difference between the amount of protein added and the amount of protein in the washes. See Experimental for details. ○ = Conalbumin; ▲ = α-chymotrypsin; ● = α-chymotrypsinogen A; □ = ribonuclease A; ◆ = lysozyme; ■ = avidin.

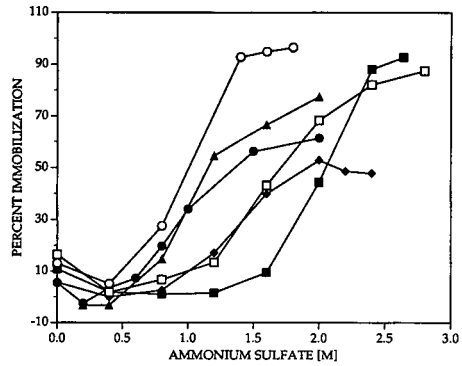

Fig. 2. Percent immobilization of proteins on an epoxy affinity support *vs.* ammonium sulfate concentration for proteins which did not exhibit elevated immobilization at zero salt concentration. See Fig. 1 for details. ○ = IgG_1k; □ = transferrin; ▲ = α-lactalbumin; ■ = myoglobin; ● = bovine serum albumin; △ = carbonic anhydrase; ◆ = β-lactoglobulin B.

The strong dependence of the degree of protein immobilization on the affinity support with respect to ammonium sulfate concentration led us to examine the fraction of immobilization of protein as a function of salt concentration. Although all the proteins exhibited increases in immobilization beginning at some concentration of salt, the concentration thresholds at which this was observed varied widely among the proteins examined. For some proteins, such as IgG, transferrin and β-lactoglobulin B, shown in Fig. 1, increases in immobilization were first observed at salt concentrations below 0.5 *M*. Others, such as avidin and ribonuclease A, shown in Fig. 2, required concentrations above 1.0 *M* to exhibit significant increases.

The reaction between proteins and the epoxide ligands on the affinity support can be represented by the reaction scheme

$$P + L \underset{k_{-1}}{\overset{k_{+1}}{\rightleftharpoons}} P \cdot L \xrightarrow{k_2} P - L$$

where P is free protein in solution, L is the stationary phase containing the epoxy groups, $P \cdot L$ is the noncovalently bound protein on the stationary phase, and P–L is the protein covalently bound to the surface through reaction with the epoxy groups. According to this model, any perturbation in the immobilization mixture

TABLE I

AMMONIUM SULFATE CONCENTRATION REQUIRED FOR 90% IMMOBILIZATION OF PROTEINS ON HYDROPORE-EP EPOXIDE AFFINITY SUPPORT

Protein	Molecular weight	p*I*	Ammonium sulfate concentration (*M*)
Lysozyme[a]	14 000	11.0	–
Avidin	68 000	10–10.5	2.4
α-Chymotrypsinogen A [a]	25 000	9.5	–
Carbonic anhydrase[b]	29 000	5.4, 5.9, 6.6	1.7
Ribonuclease A [c]	13 700	9.4	2.8 (87%)
α-Chymotrypsin[c]	21 600	8.8	2.0 (77%)
Myoglobin	17 500	7.1	1.3
IgG_1k monoclonal antibody	55 000	NA	0.4
Conalbumin	77 000	6.5	1.4
Transferrin	77 000	5–6	0.8
β-Lactoglobulin B	35 000	5.1	1.6
Serum albumin (bovine)	68 000	4.4–4.8	1.1
α-Lactalbumin	14 200	4.5–4.7	0.9

[a] These proteins were not 90% immobilized. See text.
[b] The isoelectric points shown represent three isozymes, all or part of which may have been present.
[c] This was the highest concentration examined.
NA = Not available.

which shifts the equilibrium to increase the ratio of $[P \cdot L]/[P][L]$ will increase the concentration of protein near the epoxide groups along the surface of the support. An increase in the concentration of $P \cdot L$ will result in a faster rate in the formation of the product $P - L$.

When the reaction is stopped after 20 h the amount of protein (P_m) measured in solution is the sum of P and $P \cdot L$. The rate constant (k_2) for the attack of a protein associated nucleophile on an epoxy group is assumed to be small compared to both the rate constant of formation (k_{+1}) and the rate constant (k_{-1}) for breakdown of $P \cdot L$.

Based on this assumption the concentration of $P \cdot L$ can be represented as

$$[P \cdot L] = [P][L]K \quad (1)$$

where $K = k_{+1}/k_{-1}$.

Then

$$d[P - L]/dt = k_2[P \cdot L] = k_2K[L][P]$$
$$= k_2K[L_0][P] \quad (2)$$

where $[L_0]$ is the initial concentration of epoxide ligands on the stationary phase and is large compared to $[P \cdot L] + [P - L]$. From the identities $[P_0] - [P_m] = [P - L]$ and $[P_m] = [P]\ (1 + K[L_0])$ eqn. 2 can be modified and integrated to yield

$$\log f = -k_2K[L_0]t/(2.3)(1 + K[L_0]) \quad (3)$$

where f is the fraction of protein which is not covalently bound to the stationary phase and is equal to $[Pm]/[P_0]$. In these experiments f was determined after a constant time (20 h). A plot of log f_a (f_a is the fraction of free protein remaining in solution after 20 h) as a function of ammonium sulfate concentration for ribonuclease A, lysozyme and α-chymotrypsinogen A is shown in Fig. 3.

At ammonium sulfate concentrations where K is small eqn. 3 reduces to

$$\log f_a = -k_2K[L_0]t_a/2.3 \quad (4)$$

where t_a is the duration of the reaction (20 h). According to eqn. 4 log f_a is directly proportional to K. Partition of the protein along the epoxide phase, represented by the equilibrium constant K in eqn. 4, is assumed to be a function

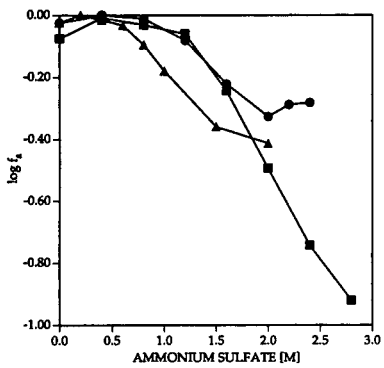

Fig. 3. Log f_a *vs.* ammonium sulfate concentration. See Fig. 1 for details. ■ = Ribonuclease A; ● = lysozyme; ▲ = α-chymotrypsinogen.

of salt concentration, analogous to the salt induced associations which occur between proteins and the stationary phase in hydrophobic interaction chromatography (HIC). Horváth and coworkers [2,3] have shown that for HIC the distribution of the protein solute between the stationary and mobile phases parallels the dependence of protein solubility on salt concentration. Protein solubility at very low salt concentrations at first increases with increasing salt concentration (the salting-in effect), and then decreases as the salt approaches high concentration (the salting-out effect). The logarithmic dependence of protein solubility is non-linear with respect to salt at low concentrations and becomes linear at higher concentrations, a characteristic which is also found for log k' *vs.* salt concentration in HIC [2]. In this study trends similar to these were found for the salt dependence of protein immobilization on the epoxide support. The dependence of log f_a (or percent immobilization) on ammonium sulfate concentration appears to be non-linear at low salt concentrations and approaches a linear dependence at higher concentrations. Plots of log f_a *vs.* ammonium sulfate concentration are shown in Fig. 3 for three proteins.

Some of the proteins in this study, seen in Fig. 1, also exhibited a slight increase in immobilization (lowered f_a) as the concentration of ammonium sulfate approached zero. Such an increase in immobilization could occur, according to the above argument, as a result of an enhanced association between the protein and support in the absence of salt. Protein–stationary phase associations like these have been reported [10] for the isocratic retention of proteins on a silica-based HIC stationary phase (polyvinyl alcohol). In that study the retention of some proteins first declined as ammonium sulfate concentration increased just above zero concentration. Although increases in HIC protein retention in the absence of salt or the increases in immobilization seen in this study are reminiscent of the salting-in effect, another explanation is possible. The proteins which demonstrated this characteristic were all basic (except conalbumin, p*I* 6.5) and should possess a net positive charge at pH 7 while the epoxy phase would be expected to have a net negative charge due to any unreacted silanols present on the underlying surface of the silica. In the absence of ammonium sulfate these proteins would show enhanced association with the solid phase through ionic interactions which would lead to relative increases in immobilization. In the HIC study described above the proteins which exhibited low salt associations with the stationary phase were also basic proteins. It can also be noted that the proteins in this study which did not show elevated immobilization at zero salt concentration all possess isoelectric points near or below p*I* 7.0. These proteins are shown in Fig. 2.

When K becomes large eqn. 3 reduces to

$$\log f_a = -k_2 t_a / 2.3 \quad (5)$$

which defines a region of salt concentrations where the fraction of immobilized protein is independent of K. In this region of salt concentrations a large fraction of the protein is already associated with the solid phase and any increase in salt concentration would not lead to an appreciable increase in P·L. The extent of immobilization in this region of salt concentrations is only a function of the rate constant k_2. For most proteins studied (*e.g.*, ribonuclease A in Fig. 3) the rate constant k_2 is large enough that complete immobilization occurs within 20 h under the conditions described by eqn. 5. For two proteins, lysozyme and α-chymotrypsinogen A, k_2 is small, and less than complete immobili-

zation occurs in 20 h even though all the protein is associated with the stationary phase (Fig. 3).

These results clearly indicate that relatively high concentrations of ammonium sulfate are required for satisfactory immobilization of proteins on the epoxide support, and that, in most cases, very high coupling efficiencies can be achieved if this condition is met. The ability to achieve high coupling efficiencies at a neutral pH allows immobilization to be performed in the absence of pH extremes and without the addition of potentially denaturing reagents, thereby helping to preserve the integrity of the immobilized ligand in the coupling process.

ACKNOWLEDGEMENTS

This work was supported by Rainin Instrument Company, Inc.

REFERENCES

1 J.B. Wheatley, *J. Chromatogr.*, 548 (1991) 243.
2 W. Melander and Cs. Horváth, *Arch. Biochem. Biophys.*, 183 (1977) 200.
3 W.R. Melander, D. Corradini and Cs. Horváth, *J. Chromatogr.*, 317 (1984) 67.
4 T. Arakawa and S.N. Timasheff, in H.W. Wyckoff, C.H.W. Hirs and S.N. Timasheff (Editors), *Methods in Enzymology*, Academic Press, Orlando, 1988 (114), p. 49.
5 K. Smalla, J. Turkova, J. Coupek and P. Hermann, *Biotech. Appl. Biochem.*, 10 (1988) 21.
6 D.F. Hollis, S. Ralston, E. Suen, N. Cooke and R.G.L. Shorr, *J. Liq. Chromatogr.*, 10 (1987) 2349.
7 D.J. Phillips, B. Bell-Alden, M. Cava, E.R. Grover, W.H. Mandeville, R. Mastico, W. Sawlivich, G. Vella and A. Weston, *J. Chromatogr.*, 536 (1991) 95.
8 O. Hannibal-Friedrich, M. Chun and M. Sernetz, *Biotech. Bioeng.*, 22 (1980) 157.
9 P.L. Coleman, M.M. Walker, D.S. Milbrath, D.M. Stauffer, J.K. Rasmussen, L.R. Krepski and S.M. Heilmann, *J. Chromatogr.*, 512 (1990) 345.
10 Z. El Rassi and Cs. Horváth, *J. Liq. Chromatogr.*, 9 (1986) 3245.

Journal of Chromatography, 644 (1993) 17–24
Elsevier Science Publishers B.V., Amsterdam

CHROM. 25 146

Molecular mass determination of low-molecular-mass heparins

Application of wide collection angle measurements of light scattering using a high-performance gel permeation chromatographic system equipped with a low-angle laser light-scattering photometer

Hiroaki Komatsu*, Kimihiko Yoshii, Susumu Ishimitsu and Satoshi Okada

Division of Drugs, National Institute of Hygienic Sciences, Osaka Branch, 1-1-43, Hoenzaka, Chuo-ku, Osaka 540 (Japan)

Tomoko Takahata

Osaka College of Pharmacy, Matsubara 580 (Japan)

(First received December 8th, 1992; revised manuscript received March 2nd, 1993)

ABSTRACT

A high-performance gel permeation chromatographic system with on-line low-angle laser light-scattering detection (HPGPC–LALLS) was used to determine molecular masses of low-molecular-mass heparins (LMMHs). Measurements at wide and narrow collection angles were compared and the application of the HPGPC–LALLS method to small molecules, with molecular masses in the range 1000–10 000, was assessed. The molecular mass averages of fractionated heparins and commercially available LMMHs were also determined by ordinary HPGPC analysis using an LMMH molecular-mass calibrant, supplied by the National Institute for Biological Standards and Control for the calibration of columns. The LALLS intensity at the routinely used narrow collection angle ($\theta_{col} = 1°$) about doubled at the wide collection angle ($\theta_{col} = 2°$) and the signal-to-noise ratio was improved. The present study thus indicates that wide collection angle measurement of light scattering allows the application of the HPGPC–LALLS method to very small biopolymers of molecular mass <10 000.

INTRODUCTION

Recently, a great deal of research on the chemical, biological and therapeutic properties of low-molecular-mass heparins (LMMHs) has been carried out [1–9]. LMMHs are generally prepared by the enrichment of low-molecular-mass fractions or by the depolymerization of unfractionated heparins [10,11], which are polysaccharides composed of alternate sequences of differently sulphated residues of uronic acid (usually α-L-iduronic acid) and α-D-glucosamine-linked α(1→4) bonds [12] with a wide molecular mass range between 3000 and 40 000 [12,13]. LMMHs are claimed to possess anticoagulant properties with reduced bleeding, greater bio-

* Corresponding author.

0021-9673/93/$06.00

availability and longer biological half-lives than unfractionated heparins [7,14].

Commercially available LMMHs from different manufacturers differ in their molecular mass distribution and in end-unit chemical structure according to the preparation. Recent production methods involve chemical depolymerization using nitrous acid or hydrogen peroxide [10] and enzymatic depolymerization [11], the resultant LMMHs varying in structure, molecular mass distribution, anticoagulant activities and pharmacological properties [5,6,10]. The anticoagulant properties in particular are related to the molecular mass distribution [14] and therefore the determination of the molecular mass averages and ranges is important for batch characterization.

Several methods for the measurement of heparin molecular mass have been commonly used [5,8,15–19]. Recently, it was shown that low-angle laser light-scattering (LALLS), incorporating high-performance gel permeation chromatography (HPGPC) coupled to an absolute molecular mass detector, can provide molecular mass profiles of heparins [20], but there are only a few data available on LMMHs. For LMMHs having molecular mass averages of about 6000, reliable evaluation is difficult because of the weak light-scattering intensity inherent with very small molecules.

Takagi and co-workers [21–24] applied HPGPC–LALLS to determine the molecular mass of biopolymers and have published extensively on molecular mass measurements of membrane proteins. Krull and co-workers have demonstrated that these detectors can be used to determine biopolymer molecular masses when coupled with reversed-phase [25] and hydrophobic interaction [26] chromatography. Recently, Dollinger *et al.* [27] demonstrated that a simple fluorimeter for high-performance liquid chromatography can be used as a 90° (corresponding to θ_{obs} in Fig. 1) classical light-scattering detector for the on-line molecular mass determination of biopolymers. This detector was shown to be sensitive, relatively immune to dust and column particles and easy to use.

In this study, in an attempt to improve the application of HPGPC–LALLS analysis to

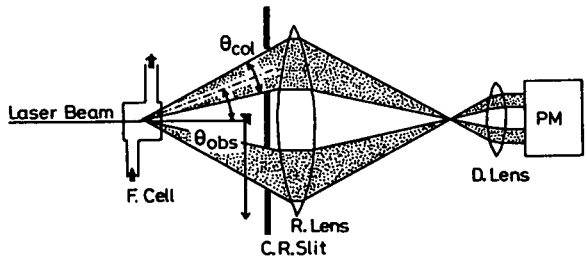

Fig. 1. Schematic illustration of light-scattering collection in a LALLS detector. F. Cell = Flow cell; C.R. Slit = circular ring slit; PM = photomultiplier; R. Lens = relay lens; D. Lens = detector lens.

LMMHs, light scattering was measured at a wider collection angle ($\theta_{col} = 2°$; see Fig. 1) than that routinely used ($\theta_{col} = 1°$) for the determination of the absolute molecular masses of polymers and proteins with values above 10 000 [21–24,26].

EXPERIMENTAL

Materials

Commercially available LMMHs, Enoxaparin (lot R573), Fraxiparine (9NDE104), Sandoparin (80005), Fluxum (B72315), Fragmin A (84920-51) and B (84921-51), Logiparin (9005A) and the Japanese Pharmacopoeia Standard for LMMH (JRS-LMMH) (lot JP911) were purchased from Pharmuka Laboratories (Gennevilliers, France), Sanofi Chimie (N.D.-de-Bondeville, France), Sandoz-Wander Pharma (Berne, Switzerland), Opocrin (Corlo, Italy), Kabi-Vitrum (Stockholm, Sweden), Novo-Nordisk Pharma (Gentofte, Denmark) and the National Institute of Hygienic Sciences (Tokyo, Japan), respectively. Fractionated heparins, N-17 (lot KBJ6056-1), N-10 (KBJ6104-1), N-6 (KBJ6076-4), N-3 (KBJ890315) were kindly provided by Novo-Nordisk Pharma, K-6 (DxN89) and K-4 (DxN49) were gifts from Kabi-Vitrum and S-5 (97F0454) and S-3 (97F0455) were obtained from Sigma (St. Louis, MO, USA). An LMMH molecular mass calibrant (Code 90/686) was supplied by the National Institute for Biological Standards and Control (NIBSC), (Potter's Bar, Hertfordshire, UK). All heparins were obtained in powdered form except for Sandoparin, which was provided as a physiological salt solution.

Pullulan P-400 (average molecular mass 380 000 and dispersitivity 1.12) was obtained from Showa Denko (Tokyo, Japan). Water for injection (Ohtsuka Pharmaceuticals, Tokushima, Japan) was used for the preparation of eluent and sample solutions. All reagents were of analytical-reagent grade.

Chromatographic conditions

The eluent used was 0.2 *M* aqueous sodium sulphate and 50 m*M* Tris–HCl (pH 7.0), filtered using a 0.2-μm pore-size filter (Japan Millipore, Tokyo, Japan) and degassed before use. Elution was performed at a flow-rate of 0.6 ml/min.

HPGPC analysis. A system consisting of an on-line degasser (Model SD-8012, Tosoh, Tokyo, Japan), a pump (Tosoh Model CCPD), an injector (Rheodyne Model 7125) equipped with a 100-μl loop, a guard column for gel permeation (Tosoh TSK guard column SWxl, 40 mm × 6.0 mm I.D.), gel permeation columns (Tosoh TSK gel G2000 SWxl and G3000 SWxl, both 300 mm × 7.8 mm I.D.) and a precision differential refractometer (Tosoh Model RI-8011; light source, photodiode with an effective wavelength of 660 nm) kept at 35°C were used. The columns were maintained at 30°C using a column oven (Tosoh CO-8010). For the calibration of the columns, especially using the NIBSC LMMH molecular mass calibrant as a standard, the absorbance at 235 nm was also monitored at the same time as the differential refractive index (RI) at room temperature (about 20°C) with a Model SPD-6A UV spectrophotometer (Shimadzu, Kyoto, Japan). The detector outputs were fed into a computer (PC-9801DA; NEC, Tokyo, Japan) and used to calculate the molecular mass profiles of the various LMMHs using the program Chromato Data Processor Ver. 2.03, supplied by Tosoh, in a gel permeation chromatographic mode.

The concentration of each sample was *ca.* 10 mg/ml, except for Sandoparin (70 mg/ml). Heparins are usually hygroscopic. In this study, therefore, their water contents were determined by thermogravimetric analysis under the assumption that the decrease in sample mass can be ascribed to evaporation of water. The concentrations of heparins were then corrected for the water content. The sample injection volume was 50 μl, except for Sandoparin (20 μl).

HPGPC–LALLS analysis. In the measurement of LALLS, a guard column for gel permeation (Tosoh TSK guard column PWxl, 40 mm × 6.0 mm I.D.) and a gel permeation column (Tosoh TSK gel G3000 PWxl, 300 mm × 7.8 mm I.D.), were used instead of SW-type columns. Although the latter have a higher resolution they release small particles during experiments, which render them unreliable for use with subtle LALLS detection systems (too much background noise on the LALLS recorder signal in spite of careful experiments), as pointed out by Hennink *et al.* [20]. A LALLS photometer (Tosoh Model LS-8000), whose introduction was described in detail in a recent review [24], and a differential refractometer were used as detectors. The ligh source of the LALLS photometer is a 5-mW helium–neon laser with a wavelength of 633 nm. A circular light slit with an aperture wider ($\theta_{col} = 2°$) than the conventional one ($\theta_{col} = 1°$) is an option which was obtained from the manufacturer (Tosoh). The columns were kept at 40°C. An ultrafilter with pore size 0.45 μm (Type FP-045; Sumitomo Electric, Tokyo, Japan) was connected between the columns and the LALLS photometer. Other components were the same as for HPGPC analysis. The sample concentrations and injection volumes were determined as the maximum values, at which RI detector saturation did not occur, being *ca.* 10 mg/ml and 80 μl, respectively, except for Sandoparin case (35 mg/ml and 30 μl). The molecular mass profiles of LMMHs were calculated using the analysis program in the LALLS mode.

RESULTS AND DISCUSSION

HPGPC measurements

Calibration of columns using an NIBSC LMMH molecular mass calibrant. The method adopted in this study is based on that of Van Dedem and Nielsen [28]. The principle is as follows: the molecular mass calibrant is a sample of bovine mucosal heparin partially degraded by *endo*-lyse heparinase. Cleavage with this enzyme leaves an unsaturated uronic acid residue at the

non-reducing end of the resulting fragment, which demonstrates UV absorption with a λ_{max} at 235 nm. The action of heparinase is assumed to be random with regard to the substrate size and position of the bonds broken. The UV absorption at 235 nm may, therefore, be assumed to give a relative measure of molar concentration over the whole molecular mass range of the material. It is further assumed that the RI is a relative measure of mass concentration and that, accordingly, the RI/UV ratio is a relative measure of molecular mass. The resolved peaks of the RI and UV outputs on the chromatogram correspond to the low-molecular mass-end and the peak positions (retention times) are assigned to degrees of polymerization. At the top of each peak, the RI/UV ratios correspond to an integral multiple of molecular masses for a disaccharide unit approximated as 600. The resulting data for retention times and molecular masses at the resolved peaks were used to derive a calibration for the chromatographic system by fitting the equation $\log M = at^3 + bt^2 + ct + d$, where t is the retention time, and a, b, c and d are parameters calculated in the fitting process. The values for the parameters were $a = -2.952 \cdot 10^{-4}$, $b = 3.040 \cdot 10^{-2}$, $c = -1.092$ and $d = 17.63$.

Measurements of the molecular mass profiles of heparins. After calibration of the system, RI detection alone was used for LMMHs of unknown molecular mass distributions. One of the molecular mass parameters, the mass-average molecular mass (M_w), was calculated from these data.

Table I gives the evaluated M_w values of various LMMHs together with a variety of fractionated heparins. Wide variations were observed in the M_w values. These findings are compatible with the results of Fareed *et al.* [8].

HPGPC–LALLS measurements

Data handling. The outputs of the LALLS and RI detectors on chromatograms are related to the molecular mass (M_t) of the sample at the retention time t according to the following equa-

TABLE I

MASS-AVERAGE MOLECULAR MASSES (M_w) OF VARIOUS LMMHS AND FRACTIONATED HEPARINS

LMMH	M_w		
	HPGPC	HPGPC–LALLS	
		Wide angle	Narrow angle
Fraxiparine	4519 ± 31[a]	–[b]	–[b]
Enoxaparin	4206 ± 35	4230 ± 57	5035 ± 85
Logiparin	6742 ± 30	6713 ± 45	7301 ± 43
Fragmin A	5946 ± 19	5779 ± 56	6050 ± 54
Fragmin B	6071 ± 22	5910 ± 48	6042 ± 63
Fluxum	5819 ± 29	6077 ± 50	6395 ± 72
Sandoparin	5087 ± 40	5094 ± 42	5652 ± 70
LMMH-JRS	6216 ± 27	5964 ± 51	–[b]
N-6	8291 ± 20	8272 ± 38	7806 ± 55
N-3	3682 ± 10	3637 ± 71	3986 ± 109
K-6	6983 ± 25	–[b]	6246 ± 51
K-4	5067 ± 25	5030 ± 45	–[b]
S-5	6136 ± 28	6023 ± 46	–[b]
S-3	3042 ± 9	2932 ± 85	–[b]

[a] Mean ± S.D. (values for data from three determinations).
[b] Not measured.

tion, which is derived from the classical Rayleigh equation [29]:

$$\frac{(LS)_t}{(RI)_t} = k_1(\mathrm{d}n/\mathrm{d}c)_t M_t \quad (1)$$

where $(LS)_t$ and $(RI)_t$ are the LALLS and RI detector outputs, respectively, k_1 is a constant and $(\mathrm{d}n/\mathrm{d}c)_t$ is the specific refractive index increment at the retention time t. This equation is valid when both the heparin concentration and light-scattering angle (θ_{obs}; see Fig. 1) are small enough to allow the concentration-dependent terms in the Rayleigh light-scattering equation to be ignored [29]. Using the present system, these requirements were satisfied in most instances.

If k_1 and $(\mathrm{d}n/\mathrm{d}c)_t$ are determined using a standard substance, for which the M_w is already known, the molecular mass distribution can be calculated from the LALLS to RI output ratio on the chromatogram. However, even if heparin is adopted as a standard of known molecular mass, the correctness of the following two assumptions should be ascertained: (1) the $(\mathrm{d}n/\mathrm{d}c)_t$ of the samples is equal to that of the standard, and (2) $(\mathrm{d}n/\mathrm{d}c)_t$ is independent of the molecular mass and is constant in the molecular mass range studied.

The specific refractive increment, $(\mathrm{d}n/\mathrm{d}c)$, can be assumed to be proportional to RI_{area}/C, where RI_{area} and C are the area on the RI chromatogram and the molar concentration, respectively. Fig. 2 depicts the dependence of RI_{area}/C values for the various fractionated heparins on the molecular masses. Open circles show the RI_{area}/C values for a variety of fractionated heparins prepared by Kabi-Vitrum, these being almost constant and independent of molecular mass. Such a small molecular mass effect is uncommon for the molecular mass range studied [30]. For small molecules of molecular mass below 20 000, usually the $\mathrm{d}n/\mathrm{d}c$ slightly decreases with increase in molecular mass [30]. On the other hand, it is almost constant and independent of the molecular mass for large molecules with molecular mass above about 20 000 [30]. This behaviour was found with polystyrenes and also with pullulans and has been ascribed to changes in specific volume

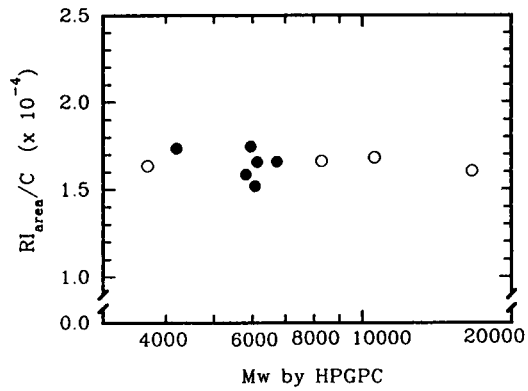

Fig. 2. Dependence of the ratio of area on the RI chromatogram to molar concentration (RI_{area}/C) of various fractionated heparins on the molecular mass. ○ = RI_{area}/C values for a variety of fractionated heparins prepared by Kabi-Vitrum; ● = RI_{area}/C values for various LMMHs. Standard deviations evaluated from at least three determinations are within the size of the circles.

caused by the end-groups of molecules [30]. The fractionated heparins in this study were all prepared by the same depolymerization and enrichment procedures but although they seem to have the same end-groups, the behaviour of $\mathrm{d}n/\mathrm{d}c$ differed. The results indicate that $(\mathrm{d}n/\mathrm{d}c)_t$ is almost independent of the molecular mass of LMMHs and may be assumed to be constant in the molecular mass range studied.

As represented by the filled circles in Fig. 2, the RI_{area}/C values varied from heparin to heparin, being sensitive to the depolymerization process and/or organ of origin. Therefore, differences in $\mathrm{d}n/\mathrm{d}c$ between standards and samples should be take into account even if heparin is used as the standard.

As $\mathrm{d}n/\mathrm{d}c$ is proportional to RI_{area}/C, eqn. 1 can be accordingly modified to give the following equation:

$$\frac{(LS)_t}{(RI)_t} = k_2 \cdot \frac{RI_{areaSTD}/C_{STD}}{RI_{areaSMP}/C_{SMP}} \cdot M_t \quad (2)$$

where $RI_{areaSTD}$ and C_{STD} are the RI_{area} and C of standard heparin and $RI_{areaSMP}$ and C_{SMP} are those of sample heparins, respectively, and k_2 is a constant dependent on the apparatus. In the present study, N-6 ($M_w = 8291$, determined by HPGPC) was used as a standard for the determination of k_2.

Measurements at wide and narrow collection angles. With our instrument, measurements by the LALLS method were usually carried out at the narrow collection angle ($\theta_{col} = 1°$, $\theta_{obs} = 4.5–5.5°$). For large molecules with molecular mass above 10 000, the signal-to-noise ratio is high enough to evaluate the molecular mass distributions at this regular angle because of the strong light scattering by the molecules. In most instances with small molecules, however, the light-scattering intensity is very weak and it is difficult to calculate the molecular masses. In this study, this problem was overcome by making the collection angle wider. Fig. 3 shows the elution profiles with RI and LALLS at both wide ($\theta_{col} = 2°$, $\theta_{obs} = 5.0–7.0°$) and narrow collection angles. The LALLS intensity became about twice as strong when the angle was widened and the signal-to-noise ratio was improved.

The LALLS signal-to-noise ratio is not only a factor of the collection angle for a fixed scatter angle but also, and most importantly, of the concentrations of samples injected. Higher concentrations at a narrow collection angle could have resulted in molecular masses as accurate and precise as those reported for lower concentrations injected with a wider collection angle. In our case, however, saturation of the RI detector occurred using higher concentrations because of the very low molecular masses of LMMHs and fractionated heparins. Therefore, with such small molecules the use of a wide collection angle appears to be the most useful approach to improving the signal-to-noise ratio. This method is also effective in the case of measurements where the amount of sample available is limited.

The lower part of Fig. 4 illustrates the relationships between the k_2 values of various LMMHs and fractionated heparins and their molecular mass averages. The k_2 values are theoretically constant and independent of the molecular mass. The scatter of k_2 in Fig. 4 accordingly corresponds to the error of measurement. In order to clarify this scatter, the ratios of k_2 to average values are depicted in the upper part of Fig. 4. Observation at the wide collection angle was associated with a smaller scatter and an increment in the signal-to-noise ratio. This suggests that observation at the wide angle results in an increase in the accuracy of measurement.

Table I gives the molecular masses of various LMMHs and fractionated heparins measured by HPGPC–LALLS at wide or narrow collection angles. At the wide angle, the molecular mass values obtained by the HPGPC–LALLS method were near to those obtained by the HPGPC

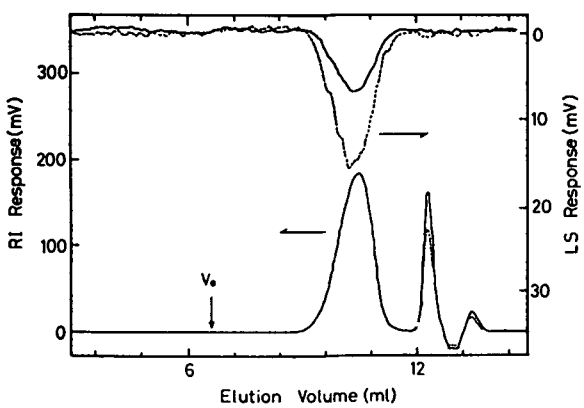

Fig. 3. Elution profiles of Fragmin B observed by RI and LALLS detectors with wide- and narrow-angle measurements. Solid line, with the narrow collection angle ($\theta_{col} = 1°$, $\theta_{obs} = 4.5–5.5°$); dotted line, with the wide collection angle ($\theta_{col} = 2°$, $\theta_{obs} = 5.0–7.0°$). The sample size of Fragmin B was 70 μl of a 8.5 mg/ml solution. V_0 indicates the void volume of the column, detected by the RI detector using pullulan P-400 as a marker.

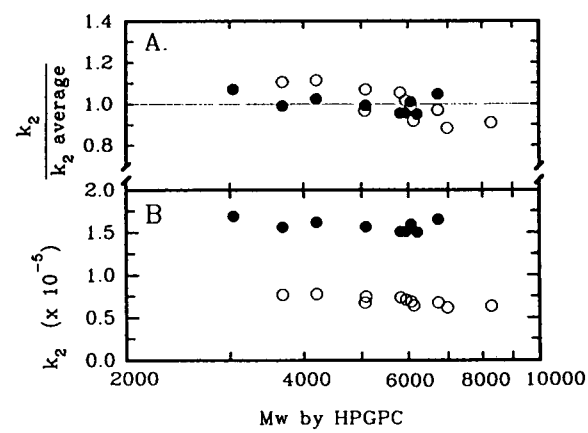

Fig. 4. The k_2 values of various LMMHs and fractionated heparins plotted against their mass-average molecular masses with wide- and narrow-angle measurements. (A) ratios of k_2 to average values; (B) k_2 values. ● = With the wide collection angle ($\theta_{col} = 2°$, $\theta_{obs} = 5.0–7.0°$); ○ = with the narrow collection angle ($\theta_{col} = 1°$, $\theta_{obs} = 4.5–5.5°$).

method, whereas the conformity was not so good with the narrow angle.

Methodological comparison of HPGPC–LALLS with HPGPC. Several methods have commonly been used to assess the molecular masses of heparins [5,8,15–19]. The HPGPC mode in HPLC with RI detection has been developed, and heparins with poorly defined molecular masses and wide molecular mass ranges have been used for calibration. It has already been shown that the application of HPGPC using other polymers such as dextrans [17], polyethylene glycols or pullulans [31] for the calibration of columns leads to wrong results because of the high negative charge of heparins. HPGPC is not the ideal way to determine accurate molecular masses, even though defined standards are available, and usually the HPGPC calibration graph, as shown in this study, is not linear. Therefore, a reliable method for the determination of molecular mass distributions of standard heparins is still required.

It has been demonstrated that HPGPC–LALLS provides molecular mass distributions of standard heparin samples in a rapid and reliable manner [20]. Light-scattering measurement has for some time been an important method for determining the molecular masses, molecular sizes and second virial coefficients of a variety of particles. Nevertheless, it has hitherto not become popular owing to the long time required for measurement in some instances and the poor precision achieved with a low angle. Owing to the development of laser light sources and improvements in LALLS detectors, the measurement can now be carried out easily. The extra cost of the relatively expensive LALLS detector may be warranted by the merits of the HPGPC–LALLS method: (1) a calibration graph is not necessary; and (2) only a standard for the determination of k_2 is needed, and its molecular mass need not necessarily be in the molecular mass range of the samples being studied. Also, it does not always have to be the same kind of compound.

In conclusion, although HPGPC–LALLS has distinct advantages, it has only rarely been utilized for the determination of the molecular masses of small molecules because of their weak light-scattering intensity. However, this study suggests that this difficulty can be overcome by measurement of light scattering at a wider collection angle. This should lead to the increased application of HPGPC–LALLS to very small molecules with M_w values in the range 1000–10 000.

ACKNOWLEDGEMENTS

This work was supported by Grant 2-2-2-A from the Japan Health Sciences Foundation. The authors thank various pharmaceutical companies for providing the low-molecular-mass heparins used in this study. They are grateful to Dr. Toshio Kimura of Sandoz Pharmaceuticals for helpful critical comments during this work, and Mr. Masakazu Tanaka of the Faculty of Pharmaceutical Sciences, Kyushu University, for dedicated technical assistance. They also thank Dr. Malcolm A. Moore for comments on the manuscript.

REFERENCES

1 M. Hook, I. Bjork, J.M. Walenga and U. Lindahl, *FEBS Lett.*, 66 (1976) 90.
2 S. Wessler, *Fed. Proc. Fed. Am. Soc. Exp. Biol.*, 36 (1977) 66.
3 S. Wessler and S.N. Giles, *Blood*, 53 (1979) 525.
4 J.W. Estes, *Clin. Pharmacokinet.*, 5 (1980) 204.
5 A.C. Grant, R.J. Linhardt, G.L. Fitzgerald, J.J. Park and R. Langer, *Anal. Biochem.*, 137 (1984) 25.
6 J. Fareed, J.M. Walenga, D. Hoppensteadt, X. Huan and A. Racanelli, *Haemostasis*, 18 (1988) 3.
7 J. Fareed, J.M. Walenga, D. Hoppensteadt, A. Racanelli and E. Coyne, *Semin. Thromb. Hemost.*, 15 (1989) 440.
8 J. Fareed, J.M. Walenga, D. Hoppensteadt, X. Huan and R. Nonn, *Ann. N.Y. Acad. Sci.*, 556 (1989) 333.
9 N. Volpi, G. Mascellani and P. Bianchini, *Anal. Biochem.*, 200 (1992) 100.
10 E. Holmer, in D.A. Lane and U. Lindahl (Editors), *Heparin. Chemical and Biological Properties. Clinical Applications*, Arnold, London, 1989, p. 575.
11 C.P. Dietrich, Y.M. Michelacci and H.B. Nader, *Mechanism of Saccharide Polymerization/Depolymerization*, Academic Press, New York, 1980, p. 317.
12 B. Casu, *Adv. Carbohydr. Chem. Biochem.*, 43 (1985) 51.
13 H.B. Nader, H.M. McDuffie and C.P. Dietrich, *Biochem. Biophys. Res. Commun.*, 57 (1974) 488.

14 J. Hirsh, F.A. Ofuso and M. Vevine, in M. Verstraete, J. Vermylen, R. Lijnen and J. Arnout (Editors), *Thrombosis and Haemostasis*, Leuven University Press, Leuven, 1987, p. 348.
15 G.H. Barlow, N.D. Sanderson and P.D. McNeill, *Arch. Biochem. Biophys.*, 84 (1961) 518.
16 G.B. Sumyl and C.F. Yocum, *J. Chromatogr.*, 35 (1968) 101.
17 N. Sugisaka and F.J. Peteracek, *Fed. Proc. Fed. Am. Soc. Exp. Biol.*, 36 (1977) 89.
18 H.J. Rodriguez and A.J. Vanderwielen, *J. Pharm. Sci.*, 68 (1979) 588.
19 J. Harenberg and J.X. De Vries, *J. Chromatogr.*, 261 (1983) 287.
20 W.E. Hennink, J.W.A. van den Berg and J. Feijen, *Thromb. Res.*, 45 (1987) 463.
21 Y. Hayashi, K. Mimura, H. Matsui and T. Takagi, *Biochim. Biophys. Acta*, 983 (1989) 217.
22 Y. Sato, N. Ishikawa and T. Takagi, *J. Chromatogr.*, 507 (1990) 25.
23 T. Takagi, in H. Parvez, Y. Kato and S. Parvez (Editors), *Progress in HPLC: Gel Permeation and Ion-Exchange Chromatography of Proteins and Peptides*, Vol. 1, VNU Sciences, Amsterdam, 1985, Ch. 3, p. 27.
24 T. Tagaki, *J. Chromatogr.*, 506 (1990) 409.
25 R. Mhatre, I.S. Krull and H.H. Stuting, *J. Chromatogr.*, 502 (1990) 21.
26 I.S. Krull, H.H. Stuting and S.C. Krzysko, *J. Chromatogr.*, 442 (1988) 29.
27 G. Dollinger, B. Cunico, M. Kunitani, D. Johnson and R. Jones, *J. Chromatogr.*, 592 (1992) 215.
28 G. van Dedem and J.I. Nielsen, *Pharmeuropa*, 3 (1991) 202.
29 C. Tanford, *Physical Chemistry of Macromolecules*, Wiley, New York, 1961, p. 275.
30 F. Candau, J. Francois and H. Benoit, *Polymer*, 15 (1974) 626.
31 H. Komatsu, S. Ishimitsu and S. Okada, unpublished results.

Journal of Chromatography, 644 (1993) 25–33
Elsevier Science Publishers B.V., Amsterdam

CHROM. 25 095

Recognition and separation of isoenzymes by metal chelates

Immobilized metal ion affinity partitioning of lactate dehydrogenase isoenzymes

Andreas Otto and Gerd Birkenmeier*

Institute of Biochemistry, University of Leipzig, Liebigstrasse 16, O-7010 Leipzig (Germany)

(First received October 1st, 1992; revised manuscript received March 8th, 1993)

ABSTRACT

Poly(ethylene glycol) (PEG)-bound chelated metal ions partition preferentially into the top, PEG-rich, phase of a PEG–salt or PEG–dextran aqueous two-phase system. Extraction by this soluble affinity ligand of proteins is due to a selective interaction of the chelated metal ion with accessible histidine residues on the protein surface. Using Cu–iminodiacetate–PEG (Cu–IDA–PEG) the surface of lactate dehydrogenase (LDH) isoenzymes from different species was probed for the presence of metal chelate binding sites. It was demonstrated that the homotetramers (LDH-1)(H_4) from rabbit, bovine and pig displayed weak binding to chelated copper whereas the M_4-type isoenzymes (LDH-5) bound strongly to this ligand. The binding of the different heterotetramers increases as the number of M-type subunits increases. In contrast, the human isoenzymes are bound to chelated copper in a reversed sequence. The comparison of the affinity partitioning effect of Cu–IDA–PEG in PEG–salt and PEG–dextran systems revealed that the discriminatory effect of copper is promoted by high salt concentrations. Resolution of isoenzymes by multiple extraction using counter-current distribution provides valuable data on the partitioning of enzymes relative to that of the bulk proteins. The efficacy of metal chelate affinity partitioning for the purification of LDH from tissue samples by batchwise extraction was also demonstrated.

INTRODUCTION

Partitioning in aqueous two-phase systems is a well established method for the separation and fractionation of proteins, cells and cell particles [1,2]. The range of applicability of this method has been extended by utilizing the interaction of proteins with affinity ligands which were covalently attached to one of the phase-forming polymer, *e.g.*, poly(ethylene glycol) (PEG) [3–5].

Recently, chelated transition metal ions covalently linked to soluble or insoluble polymers have been used to increase the selectivity of separation in chromatography and phase partitioning [6–10]. This interaction is due to the coordination of immobilized metal ions with electron-rich ligands on the protein surface. It is now well established that accessible histidine residues localized in a favourable orientation on the protein surface serve as predominant metal binding sites [7,11,12]. Experiments with metal chelate-derivatized PEG in PEG–dextran and PEG–salt two-phase systems indicate that extraction of proteins by these ligands is histidine-mediated [8].

In this work, we used metal–IDA–PEG as

* Corresponding author.

0021-9673/93/$06.00

probes for the recognition of surface differences in LDH isoenzymes from different sources and species. Substantial differences in the binding of isoenzymes to the chelated metal were found and can be exploited for isoenzyme separation by immobilized metal ion affinity partitioning. The difference in binding of isoenzymes to the affinity ligand is discussed on the basis of their primary structure with respect to the content and distribution of histidine residues.

EXPERIMENTAL

Materials

PEG 6000 and 1550 were obtained from Serva (Heidelberg, Germany), monomethoxy-PEG 5000 from Sigma (St. Louis, MO, USA) and Dextran T 70 from Pharmacia (Uppsala, Sweden). Lactate dehydrogenase (EC 1.1.1.27) isoenzymes from rabbit heart (LDH-1) and the human isoenzymes LDH-1, LDH-2, LDH-3 and LDH-5 were purchased from Sigma, LDH-3 from rabbit from Arzneittelwerk Dresden (Dresden, Germany) and LDH from pig muscle (LDH-5), pig heart (LDH-1), bovine heart (LDH-1) and rabbit muscle (LDH-5) from Boehringer (Mannheim, Germany).

Preparation of metal chelate–PEG

Iminodiacetate–PEG (IDA–PEG) was synthesized by the reaction of bromoacetic acid with aminomonomethoxy–PEG as described previously [10]. Charging of IDA–PEG with metal ions [*e.g.*, Cu(II), Zn(II) and Ni(II)] was performed in 50 m*M* sodium acetate buffer (pH 4.0). The product was extracted repeatedly with chloroform. The contents of Cu(II), Zn(II), and Ni(II) per mole of IDA–PEG were 0.83, 0.8 and 0.3 mol, respectively.

Partition experiments

Aqueous two-phase systems of PEG–dextran were prepared from stock solutions of dextran T 70 (20%, w/w), PEG 6000 (40%, w/w) and 0.1 *M* sodium-phosphate–1.5 *M* Na_2SO_4 (pH 7.0). Stock solutions used for PEG–salt systems were PEG 1550 (40%, w/w), PEG 6000 (40%, w/w), 20% (w/w) Na_2SO_4 and 0.1 *M* sodium phosphate buffer (pH 7.0). The solutions were weighed out in appropriate amounts to yield the required mass of the desired phase systems. PEG–dextran systems (total mass 2 g) used for partitioning had the following composition: 5% PEG 6000 (including metal–IDA–PEG), 7.5% dextran T 70, 0.15 *M* Na_2SO_4, 0.01 *M* sodium phosphate buffer (pH 7.0). PEG–salt systems of 2 g were composed of 10% PEG 1550, 2% PEG 6000 (including metal–IDA–PEG), 10% Na_2SO_4 and 0.01 *M* sodium phosphate buffer (pH 7.0). The phase systems were equilibrated at 22°C before adding the desired amounts of the enzymes. The systems were mixed by 20 inversions and phase separation was achieved by brief centrifugation (2 min at 2000 *g*). Aliquots were immediately withdrawn from the top and bottom phase and analysed for enzyme activity. The partitioning of the enzyme between the two phases is defined as K, expressing the ratio of the concentrations (activities) of the enzyme in the top and bottom phases. The change in the partition coefficient of the enzyme which is due to binding to metal chelate–PEG is expressed as $\Delta \log K$, given as $\Delta \log K = \log K_{aff} - \log K_0$, where K_{aff} and K_0 are the partition coefficients of the protein in the presence and the absence of the affinity ligand in the phase system, respectively, other conditions being identical.

Preparative extraction of LDH

Heart and skeletal muscle extracts from rabbit were prepared by homogenizing minced muscle in 50 m*M* sodium phosphate buffer (pH 7.0) using a Potter homogenizer. After centrifugation (30 min at 5000 *g*), the supernatant was used for partitioning experiments. The specific activity of LDH in heart and skeletal muscle extract was 1.9 and 16.3 U/mg protein, respectively.

The preparative two-step extraction was performed as follows. An 8-g phase system was prepared containing 10% PEG 1550, 2% Cu–IDA–PEG, 10% Na_2SO_4 and 2 ml of rabbit heart extract (27 U) or rabbit muscle extract (312 U). The phases having a volume ratio of 0.58 (top/bottom phase) were mixed at 22°C and separated by centrifugation (10 min at 4000 *g*). The enzymatic activity and the protein content were determined in the top phase (T1) and in the bottom phase (B1). For extraction of heart

LDH, the bottom phase (B1) was then mixed again with fresh top phase of a pre-equilibrated two-phase system of the same composition but without protein. The phases T2 and B2 thus obtained after centrifugation were subjected to analysis. With rabbit skeletal muscle LDH, T1 was re-extracted with fresh bottom phase to remove material with low partition coefficients. Sodium dodecyl sulphate polyacrylamide gel electrophoresis (SDS-PAGE) was performed according to Laemmli [13]. The type of isoenzymes was determined by the ability of the enzyme to reduce 2-oxobutyrate [14].

Counter-current distribution

Repeated extraction of LDH was performed by counter-current distribution (CCD) using a standard apparatus with 60 cavities as described by Albertsson [1]. The chambers were loaded with 0.78 ml of the lower phase and 0.78 ml of the upper phase of a pre-equilibrated two-phase system composed of 10% PEG 1550, 10% Na_2SO_4, 2% PEG 6000 (or 2% Cu–IDA–PEG) and 0.01 *M* sodium phosphate buffer (pH 7.0). Sample systems (1.56 g) were prepared by including 200 μl of rabbit heart or muscle extract into the phase systems which were loaded into the chamber 0. Twenty-seven transfers were carried out at 22°C. The shaking time was 60 s and the settling time 6 min per transfer cycle. After the run 300 μl of water were added to each chamber, yielding a homogeneous phase. The fractions were analysed for enzyme activity and for protein using the method of Bradford [15].

Enzyme assay

The activity of the LDH isoenzymes was assayed at 25°C as described by Bergmeyer [16] using 0.6 m*M* pyruvate and 0.18 m*M* NADH as substrates in 50 m*M* sodium phosphate buffer (pH 7.5). One unit of the activity is defined as the amount of the enzyme catalysing the conversion of 1 μmol of substrate per minute at 25°C.

RESULTS

Fig. 1 illustrates the effect of immobilized copper (Cu–IDA–PEG) on the partitioning of LDH isoenzymes from rabbit in PEG–salt

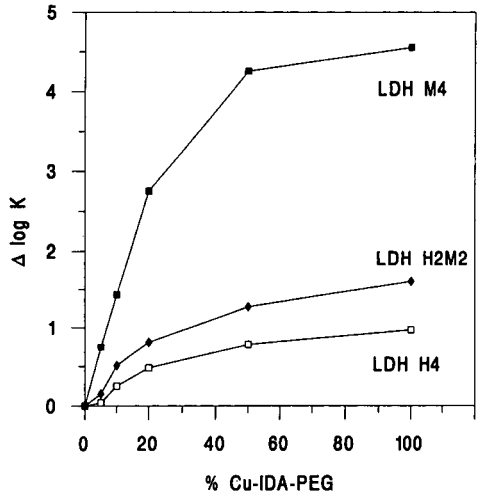

Fig. 1. Metal chelate affinity partitioning of LDH isoenzymes from rabbit. 5–10 units of each purified isoenzyme were partitioned in two-phase systems (2 g) composed of 10% PEG 1550, 10% Na_2SO_4, 2% PEG 6000 (or increasing substituting concentrations of Cu–IDA–PEG) and 0.01 *M* sodium phosphate buffer (pH 7.0). The concentration of Cu–IDA–PEG is expressed as a percentage of the total PEG 6000 that is replaced by Cu–IDA–PEG. □ = LDH-1 (H_4-type); ◆ = LDH-3 (H_2M_2-type); ■ = LDH-5 (M_4-type). Partitioning was performed at 22°C.

systems. In the absence of the metal ion the partition coefficient, *K*, does not vary greatly among the isoenzymes and was measured to be between 0.010 and 0.013. This was to be expected because in the presence of high salt concentrations the influence of charges on the partitioning of proteins is suppressed. Addition of Cu–IDA–PEG increases the partitioning of the isoenzymes into the top, PEG-rich, phase and dramatically changes the partitioning of LDH-5 (M_4-type). Owing to the binding to the affinity ligand, the *K* value of LDH-5 is changed 50 000-fold, from 0.01 to about 500, yielding $\Delta \log K = 4.6$ at the maximum ligand concentration. The isoenzyme LDH-3 (H_2M_2-type) displayed much weaker binding to the polymer-bound metal than the M_4-isoenzyme. The lowest binding was found for the homotetramer H_4. Despite the lack of LDH-4 and LDH-2 in our study, it could be observed that the binding of LDH isoenzymes to chelated copper increases with increasing number of the M-type subunit in the oligomer.

The partitioning of human LDH isoenzymes in

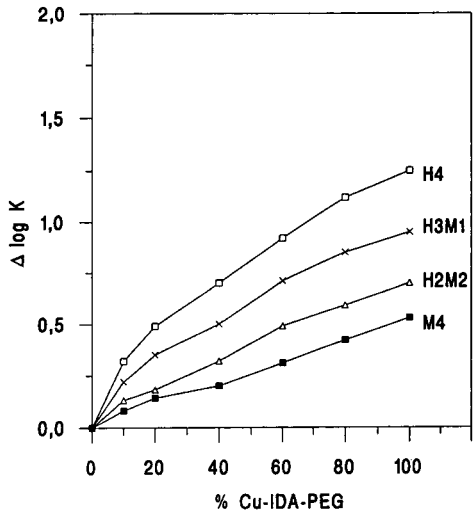

Fig. 2. Metal chelate affinity partitioning of human LDH isoenzymes. 2–6 units of each purified isoenzyme were partitioned in two-phase systems (2 g) composed of 10% PEG 1550, 10% Na_2SO_4, 2% PEG 6000 (or increasing substituting concentrations of Cu–IDA–PEG) and 0.01 *M* sodium phosphate buffer (pH 7.0). The concentration of Cu–IDA–PEG is expressed as a percentage of the total PEG 6000 that is replaced by Cu–IDA–PEG. □ = LDH-1 (H_4-type); × = LDH-2 (H_3M_1-type); △ = LDH-3 (H_2M_2-type); ■ = LDH-5 (M_4-type). Partitioning was performed at 22°C.

PEG–salt systems and the effect of Cu–IDA–PEG are demonstrated in Fig. 2. In the absence of the affinity ligand all isoenzymes partition preferentially into the bottom, salt-rich, phase with *K* values near 0.01. As can be seen, on average, the interaction of the human isoenzymes to immobilized copper is significantly lower compared with the rabbit species. Further, the sequence of extraction of the different isoenzymes is reversed, meaning that the homotetramer H_4 displayed stronger binding to copper than the homotetramer M_4. The heterotetrameric forms of LDH are extracted in the sequence of their increased number of H-type subunits in the molecule.

The species-dependent affinity partitioning of LDH isoenzymes is summarized in Table I. In addition to the effect of copper, the influence of zinc and nickel on isoenzyme partitioning has also been included. Typically, all isoenzymes bound most strongly to chelated copper. Note again the low affinity of bovine LDH-1 and pig LDH-1 and the high affinity of pig LDH-5 to this metal. In contrast, zinc had only marginal effects on the enzyme partitioning and could not dis-

TABLE I

EFFECT OF CHELATED METAL IONS ON PARTITIONING OF ISOENZYMES FROM DIFFERENT SPECIES

Between 2 and 10 units of LDH isoenzymes were partitioned in PEG–salt systems (2 g) composed of 10% PEG 1550, 2% PEG 6000 (or 2% metal–IDA–PEG), 10% Na_2SO_4 and 0.01 *M* sodium phosphate buffer (pH 7.0). Temperature, 22°C.

Species	Isoenzyme	Δ log *K*		
		Cu–IDA–PEG	Zn–IDA–PEG	Ni–IDA–PEG
Rabbit	H_4	0.9	0.2	0.5
	H_2M_2	1.6	0.2	0.8
	M_4	4.5	0.2	1.2
Bovine	H_4	0.5	0.3	0.3
Pig	H_4	0.4	0	0.2
	M_4	3.8	0.2	0.8
Human	H_4	1.3	0.3	0.6
	H_3M_1	1.1	0.4	0.6
	H_2M_2	0.9	0.2	0.8
	M_4	0.5	0.2	0.6

criminate between different isoenzymes. Interestingly, binding to Ni–IDA–PEG is less compared with the effect of copper, but some similarities in the sequence of extraction could be observed.

A comparison of affinity partitioning of isoenzymes in PEG–salt and PEG–dextran systems is shown in Fig. 3. As can be seen, the inverse sequence of extraction of rabbit and human isoenzymes in PEG–salt systems is apparent again. The very similar Δ log K values found for LDH-1 (rabbit) and LDH-1 (human) may argue for a similar number of metal chelate binding sites on the surface of these proteins. Partitioning in PEG–dextran systems at lower salt concentrations revealed that the affinity of the rabbit isoenzymes to copper is considerably reduced. Further, the discriminatory effect of copper for isoenzyme recognition is also decreased. For example, the differences in the Δ log K values of rabbit LDH-1 and LDH-5 amount to 1.85 in the PEG–dextran system, which is much less than the value of 3.6 obtained in the PEG–salt system. Cu–IDA–PEG was not capable of recognizing obvious differences in the protein surface of human isoenzymes in PEG–dextran systems. This means that high concentrations of sulphate promote the protein–metal chelate interaction and increase the discriminatory ability of copper in isoenzyme recognition.

Counter-current distribution of LDH isoenzymes

To increase the separatory effect of two-phase systems, multiple-step extractions were performed by CCD. The resolution of LDH from rabbit muscle and heart in the presence and absence of Cu–IDA–PEG is shown in Fig. 4. In the absence of the metal chelate the LDH activity was found at the far left site of the train with peak position in fractions 1 and 2. The bulk proteins partitioned also in favour of the salt-rich phase (Fig. 4A).

Addition of Cu–IDA–PEG causes extraction of muscle LDH into the top phase occupying the far right site of the train (Fig. 4B). The peak of activity preferentially contained LDH-5 and LDH-4, which is due to their high affinity to the ligand. Even the bulk proteins displayed binding to the ligand and were co-extracted with the enzyme. CCD of the heart extract revealed that Cu–IDA–PEG pulls out the bulk proteins into the top phase whilst having little effect on partitioning of the enzyme (Fig. 4C and D). The splitting of the activity peak is attributed to the partial separation of LDH-1 and LDH-2. The results demonstrate that separation of isoenzymes by CCD is possible.

Extractive purification of LDH

The results of the CCD experiments gave valuable information for carrying out batchwise

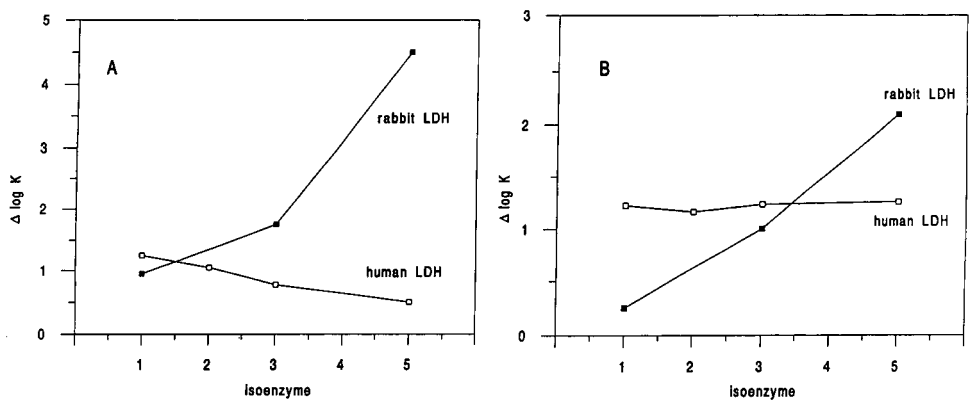

Fig. 3. Effect of Cu–IDA–PEG on partitioning of LDH isoenzymes in PEG–salt and PEG–dextran systems. Between 2 and 10 units of each isoenzyme were partitioned in two-phase systems (2 g) composed of (A) 10% PEG 1550, 10% Na_2SO_4, 2% PEG 6000 (or 2% Cu–IDA–PEG) and 0.01 M sodium phosphate buffer (pH 7.0) and (B) 5% PEG 6000 (or substituted totally by Cu–IDA–PEG for human LDH, or substituted by 10% Cu–IDA–PEG for rabbit LDH), 7.5% dextran T 70, 0.15 M Na_2SO_4 and 0.01 M sodium phosphate buffer (pH 7.0).

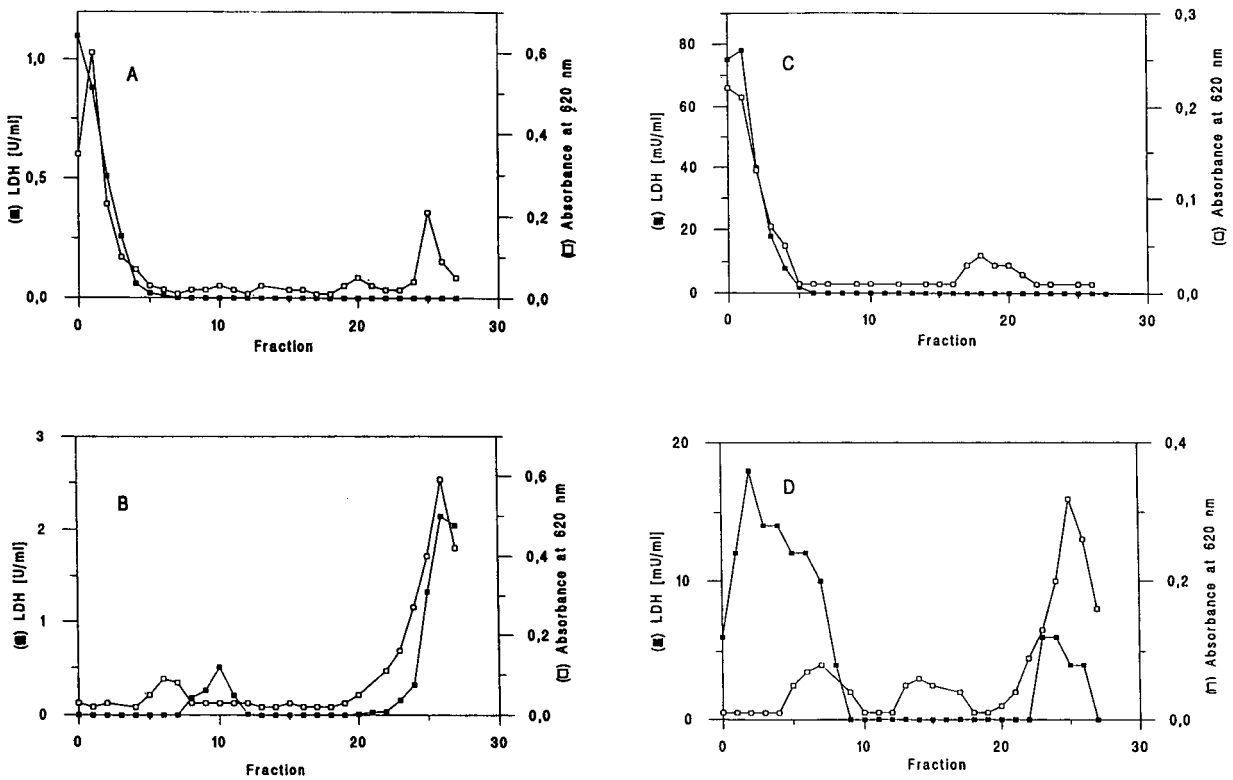

Fig. 4. Counter-current distribution of rabbit LDH from heart and skeletal muscle extract. Distribution pattern of (A and B) muscle and (C and D) heart extract, (A and C) in the absence and (B and D) in the presence of Cu–IDA–PEG. The phase systems were composed of 10% PEG 1550, 10% Na_2SO_4, 2% PEG 6000 (or 2% Cu–IDA–PEG) and 0.01 *M* sodium phosphate buffer (pH 7.0). After 27 transfers at 22°C the fractions were analysed for (■) enzyme activity and (□) protein content.

extraction by showing how bulk proteins partition relative to the target enzyme.

Table II illustrates the efficacy of purification of LDH from heart extract by batchwise two-step affinity extraction in PEG–salt systems. As can be seen, Cu–IDA–PEG, in the first extrac-

TABLE II

EXTRACTIVE PURIFICATION OF RABBIT LDH BY TWO-STEP AFFINITY PARTITIONING

Heart extract was partitioned at 22°C in a PEG–salt system composed of 10% PEG 1550, 2% Cu–IDA–PEG, 10% Na_2SO_4 and 0.01 *M* sodium phosphate buffer (pH 7.0). The bottom phase obtained after the first partitioning step was re-extracted with fresh ligand-containing top phase in the second partitioning step as described under Experimental. The specific activity of LDH in the starting sample was 1.9 U/mg.

Extraction step	Phase volume (ml)	Activity (U/ml)	Total activity (U)	Protein (mg/ml)	Specific activity (U/mg)
T1	2.8	0.8	2.2	3.6	0.2
B1	4.8	3.8	18.3	0.4	9.5
T2	2.8	0.88	2.4	0.1	8.8
B2	4.8	3.0	14.4	0.12	25.0

tion step, pulls out the bulk proteins into the top phase. This results in a fivefold increase in the specific activity of LDH in the bottom phase. Re-extraction of material from the bottom phase by mixing with fresh ligand-containing top phase increases the purity of LDH further to about thirteenfold. The recovery of enzyme activity after the second extraction step was about 62%. The major loss of activity was found in the first extraction due to partial coprecipitation of LDH with bulk proteins at the interphase.

The performance of extraction is shown by SDS-PAGE (Fig. 5). Most of the bulk proteins of the crude material (lane 2) were extracted into the Cu–IDA–PEG phase in the first extraction step, while the enzyme activity remained substantially enriched in the salt-rich bottom phase (lane 4). Isoenzyme determination in the bottom phase was performed by measuring the ability to reduce 2-oxobutyrate. The rate of conversion of 2-oxobutyrate was 92% compared with pyruvate. This indicates the predominance of LDH-1 in the salt-rich bottom phase.

On the other hand, attempts to purify LDH from muscle by two-phase partitioning failed because of the similar binding properties of this enzyme and the bulk proteins to chelated copper, as already demonstrated by CCD.

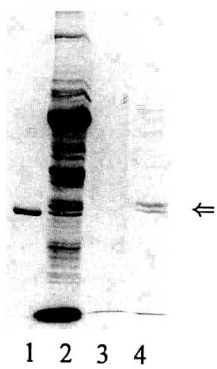

Fig. 5. SDS-PAGE of extracted LDH. LDH from heart extract was purified by two-step partitioning. SDS-PAGE was carried out in 8% polyacrylamide gels at 40 mA and 220 V for 2.5 h at room temperature. Lanes: 1 = 10 μg of commercial LDH-1; 2 = 300 μg of protein of heart extract; 3 = 28 μg of protein of the top phase (T2); 4 = 25 μg of protein of the bottom phase (B2). The arrow indicates the position of LDH.

DISCUSSION

Affinity partitioning in aqueous two-phase systems has been widely used for the study and separation of proteins [2,4,5] and cells [2,17]. Different polymer-bound ligands, *e.g.*, dyes [4,5], palmitate [3] and others [2], were applied to recognize binding sites on the protein surface. Recently, immobilized metal ions have been introduced as affinity ligands in the two-phase separation technique for the extraction of proteins [8–10] and cells [18,19]. As corroborated by a number of experimental data, the binding of chelated metal ions to proteins occurs via electron-donating side-chains of amino acids. Accessible histidine residues on the protein surface have been reported to serve as predominant metal-binding sites.

As shown in this study, PEG-bound metal ions were capable of recognizing and differentiating isoenzymes of LDH. The different partitioning behaviour of the isoenzymes studied can be explained by assuming that the binding ($\Delta \log K$) is proportionally related to the number of histidine residues. At present, owing to the lack of a crystal structure analysis of the isoenzymes used, we are unable to define the histidine residues that are exposed to the solvent and thereby accessible for metal–IDA–PEG interaction. Nevertheless, a correlation between the $\Delta \log K$ of various proteins and their total number of histidines has been demonstrated [20]. This assumption can be approximated because histidines have been shown to be distributed more or less evenly between the interior and the exterior of proteins [21].

The H-type subunit of rabbit LDH contains six and the M-type subunit contains eleven histidines [22]. The latter apparently binds much more strongly to chelated copper than the H-type subunit. Although demonstrated for only three isoenzymes, it can be deduced that the increase in the partitioning ($\Delta \log K$) is proportional to the number of M-type subunits in the different isoenzymes (Fig. 3). A similar tendency became apparent for LDH from pig.

In contrast, for human LDH a reversed binding of the H- and M-types to immobilized copper was found. The increments in affinity of these

isoenzymes to copper were found to be proportional to the number of H-subunits in the tetrameric molecule. This indicates that the relative contribution of each H-subunit for the binding is equal. The overall lower binding of human LDH to copper compared with the rabbit enzymes implies a reduced number of metal chelate binding sites. The human H- and M-types possess only seven histidines [23,24]. Hence a Δ log K that is near to the value for rabbit LDH-1 was to be expected. However, despite having a similar histidine content, fine differences in the metal chelate binding properties of the human isoenzymes were confirmed. The amino acid sequences of the H- and M-types show 74.3% identities. Out of seven histidines, six His residues (His_{67}, His_{181}, His_{186}, His_{193}, His_{231} and His_{271}) are in identical positions. The position of one histidine is different: the H-type contains His_{156} and the M-type His_{215}. One is tempted to assume that the different affinity of the human isoenzymes could arise from the different availabilities of these His residues for Cu–IDA–PEG. Nevertheless, these results show that Cu–IDA–PEG is a very sensitive probe to detect fine differences in surface properties as shown in the case of closely related isoenzymes.

Suh *et al.* [9] have recently demonstrated that high stability constants for Cu–IDA–PEG–protein complexes are found when specific His–X_3–His configurations are available in α-helical regions of the proteins. There are no indications of such specific sites in the LDH isoenzymes studied. Thus, the strong binding of, *e.g.*, rabbit LDH-5 to Cu–IDA–PEG may be the result of metal binding to obviously a number of but single histidine side-chain residues. Special attention was paid to the difference in the partitioning behaviour of LDH isoenzymes in PEG–salt and PEG–dextran systems. The experiments clearly indicate that the partitioning in PEG–salt increases the discriminatory capability of chelated copper for isoenzyme recognition. Thus, sulphate ions seem to promote complex stability. Interestingly, phosphate ions when used to prepare PEG–salt systems were found to lack this property (unpublished results). Generally, water-stabilizing ions seem to increase the interaction of proteins and Cu–IDA–PEG [25]. Owing to its antichaotropic and water-stabilizing character, sulphate ions reduce the ability of water to coordinate to the metal and to compete with the histidines for binding to the metal ion. Therefore, sulphate ions may increase the complex stability by changing the structure of the solvent and by reducing its ability to coordinate itself. Similar effects to those found for sulphate have been reported for NaCl when used in high concentrations in metal chelate affinity chromatography [25].

The fact that high salt concentrations confer high stability of coordination to metals offers an excellent possibility to carry out preparative affinity extraction in inexpensive PEG–salt systems. We have tested the ability to separate isoenzymes that differ in their binding to copper by multi-stage and two-stage extraction. Counter-current distribution was demonstrated to be a very efficient method for the affinity extraction of isoenzymes. Valuable data on the partition coefficients of the target enzyme relative to the bulk proteins can be obtained. Hence it could be demonstrated that extractive purification of LDH-5 failed despite its strong binding to Cu–IDA–PEG because of the co-extraction of most of the bulk proteins. On the other hand, the thirteenfold enrichment of LDH-1 by two-stage affinity extraction provides an example of the efficacy of this step.

Purification by negative affinity extraction may be useful if bulk proteins have to be separated from proteins with low affinity and which remain in the salt-rich bottom phase. However, this is limited by the capacity of the Cu–IDA–PEG-containing top phase. It is therefore advisable to use such a fast and efficient extraction step for refined purification or separation of these enzymes. Nevertheless, partitioning studies with other proteins revealed that the protein load of the top phase containing the chelated metal ion is high, ranging between 10 and 20 mg/ml [20]. Increasing the top phase volume and/or increasing the Cu–IDA–PEG content would lead to a further increase in the extraction capacity.

For the separation of isoenzymes of LDH, electrophoretic methods, ion-exchange chromatography and affinity chromatography have been used, expoiting differences in charges or affinity

to certain immobilized ligands [26,27]. Recently, Kirchberger *et al.* [28] were able to separate LDH-1 and LDH-5 from rabbit by partitioning owing to their different affinities to PEG-bound dyes. Disadvantageously, this method cannot be performed in PEG–salt systems because of the breakdown of dye–protein complexes at high salt concentrations. Further, Cu–IDA–PEG was found to possess a much higher discriminating ability among the isoenzymes than the dyes.

CONCLUSIONS

Metal chelate affinity partitioning in aqueous two-phase systems was found to be a very attractive method for the separation of isoenzymes of LDH. Cu–IDA–PEG has been demonstrated to be a sensitive probe for the recognition of distinct surface differences of closely related proteins. From analytical studies suitably done by CCD, data can be obtained to create affinity phase systems designed for the preparative extraction of proteins on the basis of their different contents and distributions of histidine residues. It can be expected that Cu–IDA–PEG may also serve as an affinity ligand for the recognition of multiple forms of other enzymes and proteins.

ACKNOWLEDGEMENT

This work was supported by the German Ministry of Science and Technology (0319792A).

REFERENCES

1 P.-A. Albertsson, *Partition of Cell Particles and Macromolecules*, Wiley, New York, 3rd ed., 1986.
2 H. Walter, D.E. Brooks and D. Fisher, *Partitioning in Aqueous Two-phase Systems. Theory, Methods, Uses and Applications to Biotechnology*, Academic Press, Orlando, FL, 1985.
3 V.P. Shanbhag and G. Johansson, *Biochem. Biophys. Res. Commun.*, 61 (1974) 1141.
4 G. Johansson, G. Kopperschläger and P.-A. Albertsson, *Eur. J. Biochem.*, 131 (1983) 589.
5 G. Birkenmeier, G. Kopperschläger and G. Johansson, *Biomed. Chromatogr.*, 1 (1986) 64.
6 J. Porath, J. Carlsson, I. Olsson and G. Belfrage, *Nature*, 258 (1975) 598.
7 E.S. Hemdan, Y.-J. Zhao, E. Sulkowski and J. Porath, *Proc. Natl. Acad. Sci. U.S.A.*, 86 (1989) 1811.
8 S.-S. Suh and F.H. Arnold, *Biotechnol. Bioeng.*, 35 (1990) 682.
9 S.-S. Suh, B.L. Haymore and F.H. Arnold, *Protein Eng.*, 4 (1991) 301.
10 G. Birkenmeier, M.A. Vijayalakshmi, T. Stigbrand and G. Kopperschläger, *J. Chromatogr.*, 539 (1991) 267.
11 R.J. Sundberg and R.B. Martin, *Chem. Rev.*, 74 (1974) 471.
12 R.J. Todd, M.E. Van Dam, D. Casimiro, B.L. Haymore and F.H. Arnold, *Proteins Struct. Funct. Genet.*, 10 (1991) 156.
13 U.K. Laemmli, *Nature*, 227 (1970) 248.
14 H.U. Bergmeyer, *Methods of Enzymatic Analysis*, Vol. 3, Verlag Chemie, Weinheim, 1983, p. 150.
15 M.M. Bradford, *Anal. Biochem.*, 72 (1976) 248.
16 H.U. Bergmeyer, *Methods of Enzymatic Analysis*, Vol. 2, Academic Press, New York, 1974, p. 574.
17 H. Walter and G. Johansson, *Anal. Biochem.*, 155 (1986) 215.
18 H. Goubran-Botros, G. Birkenmeier, A. Otto, G. Kopperschläger and M.A. Vijayalakshmi, *Biochim. Biophys. Acta*, 1074 (1991) 69.
19 H. Walter, K.E. Widen and G. Birkenmeier, *J. Chromatogr.*, submitted for publication.
20 G. Birkenmeier, in preparation.
21 H. Meirovitch and H.A. Scheraga, *Macromolecules*, 13 (1989) 1406.
22 C. Sass, M. Briand, S. Benslimane, M. Renaud and Y. Briand, *J. Biol. Chem.*, 264 (1989) 4076.
23 T. Takeno and S.S.-L. Li, *Biochem. J.*, 257 (1989) 921.
24 H. Tsujibo, H.F. Tiano and S.S.-L. Li, *Eur. J. Biochem.*, 147 (1985) 9.
25 J. Porath, *J. Chromatogr.*, 376 (1986) 331.
26 E.D. Wachsmuth and G. Pfleiderer, *Biochem. Z.*, 336 (1963) 556.
27 G. Kopperschläger, H.-J. Böhme and E. Hofmann, in T.K. Ghose, A. Fiechter and N. Blakebrough (Editors), *Advances in Biochemical Engineering*, Springer, Heidelberg, 1982, p. 101.
28 J. Kirchberger, G. Kopperschläger and M.A. Vijayalakshmi, *J. Chromatogr.*, 557 (1991) 325.

Journal of Chromatography, 644 (1993) 35–41
Elsevier Science Publishers B.V., Amsterdam

CHROM. 25 147

Isolation of chitin deacetylase from *Mucor rouxii* by immunoaffinity chromatography

A. Martinou, D. Kafetzopoulos and V. Bouriotis*

Institute of Molecular Biology and Biotechnology, Enzyme Technology Division, P.O. Box 1515, Heraklion 711 10, Crete (Greece) and Department of Biology, Division of Applied Biology and Biotechnology, University of Crete, P.O. Box 1470, Heraklion 711 10, Crete (Greece)

(First received November 30th, 1992; revised manuscript received March 29th, 1993)

ABSTRACT

The purification of chitin deacetylase from *Mucor rouxii* to homogeneity employing conventional methods has already been described. However, a lengthy protocol is required resulting in a low yield and specific activity for the enzyme. A 169-fold one-step purification of chitin deacetylase by immunoaffinity chromatography is reported, resulting in a homogeneous enzyme preparation. The enzyme purified using this procedure was judged to be electrophoretically homogeneous as tested by both native polyacrylamide gel electrophoresis (PAGE) and sodium dodecyl sulphate PAGE. Using antibodies of lower affinity, less severe chemical conditions were required for the desorption of immunoadsorbents. Chitin deacetylase purified by immunoaffinity chromatography exhibited a specific activity of 13 U mg^{-1} while a 30% yield was obtained, both much higher than the respective values obtained using conventional methodology.

INTRODUCTION

Chitin, a polymer of N-acetyglucosamine and the second most abundant polymer in nature after cellulose, occurs widely in the exoskeletons of many invertebrates and in the cell walls of most fungi and some algae [1,2]. Chitin is an insoluble material and has limited industrial use, whereas chitosan, a partially deacetylated form of chitin, occurring in several Zygomycetes species [3,4], is water soluble and has a large number and a wide variety of important applications [5–7]. Chitosan is produced by the thermochemical deacetylation of chitin, which leads to a highly heterogeneous end-product owing to the severity of the treatment [8]. An alternative or complementary procedure exploiting the enzymatic deacetylation of chitin could potentially be employed, especially when a controlled, non-degradative and well defined process is required.

Chitin deacetylase (CDA) catalyses the conversion of chitin to chitosan by deacetylating N-acetylglucosamine residues. It was first identified and partially purified from extracts of the fungus *Mucor rouxii* [9]. Since then, a similar enzyme activity has been reported in several other fungi [10,11] and in some insect species [12].

Chitin deacetylase from *Mucor rouxii* has been purified to homogeneity and further characterized by employing conventional chromatographic procedures [13]. However, conventional methods require the use of a series of purification steps, which is time consuming and results in low yield and specific activity for the enzyme.

Although there are some fundamental limitations, immunoaffinity chromatography has been used increasingly and successfully for enzyme

* Corresponding author. Address for correspondence: Institute of Molecular Biology and Biotechnology, Enzyme Technology Division, P.O. Box 1515, Heraklion 711 10, Crete, Greece.

0021-9673/93/$06.00

purification [14]. A main drawback of this technique is that the deforming agents usually required for desorption often denature and inactivate labile proteins. However, low-affinity antibodies require less severe desorption conditions. A review of the literature suggests that a proper choice of intermediate affinity antibodies for the preparation of an immunoaffinity column can lead to high yields and rapid purification procedures for enzymes [14,15].

This paper describes the isolation of chitin deacetylase from *Mucor rouxii* to homogeneity employing immunoaffinity chromatography in a one-step procedure.

EXPERIMENTAL

Materials

Mucor rouxii (ATCC 24905) was obtained from American Type Culture Collection. Glycol chitosan and glass beads (425–600 μm) were purchased from Sigma, [^{3}H]acetic anhydride from DuPont New England Nuclear and enzymes and reagents for acetic acid determination from Boehringer Mannheim Biochemica. All chromatographic media (Phenyl Sepharose CL-4B, Q Sepharose Fast Flow, S Sepharose Fast Flow, cyanogen bromide-activated Sepharose) and molecular mass markers were obtained from Pharmacia and ultrafiltration membranes from Amicon. Chitohexaose was purchased from BioCarb, enzyme-linked immunosorbent assay (ELISA) microtitre plates from Nunc and anti-rabbit immunoglobulin G (IgG) conjugated to horseradish peroxidase from NIDA Biotechnology. All other chemicals were of the highest purity commercially available.

Enzyme assays

We employed two different assays for the determination of chitin deacetylase activity, as follows.

(I) Chitin deacetylase activity was determined using as the substrate partially O-hydroxyethylated chitin (glycol chitin), radiolabelled in the N-acetyl groups. The substrate was prepared according to Araki and Ito [9] from glycol chitosan and [^{3}H]acetic anhydride. Enzyme assays were performed as described previously [9], with the following modifications: 25 m*M* sodium glutamate (pH 4.5) was used as the buffer and BSA (0.1 mg ml^{-1}) was added to the assay mixture. The incubation time was 10 min at 50°C.

(II) Acetic acid released by the action of chitin deacetylase on various chitinous substrates was determined by the enzymatic method of Bergmeyer [16] via three coupled enzyme reactions. Units of enzyme activity were determined using 166 nmol of chitohexaose in a total volume of 500 μl buffered with 25 m*M* sodium glutamate (pH 4.5). The incubation time was 10 min at 50°C and the reaction was terminated by heating at 100°C prior to acetic acid determination.

Protein assay and electrophoretic techniques

Protein content was determined by the method of Lowry *et al.* [17] using bovine serum albumin as a standard. Slab-gel electrophoresis using gradient or homogeneous polyacrylamide gels and discontinuous buffer systems under denaturing and reducing conditions were performed as described by Laemmli [18]. Non-denaturing polyacrylamide gels were prepared by the method of Davis [19]. Protein markers were α-lactalbumin (M_r = 14 400), soybean trypsin inhibitor (20 100) carbonic anhydrase (30 000), ovalbumin (43 000), bovine serum albumin (67 000) and β-phosphorylase (94 000). Protein bands were revealed by staining with Coomassie Brilliant Blue R.

Production of antibodies

An adult male white New Zealand rabbit was immunized with 500 μg of CDA [1 mg/ml in 0.010 *M* phosphate-buffered saline (PBS) containing 0.15 *M* NaCl (pH 7.4)], purified from the fungus *Mucor rouxii*, emulsified with an equal volume of Freund's complete adjuvant in a total volume of 1 ml. It was administered intradermally as described previously [20]. Further booster doses of 150 μg of CDA emulsified in Freund's incomplete adjuvant were administered at 4-week intervals. Test bleeds from the marginal ear vein were used to monitor the serum anti-

body titre by ELISA. The blood was allowed to clot at 37°C for 1 h and then stored at 0°C overnight. After the blood clot had been removed, the rabbit sera were aliquoted and stored at −20°C. Control serum was taken prior to immunization.

The antibody titre was monitored using a non-competitive ELISA [21]. CDA was immobilized on flat-bottomed microtitre plates at 2 μg ml^{-1} of buffer containing 0.05 *M* sodium carbonate and sodium hydrogencarbonate (pH 9.6) by incubation overnight at 4°C. The wells were washed with a 0.05% aqueous solution of Tween 20, followed by two washes with distilled water. Subsequently, 200 μl of blocking agent solution per well were incubated for 1 h at room temperature. The blocking agent consisted of 1 g of bovine serum albumin dissolved in 100 ml of 0.010 *M* PBS containing 0.15 *M* NaCl (pH 7.4). The wells were washed as described above. An anti-rabbit IgG antiserum conjugated to horseradish peroxidase was used to detect indirectly specific IgG bound to immobilized CDA. The conjugate was diluted 10 000-fold in 0.010 *M* PBS containing 0.15 *M* NaCl (pH 7.4) and incubated at 100 μl per well for 1 h at room temperature. The wells were washed with aqueous Tween 20 solution as described above, followed by two washes with distilled water. The wells were aspirated and incubated with 100 μl of substrate–chromogen solution made up just prior to use as follows: 3 ml of substrate [0.08% (v/v) hydrogen peroxide solution] were mixed with 12 ml of 0.25 m*M* chromogen (3,3′,5,5′-tetramethylbenzidine–HCl) and the reaction was stopped after 15 min by addition of 50 μl of 4 *M* sulphuric acid per well. The absorbance was read at 450 nm using an ELISA reader (Titertek, Multiskan Plus).

The concentration of antibody in solution was determined by measuring the absorbance at 280 nm using an average molar absorptivity for antibodies of 1.45 l mol^{-1} cm^{-1} for a solution of 1 mg ml^{-1} protein using a 1-cm path-length cell [22].

The enzyme activity of a defined amount of purified CDA (control activity 0.45 mU μl^{-1}) was measured after incubation with various amounts of antiserum [23]. The difference between the measured enzyme activity and the control activity was expressed as percentage inhibition of the control activity.

Purification of IgG

CDA was purified to homogeneity from mycelial extracts of the fungus *Mucor rouxii* as described previously [13]. The mycelial extract was subjected to 52% ammonium sulphate fractionation and 50°C heat treatment and subsequently chromatographed on Phenyl-Sepharose CL-4B, Q-Sepharose Fast-Flow and S-Sepharose Fast-Flow.

Specific anti-CDA IgG was affinity purified from rabbit serum using a CDA–Sepharose-4B adsorbent. CDA was immobilized on cyanogen bromide-activated Sepharose 4B according to the manufacturer's instructions, resulting in 1.3 mg of CDA immobilized per ml of gel (90% coupling efficiency).

Rabbit antiserum against CDA obtained from two bleedings was subjected to 40% ammonium sulphate fractionation. The immunoglobulin-containing precipitate was dissolved and dialysed extensively against 0.025 *M* Tris–HCl–0.2 *M* sodium chloride (pH 7.4) and subsequently loaded on to the CDA-linked Sepharose 4B column (2.2 × 2 cm I.D.; 7.5 ml). The adsorbent was initially washed with ten column volumes of 0.025 *M* Tris–HCl–0.2 *M* NaCl (pH 7.4) and subsequently with two column volumes of 0.025 *M* Tris–HCl–1 *M* NaCl (pH 7.4) in order to remove nonspecifically bound proteins. A batch of IgG was eluted with two column volumes of 0.2 *M* glycine–HCl buffer (pH 2.8). A further batch of higher affinity IgG was eluted with two column volumes of 0.2 *M* glycine–HCl buffer (pH 2.2) (data not shown). All fractions were immediately adjusted to pH 7.0 with 1 *M* Tris–HCl (pH 9.0). The two populations of IgG fractions were pooled separately and concentrated by ultrafiltration, prior to dialysis against 0.025 *M* Tris–HCl (pH 7.4). The purified specific IgG shows the characteristic abbit IgG pattern in sodium dodecyl sulphate–polyacrylamide gel electrophoresis (SDS-PAGE) (data not shown). Pure specific IgG was stored at −20°C at a concentration >1 mg ml^{-1} in 0.010 *M* Tris–HCl–0.1 *M* sodium chloride (pH 7.4).

Purification of CDA

The immunoadsorbent was prepared as follows. Pure lower affinity IgG (5.9 mg) was dialysed against buffer containing 0.1 *M* sodium hydrogencarbonate and 0.5 *M* sodium chloride pH 8.3 and mixed with preswollen cyanogen bromide-activated Sepharose 4B (5 ml) and subsequently immobilized according to the manufacturer's instructions. The ligand concentration was estimated to be 1 mg IgG per ml gel (85% coupling efficiency).

Frozen mycelia (2 g) were thawed, minced and homogenized in 10 ml of 0.05 *M* Tris–HCl buffer (pH 7.4) containing 0.5 m*M* phenylmethylsulphonyl fluoride, 0.1 m*M* N-ethylmaleimide and 150 m*M* NaCl, using an improvised glass-bead miller (2 g of glass beads per gram of wet mycelia). All steps were performed at 4°C. The resulting homogenate was centrifuged at 15 000 *g* for 30 min at 4°C. The supernatant (12.2 ml; 4.6 mg ml^{-1}; 56.0 mg) was then incubated in a water-bath set at 50°C for 15 min and rapidly cooled in ice. Precipitated protein was removed by centrifugation at 136 000 *g* for 45 min at 4°C. The supernatant (11.5 ml; 0.54 mg ml^{-1}; 6.2 mg) was loaded on to the immunoadsorbent (2 × 1.6 cm I.D.; 5 ml) previously equilibrated in 25 m*M* Tris–HCl buffer (pH 7.4) containing 150 m*M* NaCl (buffer A). The column was washed with buffer A (50 ml) and subsequently with 25 m*M* Tris–HCl (pH 7.4)–1 *M* NaCl (10 ml) in order to remove non-specifically bound proteins. CDA was eluted using 0.2 *M* glycine–HCl buffer (pH 2.8) at a flow-rate of 35 ml h^{-1}. The eluate was immediately adjusted to pH 7.0 with 1 *M* Tris–HCl (pH 9.0), dialysed against buffer A and concentrated by ultrafiltration (300 μl; 40 μg ml^{-1}; 12 μg; 160 mU).

RESULTS AND DISCUSSION

Chitosan is produced from chitin by thermochemical deacetylation. This process results in a polymer product having a broad distribution of molecular mass and a heterogeneous extent of deacetylation. However, for many potentially important applications, uniform material with specific physical and chemical properties is required. The development of a controllable process, employing the enzymatic deacetylation of chitinous substrates, presents an attractive alternative as degradation of chitin is prevented and control of the degree of deacetylation can be effected after optimization of the enzymatic reaction.

The purification of chitin deacetylase from *Mucor rouxii* to homogeneity employing conventional purification methodology has been reported [13]. The enzyme is a high-mannose glycoprotein and exists as a monomer with an apparent molecular mass of 75 000–80 000. However, this purification scheme is time consuming and results in low yields (11.8%) and specific activity (2.9 U mg^{-1}) for the enzyme, which is a limiting factor for large-scale applications.

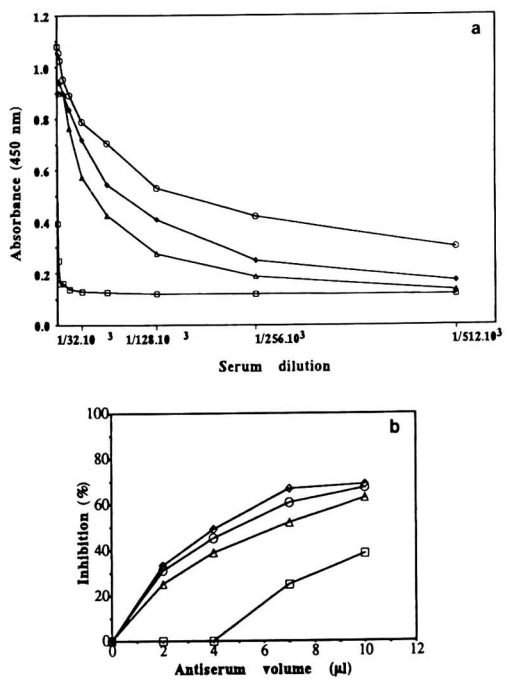

Fig. 1. Determination of the titre of the antiserum. Antisera were obtained at (□) 0 (normal serum), (○) 6, (◇) 23 and (△) 40 weeks after priming. (a) By a non-competitive ELISA: titre was determined at the serum dilution used to obtain half of the maximum absorbance value observed. (b) By immunoinhibition of chitin deacetylase (control activity: 0.45 mU ml^{-1}), after incubation with various amounts of anti-CDA immune sera. The difference between the measured enzyme activity and control activity was expressed as percentage inhibition of the control activity.

In this study, immunoaffinity chromatography was examined as an alternative purification procedure for the rapid isolation of the enzyme in large amounts. We immunized a rabbit with a purified antigen preparation in order to obtain specific antibodies of the enzyme for the development of an immunoaffinity column. The titre of the antisera obtained was exceptionally good, as evidenced by non-competitive ELISA studies (Fig. 1a), probably owing to the glycosylated nature of the enzyme [13]. As the antiserum titre as determined by ELISA is high (>1:50 000 against 800 for normal serum), it is expected that a fraction of the specific antibodies will recognize the epitope at or near the active site of the enzyme (Fig. 1b). The antisera obtained showed no detectable cross-reactivity against other proteins contained in the crude extract of *Mucor rouxii*.

Employing immunoaffinity chromatography, a homogeneous enzyme preparation could be obtained within a day (Figs. 2 and 3). The enzyme purified with this procedure was judged to be electrophoretically homogeneous, as tested by both native PAGE and SDS-PAGE. Enzyme

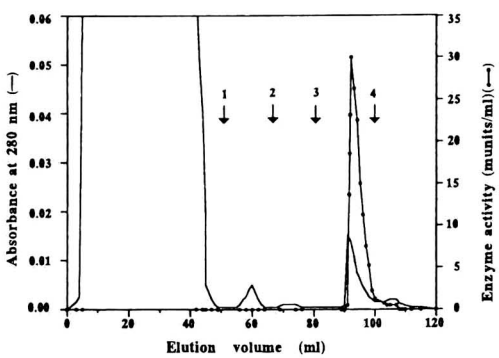

Fig. 2. Purification of chitin deacetylase by immunoaffinity chromatography. A sample (11.5 ml, 6.2 mg; 0.49 U) of partially purified chitin deacetylase was applied to an immunoadsorbent (2 × 1.6 cm I.D.; 5 ml) previously equilibrated in buffer A. The column was washed with buffer A and subsequently with buffer A containing 1 *M* NaCl (1), followed by buffer A (2), 0.2 *M* Glycine–HCl (pH 2.8) (3) and finally with 25 m*M* Tris–HCl (pH 7.4) (4). Fractions (1 ml) with chitin deacetylase activity were collected during the 0.2 *M* glycine–HCl (pH 2.8) wash. The protein content was followed by UV spectrophotometry at 280 nm.

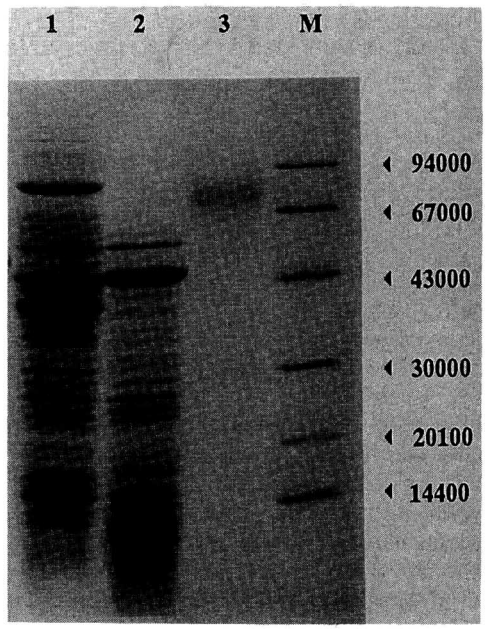

Fig. 3. Denaturing PAGE of the eluate containing chitin deacetylase activity and obtained from the immunoadsorbent. Lanes: 1 = crude protein mixture obtained from *Mucor rouxii* strain after cell lysis (150 μg); 2 = protein mixture obtained after 50°C treatment (150 μg); 3 = fractions with chitin deacetylase activity eluted from the immunoadsorbent (15 μg); M = molecular mass markers (molecular masses are given on the right).

activity assays using the gel slices obtained from gradient (5–20%) native PAGE exhibited chitin deacetylase activity coinciding with the detected protein band. Purified chitin deacetylase subjected to gel filtration on Sephacryl S-200 HR was eluted as a single peak exhibiting chitin deacetylase activity. Purified enzyme preparations exhibited a specific activity of 13.3 U mg^{-1} while a 30% overall yield was obtained (Table I), which represents increases of four- and threefold, respectively, in comparison with the previously reported purification scheme [13]. Further, employing conventional methodology for the isolation of the enzyme, traces of chitinase activity were detected which could degrade the polymer substrate (chitin). In contrast, enzyme preparations obtained from the immunoadsorbent were free of chitinase activity. The immunoadsorbent could be used repeatedly

TABLE I

SUMMARY OF THE PURIFICATION PROTOCOL FOR CHITIN DEACETYLASE

Step	Total protein (mg)	Enzyme activity (U)[a]	Specific activity (U mg^{-1})	Purification (fold)	Yield (%)
Crude extract	56.000	0.55	0.010	1.0	100.0
50°C treatment	6.200	0.49	0.079	7.9	89.0
Immunoadsorbent	0.012	0.16	13.333	1333.0	29.1

[a] One unit of the enzyme activity is defined as the amount of the enzyme required to produce 1 μmol of acetic acid per minute when incubated with 16.6 nmol of chitohexaose under optimum pH (4.5) and temperature (50°C) conditions.

more than twenty times to isolate chitin deacetylase without any decrease in its enzyme-purifying ability. The successful isolation of the enzyme is mainly due to the effectiveness of the immunoadsorbent where the enzyme was enriched 169-fold (Table I).

The binding capacity of the CDA–Sepharose 4B for anti-CDA antibodies was determined to be *ca.* 1.2 mg of IgG per mg of immobilized CDA. This high binding capacity is due to the fact that a number of IgG molecules can bind to a CDA molecule depending on antigenic valency.

The capacity of the immunoadsorbent used in this study, although not optimized, was determined to be higher than 42 μg of chitin deacetylase per ml of immunoadsorbent (4% of the theoretical maximum capacity). The maximum theoretical binding capacity of the immunoadsorbent occurs when both binding sites of each immobilized antibody molecule bind a molecule of CDA. Assuming that the molecular masses of CDA and IgG are 80 000 and 160 000, respectively, 1 mg of immobilized IgG could bind 1 mg of CDA. However, in practice only a small percentage of antigen binding sites remain available for binding the antigen after covalent immobilization on a matrix.

After isolation and subsequent immobilization of lower affinity antibodies, less severe chemical conditions were required for the desorption of the immunoadsorbent. Two separate batches of IgG were eluted from the CDA–Sepharose 4B column. The first batch was eluted with 0.2 *M* glycine–HCl buffer (pH 2.8) and the second batch with 0.2 *M* glycine–HCl buffer (pH 2.2). As elution of the immunoadsorbent at pH 2.2 represents a more drastic procedure compared with the pH 2.8 elution procedure, IgG fractions eluted with 0.2 *M* glycine–HCl (pH 2.8) (lower affinity IgG) were used for the preparation of the immunoadsorbent. An immunoadsorbent having immobilized specific IgG instead of crude polyclonal antibody was employed in order to increase the specificity of the adsorbent for the enzyme. It is expected that the half-life of the immunoadsorbent having immobilized lower affinity antibodies will be increased by preventing irreversible binding of chitin deacetylase to higher affinity IgG after successive chitin deacetylase purifications [the term "affinity" used in the text refers to the functional affinity (avidity) as polyclonal antibodies are used].

The same immunoadsorbent could potentially be employed for the isolation of chitin deacetylases from other Zygomycetes species, as an inter-species homology has been observed by Western blot assays (data not shown). In this way, a comparative study of chitin deacetylases from various sources can be performed.

During the isolation of the enzyme by conventional methods, a second chitin deacetylase activity of molecular mass 38 000 was identified, which is more likely a degradation product of full-length chitin deacetylase [13]. Employing immunoaffinity chromatography only one form of the enzyme could be identified, of molecular mass 75 000–80 000, suggesting that degradation products of the protein can be avoided using this rapid purification scheme.

This study has demonstrated the effectiveness of immunoaffinity chromatography for the isolation of chitin deacetylase from *Mucor rouxii* in a one-step procedure. Bearing in mind the potential application of the enzyme in large-scale deacetylation processes, we are presently focusing on the evaluation of other enzyme sources for the identification of the best producer species, overproduction of the enzyme in a suitable system after cloning the gene from a cDNA library we have constructed and optimization of substrate pretreatment requirements.

CONCLUSIONS

Chitin deacetylase from *Mucor rouxii* has been purified to homogeneity in a one-step procedure employing immunoaffinity chromatography. Using antibodies of lower affinity, less severe chemical conditions were required for the desorption of immunoadsorbents. A 169-fold purification of the enzyme was achieved while purified enzyme preparations exhibited a specific activity of 13 U mg^{-1} and a 30% yield was obtained.

ACKNOWLEDGEMENTS

We thank Dr. J. Vournakis and Dr. G. Papadopoulos for critical reading of the manuscript. We also acknowledge Dr. Elias Krambovitis for his advice and essential help in obtaining specific antibodies and Georgia Plousi and George Hatzidakis for providing excellent technical assistance with immunizations and serum characterizations.

REFERENCES

1 C. Jeuniaux, *Bull. Soc. Zool. Fr.*, 107 (1982) 363–386.
2 J. Ruiz-Herrera, in R.A.A. Muzzarelli and R.E. Pariser (Editors), *Proceedings of the First International Conference on Chitin/Chitosan, Boston, 1977, MIT Sea Grant Rep. MITSG*, 78-7 1978, pp. 11–21.
3 S. Bartnicki-Garcia and W.J. Nickerson, *Biochim. Biophys. Acta*, 58 (1962) 102–119.
4 K. Shimahara, Y. Takiguchi, T. Kobayashi, K. Uda and T. Sannan, in G. Skjak-Braek, T. Anthonsen and P. Sandford (Editors), *Chitin and Chitosan*, Elsevier Applied Science, Barking, 1989, pp. 171–178.
5 C.K. Rha, D. Rodriguez-Sanchez and C. Kienzle-Sterzer, in R.R. Colwell, E.R. Pariser and J.A. Sinskey (Editors), *Biotechnology of Marine Polysaccharides*, Hemisphere, Washington, New York, London, 1984, pp. 283–311.
6 D. Knorr, in R.R. Colwell, R.E. Pariser and A.J. Sinskey (Editors), *Biotechnology of Marine Polysaccharides*, Hemisphere, Washington, New York, London, 1984, pp. 313–332.
7 S. Hirano, in G. Skjak-Braek, T. Anthonsen and P. Sandford (Editors), *Chitin and Chinosan*, Elsevier Applied Science, Barking, 1989, pp. 37–43.
8 T. Sannan, K. Kurita and Y. Iwakura, *Makromol. Chem.*, 177 (1976) 3589–3600.
9 Y. Araki and E. Ito, *Eur. J. Biochem.*, 55 (1975) 71–78.
10 H. Kauss, W. Jeblick and D.H. Young, *Plant Sci. Lett.*, 28 (1983) 231–236.
11 J. Trudel and A. Asselain, *Anal. Biochem.*, 189 (1990) 249–253.
12 M. Aruchami, N. Gowri and G. Sundara-Rajulu, in R. Muzzareli, C. Jeuniaux and G.W. Gooday (Editors), *Chitin in Nature and Technology*, Plenum Press, New York, 1986, pp. 263–268.
13 D. Kafetzopoulos, A. Martinou and V. Bouriotis, *Proc. Natl. Acad. Sci. U.S.A.*, 90 (1993) 2564–2568.
14 H. Ehle and A. Horn, *Bioseparation*, 1 (1990) 97–110.
15 J.M Leah, E.E. Billett and T. Palmer, *Anal. Biochem.*, 170 (1988) 495–501.
16 H.U. Bergmeyer, in H.U. Bergmeyer (Editor), *Methods of Enzymatic Analysis*, Vol. 1, Academic Press, New York, 2nd ed., 1974, pp. 112–117.
17 O.H. Lowry, M.J. Resebrough, A.L. Farr and R.J. Randall, *J. Biol. Chem.*, 193 (1951) 265–275.
18 U.K. Laemmli, *Nature*, 227 (1970) 680–685.
19 B.J. Davis, *Ann. N.Y. Acad. Sci.*, 121 (1964) 404–427.
20 R.J. Mayer and J.H. Walker, *Immunochemical Methods in the Biological Sciences. Enzymes and Proteins*, Academic Press, New York, 1980, pp. 148–149.
21 A. Voller, D.E. Bidwell and A. Bartlett, *The Enzyme Linked Immunosorbent Assay (ELISA), a Guide with Abstracts of Microplate Applications*, Dynatech Europe, Borough House, Guernsey, 1979, pp. 18–26.
22 D. Catty, *Antibodies, Vol. 1, a Practical Approach*, IRL Press, Oxford, 1988, p. 73.
23 H. Ehle and A. Bublitz, *Biomed. Biochim. Acta*, 44 (1985) 223–233.

Journal of Chromatography, 644 (1993) 43–48
Elsevier Science Publishers B.V., Amsterdam

CHROM. 25 128

Determination and quantitative analysis of *Aconitum* alkaloids in plants by liquid chromatography–atmospheric pressure chemical ionization mass spectrometry

Koji Wada*, Hideo Bando and Norio Kawahara

Hokkaido Institute of Pharmaceutical Sciences, 7-1, Katsuraoka-cho, Otaru 047-02 (Japan)

(First received January 4th, 1993; revised manuscript received March 30th, 1993)

ABSTRACT

A high-performance liquid chromatography–atmospheric pressure chemical ionization mass spectrometry method was useful for the simultaneous determination of *Aconitum* alkaloids, kobusine, pseudokobusine, dehydroluciduscuIine, luciduscuIine, delcosine and 14-acetyldelcosine, found in the *Aconitum yesoense* var. *macroyesoense*. These compounds were chromatographed by definite elution in 10 min and were quantitated by selected-ion monitoring of the protonated molecules. The method is linear over the range 10 ng to 10 μg of alkaloids per injection. The detection limits of alkaloids were *ca.* 1–5 ng per injection.

INTRODUCTION

Various *Aconitum* (Ranunculaceae) plants produce C_{19}- and C_{20}-diterpenoid alkaloids [1]. The tubers of *Aconitum* plants, called "busi", have been employed as an oriental drug in Japan and China. The crude drug "busi" has been consumed clinically in large quantities in East Asia.

A number of reports on the analysis of trimethylsilylated aconitine-type alkaloids by gas chromatography [2] and toxic C_{19}-diterpenoid alkaloids by high-performance liquid chromatography (HPLC) have appeared in recent years [3–7]. These alkaloids have a moiety of aromatic ester (such as benzoyl and anisoyl groups), and can be applied directly to the method with UV detection. However, no report exists on the investigation of the separation and the simultaneous determination of C_{19}- (no aromatic ester group) and C_{20}-diterpenoid alkaloids.

Recently, the use of high-performance liquid chromatography–mass spectrometry (HPLC–MS) for analysis in various fields has been reported. HPLC–MS has proved effective for the detection of various alkaloids, for example strychnine [8], nicotine [9], indole alkaloids [10–13], ergot alkaloids [14–16] and tropane alkaloids [17].

In the present paper we report on the analytical conditions for the determination and the quantitative analysis of kobusine (KB), pseudokobusine (PK), dehydroluciduscuIine (DL), luciduscuIine (LD), delcosine (DC) and 14-acetyldelcosine (AD) (Fig. 1), using high-performance liquid chromatography–atmospheric pressure chemical ionization mass spectrometry (HPLC–APCI-MS). A method using selected-ion monitoring (SIM) of protonated molecules ($[M + H]^+$) was developed for the verification of the HPLC peak and for the quantitation of

* Corresponding author.

0021-9673/93/$06.00

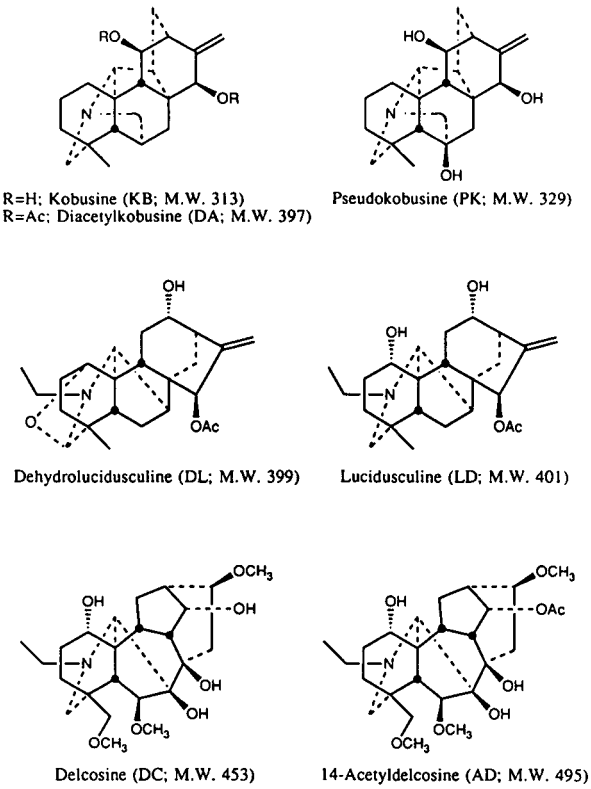

Fig. 1. Structures and molecular mass (M.W.) of the investigated *Aconitum* alkaloids and internal standard alkaloid.

diterpenoid alkaloid in plant extracts of *Aconitum yesoense* var. *macroyesoense* (Nakai) Tamura.

EXPERIMENTAL

Materials

Kobusine (KB), pseudokobusine (PK), dehydroluciduscuiline (DL), luciduscuiline (LD), delcosine (DC) and 14-acetyldelcosine (AD) were purified from *Aconitum yesoense* var. *macroyesoense* roots and identified as described previously [18]. Diacetylkobusine (DA) used as an internal standard was synthesized from kobusine (KB). Ammonium acetate of reagent grade was purchased from Kanto Chemicals (Tokyo, Japan), and acetonitrile and tetrahydrofuran of HPLC grade were purchased from Wako Pure Chemical Industries (Osaka, Japan).

Apparatus

IR spectra in potassium bromide discs were taken with a Model IRA-2 spectrometer (Jasco, Tokyo, Japan). NMR spectra were measured in deuterated trichloromethane solution with a Model GX-270 spectrometer (JEOL, Tokyo, Japan) using TMS as an internal standard. MS was performed with a Model M-2000 mass spectrometer (Hitachi, Tokyo, Japan). A Model M-2000 mass spectrometer through the APCI interface was used as the HPLC–APCI-MS system.

Diacetylkobusine

M.p., 139–141°C (from ether–hexane); IR, 1730, 1370 cm^{-1}; ^1H NMR, δ 0.97 (3H, s, 18-CH_3), 2.00 and 2.09 (each 3H, s, OAc), 5.00 and 5.18 (each 1H, s, 17-H_2), 5.08 (1H, d, $J = 5$ Hz, 11-H), 5.42 (1H, s, 15-H); MS, m/z 397 (M^+, base peak), 354, 338.

HPLC–APCI-MS conditions

The HPLC system consisted of a Model L-6200 chromatographic pump (Hitachi, Tokyo, Japan) and a Rheodyne 7125 injector (Rheodyne, Cotati, CA, USA) with a 20-μl loop. The HPLC column was an Inertsil ODS-2 (150 × 4.6 mm I.D., 5 μm; GL Sciences, Tokyo, Japan), and the definite eluent consisted of 0.05 *M* ammonium acetate–acetonitrile–tetrahydrofuran (60:25:15, v/v/v) at a flow-rate of 0.8 ml/min. The interface consisted of nebulizing and vaporizing unit. The temperature of the nebulizer was set to 370°C to give the strong intensity of target ions. The desolvater temperature was set to 400°C.

Vaporized sample and solvent molecules were led into the ion source of the APCI–MS system, the solvent molecules were ionized by corona discharge and then the sample molecules and ionized solvent molecules underwent ion–molecule reactions.

The mass spectrometer was operated in the APCI mode, the drift voltage was set to 143 V and the scan ranges were 280–510 u.

Sample preparation

The *A. yesoense* var. *macroyesoense* samples were obtained from the root of Jozankei, the city

of Sapporo, Hokkaido, Japan. The root samples were freeze-dried and ground. The samples (1 g) were stirred with organic solvents (ether, chloroform or methanol, 10 ml) containing 10% aqueous ammonia (0.5 ml) at room temperature for 30 min [6]. Water (0.5 ml) was added to the solution. The liquid phase was filtered and the residue was further extracted twice in the same manner with the same solvent (10 ml each), but no water was added. The combined solutions were evaporated to dryness. The extract was dissolved with HPLC mobile phase (5 ml), and filtered with a 0.5-μm filter. Internal standard (10 μg per 20 μl of diacetylkobusine) was added to the filtrated solution (180 μl), and this solution (10 μl) was injected into the HPLC–APCI-MS system. The content of alkaloids was calculated.

The recovery of extracted alkaloids from root samples was determined by addition of kobusine, luciduscuiline and delcosine at 400 μg to the root samples. The recoveries of alkaloids were compared with those from root extract samples to which no alkaloids had been added. The extraction procedure was the same as above.

Calibration curves and quality control of assay

The calibration curves (10, 100 and 500 ng and 1 and 10 μg per injection) were prepared using standard solutions of each alkaloid. At same time, the internal standard (500 ng per injection of diacetylkobusine) was added to each solution, and 10-μl aliquots of the solutions were injected into the HPLC–APCI-MS system. The calibration curves were calculated by the internal standard method for each peak area. Relative standard deviations (R.S.D.s) were determined using 10 ng and 100 ng of alkaloids.

RESULTS AND DISCUSSION

The mass spectra show protonated molecules ($[M + H]^+$) for kobusine at m/z 314, for pseudokobusine at m/z 330, for dehydroluciduscuiline at m/z 400, for luciduscuiline at m/z 402, for delcosine at m/z 454, for 14-acetyldelcosine at m/z 496 and for diacetylkobusine (internal standard) at m/z 398 (Fig. 2). However, the characteristic clusters produced by water or ammonia

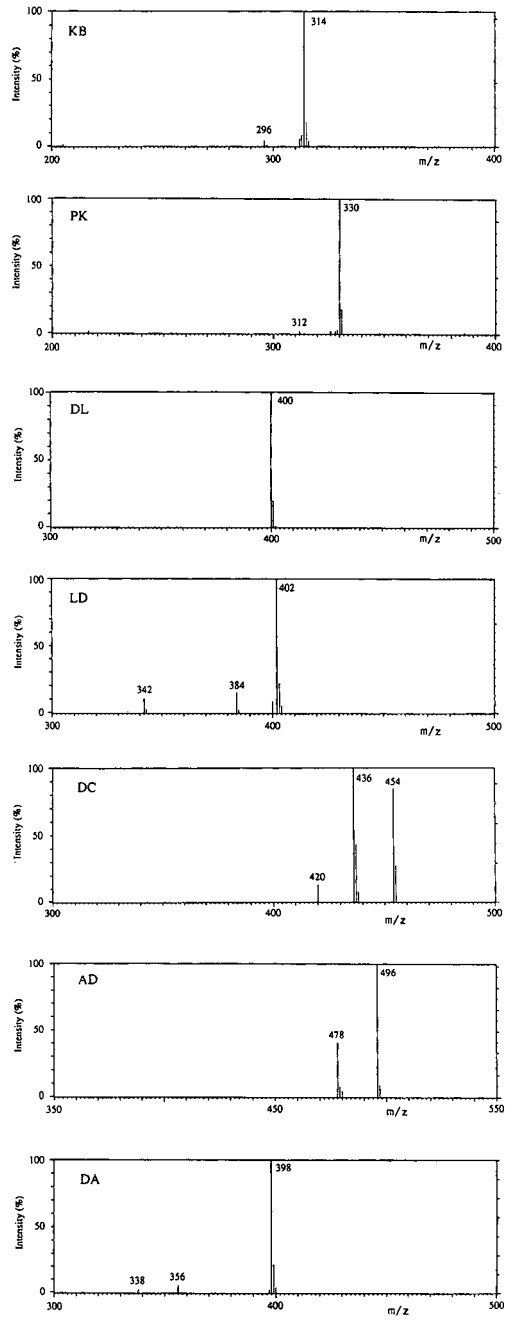

Fig. 2. Mass spectra for kobusine (KB), pseudokobusine (PK), dehydroluciduscuiline (DL), luciduscuiline (LD), delcosine (DC), 14-acetyldelcosine (AD) and diacetylkobusine (DA; internal standard). The compounds (2 μg) were injected via the column. Conditions: Inertsil ODS-2 column, 150 × 4.6 mm I.D., 5 μm; mobile phase, 0.05 *M* ammonium acetate–acetonitrile–tetrahydrofuran (60:25:15, v/v); flow-rate 0.8 ml/min; nebulizer temperature, 370°C; desolvater temperature, 400°C.

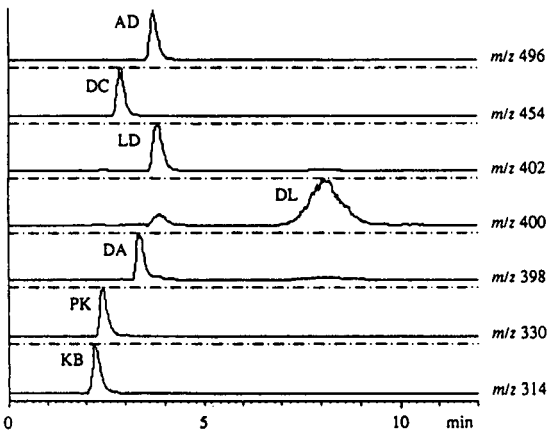

Fig. 3. Mass fragmentograms of kobusine (KB), pseudokobusine (PK), dehydroluciduscuIine (DL), luciduscuIine (LD), delcosine (DC), 14-acetyldelcosine (AD) and diacetylkobusine (DA; internal standard) using the selected-ion monitoring method. Conditions as in Fig. 2.

ion attachment to each $[M+H]^+$ were not observed. The mass spectrum of kobusine shows a fragment ion at m/z 296 ($[M+H-water]^+$). The mass spectrum of pseudokobusine shows a fragment ion at m/z 312 ($[M+H-water]^+$). The mass spectrum of dehydroluciduscuIine shows no fragment ion. The mass spectrum of luciduscuIine shows fragment ions at m/z 384 ($[M+H-water]^+$) and 342 ($[M+H-acetic\ acid]^+$). The mass spectrum of delcosine shows fragment ions at m/z 436 ($[M+H-water]^+$) and 420 ($[M+H-CH_4-water]^+$). The mass spectrum of 14-acetyldelcosine shows a fragment ion at m/z 478 ($[M+H-water]^+$). The mass spectrum of diacetylkobusine (as an internal standard) shows fragment ions at m/z 356 ($[M+H-CH_2CO]^+$) and 338 ($[M+H-acetic\ acid]^+$).

The $[M+H]^+$ ion showed high intensity in the mass spectra of kobusine, pseudokobusine, dehydroluciduscuIine, luciduscuIine, delcosine and 14-acetyldelcosine, and selected-ion monitoring (SIM) of the $[M+H]^+$ ions was a useful technique for the quantitation of their compounds. *Aconitum* alkaloids were unambiguously determined by the SIM method under these conditions (Fig. 3). Good linearity was observed ($r > 0.997$ in all instances) when *Aconitum* alkaloids and internal standard peak-area ratios were plotted for the range 10 ng to 10 μg per injection. The reproducibility of the measurement was investigated by analysing known amounts (10 and 100 ng) of *Aconitum* alkaloids. The relative standard deviations (%) were obtained by calculating the ratio of the peak intensities of *Aconitum* alkaloids against the intensity of internal standard (Table I). The reproducibility of the result was found to be within the acceptable limit.

The HPLC–APCI-MS method with SIM was applied to the determination of *Aconitum* alkaloids in plants, and the elution at a flow-rate of 0.8 ml/min resulted in good chromatographic separation of the alkaloids within 10 min using the definite solvent system, and buffer ionization

TABLE I

REGRESSION PARAMETERS OF THE HPLC–APCI-MS ASSAY OF *ACONITUM* ALKALOIDS

r = Coefficient of correlation; R.S.D. = relative standard deviation; x = amount of analyte in ng; y = peak-area ratio of analyte and internal standard.

Compound	Curve equation	r	R.S.D. (%, $n=7$)	
			10 ng	100 ng
Kobusine	$y = 6.607 \cdot 10^{-3}x + 9.462 \cdot 10^{-4}$	0.9967	10.1	11.1
Pseudokobusine	$y = 6.487 \cdot 10^{-3}x - 1.678 \cdot 10^{-4}$	0.9990	9.1	11.7
Dehydrolucidusculine	$y = 1.511 \cdot 10^{-3}x + 2.641 \cdot 10^{-3}$	0.9962	13.3	10.4
Lucidusculine	$y = 6.532 \cdot 10^{-4}x + 6.715 \cdot 10^{-3}$	0.9994	10.6	2.9
Delcosine	$y = 1.906 \cdot 10^{-4}x + 8.192 \cdot 10^{-4}$	0.9976	17.3	6.4
14-Acetyldelcosine	$y = 1.681 \cdot 10^{-4}x - 4.458 \cdot 10^{-5}$	0.9972	9.1	11.7

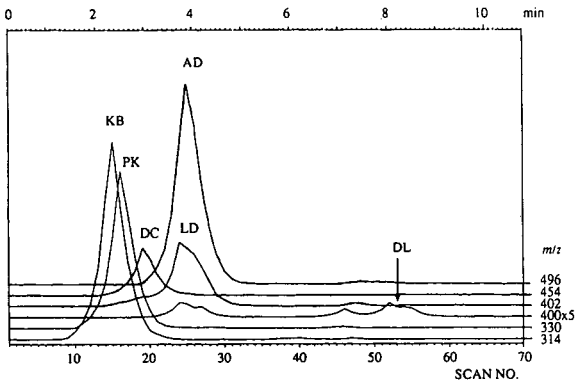

Fig. 4. Mass chromatograms of a plant sample of *A. yesoense* var. *macroyesoense*. Compounds monitored: kobusine (KB) at *m/z* 314, pseudokobusine (PK) at *m/z* 330, dehydrolucidusculine (DL) at *m/z* 400, lucidusculine (LD) at *m/z* 402, delcosine (DC) at *m/z* 454, 14-acetyldelcosine (AD) at *m/z* 496. Conditions as in Fig. 2.

was stable and the background noise was a low enough to allow good net peaks for 1–5 ng samples of the alkaloids.

In order to verify the applicability of this procedure, *Aconitum* root was assayed by employing the above procedure. The mass chromatograms of a plant sample are shown in Fig. 4. A comparative assessment of various solvents for extraction of *Aconitum* alkaloids from aconite was made to examine the efficiency of different extraction procedures. The results are shown in Table II. In the chloroform extraction procedure, the recovery of kobusine, lucidusculine and delcosine was found to be 95.4, 97.4 and 94.3%, respectively, and the extraction method was considered to be the most satisfactory. The contents of 14-acetyldelcosine was found to be the highest in *Aconitum* alkaloids.

CONCLUSIONS

It has been demonstrated that HPLC–APCI-MS can give $[M + H]^+$ ions species of *Aconitum* alkaloids, and that the method is useful for the separation and simultaneous determination of *Aconitum* alkaloids in plant samples. The wide linear range of the assay is applicable to determination with respect to a variety of contents in samples from different sources. The precision of the method is adequate for screening the *Aconitum* alkaloid content of plant extracts and can be also applied to the identification of *Aconitum* alkaloid metabolites in biological samples.

REFERENCES

1 T. Amiya and H. Bando, in A. Brossi (Editor), *The Alkaloids*, Vol. 34, Academic Press, San Diego, 1988, p. 95.
2 H. Kikino, C. Yamada, K. Nakamura, H. Sato, Y. Ohizumi and K. Endo, *Yakugaku Zasshi*, 97 (1977) 359.
3 H. Hikino, C. Konno, H. Watanabe and O. Ishikawa, *J. Chromatogr.*, 211 (1981) 107.
4 H. Hikino, M. Murakami, C. Konno and H. Watanabe, *Planta Med.*, 48 (1983) 67.
5 I. Kitagawa, Z.L. Chen, M. Yoshihara and M. Yoshikawa, *Yakugaku Zasshi*, 104 (1984) 867.
6 H. Bando, K. Wada, M. Watanabe, T. Mori and T. Amiya, *Chem. Pharm. Bull.*, 33 (1985) 4717.
7 P. Kulanthaivel and S.W. Pelletier, *J. Chromatogr.*, 402 (1987) 366.
8 J.D. Henion, *Anal. Chem.*, 50 (1978) 1687.

TABLE II

CONTENTS OF ALKALOIDS IN *A. YESOENSE* VAR. *MACROYESOENSE*

Compound	Extracting solvents (μg/g ± S.D.)			Recovery (%)		
	Ether	Chloroform	Methanol	Ether	Chloroform	Methanol
Kobusine	409 ± 27.7	443 ± 41.0	449 ± 17.9	39.5	95.4	79.8
Pseudokobusine	263 ± 9.85	384 ± 21.2	344 ± 18.5	–	–	–
Dehydrolucidusculine	186 ± 12.9	44.8 ± 1.77	7.15 ± 0.699	–	–	–
Lucidusculine	$1.28 \cdot 10^3 \pm 51.6$	$1.53 \cdot 10^3 \pm 108$	$1.35 \cdot 10^3 \pm 76.9$	97.2	97.4	98.3
Delcosine	632 ± 30.0	778 ± 58.8	723 ± 59.7	94.6	94.3	94.3
14-Acetyldelcosine	$7.07 \cdot 10^3 \pm 632$	$6.06 \cdot 10^3 \pm 742$	$5.87 \cdot 10^3 \pm 364$	–	–	–

9 K.T. McManus, J.D. de Bethizy, D.A. Garteiz, G.A. Kyerematen and E.S. Vesell, *J. Chromatogr. Sci.*, 28 (1990) 510.
10 S. Auriola, V.P. Ranta, T. Naaranlahti and S.P. Lapinjoki, *J. Chromatogr.*, 474 (1989) 181.
11 S. Auriola, T. Naaranlahti, R. Kostiainen and S.P. Lapinjoki, *Biomed. Environ. Mass Spectrom.*, 19 (1990) 609.
12 S. Auriola, T. Naaranlahti and S.P. Lapinjoki, *J. Chromatogr.*, 554 (1991) 227.
13 R. Le Verge, P. Le Corre, F. Chevanne, M.D. De Maindreville, D. Royer and J. Levy, *J. Chromatogr.*, 574 (1992) 283.
14 K.H. Schellenberg, M. Linder, A. Groeppelin and F. Erni, *J. Chromatogr.*, 394 (1987) 239.
15 K. Banno and S. Horimoto, *J. Chromatogr.*, 31 (1991) 50.
16 K. Banno, S. Horimoto and M. Mabuchi, *J. Chromatogr.*, 568 (1991) 375.
17 S. Auriola, A. Martinsen, K. Oksman-Caldentey and T. Naaranlahti, *J. Chromatogr.*, 562 (1991) 737.
18 H. Bando, K. Wada, T. Amiya, K. Kobayashi, Y. Fujimoto and T. Sakurai, *Heterocycles*, 26 (1987) 2623.

Journal of Chromatography, 644 (1993) 49–58
Elsevier Science Publishers B.V., Amsterdam

CHROM. 25 079

Automated high-performance liquid chromatographic method for the determination of organophosphorus pesticides in waters with dual electrochemical (reductive–oxidative) detection

R. Carabias Martínez*, E. Rodríguez Gonzalo, F. Garay García and J. Hernández Méndez

Departamento de Química Analítica, Nutrición y Bromatología, Universidad de Salamanca, 37008 Salamanca (Spain)

(First received November 25th, 1992; revised manuscript received March 16th, 1993)

ABSTRACT

A highly sensitive method for multi-residue analysis of organophosphorus pesticides by HPLC with dual electrochemical detection has been developed. It involves the detection of reduction products from the upstream electrode in an oxidative mode at the downstream electrode. This reductive–oxidative detection mode allows detection limits below 4 μg/l. When a preconcentration device was coupled on-line with the HPLC system, detection limits as low as 0.03 μg/l were achieved for only 100 ml of sample. The relative standard deviations were in an acceptable range for trace analysis. The overall analysis time for the five pesticides investigated (paraoxon, guthion, methyl-parathion, ethyl-parathion and fenitrothion) was 25 min.

INTRODUCTION

Organophosphorus pesticides are in widespread use because of their relatively rapid decomposition and low accumulation in the biological food chain. Because there is a need to determine trace levels of pesticides in complex matrices such as water, soil and crops, analytical methods have to be both highly sensitive and selective. Organophosphorus pesticides are mainly determined by using chromatographic techniques [1]. As far as HPLC, which is the only separation technique to be discussed in this paper, is concerned, ultraviolet detection is the most common choice [2–4], but electrochemical detection (HPLC–ED) is becoming a popular technique [5,6]. Most reports describe the use of amperometric detectors with only a single working electrode, but dual-electrode detectors (series or parallel configuration) are more versatile; they can provide improved analyte specificity and lower detection limits, especially in the series (upstream–downstream) configuration [7,8]. The series configuration is also applied for electrochemical derivatization of the analyte to a product with favourable properties for electrochemical detection.

This paper describes an HPLC method for the determination of paraoxon, methyl-parathion, ethyl-parathion, guthion and fenitrothion in a reductive–oxidative detection mode with a series dual-electrode system. These organophosphorus pesticides can be directly determined by reductive electrochemical detection due to the presence of nitro or azo groups in their structures. However, reductive HPLC–ED requires an exhaustive deoxygenation because of the high

* Corresponding author.

0021-9673/93/$06.00

residual current due to the reduction of dissolved oxygen. Although direct oxidative electrochemical detection is not possible for these pesticides, they can be electrochemically converted into derivatives which are then suitable for oxidative detection. A dual-electrode detector in the series mode provides a simple and rapid way for performing this detection. Improvements in electrochemical detection are described here, the detection limits obtained being a significant improvement over the results of all other HPLC methods previously reported [9–12].

The proposed method was applied to the determination of pesticide residues in waters. Preconcentration prior to HPLC–ED is required when it is desirable to measure analyte concentrations of less than 0.1 μg/l. In recent years, much attention has been paid to sample preconcentration techniques involving the use of a solid-phase sorbent, as an alternative to conventional liquid–liquid extraction techniques [13–17].

In a previous work [12], extraction and preconcentration of organophosphorus pesticides on a C_{18}-bonded phase silica cartridge were successfully accomplished. In this paper, a microprocessor-controlled system for automated on-line pesticide extraction and preconcentration is described, the solid-phase sorbent cartridge being placed in the sample loop of a six-port valve. The overall HPLC–ED system was optimized.

EXPERIMENTAL

Apparatus

The HPLC system consisted of a Spectra-Physics Model SP-8800 ternary pump, a PAR 400 electrochemical detector equipped with an MP 1304 glassy carbon series dual electrode, an Ag/AgCl/1.0 *M* KCl reference electrode and a gold auxiliary electrode and a Spectra-Physics SP 4290 integrator. A Rheodyne injection valve with a 10-μl sample loop and a 5-μm Spheri-5-RP-18 column (250 × 4.6 mm I.D.) from Brownlee Labs. were used in all experiments. All solvents and samples were filtered through 0.45 μm pore-size nylon membrane filters (Millipore).

A PAR 384 B polarograph with a Metrohm E-628 glassy carbon rotating electrode, a platinum auxiliary electrode and a saturated calomel reference electrode was used for cyclic and anodic stripping voltammetry.

The on-line preconcentration system consisted of commercially available Sep-Pak C_{18} bonded-phase silica cartridges (Waters) placed in the sample loop of a Rheodyne Model 5020 six-port injection valve; a Gilson 231-401 microprocessor-controlled diluter–autosampling injector, equipped with a piston pump and a fraction collector, was used to elute and inject the sample into the chromatograph. A Gilson Minipuls-3 peristaltic pump with vinyl tubing was used for pumping the pesticides through the cartridge.

Reagents

All organophoshorus pesticides were obtained from Riedel-de Haën (Seelze-Hannover, Germany); the purities of the individual standards ranged from 97 to 99%. The pesticides, listed in the order in which they appear in the chromatograms, were (1) paraoxon, (2) guthion, (3) methyl-parathion, (4) fenitrothion and (5) ethyl-parathion. Ultra-high-quality water was obtained with an Elgastat UHQ water-purification system. Standard solutions were prepared in HPLC-grade methanol (Carlo Erba, Milan, Italy). All other chemicals were of analytical-reagent grade.

Water samples

Stock standard solutions containing a mixture of the five pesticides were prepared in pure methanol. Working standard aqueous samples were prepared by diluting 1.0 ml of the stock standard solution to 100.0 ml with ultra-pure water. River water samples investigated were taken from the Tormes river (Salamanca, Spain) as representative samples of surface waters in this agricultural area. They were collected directly in 1-l glass containers, stored at 4°C in the dark and analysed within 24 h after collection. All river water samples were filtered through sintered-glass filters (No. 5) to remove suspended particulate matter.

Procedure

The HPLC operating conditions were optimized in a previous study [12], the mobile phase

being methanol–water (70:30, v/v) containing 0.025 *M* acetic acid–acetate buffer (pH 4.8). The flow-rate was set at 1.25 ml/min.

Electrochemical detection with series dual electrodes was carried out as follows: pesticides were reduced at the upstream electrode (W_1) set at a potential $E_1 = -1.500$ V, the reduction products being detected in an oxidative mode at the downstream electrode (W_2) set at $E_2 = 0.400$ V. Both electrodes were electrochemically pretreated every day. Injected amounts higher than 20 ng required reactivation of the upstream electrode at a potential of +1.600 V for 5 min prior to each measurement.

Determination of pesticides in waters. The preconcentration step was carried out with the on-line system depicted schematically in Fig. 1. Analytes were adsorbed in the cartridge by a single pass of a 100-ml water sample with a peristaltic pump (B_1) at a flow-rate of 10 ml/min. The valve was then switched to the injection position and the cartridge eluted with 2.0 ml of pure methanol using a piston pump (B_2); the microprocessor-controlled diluter–injector allowed the collection, in a conical vial, of the fraction eluting between 1.0 and 1.4 ml, sending to waste the remainder of the liquid eluted. A 10-μl aliquot of the 400 μl collected was injected into the chromatographic system. The cartridge was rinsed with 10.0 ml of methanol and the system was then ready for the next sample. All

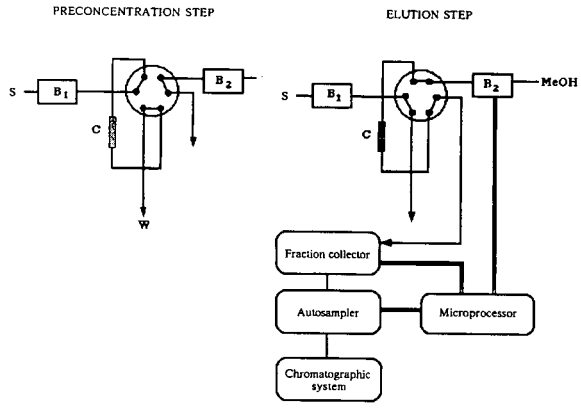

Fig. 1. Schematic diagram of the automatic on line preconcentration system used for river water analysis. B_1, B_2 = Peristaltic and piston pumps, respectively; S = sample; C = preconcentration cartridge; W = waste.

operations (cartridge elution, fraction collection, sample injection and wash cycle) were done automatically under the control of the microprocessor.

The cartridges were equilibrated with 5.0 ml of methanol and 5.0 ml of ultra-pure water before use for pesticide concentration. In the analysis of river waters, a new cartridge was used for each sample.

Quantification was carried out by using the external standard method, bracketing samples and standards under identical conditions (preconcentration, elution and injection) and taking the mean peak area value of three injections.

RESULTS AND DISCUSSION

Voltammetric studies

An initial study by cyclic voltammetry was performed on solutions of the same composition as the chromatographic mobile phase. Moreover, in order to check whether the products generated by electrochemical reduction are available for oxidative detection, anodic stripping voltammetry after application of an extreme reduction potential was also investigated.

Cyclic voltammograms of paraoxon (Fig. 2a) were scanned from 0.800 to −1.200 V; this pesticide exhibits a cathodic peak at −0.930 V and an ill-defined anodic peak at 0.300 V on the reverse scan, which represent the oxidation of the species generated in the reduction process. The anodic stripping voltammogram (Fig. 2b) obtained by an anodic potential sweep in the differential pulse mode, after preconcentration at −1.200 V, showed two well defined peaks, one of them due to reduction of pesticide free in solution and another (at $E = 0.270$ V) due to oxidation of the reduced product at −1.200 V. These results are consistent with those described by Toral *et al.* [18], who suggested that the cathodic peak represented the reduction of the nitro group to hydroxylamine, while the anodic peak was derived from the oxidation of the hydroxylamine to a nitroso derivative. A similar electrochemical behaviour was exhibited by fenitrothion and ethyl- and methyl-parathion because they all have the same electroactive aromatic nitro group.

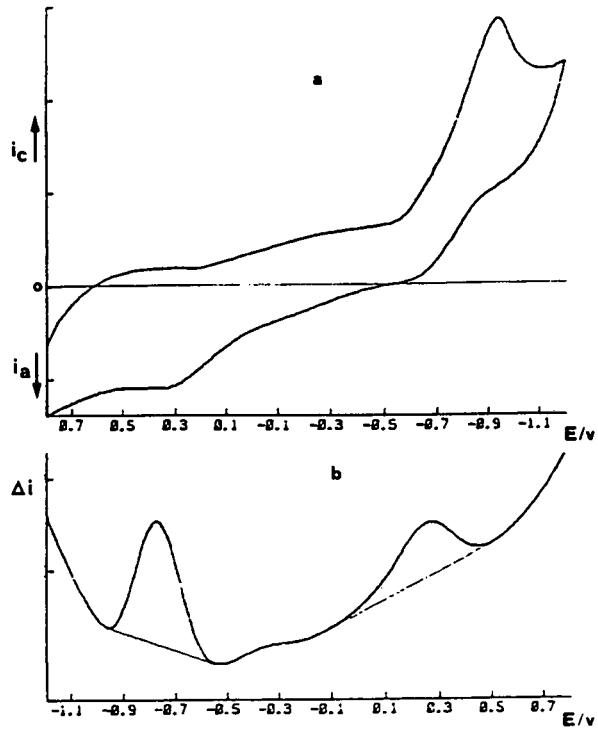

Fig. 2. (a) Cyclic voltammogram for paraoxon. $E_{initial} = 0.800$ V; $E_{final} = -1.200$ V; scan rate, 50 mV/s. (b) Anodic stripping voltammogram. $E_{preconcentration} = -1.200$ V.

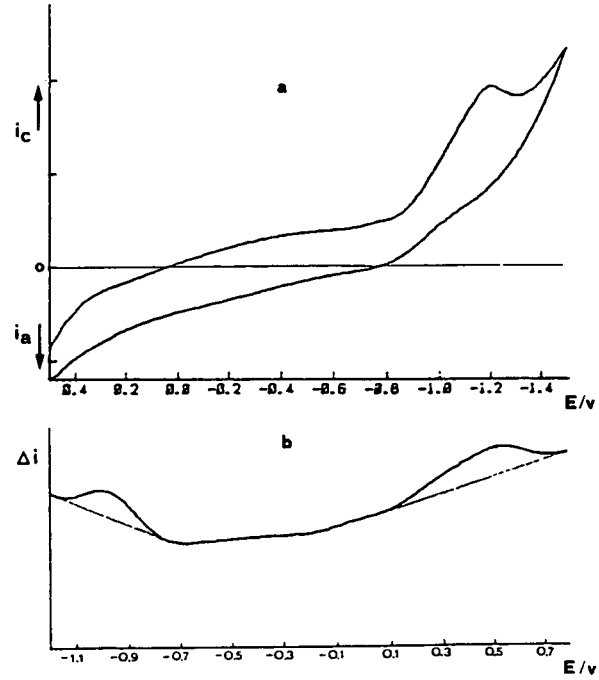

Fig. 3. (a) Cyclic voltammogram for guthion. $E_{initial} = 0.500$ V; $E_{final} = -1.500$ V; scan rate, 50 mV/s. (b) Anodic stripping voltammogram. $E_{preconcentration} = -1.200$ V.

Cyclic and anodic stripping voltammograms for guthion with a glassy carbon electrode are shown in Fig. 3. The voltammograms for this pesticide (which has an –N=N– electroactive group) exhibit a reduction process at more negative potentials (−1.200 V) than the other pesticides investigated, the oxidation of the reduced products having taken place at 0.500 V.

It can be concluded that electrochemical detection is feasible either by using a single working electrode set at a high cathodic potential or with a series dual-electrode device, the upstream electrode operating as a "generator" electrode to convert the analyte into its reduced form which will be detected in the oxidative mode at the downstream "detector" electrode.

Single-electrode detection

The high negative potential required for the reduction of guthion (−1.400 V) makes direct reductive (single-electrode) electrochemical detection of organophosphorus pesticides unsuitable for trace determinations as the residual current and noise level become very high. Thus, detection limits calculated by reductive electro-

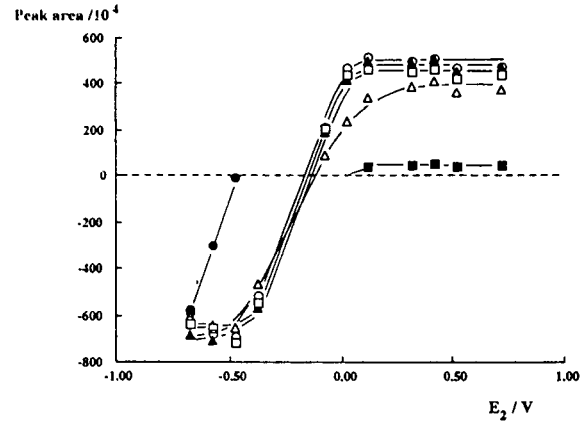

Fig. 4. Influence of downstream electrode potential (E_2) on the analytical signals. Upstream electrode potential $E_1 = -1.200$ V in all experiments. Amount injected, *ca.* 275 ng of each pesticide. Negative peak area means reduction peak. △ = Paraoxon; ■ = guthion; ▲ = methyl-parathion; ○ = fenitrothion; □ = parathion; ● = oxygen.

chemical detection, on a single electrode, are similar to those previously obtained with ultraviolet detection [12], but no improvements are achieved.

Series dual-electrode detection

The primary advantage of the series dual-electrode approach is the ability to employ the upstream electrode as a "generator" electrode essentially ignoring the unwieldy background current and other problems associated with the high potential. The downstream electrode is then the "detector" electrode, which will remain unaffected.

Hydrodynamic voltammograms were obtained considering $E_1 = -1.200$ V as the operating potential for the upstream electrode (W_1) and incrementally changing the potential E_2 of the downstream electrode (W_2) from -0.700 to 0.700 V (Fig. 4). Signals for dissolved oxygen were only obtained when the downstream electrode (W_2) was set at potentials lower than -0.500 V. The responses for paraoxon, methyl-parathion, fenitrothion and ethyl-parathion were very similar, as expected from their similar structures, reaching a limiting plateau at potentials higher than 0.400 V. Guthion did not exhibit an analytically useful response at any of these potentials. It was necessary to set the upstream electrode (W_1) potential at $E_1 = -1.500$ V in order to increase the oxidative current of guthion in the downstream electrode (Table I).

Optimum potential values of $E_1 = -1.500$ V and $E_2 = 0.400$ V for the upstream (W_1) and downstream (W_2) electrodes, respectively, were

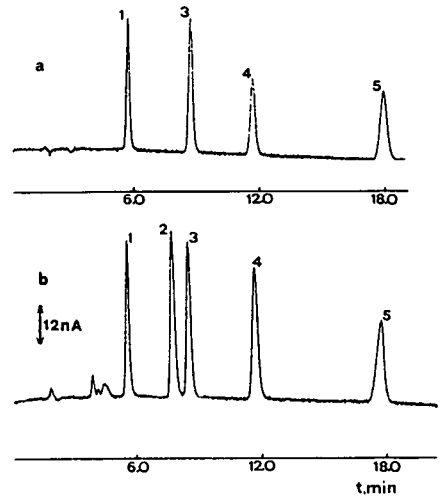

Fig. 5. Chromatogram for dual-electrode detection. (a) Poorly deoxygenated mobile phase and (b) mobile phase continuously deoxygenated by bubbling helium. Experimental conditions and numbers on peaks as described under Experimental.

therefore chosen for further experiments, to permit the most universal practical response for the five pesticides. Under these conditions, an anomalous behaviour for guthion was again observed: no response at all for this pesticide was obtained when the mobile phase was poorly deoxygenated (Fig. 5a); when helium was continuously bubbled through the mobile phase, guthion exhibited a good and reproducible response (Fig. 5b). The electrochemical behaviour of guthion has been described by Hernandez Méndez *et al.* [19]; the electrochemically reduced form of this pesticide is unstable, being subject

TABLE I

INFLUENCE OF UPSTREAM ELECTRODE APPLIED POTENTIAL (E_1) ON THE ANALYTICAL SIGNALS

Downstream electrode potential $E_2 = 0.400$ V in all experiments. Amounts injected as in Fig. 4.

E_1(V)	10^4 Area units				
	Paraoxon	Guthion	Methyl-parathion	Fenitrothion	Parathion
−1.200	384	29	479	487	436
−1.300	416	314	514	523	458
−1.400	406	443	498	499	444
−1.500	374	467	459	456	405

to subsequent chemical reactions with oxygen. According to the reported mechanism, the upstream reduced guthion is oxidized by dissolved oxygen, leading to compounds that are electroinactive at the downstream detector. Therefore, a rigorous and continuous deoxygenation of the mobile phase was required to ensure sufficient removal of any oxygen.

Electrode pretreatment

Solid electrodes are known to be subject to fouling of their surfaces, resulting in decreased sensitivity. At present, there is no simple solution to the problem of electrode poisoning and many procedures have been reported, including electrochemical treatments [20,21], to avoid or minimize the gradual decrease in activity.

To improve the detector performance, different kinds of electrochemical pretreatments were tested, the most efficient being the application to both electrodes of several potential pulses (Fig. 6). Even applying such pretreatment everyday, a gradual diminution of chromatographic signals with time was still observed (Fig. 7a). However, the signal reproducibility was improved when, in addition to this daily pretreatment, a potential of 1.600 V was applied for 5 min to the upstream electrode (W_1) after each injection (Fig. 7b). The possibility of applying a positive potential pulse to the upstream electrode (reduction process) without any noticeable deterioration of the baseline at the downstream detector is another important advantage of series dual-electrode detection that allows the injection to be made once the cleaning pulse is finished. By

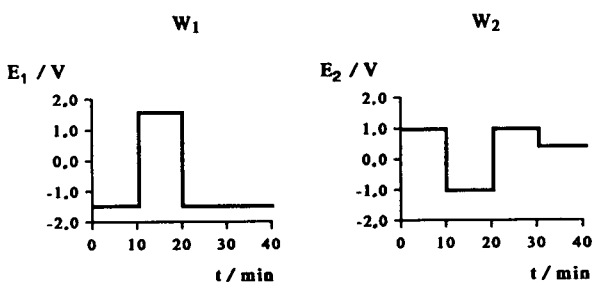

Fig. 6. Electrochemical pretreatment for series dual-electrode detection. Applied potential *versus* time for both electrodes (W_1 and W_2).

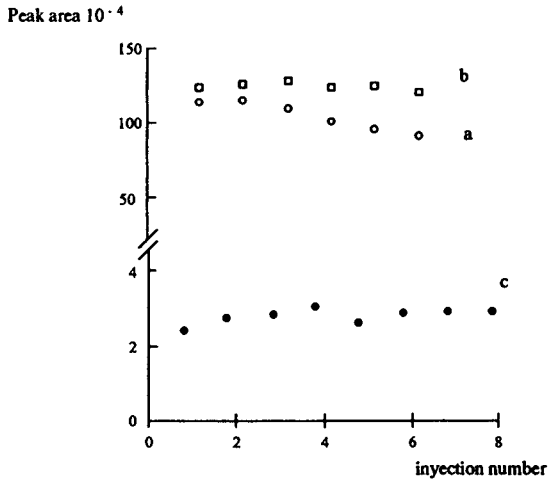

Fig. 7. Enhancement of reproducibility of response with the electrode pretreatment. (a) Signals for 138 ng of paraoxon injected, electrodes being pretreated daily as described in Fig. 6; (b) same as (a) but including an additional step where W_1 was set at 1.600 V for 5 min before each injection; (c) same as (a) for a smaller amount injected (4.2 ng of paraoxon).

using this upstream electrode reactivation step, the precision of the analytical responses for repetitive injections, expressed as their relative standard deviations, were in the range 1.6–4.9%.

As the decrease in electrode performance depends on the concentration injected, it was checked that no upstream electrode (W_1) reactivation was required for injected amounts lower than 20 ng (Fig. 7c).

Influence of flow-rate on the optimum electrochemical detection

Flow-rate is an important parameter in HPLC–ED because it determines not only the chromatographic separation but also the optimum electrochemical detection as hydrodynamic conditions influence the detector response for a given flow cell geometry. The experimental relationship between peak area (A) and flow-rate (q) was as predicted for a thin-layer flow cell configuration [22], fitting the equation $A = \text{constant} \cdot q^{-0.64}$ ($r = 0.98$) in the range investigated (0.50–1.75 ml/min) for all pesticides except guthion. For this pesticide, its behaviour was as expected theoretically only at

flow-rates higher than 0.90 ml/min because at lower flow-rates the electrochemically reduced form of guthion can be chemically oxidized [19] by traces of oxygen in the mobile phase.

Although exhaustive deoxygenation of the mobile phase was shown to be very efficient at moderate flow-rates, at lower flow-rates, when the time delay between upstream reduction and downstream oxidative detection becomes significant, even traces of oxygen in the mobile phase seem to be sufficient for chemical oxidation of the reduction products of guthion and, consequently, a decreased oxidative response at downstream electrode is observed. Hence flow-rates higher than 0.90 ml/min are recommended in order to prevent these products becoming electroinactive before downstream detection.

According to all these results and bearing in mind the requirements for the chromatographic separation [12], a flow-rate of 1.25 ml/min was considered the most appropriate for optimum overall performance.

Analytical data

Under the optimum conditions described above, linear relationships were found between peak area and pesticide concentration over the whole range studied, between about 0.1 and 280 ng injected for each pesticide. The calculated detection limits, for a signal-to-noise ratio of 2, are given in Table II. These values, about 40 pg of injected pesticide, represent a considerable improvement on those reported by Clark *et al.* [11] for electrochemical determination of ethyl- and methyl-parathion with a single-electrode detector (0.8–0.9 ng injected) and to those reported by Ding and Krull [10] for guthion and ethyl-parathion (0.20 and 0.2 mg/l, respectively) using photolysis followed by electrochemical detection. The sensitivity is also ten times higher than that reported for ultraviolet detection [12] under the same chromatographic conditions.

The relative standard deviations at a concentration level of 4.2 ng injected were in the range 4–11% (Table II); the values decreased to 2–5% when 138 ng of each pesticide were injected.

Determination of pesticides in river waters

There is an increasing need for sensitive and reliable methods to determine pesticide concentrations below μg/l levels in natural waters. The maximum concentration of individual pesticides in drinking waters allowed by European Community (EC) legislation is 0.1 μg/l [23]; hence analyte preconcentration prior to HPLC–ED determination is required in order to reach sensitivity levels below the legal limits.

Most reported methods for pesticide analysis involve liquid–liquid extraction for analyte isolation and sample handling, but such procedures frequently require hazardous solvents and make automation of the analysis more difficult. Nowa-

TABLE II

CALIBRATION FITS WITHOUT PRECONCENTRATION

Concentration range between *ca.* 0.1 and 275 ng injected of each pesticide.

Pesticide	Intercept (10^2 area units)	Slope (10^4 area units/mg l^{-1})	Correlation coefficient	R.S.D. (%)[a]		DL (mg/l)[b]
				A	B	
Paraoxon	4.8 ± 3.1	5.57 ± 0.03	0.9998	4.8	1.9	0.004
Guthion	3.4 ± 3.6	5.59 ± 0.03	0.9998	3.7	3.2	0.004
Methyl-parathion	4.8 ± 2.7	6.23 ± 0.03	0.9999	3.5	1.6	0.003
Fenitrothion	5.7 ± 5.6	6.42 ± 0.05	0.9995	4.5	2.5	0.003
Ethyl-parathion	6.8 ± 8.2	5.21 ± 0.08	0.9985	11.0	4.9	0.004

[a] R.S.D. = Relative standard deviation ($n = 10$); (A) 4.2 ng of each pesticide, only daily electrode pretreatment; (B) 138 ng of each pesticide, daily pretreatment plus a pulse of 1.600 V to the upstream electrode (W_1) prior to each measurement.

[b] DL = Detection limit ($2N/m$, where N is the noise and m is the slope of the calibration graph).

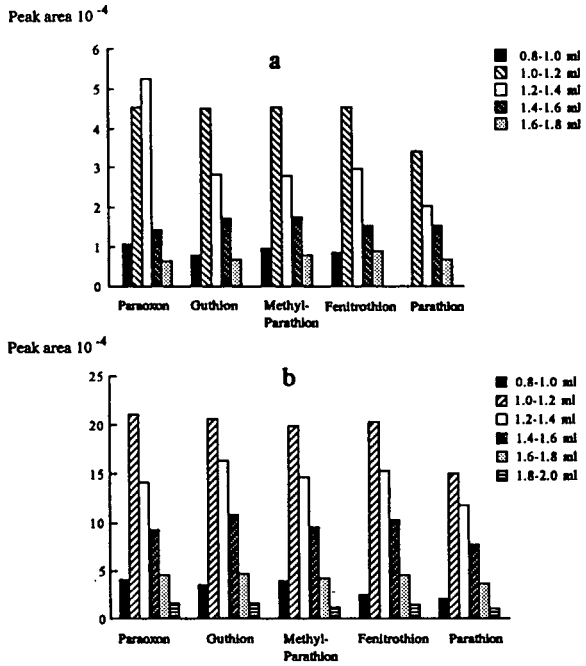

Fig. 8. Elution profiles for each pesticide from different volume fractions collected. (a) 4.2 μg/l; (b) 19 μg/l.

days, investigations are focused on the optimization of solid–liquid extraction procedures.

Standard samples in ultra-pure water were used to check the automated on-line preconcentration system (Fig. 1) in the different steps in the overall process. After sorption of pesticides in the solid-phase cartridge, the latter was eluted with 2.0 ml of methanol; elution profiles for each pesticide were determined by analysing the different volume fractions eluted (0.2 ml each). For the five pesticides and at all concentrations tested (0.1–19 μg/l), the richest fractions were the sixth and the seventh (between 1.0–1.2 and 1.2–1.4 ml) (Fig. 8). Once the richest fractions were known, subsequent studies were made by programming the diluter–injector to collect solely the fraction between 1.0 and 1.4 ml and injecting a 10-μl aliquot.

The experimental relationships between peak area and pesticide concentration in water samples were found to be linear over the whole range tested (Table III). Detection limits, calculated at a signal-to-noise ratio of 2, were 0.03 μg/l for ethyl-parathion and 0.02 μg/l for all others pesticides investigated, all of them being 3–5 times lower than the legal limits allowed in drinking waters. The lowest detectable concentration can be improved by using sample volumes greater than 100 ml; the recovery data obtained showed that no loss of pesticide occurred on increasing the water volume passed through the extraction cartridge from 100 to 1000 ml. Relative standard deviations for ten replicates at concentration levels of 4.2 and 0.2 μg/l are also given in Table III.

In order to check the applicability of the proposed method to real matrices, river water samples from different points of the Tormes river (Salamanca, Spain) were analysed (Fig. 9).

TABLE III

CALIBRATION FITS WITH PRECONCENTRATION

Concentration range between *ca.* 0.1 and 6 μg/l of each pesticide. Preconcentration of 100 ml of sample.

Pesticide	Intercept (10^3 area units)	Slope (10^3 area units/μg l^{-1})	Correlation coefficient	R.S.D. (%)[a]		DL (μg/l)[b]
				A	B	
Paraoxon	−1.2 ± 0.8	8.5 ± 0.2	0.9991	9.4	12.3	0.02
Guthion	−2.1 ± 0.9	9.3 ± 0.2	0.9992	6.8	10.8	0.02
Methyl-parathion	−0.9 ± 0.8	9.3 ± 0.2	0.9990	6.4	8.6	0.02
Fenitrothion	0.3 ± 0.5	9.0 ± 0.1	0.9997	8.6	10.9	0.02
Ethyl-parathion	1.3 ± 0.5	6.9 ± 0.1	0.9994	9.3	12.8	0.03

[a] R.S.D. = Relative standard deviation (n = 10). Fortification level: (A) 4.2 μg/l; (B) 0.2 μg/l.
[b] DL = Detection limit, defined as in Table II.

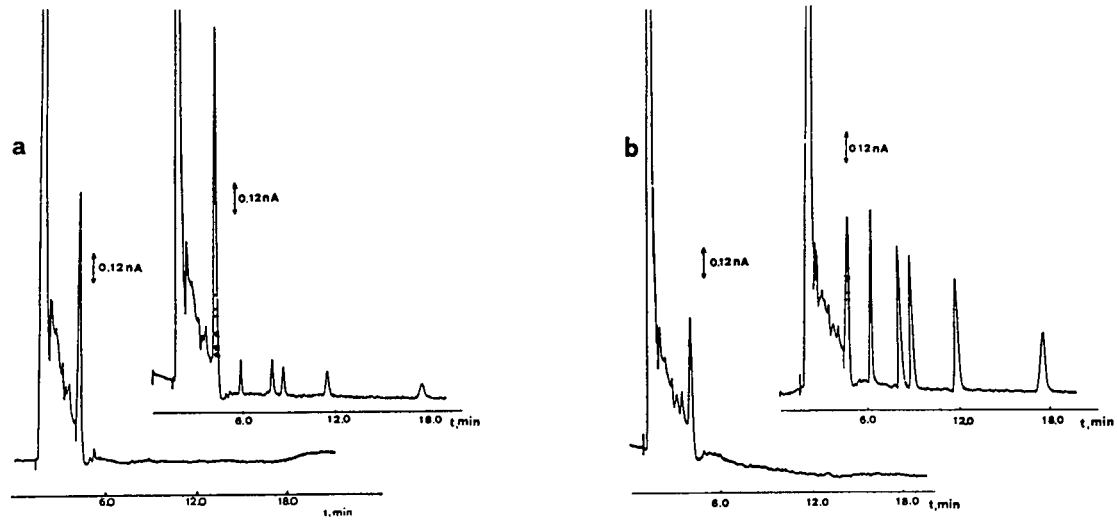

Fig. 9. Chromatograms of river water samples from different points of the Tormes river fortified at (a) 0.2 and (b) 1.4 μg/l.

A 100-ml aliquot of each sample was firstly analysed following the same procedure to provide ambient-level analyte concentrations; none of the samples showed naturally occurring pesticides. Samples were then fortified at four concentration levels between *ca.* 0.2 and 2 μg/l of each pesticide. The analytical recoveries from this matrix ranged from 84% to 124% (Table IV).

TABLE IV

PESTICIDE RECOVERIES FROM RIVER WATER SAMPLES

Pesticide	Fortification level (μg/l)	Recovery (%)	*n*
Paraoxon	0.20	114	2
	0.42	108	2
	1.47	91	4
	2.11	105	4
Guthion	0.20	124	2
	0.44	113	2
	1.73	84	4
	2.22	103	4
Methyl-parathion	0.19	100	2
	0.41	112	2
	1.62	86	4
	2.15	109	4
Fenitrothion	0.20	100	2
	0.44	113	2
	1.66	90	4
	2.20	109	4
Ethyl-parathion	0.20	98	2
	0.44	95	2
	1.57	92	4
	2.26	100	4

CONCLUSIONS

HPLC coupled with dual electrochemical detection in the reductive–oxidative mode was applied to multi-residue organophosphorus pesticide analysis, the proposed method being more sensitive than all other HPLC methods previously reported. An improvement in electrochemical detection by using a series dual-electrode detector was established; the possibility of activation of the upstream electrode by applying a high-potential pulse prior to each analysis, without any baseline deterioration at the downstream detector, is an important advantage of the series dual-electrode configuration, not previously reported; this treatment was shown to be the best way to obtain good signal reproducibility independent of the working time (without problems of electrode surface activity).

In the computer-controlled on-line preconcentration scheme proposed, problems with analyte losses or contamination are minimal because the extracts could be injected automatically into the

chromatographic system, having the important advantage of eliminating the solvent-removal step, which in some instances is extremely critical. The linearity of the calibration graphs show the integrity of the overall system, including adsorption, desorption, chromatographic separation and dual-electrode detection. The limits of sensitivity of this method for organophosphorus pesticides were set at sub-pg levels by sampling only 100 ml of water, whereas most extraction procedures require 1–2 l of water. The relative standard deviations obtained are in an acceptable range for trace analysis.

The method of on-line preconcentration with an automated sampling device provides a rapid and easy means of pesticide trace enrichment prior to their analysis by HPLC and it is obviously advantageous from the viewpoint of sensitivity, rapid sample handling and costs, when large monitoring programmes are to be performed.

ACKNOWLEDGEMENT

The Dirección General de Investigación Científica y Técnica (DGICYT, Spain) is gratefully acknowledged for financial support of this work (Project No. PB89-0397).

REFERENCES

1 D. Barceló, *Analyst*, 116 (1991) 681–698.
2 E.R. Brouwer, H. Lingeman and U.A.Th. Brinkman, *Chromatographia*, 29 (1990) 415–422.
3 D.C. Paschal, R. Bicknell and D. Dresbach, *Anal. Chem.*, 49 (1977) 1551–1554.
4 V. Pacakova, K. Stulik and M. Prihoda, *J. Chromatogr.*, 442 (1988) 147–161.
5 R.E. Shoup (Editor), *Bibliography of Recent Reports of Electrochemical Detection*, BAS Press, West Lafayette, IN, 1981.
6 W.J. Bachman and J.T. Stewart, *J. Chromatogr.*, 481 (1989) 121–133.
7 C.E. Lunte, P.T. Kissinger and R.E. Shoup, *Anal. Chem.*, 57 (1985) 1541–1548.
8 L.A. Allisson and R.E. Shoup, *Anal. Chem.*, 55 (1983) 8–12.
9 J.G. Koen and J.F.K. Huber, *Anal. Chim. Acta*, 51 (1970) 303–307.
10 X.D. Ding and I.S. Krull, *J. Agric. Food Chem.*, 32 (1984) 622–628.
11 G.J. Clark, R.R. Goodin and J.W. Smiley, *Anal. Chem.*, 57 (1985) 2223–2228.
12 R. Carabias Martínez, E. Rodríguez Gonzalo, M.J. Amigo Morán and J. Hernández Méndez, *J. Chromatogr.*, 607 (1992) 37–42.
13 C.H. Marvin, I.D. Brindle, C.D. Hall and M. Chiba, *J. Chromatogr.*, 503 (1990) 167–176.
14 M.W.F. Nielen, U.A.Th. Brinkman and R.W. Frei, *Anal. Chem.*, 57 (1985) 806–810.
15 T.A. Bellar and W.L. Budde, *Anal. Chem.*, 60 (1988) 2076–2083.
16 R.B. Geerdink, C.A. van Balkom and H.J. Brouwer, *J. Chromatogr.*, 481 (1989) 275–280.
17 I. Liska, E.R. Brouwer, A.G.L. Ostheimer, H. Lingeman, U.A.Th. Brinkman, R.B. Geerdink and W.H. Mulder, *Int. J. Environ. Anal. Chem.*, 47 (1992) 267–291.
18 M.I. Toral, P. Ritcher and A. Miranda, *An. Quim. B*, 86 (1990) 461–466.
19 J. Hernández Méndez, R. Carabias Martínez and E. Rodríguez Gonzalo, *J. Electroanal. Chem.*, 244 (1988) 221–233.
20 J. Wang and L.D. Hutchins, *Anal. Chim. Acta*, 167 (1985) 325–334.
21 G. Sittampalam and G.S. Wilson, *Anal. Chem.*, 55 (1983) 1608.
22 J.M. Elbicki, D.M. Morgan and S.G. Weber, *Anal. Chem.*, 56 (1984) 978–985.
23 EEC Drinking Water Guideline 80/778/EEC, *Off. J. Eur. Commun.*, No. L229/11-29, August 30th (1980).

Journal of Chromatography, 644 (1993) 59–71
Elsevier Science Publishers B.V., Amsterdam

CHROM. 25 033

Reversed-phase high-performance liquid chromatographic determination of linear alkylbenzene sulphonates, nonylphenol polyethoxylates and their carboxylic biotransformation products

Antonio Marcomini*

Department of Environmental Sciences, University of Venice, Calle Larga S. Marta 2137, I-30123 Venice (Italy)

Antonio Di Corcia and Roberto Samperi

Department of Chemistry, University La Sapienza, P.le A. Moro 5, I-00195 Rome (Italy)

Silvio Capri

Water Research Institute (CNR–IRSA), via Reno 1, I-00198 Rome (Italy)

(First received December 11th, 1992; revised manuscript received March 3rd, 1993)

ABSTRACT

The possibility was investigated of simultaneously determining linear alkylbenzene sulphonates, nonylphenol polyethoxylates and their respective biotransformation products, namely sulphophenyl carboxylates (SPC) and nonylphenoxy carboxylates, by reversed-phase high-performance liquid chromatography with UV and fluorescence detection. Both the ion-suppression and the ion-pair techniques were taken into account for separating the compounds of interest. Each technique exhibited peculiar characteristics of resolution and sensitivity. Differences in the selectivity of the chromatographic system on using either methanol or acetonitrile as organic modifier were also considered. Liquid–solid extraction by an octadecyl-bonded silica (C_{18}) cartridge was employed to isolate all the compounds considered from a sewage treatment plant effluent sample. The recovery of SPC with up to six carbons in the carboxylate chain was unsatisfactory. The SPC distribution appeared to be dominated by the homologues having 5–8 carbon atoms in the carboxylate chain.

INTRODUCTION

Linear alkylbenzene sulphonates (LAS) and alkylphenol polyethoxylates (NPEO) are anionic and non-ionic surfactants widely used in domestic and industrial detergents, respectively. The annual world production was 1.8 million tons of LAS in 1987 [1] and *ca.* 0.3 million tons of NPEO in 1990 [2]. The structures of LAS, NPEO and their biotransformation products are shown in Fig. 1. LAS are present in commercial formulations as complex mixtures of C_{10}–C_{13} homologues and of positional isomers resulting from the attachment of the phenyl ring to the carbon atoms (from the second to the central one) of the linear alkyl chain. Commercial NPEO are mixtures of oligomers and isomers, the latter involving different degrees of branching of the alkyl chain.

Laboratory biodegradation studies showed sulphophenyl carboxylates (SPC) to be the only

* Corresponding author.

0021-9673/93/$06.00

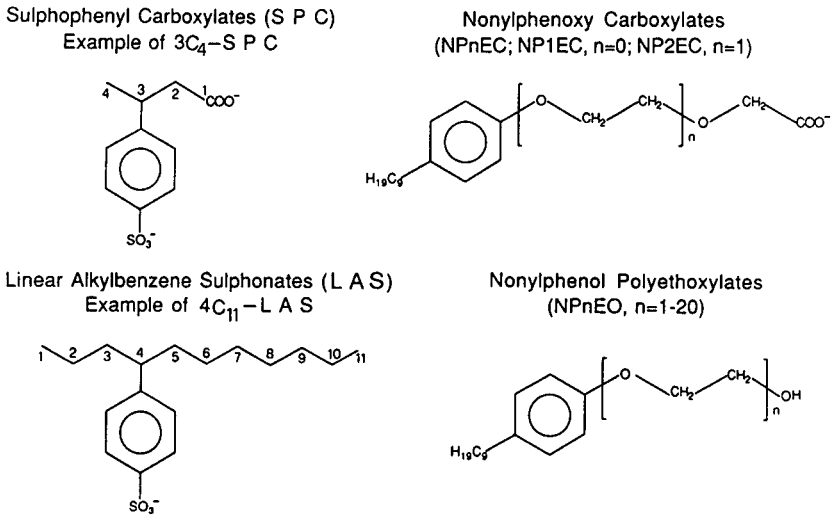

Fig. 1. Structures and abbreviations of sulphophenyl carboxylates (SPC), nonylphenoxyacetic acid (NP1EC) and nonylphenoxyethoxyacetic acid (NP2EC), linear alkylbenzene sulphonates (LAS) and nonylphenol polyethoxylates (NPEO).

biodegradation intermediates of LAS [3,4]. From these studies, it was believed that short-chain SPC could be the most probably occurring LAS metabolites in aqueous environmental samples. A recent investigation, however, identified in treated sewage and groundwater samples SPC containing 3–10 carbon atoms in the alkyl chain [5].

Nonylphenoxy carboxylic acids (NPEC) are formed by biodegradation of NPEO under aerobic conditions [6], especially during activated sludge treatment in sewage treatment plants (STPs) [7]. They constitute the majority of NPEO biodegradation products in the secondary effluent of STPs, together with lower NPEO oligomers (NP1EO and NP2EO) and the completely de-ethoxylated product nonylphenol (NP) [8]. The only NPEC detected in environmental samples were NP1EC and NP2EC [7]. In contrast to SPC, NPEC retain surface-active properties.

High-performance liquid chromatography (HPLC) [9–19] has been preferred to gas chromatography (GC) or GC–mass spectrometry (GC–MS) [20–24] for the specific routine determination in environmental samples of both LAS and NPEO, as it does not require derivatization of LAS and of the higher NPEO oligomers. Another great advantage shown by RP-HPLC over the GC techniques is that the simultaneous determination of both LAS and NPEO using octyl- or octadecylsilica columns is possible [25,26]. In this instance, the LAS components are eluted according to the alkyl chain length and the attachment position of the phenyl ring in the alkyl chain, whereas the NPEO oligomers are eluted as a single peak as the chromatographic process is mainly governed by non-specific interactions occurring between the branched alkyl chain and the stationary phase. So far, few analytical procedures have been developed for determining SPC [27–30] and NPEC [7,24,31]. Most of them involved the use of GC or GC–MS techniques. The SPC were derivatized to methyl [29] or trifluoroethyl esters [30] or altered by desulphonation [28,29]. The NPEC were esterified by methylation [7]. Unaltered SPC were determined by ion-pair RP-HPLC with UV detection [32]. NPEC were analysed by normal-phase HPLC after derivatization to methyl esters [7]. The lack of commercially available standards is presumably the main cause of the scarce information on the environmental behaviour of individual SPC and NPEC.

The main objective of this work was to develop a "tailor-made" RP-HPLC system able to

yield the best fractionation of a complex mixture, such as that containing SPC, NPEC and their respective LAS and NPEO precursors. For this purpose, we evaluated the selectivity characteristics offered by the ion-suppression and the ion-pair HPLC techniques. Ion-pair HPLC was employed by adding to the mobile phase either a tetraalkylammonium salt or an inorganic salt, such as sodium perchlorate. The addition of this salt to the mobile phase has been widely adopted for fractionating LAS mixtures. A secondary objective was to evaluate the ability of an octadecyl-bonded silica (C_{18}) cartridge to extract from both treated and untreated wastewaters the compounds considered. This was done by suitably modifying previously reported methods [33,34].

EXPERIMENTAL

Materials and reagents

The LAS and NPEO standards were purchased from Carlo Erba (Milan, Italy). The average alkyl chain length of the C_{10}–C_{13} LAS mixture was $C_{11.2}$. The average polyethyoxylic chain length of NP*n*EO (n = 1–20) was 8.8. Pure C_{14} LAS homologue was kindly supplied by EniChem (Milan, Italy). Technical nonylphenol (NP) was obtained from Fluka (Buchs, Switzerland). A 75:25 (w/w) mixture of nonylphenol mono- (NP1EO) and diethoxylate (NP2EO) was obtained from Kolb (Hedingen, Switzerland). Most of the phenylalkanoic acids (phenylacetic, 2-phenylpropionic, 4-phenylbutyric, 5-phenylvaleric and phenylmalonic) were obtained from Fluka; 2- and 3-phenylbutyric and 3-phenylglutaric acid were purchased from Aldrich (Milwaukee, WI, USA). The solvents used for the syntheses were purchased from Carlo Erba and those for HPLC from Riedel-de Haën (Seelze, Germany). The HPLC mobile phase modifiers trifluoroacetic acid (TFA) and tetrabutylammonium dihydrogenphosphate (TBA-H_2PO_4) were supplied by Aldrich; sodium perchlorate was from Merck (Darmstadt, Germany). C_{18} extraction cartridges (1 g) were purchased from Supelco (Bellefonte, PA, USA). The cartridge was preconditioned with 5 ml of acetonitrile and 5 ml of methanol followed by 10 ml of distilled water.

Synthesis and characterization of carboxylic biodegradation intermediates

Synthesis of sulphophenyl carboxylates (SPC). The SPC were synthesized by sulphonation of the corresponding commercially available phenylalkanoic acids according to conditions reported by Taylor and Nickless [32]. Briefly, 20 ml of sulphuriç acids were added to 5 g of phenylcarboxylic acid and heated at 60°C with gentle stirring for 24 h. Unreacted starting material was removed with 2 × 100 ml of diethyl ether and the resulting solution was neutralized with NaOH. Three volumes of 2-propanol were added to precipitate the sodium sulphate and the mixture was left in a refrigerator overnight. The supernatant solution was filtered and evaporated to dryness on a rotary evaporator. The solid white residue was dissolved in hot methanol and reprecipitated by adding diethyl ether. Recrystallization was carried out in triplicate. The yields obtained were about 50% for monocarboxylic SPC and about 10% for bicarboxylic SPC. The sulphophenyl monocarboxylates $2C_2$-SPC, $3C_3$-SPC, $2C_4$-SPC, $3C_4$-SPC, $4C_4$-SPC and $5C_5$-SPC, and the bicarboxylates C_3-SP2C and $3C_5$-SP2C were synthesized.

Synthesis of nonylphenoxyacetic acids (NPEC). Both nonylphenoxyacetic acid (NP1EC) and nonylphenoxyethoxyacetic acid (NP2EC) were prepared by oxidation with Jones reagent (method A, see below) [23]. In addition, NP1EC was synthesized by reaction of chloroacetic acid with nonylphenol (NP) in an alkaline aqueous solution (method B) according to suitably modified conditions reported previously [35]. A common procedure was followed for the product purifications.

In method A, 11 g of NP1EO–NP2EO (75:25) mixture were added with stirring at 60°C to 100 ml of Jones reagent during 6 h. Heating of the solution was continued for about 10 h, then the mixture was left at room temperature. The desired products were recovered from the mixture by dilution with water (*ca.* 400 ml) followed by extraction with diethyl ether (8 × 100 ml). The combined green extracts were washed first

with 5% aqueous sulphuric acid (5 × 50 ml) and then with water. A green viscous oil was obtained after evaporation to dryness.

In method B, 22 g of nonylphenol were dissolved in 10 ml of ethanol. To this solution, 20 ml of aqueous NaOH and 20 ml of chloroacetic acid were added dropwise three times, at 1-h intervals. The pH during the reaction was maintained at *ca.* 10 with aqueous sodium hydroxide. The resulting solution after acidification to pH 4 and cooling was extracted with diethyl ether. The extracts obtained were washed with water, evaporated to dryness on a rotary evaporator and dried over magnesium sulphate.

The NP1EC–NP2EC mixture and NP1EC synthesized by the above two methods were purified by silica gel chromatography using a 40 × 2 cm column packed by suspending the sorbent in chloroform. The sorbent material (30–70-mesh silica; Merck) was activated at 110°C for 24 h. Aliquots of the dry residues were dissolved in a minimum volume of chloroform, transferred to the top of the column and eluted with the same solvent (500 ml). The NP1EC–NP2EC mixture obtained by method A and NP1EC obtained by method B were found in the third fraction (last 100 ml), after those containing a yellow side-product (first 100 ml) and unreacted 4-nonylphenol (next 100 ml).

Characterization of the synthesized compounds. Both SPC and NPEC were characterized by elemental analysis (Carlo Erba NA 1500 C, H, N analyzer), UV (Perkin-Elmer Lambda 5) and IR (Perkin-Elmer Model 683) spectrophotometry and ^{1}H NMR spectroscopy (Varian FT 80 A). Based on elemental analysis results, the purity of each compound, calculated from the difference between the observed recovery and the calculated recovery averaged for each element, was between 92% and 98%. The UV maxima were between 215 and 225 nm, with molar absorptivities in 1:1 water–acetonitrile of 9550–12 200 l mol^{-1} cm^{-1} for SPC and 9150–9360 l mol^{-1} cm^{-1} for NP1EC and NP2EC, respectively. The proton NMR spectra of SPC in ^2H_2O, showing a pseudo-quartet of the four aromatic protons at δ 7.60 (reference tetramethylsilane), confirmed that sulphonation had occurred at the *para* position.

HPLC apparatus and conditions

The method development work was performed on a Hewlett-Packard Model 1050 liquid chromatograph consisting of a quaternary pump, a four-bottle solvent-delivery system and a Rheodyne syringe-loading sample injector (Model 7125). The data were collected and treated by an electronic integrator (Hewlett-Packard Model 3396A). Fluorescence detection was performed by a Hewlett-Packard Model 1046A instrument (flow cell volume 10 μl). The detector was operated with an excitation wavelength of 225 nm and an emission wavelength of 295 nm, with a spectral band pass of 10 nm.

The chromatographic separation was performed in the reversed-phase mode by using an octadecylsilica column (LiChrospher RP-18, 250 × 4 mm I.D., 5-μm particle size, from Merck) equipped with a guard column and operated at room temperature.

Elution was carried out in the gradient mode, at a flow-rate of 1.0 ml min^{-1}, using aqueous acetonitrile and aqueous methanol containing alternatively $NaClO_4$, TFA and $TBAH_2PO_4$ as phase modifiers. In presence of $TBAH_2PO_4$, the pH was adjusted to 5.5 with 0.1 *M* NaOH.

The following elution programmes were used depending on the type of mixture and phase modifier.

Water–acetonitrile containing $NaClO_4$:
solvent A, acetonitrile; solvent B, water containing 14 g l^{-1} $NaClO_4$:
0– 3 min 40% A–60% B
3–23 min linear gradient to 30% B
23–26 min linear gradient to 10% B
26–30 min linear gradient to 60% B
30–32 min 40% A–60% B

Water–acetonitrile containing TFA:
solvent A acetonitrile; solvent B, water containing 0.14 g l^{-1} TFA; solvent C, water:
0 – 0.5 min 5% A–40% B–5% C
0.5–10 min linear gradient to 60% A and 40% C
10 –20 min linear gradient to 90% A and 10% C
20 –23 min 90% A–0% B–55% C
23 –28 min linear gradient to 5% A–40% B–55% C

Water–acetonitrile containing $TBAH_2PO_4$:
solvent A, acetonitrile; solvent B, water containing 3.4 g l^{-1} $TBAH_2PO_4$; solvent C, water:
0 – 0.1 min 35% A–32.5% B–32.5% C
0.1– 8 min linear gradient to 70% A–15% B–15% C
8 –15 min linear gradient to 90% A–5% B–5% C
15 –19 min linear gradient to 75% A–12.5% B–12.5% C
19 –23 min linear gradient to 35% A–32.5% B–32.5% C

Water–acetonitrile containing both $NaClO_4$ and TFA:
solvent A, acetonitrile; solvent B, water containing 0.14 g l^{-1} TFA; solvent C, water containing 14 g l^{-1} $NaClO_4$; solvent D, water:
0 – 0.5 min 5% A–40% B–0% C–55% D
0.5–10 min linear gradient to 60% A–0% B–20% C–20% D
10 –20 min linear gradient to 90% A–0% B–0% C–10% D
20 –28 min linear gradient to 5% A–40% B–0% C–55% D

Water–methanol containing $NaClO_4$:
solvent A, methanol; solvent B, water containing 14 g l^{-1} $NaClO_4$:
0–15 min 60% A–40% B
15–20 min linear gradient to 20% B
20–23 min 80% A–20% B
23–26 min linear gradient to 10% B
26–30 min linear gradient to 40% B

Water–methanol containing TFA:
solvent A, methanol; solvent B, water containing 0.14 g l^{-1} TFA; solvent C, water:
0–10 min 5% A–95% B–0% C
10–20 min linear gradient to 60% A and 40% C
20–30 min linear gradient to 70% A and 30% C
30–32 min linear gradient to 85% A and 15% C
32–37 min linear gradient to 5% A–95% B–0% C

Water–methanol containing $TBAH_2PO_4$:
solvent A, methanol; solvent B, water containing 3.4 g l^{-1} $TBAH_2PO_4$; solvent C, water:
0 – 0.1 min 20% A–50% B–0% C–30% D
0.1–10 min linear gradient to 60% A–0% B–8% C–32% D
10 –20 min linear gradient to 70% A–0% B–6% C–24% D
20 –28 min linear gradient to 85% A–0% B–3% C–12% D
28 –34 min 85% A–0% B–3% C–12% D
34 –39 min linear gradient to 20% A–50% B–0% C–30% D

Water–methanol containing both $NaClO_4$ and TFA:
solvent A, methanol; solvent B, water containing 0.14 g l^{-1} TFA; solvent C, water containing 14 g l^{-1} $NaClO_4$; solvent D, water:
0 – 0.5 min 5% A–40% B–0% C–55% D
0.5–10 min linear gradient to 60 % A–0% B–20% C–20% D
10 –20 min linear gradient to 90% A–0% B–0% C–10% D
20 –28 min linear gradient to 5% A–40% B–0% C–55% D

Samples

Influent and final effluent water were 24-h composite samples. They were taken from mechanical–biological sewage treatment facilities. All specimens were immediately passed through glass-fibre filters (0.2 μm) (Whatman), 1% of formaldehyde (37%; Merck) was added and the mixtures were stored at 4°C.

Isolation and identification procedures

The isolation of SPC and NPEC, and of LAS and NPEO, from filtered (0.2-μm glass-fibre filters; Whatman) aqueous samples was carried out by the following two procedures. One involved the removal of water by rotary evaporation of 10 ml of influent, 50 ml of final effluent and 200 ml of river water. The semi-dried residue was dissolved by ultrasonication for 5 min in 5 ml of methanol containing 0.05 *M* sodium dodecyl sulphate (SDS) that was used to aid the resolubilization of the surfactants. The aqueous methanol extracts were concentrated by evaporation on a steam-bath to *ca.* 0.5–2 ml, depending on the type of sample. The alternative isolation procedure followed in this work em-

ployed commercially available C_{18} extraction cartridges. After acidification of the aqueous sample with HCl (pH 2) and conditioning of the cartridge as described above, 10 ml of influent, 50 ml of effluent and 200 ml of river water were passed through the C_{18} cartridge. After extraction, SPC, NPEC, LAS and NPEO were eluted with 5 ml of methanol. Blow-down of the methanolic eluate was carried out in a water-bath under a stream of nitrogen to 0.5–1.5 ml, depending on the type of sample.

The SPC and NPEC in environmental aqueous samples were identified both from the retention times and by external addition of both the synthesized compounds and a series of SPC which were obtained by LAS biodegradation experiments. The latter were formed during the run of the Modified OECD Biodegradation Screening Test [36] carried out under mild inoculum (fertile soil) conditions [37,38]. Analysis performed by both GC–MS and RP-HPLC provided the identification and quantification of isomers of the C_6–C_8 SPC homologues (*i.e.*, 2,3C_6-SPC, 3,4C_7-SPC and 3,4,5C_8-SPC) and of bicarboxylate SPC not synthesized, namely the succinic (C_4-SP2C) and adipic (C_6-SP2C) compounds. The amounts of biologically generated SPC were sufficiently high to allow standard addition and recovery experiments to be carried out [37,38].

Quantification

SPC, NPEC, LAS and NPEO were determined using calibration graphs. When necessary, the standard addition method was applied to the determination of the compounds considered in environmental samples. The calibration graphs were obtained by dissolving in water–acetonitrile (50:50, v/v) 0.02–0.25 mg ml^{-1} of LAS, 0.005–0.15 mg ml^{-1} of NPEO and 0.002–0.08 mg ml^{-1} of each synthesized SPC and NPEC compound. Recovery experiments and standard additions were performed by adding to the aqueous environomental sample prior to the extraction or to the final extracts, respectively, 5–125 μg of each compound class. The additions were made according to the criterion of approximately doubling the original concentrations.

By using $NaClO_4$ as phase modifier, SPC were eluted as a single peak. In this instance, the calibration graph was constructed using the biologically generated SPC because their distribution was similar to that found in the environmental samples.

The column injection volumes of both standard solutions and environmental samples were 20–100 μl and contained *ca.* 0.6–12 μg of SPC, 0.4–7.5 μg of LAS, 0.05–1.4 μg of NPEC and 0.1–4.5 μg of NPEO.

RESULTS AND DISCUSSION

The chromatographic behaviours of the components of the mixtures containing the surfactants and some of their synthesized biointermediates were altered by varying both the organic modifier, namely acetonitrile and methanol, and the phase modifier, that is $NaClO_4$, trifluoroacetic acid (TFA) and tetrabutylammonium dihydrogenphosphate ($TBAH_2PO_4$). For the sake of clarity, the effects observed on adding the three phase modifiers, individually or in combination, to water–acetonitrile mixtures will be discussed separately from those obtained with water–methanol mixtures.

With water–acetonitrile mixtures

The chromatograms showing the separations of the considered compounds obtained by gradient elution of aqueous acetonitrile mixtures containing (A) $NaClO_4$, (B) TFA, (C) $TBAH_2PO_4$ and (D) both $NaClO_4$ and TFA are shown in Fig. 2. As already indicated, to determine LAS by RP-HPLC, mobile phases of different compositions containing almost invariably relatively high concentrations of $NaClO_4$ as ion-pair phase modifier have frequently been proposed [9–15]. By considering the nature of the counter ion, this chromatographic system could be called "soft" ion-pair chromatography. By suitably adjusting some chromatographic parameters, the capacity of this technique for fractionating the mixture of interest was evaluated (Fig. 2A). As can be seen, both SPC and the two NPEC were eluted before LAS and NPEO, as expected considering that the first two compound classes are more polar

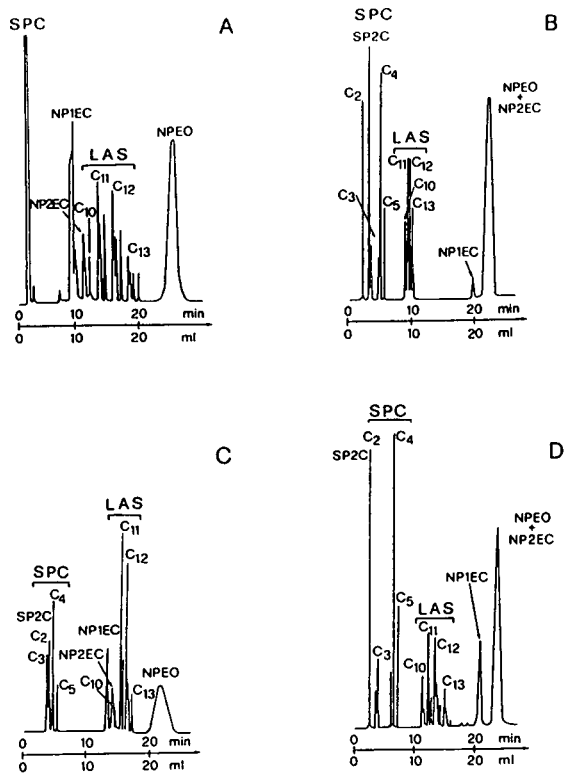

Fig. 2. RP-HPLC-fluorescence detection chromatograms showing the elution of SPC, LAS, NPEC and NPEO with aqueous acetonitrile mixtures containing (A) $NaClO_4$, (B) TFA, (C) $TBAH_2PO_4$ and (D) both $NaClO_4$ and TFA.

than the third [39]. The eight synthesized SPC were only weakly retained by the stationary phase and eluted into two peaks. Several factors suggest that this technique is impracticable for determining SPC. From a qualitative point of view, no information can be obtained about the metabolic pathway of LAS. From a quantitative point of view, there is a high probability that extraneous compounds are co-eluted with SPC, resulting in overestimation of the LAS intermediates. This risk is greatly increased when using a non-selective detector, such as a UV detector. Even when using fluorescence detection, however, the quantification is made difficult if no information on the average distribution of SPC is available, as the signal intensity per unit mass decreases as the alkyl chain length of the SPC homologues is increased.

Concerning the two NPEO metabolites, NP1EC was completely resolved, but the peak for NP2EC was only partially resolved from those for the innermost isomers of the C_{10} LAS.

By comparing chromatographs obtained under the various conditions selected, it appears that the positive feature of using $NaClO_4$ as a phase modifier is that partial separations of positional isomers of LAS, and also the separation of NP1EC and partial separation of NP2EC from the innermost C_{10} LAS isomers, were obtained. The elution order of the positional isomers for each LAS homologue followed that of decreasing distance of the substituent phenyl group from the end of the alkyl chain. Although incomplete, this separation may be of interest when rapid information on the biodegradation rate of the various LAS isomers is desired.

The separation of the SPC components was achieved by using the ion-suppression technique (Fig. 2B). With the TFA concentration selected, the term partial ion suppression should more correctly be used. In fact, by increasing the amount of TFA dissolved in the mobile phase, a continuous increase in the retention times of LAS was noted to the point (corresponding to about 5 g l^{-1} TFA) that the peak for the highest LAS homologue overlapped that for NP1EC. Under the conditions selected, the elution order of SPC was $2C_2$-SPC, C_3-SP2C + $3C_5$-SP2C, $3C_3$-SPC, $2C_4$-SPC + $3C_4$-SPC + $4C_4$-SPC, $5C_5$-SPC.

Compared with the previous situation, this offers several advantages. One is that the resolution of the SPC mixture decreases the probability of overestimation of LAS biointermediates by unknown compounds. The second is that all of the isomers of each SPC homologue are lumped into one peak. This makes the determination of SPC in real water samples easy to perform by using a few synthesized SPC compounds and assuming that all of the isomers of each homologue exhibit the same fluorescence quantum yield. Finally, although not detailed, rapid information on the metabolic pathway of LAS can be achieved.

For the LAS mixture, all of the isomers of each homologue were co-eluted in a single peak. This effect can be advantageously exploited for the routine determination of traces of LAS, as

the peak for each homologue increases in intensity.

Compared with the results obtained by using $NaClO_4$, the most dramatic effect obtained on suppressing the ionization of NPEC was that they were eluted well after LAS and near NPEO with the peak for NPEC overlapped by that for its parent compounds. These effects can be explained by considering that non-ionized NPEC have a higher affinity for the stationary phase than partially dissociated LAS. In addition, interactions occurring between the stationary phase and the branched alkyl chain, common to both NPEO and NPEC, play a dominant role in determining close elutions of the two compound classes.

By classical ion-pair chromatography, achieved by using a tetralkylammonium salt as phase modifier (Fig. 2C), the elution sequence of the four classes of compounds was the same as that obtained with $NaClO_4$ as phase modifier. On the other hand, the TBA^+ naked ion was more effective than Na^+ in forming stable, hydrophobic ion pairs with SPC. As a result, they were retained by the stationary phase and, thus, partially separated from each other. The elution order of SPC was $2C_2$-SPC + $3C_3$-SPC, C_3-SP2C + $3C_5$-SP2C, $2C_4$-SPC + $3C_4$-SPC + $4C_4$-SPC, $5C_5$-SPC. It appears that the addition of an ion-pair-forming agent to the mobile phase did not allow the separation of the C_2 from the C_3 SPC homologue which was achieved by the ion-suppression retention mechanism. This was due in part to the fact that derivative formation, as occurs with the ion-pair technique, tends to obscure small differences in the chemical characteristics of solutes and in part to the low capacity factors of the first two members of SPC that resulted in a low resolving power of the chromatographic system. On the other hand, attempts to increase their retention by increasing the concentration of $TBAH_2PO_4$ caused LAS to be co-eluted with NPEO.

With respect to the elution sequence obtained by the use of ion-suppression HPLC, the elution of C_3-SPC and the two bicarboxylate forms was reversed by ion-pair formation. This effect can be ascribed to the fact that the latter two compounds form a triple derivative as they contain three negative charges, so that their actual molecular sizes are enhanced.

Compared with the ion-suppression technique, that exploiting the ion-pair retention mechanism caused NPEO to be eluted into a much broader and indented peak. This indicates that the latter technique is more selective than the former for the separation of the various NPEO oligomers, which, however, cannot be achieved owing to the limited efficiency of the HPLC column. This effect was unclear to us, taking into consideration that the two phase modifiers should not affect significantly the chromatographic process of neutral eluates, such as NPEO. From a practical point of view, it is preferable to obtain NPEO lumped into a sharp peak as this improves the detection limit of analytical procedures devoted to monitoring NPEO in natural water samples where these surfactants are present at very low parts per billion levels.

The combined effects of both $NaClO_4$ and TFA as phase modifiers were also evaluated (Fig. 2D). As mentioned above, at the low ion-suppressor concentrations used, only the dissociation of the carboxylic group, common to both SPC and NPEC, was totally enhibited. Under this hybrid situation, the elution process of LAS was controlled by the mechanism of "soft" ion-pair formation, as partial separation of the isomers of each LAS homologue was again achieved. For the other compound classes, the chromatographic process was very similar to that obtained by the addition of the sole ion-suppression agent, with the exception of the SP2C, which co-eluted with C_2-SPC.

With aqueous methanol mixtures

It is known that the nature of the organic modifier in RP-HPLC can affect the separation of a given mixture by peculiar interactions taking place between particular eluates and the organic solvent. These are the so-called "secondary effects" of the organic modifier. In order to establish whether the secondary effects could positively affect the fractionation of the mixture under consideration, acetonitrile was replaced with methanol as organic modifier. Obviously, when using methanol in place of acetonitrile, some parameters of the gradient elution process

were suitably adjusted (see Experimental) to obtain the best time–resolution combination. In Fig. 3, chromatograms are shown for the elution of the compounds considered by using the same phase modifiers as used with aqueous acetonitrile mixtures. The sequence of the chromatograms reported was the same as with the aqueous acetonitrile mixtures.

Apparently, the replacement of acetonitrile with methanol had the effect of eluting all of the NPEO oligomers into a much sharper peak. The less selective elution of the various NPEO oligomers mixture obtained with methanol as organic modifier might be ascribed to the fact that differences in polarity of the various NPEO oligomers arising from differences in the length of the polyethoxylic chain are levelled out by specific interactions taking place with the terminal hydroxyl of these eluates and that of methanol. To substantiate this hypothesis, the mixture composed of all of the NPEO oligomers was simultaneously injected into the HPLC column with that formed only by the first two members of NPEO (*i.e.*, NP1EO and NP2EO). When water–acetonitrile was used as the eluent, NP1EO and NP2EO produced a peak over lapping the final part of the peak for NPEO, whereas the opposite occurred with methanol as organic modifier.

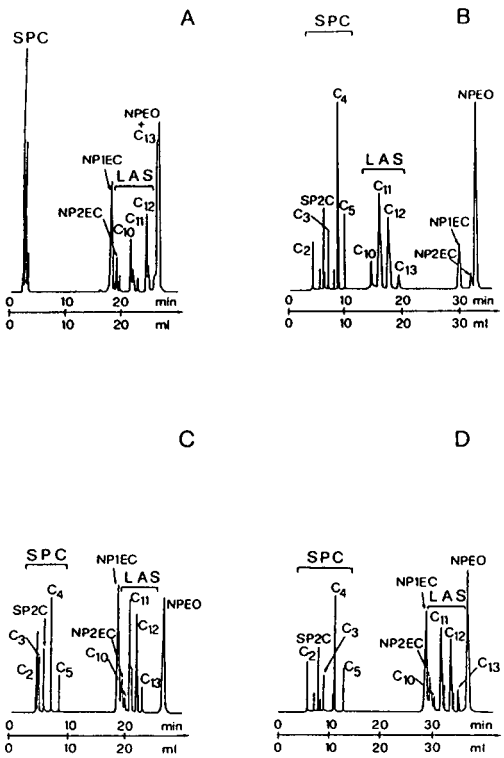

Fig. 3. RP-HPLC-fluorescence detection chromatograms showing the elution of standard solutions of SPC, LAS, NPEC and NPEO, with aqueous methanol mixtures containing (A) $NaClO_4$, (B) TFA, (C) $TBAH_2PO_4$ and (D) both $NaClO_4$ and TFA.

Under the ion-suppression conditions (Fig. 3B), the benefits of using a methanol–water as the eluent were that LAS homologues were well separated from each other and, mostly, we were able to separate NP2EC from NPEO.

Under the conditions of ion-pair formation, the replacement of acetonitrile with methanol succeeded in separating C_2-SPC from C_3-SPC (Fig. 3C).

Interestingly, under the combined ion-pair formation and ion-suppression effects provided by the simultaneous presence in the mobile phase of $NaClO_4$ and TFA (Fig. 3D), NPEC were eluted before LAS. This indicates that more stable ion pairs were formed between LAS and the Na^+ counter ion in the presence of methanol. The reason for this effect was unclear to us.

Effect of phase modifier concentration on fractionation

As is known, charged species can be chromatographed by RP-HPLC provided that either an ion-pair-forming agent or an ion-suppressor is added to the mobile phase. When this is not done, charged compounds are eluted all together with the dead volume of the column. In contrast, within certain limits, the equilibrium of the distribution of ionogenic compounds between the stationary and the mobile phases can be altered by suitably varying the concentration of the phase modifier, so that the best fractionation of a given complex mixture can be achieved.

Fig. 4 shows the effect of varying the concentration of $NACIO_4$ on the retention volumes of SPC and NPEC. The chromatographic behaviour of LAS on varying the salt concentration has already been investigated [26]. We observed that the chromatographic process of the latter com-

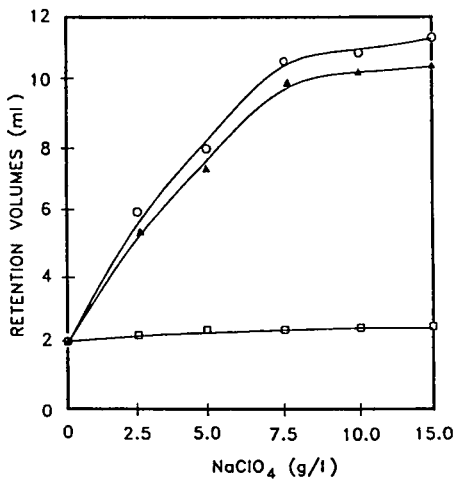

Fig. 4. Dependence of the retention volumes of NP1EC (○), NP2EC (▲) and SPC (□) on the salt concentration in aqueous acetonitrile.

pounds considered was not significantly affected by varying the nature of the inorganic salt. At any salt concentration considered, no effect on the retention of SPC was observed. Probably the ion pairs formed between SPC and the Na^+ counter ion are still so highly polar that no adsorption of them on the stationary phase can take place. In contrast, the retention of NP1EC and NP2EC steadily increased up to a salt concentration of *ca.* 7.5 g l^{-1}, where the two NPEO intermediates were fairly well separated from each other. Further increases in salt concentration up to 32 g l^{-1} did not improve the separation of the compounds considered. The plots of the retention volumes of SPC, NPEC and LAS *versus* the concentrations of the phase modifiers TFA and $TBAH_2PO_4$ were similar to that of NPEC in Fig. 4. Initial concentrations of TFA and $TBAH_2PO_4$ lower than 0.05 and 0.5 g l^{-1}, respectively, prompted an earlier elution of the compounds considered and adversely affected the resolution of the LAS, SPC and NPEC components shown in the Figs. 2 and 3. Raising the initial concentrations of both TFA and $TBAH_2PO_4$ above 0.4 and 8.0 g l^{-1}, respectively, caused a continuous increase in the retention volumes of LAS, SPC and NPEC without any further improvement in the resolution of their components.

Detection by UV and fluorescence methods

The synthesized biotransformation products of LAS and NPEO, namely SPC and NPEC, can be detected by both UV absorption at 225 nm and fluorescence with excitation and emission wavelengths of 225 and 295 nm, respectively, since they retain the spectroscopic properties of the parent compounds. A simple, inexpensive UV detector can be employed for analysing commercial products, while the monitoring in aqueous environmental samples of surfactants and their intermediates is more accurately performed by a selective detection method, such as fluorescence. Under the various chromatographic conditions examined, the detectabilities of the compounds considered were measured by connecting a UV and a fluorimetric detector in series and injecting 10 nmol of each compound.

With UV detection, some variations in the molar absorptivities of the eluates were noted, depending on the particular mobile phase selected. These fluctuations, however, were not significant enough to indicate the superiority of a particular chromatographic system in terms of selectivity.

The fluorescence signal intensities, reported in Table I, show that even the fluorescence quantum efficiency of SPC, LAS and NPEO was to some extent affected by the eluent system employed. On the other hand, an abrupt decrease in the quantum efficiency was observed for NPEC when eluted in the presence of an ion-suppression agent. No particular effect was caused by the presence of TFA in the mobile phase, as its replacement with any other ion suppressor did not lead to an increase in the quantum efficiency of the NPEO intermediates. Evidently, the sharp decrease in the quantum efficiency of the NPEO skeleton is directly related to the introduction into it of an undissociated carboxylic group. When coupled to ion-suppression chromatography, a fluorescence detector is useless for determining small amounts of NPEC.

Application to environmental samples

The RP-HPLC procedures proposed for the concurrent separation of SPC, NPEC, LAS and NPEO were applied to the analysis of aqueous

TABLE I

SIGNAL INTENSITIES WITH FLUORESCENCE DETECTION (EXCITATION AT 225 nm; EMISSION AT 295 nm) OF SPC, LAS, NP1EC AND NPEO DISSOLVED IN BOTH ACETONITRILE AND METHANOL MIXTURES WITH VARIOUS PHASE MODIFIERS

Compound	Peak area (counts × 1000)[a]					
	$NaClO_4$		TFA		$TBAH_2PO_4$	
	CH_3CN	CH_3OH	CH_3CN	CH_3OH	CH_3CN	CH_3OH
SPC	8.6	11.6	4.9	11.2	9.4	9.4
LAS	12.2	17.8	23.3	9.9	14.3	12.0
NP1EC	19.3	18.6	1.6	2.6	17.2	13.5
NPEO	67.3	66.9	67.0	80.1	63.8	69.9

[a] Values recorded by the integration corresponding to 10 nmol of each compound injected under the various chromatographic conditions reported under Experimental. The peak areas of each compound class were calculated by summing the peak areas of the individual components.

samples, such as treated and untreated wastewaters. Two sample preparation procedures were followed. One involved water removal by distillation of suitable volumes of each sample (10 ml of influent, 50 ml of final effluent) followed by dissolution of the semi-dried residue in methanol. When exploiting the selectivity of fluorescence detection, owing to the very low vapour pressure of the considered compounds and their relatively high concentration levels in wastewaters (1–10 mg l^{-1}), this sample preparation procedure is suitable for measuring the presence in the environmental samples of SPC and NPEC, and also of LAS and NPEO.

The second procedure was based on percolation through a C_{18} extraction cartridge of the same samples as reported above after adjusting their pH to about 2 and adding salt. This sample pretreatment was suggested by the observation of the synergistic effects produced by the simultaneous presence of a salt and an ion suppressor on the retention of the eluates on a reversed-phase stationary phase, as been illustrated above. Fig. 5 shows chromatographs obtained on preparing the samples by the first procedure and injecting the extract into the HPLC apparatus operating in the acetonitrile ion-suppression mode with fluorescence detection. As can be seen, no peak for NPEO and their intermediates was evident. This is because the water samples were collected in a plant treating domestic sewage. As is known, no European household formulation contains NPEO any longer [42]. The identification of SPC was done by external addition to the final extracts of authentic SPC, of both chemical and biochemical origin. In the influent, the small amounts of SPC found were bicarboxylate or

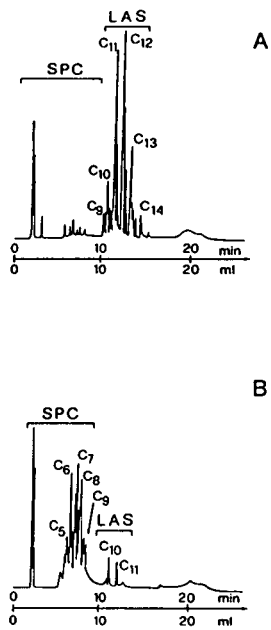

Fig. 5. RP-HPLC traces obtained on injecting the extracts obtained from (A) 10 ml of an influent and (B) 50 ml of an effluent of a plant treating domestic sewage. Fluorescence detection was used.

short-chain monocarboxylate species. In contrast, C_5–C_8 SPC homologue predominated in the effluent. The overall SPC concentrations calculated from triplicate analyses of 10 ml of influent and 50 ml of effluent were 1.4 ± 0.2 mg l^{-1} in the influent and 4.5 ± 0.5 mg l^{-1} in the effluent after water distillation and 1.1 ± 0.3 mg l^{-1} in the influent and 3.2 ± 0.4 mg l^{-1} in the effluent after percolation through the C_{18} cartridge. This suggested that SPC were partly lost on extracting 50 ml of the effluent with the C_{18} cartridge. In these same samples the LAS concentrations were 6.7 ± 0.4 mg l^{-1} in the influent and 0.08 ± 0.03 mg l^{-1} in the effluent, with no statistically significant differences between the results obtained by using the two procedures.

Recovery experiments on SPC and NPEC were conducted by spiking effluent samples and by following the two isolation procedures. The results are reported in Table II. The C_{18} extraction cartridge partially failed to retain SPC, especially those having less than six carbon atoms in the alkyl carboxylate chain. In contrast, the analyte isolation procedure by water evaporation provided quantitative recoveries (96–102%) with a good relative standard deviation (3–9%) for each of the added analytes. The recoveries of NPEC, and also those of LAS and NPEO according to previous work [33], obtained by making use of both isolation procedures were satisfactory.

TABLE II

RECOVERY OF SPC AND NPEC AFTER ADDING THEM TO 50 ml OF A SEWAGE TREATMENT PLANT EFFLUENT SAMPLE AND EXTRACTION WITH A C_{18} CARTRIDGE

Compound	Added (μg)	Recovery (%)
$2C_2$-SPC	72	12.6 ± 3.3
C_3-SP2C	88	30.3 ± 4.2
$5C_5$-SPC	76	38.0 ± 4.5
C_6-SPC[a]	70	57.3 ± 5.0
C_7-SPC[b]	104	72.0 ± 2.9
C_8-SPC[c]	76	82.7 ± 3.4
NP1EC	96	91.0 ± 2.9
NP2EC	24	87.7 ± 2.5

[a] Mixture of $2C_6$-SPC and $3C_6$-SPC.
[b] Mixture of $3C_7$-SPC and $4C_7$-SPC.
[c] Mixture of $3C_8$-SPC, $4C_8$-SPC and $5C_8$-SPC.

CONCLUSIONS

RP-HPLC coupled with fluorimetric detection can allow the simultaneous separation of the surfactants LAS, NPEO and their carboxylate biointermediates, provided that a careful choice of both the organic and phase modifiers is made. The flexibility of this chromatographic technique makes it suitable for laboratory biodegradation studies and also for field monitoring of the compounds of interest in aqueous samples. By using acetonitrile as organic modifier and simultaneously adding $NaClO_4$ and TFA to the mobile phase, the metabolic pathway of LAS, under various laboratory biodegradation test conditions, could be readily understood by following the gradual selective disappearance of peaks for the various homologues and positional isomers of LAS and the simultaneous increase in peaks for the various SPC. For monitoring the target compounds in aqueous environmental samples, the ion-pair retention mechanism with methanol–water mixtures appears to be the most selective, as it is capable of separating the two NPEC from the parent compounds.

REFERENCES

1 P. Berth and P. Jeschke, *Tenside Deterg.*, 26 (1989) 75.
2 *Seminar on Nonylphenolethoxylates (NPE) and Nonylphenol (NP), Report 3907*, Swedish Environmental Protection Agency, Stockholm, 1991, p. 7.
3 R. Swisher, *Surfactants Biodegradation*, Marcel Dekker, New York, 2nd ed., 1987.
4 P. Schöberl, *Tenside Deterg.*, 26 (1989) 86.
5 J.A. Field, J.A. Leenheer, K.A. Thorn, L.B. Barber, II, C. Rostad, D.L. Macalady and R.D. Stephen, *J. Contam. Hydrol.*, 9 (1992) 55.
6 H.A. Ball, M. Reinhard and P.L. McCarty, *Environ. Sci. Technol.*, 23 (1989) 951.
7 M. Ahel, T. Conrad and W. Giger, *Environ. Sci. Technol.*, 21 (1987) 697.
8 W. Giger, M. Ahel, M. Koch, H.U. Laubscher, C. Schaffner and J. Schneider, *Water Sci. Technol.*, 19 (1987) 449.
9 A. Nakae, K. Tsuij and M. Yamanaka, *Anal. Chem.*, 52 (1980) 2275.
10 M. Kikuchi, A. Tokai and T. Hoshida, *Water Res.*, 20 (1986) 643.

11 H. De Henau, E. Matthijs and W.D. Hopping, *Int. J. Environ. Anal. Chem.*, 26 (1986) 279.
12 P. Gerike, R. Winkler, P. Schneider and W. Jacob, *Tenside Deterg.*, 26 (1989) 136.
13 M.A. Castles, B.L. Moore and S.R. Ward, *Anal. Chem.*, 61 (1989) 2534.
14 P.D. Brunner, S. Capri, A. Marcomini and W. Giger, *Water Res.*, 22 (1989) 1465.
15 A. Marcomini, P.D. Capel, T. Lichtensteiger, P.D. Brunner and W. Giger, *J. Environ. Qual.*, 18 (1989) 523.
16 M. Ahel and W. Giger, *Anal. Chem.*, 57 (1985) 1577.
17 M. Ahel and W. Giger, *Anal. Chem.*, 57 (1985) 2584.
18 M. Kudoh, H. Ozawa, S. Fudano and K. Tsuji, *J. Chromatogr.*, 287 (1984) 337.
19 M.S. Holt, E.H. McKerrel, J. Perry and R.J. Watkinson, *J. Chromatogr.*, 362 (1986) 419.
20 J. Waters and J.T. Garrigan, *Water Res.*, 17 (1983) 1549.
21 Q.W. Osburn, *J. Am. Oil Chem. Soc.*, 63 (1986) 257.
22 J. McEvoy and W. Giger, *Environ. Sci. Technol.*, 20 (1986) 376.
23 H.A. Ball and M. Reinhard, in R.L. Jolley, *et al.* (Editors), *Water Chlorination—Chemistry, Environmental Impact and Health Effects*, Vol. 5, Lewis, Chelsea, MI, 1985, p. 1505.
24 E. Stephanou, *Int. J. Environ. Anal. Chem.*, 20 (1987) 41.
25 A. Marcomini and W. Giger, *Anal. Chem.*, 59 (1987) 1709.
26 A. Marcomini, S. Stelluto and B. Pavoni, *Int. J. Environ. Anal. Chem.*, 35 (1989) 207.
27 R.D. Swisher, *J. Water Pollut. Control Fed.*, 35 (1963) 1557.
28 H. Leidner, R. Gloor and K. Wuhrmann, *Tenside Deterg.*, 13 (1976) 122.
29 C.R. Eggert, R.G. Kaley and W.E. Gledhill, in A.W. Bourquin and P.H. Pritchard (Editors), *Proceedings of the Workshop: Microbial Degradation of Pollutants in Marine Environments, US EPA Report No. 600/9-79-012*, Environmental Protection Agency, Washington, DC, pp. 451–461.
30 M.L. Trehy, W.E. Gledhill and R.G. Orth, *Anal. Chem.*, 62 (1990) 2581.
31 E. Stephanou, R. Reinhard and H.A. Ball, *Biomed. Environ. Mass Spectrom.*, 15 (1988) 275.
32 P.W. Taylor and G. Nickless, *J. Chromatogr.*, 178 (1979) 259.
33 A. Marcomini, S. Capri and W. Giger, *J. Chromatogr.*, 403 (1987) 243.
34 A. Di Corcia, M. Marchetti, R. Samperi and A. Marcomini, *Anal. Chem.*, 63 (1991) 1179.
35 K. Yoshimura, *J. Am. Oil Chem. Soc.*, 63 (1986) 1590.
36 *Modified OECD 301E Biodegradation Screening Test, OECD Guideline for Testing of Chemicals*, Paris, June 1991.
37 A. Marcomini and L. Cavalli, in *Proceedings of the 3rd World Surfactants Congress, GOSIP, London, June 2–6, 1992*, pp. 8–16.
38 A. Di Corcia, R. Samperi and A. Marcomini, *Environm. Sci. Technol.*, submitted.
39 R.A. Kimerle and R.D. Swisher, *Water Res.*, 11 (1977) 31.
40 W.J. Weber, J.C. Morris and W. Stumm, *Anal. Chem.*, 34 (1962) 1844.
41 B. Ballarin, S. Stelluto and A. Marcomini, *Riv. Ital. Sostanze Grasse*, 66 (1989) 349.

Journal of Chromatography, 644 (1993) 73–82
Elsevier Science Publishers B.V., Amsterdam

CHROM. 25 113

Rapid and continuous ion chromatographic determination of trace heavy metal impurities in noble metals

Youbang Liu* and Qi Wang

Lanzhou Institute of Chemical Physics, Chinese Academy of Sciences, Lanzhou, Gansu (China)

(First received January 12th, 1993; revised manuscript received March 19th, 1993)

ABSTRACT

A rapid and continuous ion chromatographic method for the determination of trace heavy metal impurities in noble metals was developed. Some real samples were analysed and satisfactory results were obtained. In this method, a ternary complex eluent (sodium tartrate, sodium citrate and sodium chloride) was used to separate six heavy metal ions and the composition of the eluent was optimized by the simplex method. An on-line pre-enrichment column was used to remove the noble metal matrix in the form of chloro complex anions and to enrich trace heavy metal impurities in the form of cations in a single operation. The retained heavy metal ions were then separated on an analytical column and detected with a coulometric detector. The enrichment conditions were investigated and optimized.

INTRODUCTION

It is important to determine trace heavy metal impurities in products and intermediates of noble metals for quality control during in-plant manufacturing processes. Beamish and Van Loon [1,2] established and reviewed a series of cation-exchange methods for the separation of the noble metals platinum, palladium, rhodium, iridium and ruthenium from associated milligram amounts of the base heavy metals copper, iron, nickel, lead and zinc using the cation exchangers KU-2 and Dowex 50. The material to be analysed was treated with *aqua regia*, evaporated with hydrochloric acid and dissolved in hydrochloric acid (pH 1.0–1.5). The solution was passed through 2 g of the cation exchanger in a 200 mm × 15 mm I.D. column at 50–60 drops/min. In this procedure, the base heavy metals were retained on the cation exchanger in the form of cations while the noble metals were drained out of the column in the form of chloro complex anions. The noble metals were recovered quantitatively.

Later, Chang [3] developed another cation-exchange method for the separation of trace amounts of copper and nickel from the base noble metals platinum and palladium based on the same principle as the earlier work, using the cation exchanger Dowex 50. The samples of platinum and palladium metals and their solutions of intermediate or final products during in-plant processing were treated with a similar procedure and dissolved in hydrochloric acid (pH 1.0–1.5). The solution with a concentration of 20–50 mg/ml of noble metals was passed through a 30–50 mm × 5 mm I.D. cation-exchange column at 50–60 drops/min. The copper and nickel impurities were retained on the cation exchanger in the form of cations while the base noble metals were drained out of the column in the form of chloro complex anions. The retained

* Corresponding author. Present address: Department of Chemistry, University of Missouri–Rolla, Rolla, MO 65401, USA.

0021-9673/93/$06.00

copper and nickel ions were eluted with 1.0–2.0 *M* hydrochloric acid and the eluate was analysed by atomic absorption spectrometry (AAS). One element was determined in each operation hence this was not a rapid method. As other heavy metals such as lead, zinc, cobalt and cadmium could also be associated with noble metals, their pressure would make the AAS method very tedious and time consuming. Further, if these heavy metals interfered with each other in the AAS measurement, they would also need to be separated. To solve this kind of problem, ion chromatography obviously has advantages.

The ion exchange chromatographic separation of six heavy metal ions, Cu^{2+}, Zn^{2+}, Ni^{2+}, Pb^{2+}, Co^{2+} and Cd^{2+}, on YSG–SO_3Na cation exchanger with a binary complex eluent (sodium tartrate–sodium chloride) has been reported [4,5]. In both studies, the elution order was in the order given. For better results, baseline separations between adjacent ion pair of Cu^{2+} and Zn^{2+}, Pb^{2+} and Co^{2+}, and Co^{2+} and Cd^{2+} were obtained, but between Zn^{2+} and Ni^{2+} and between Ni^{2+} and Pb^{2+} there was only 60–70% separation. Co^{2+} was eluted at about 30 min and Cd^{2+} at about 45 min. This condition was clearly not suitable for quantitative analysis. Earlier, Takata and Muto [6] reported an ion chromatographic separation of seven heavy metal ions, Hg^{2+}, Cu^{2+}, Zn^{2+}, Ni^{2+}, Pb^{2+}, Cd^{2+} and Co^{2+}, on Hitachi 2611 cation exchanger with a binary complex eluent (sodium tartrate–sodium chloride) within about 38 min. The resolutions between each adjacent ion pairs were acceptable for quantitative analysis. However, unfortunately, this kind of stationary phase was not available to us.

The objective of this work was to develop an ion chromatographic procedure for the determination of trace heavy metal impurities in base noble metals and to use this procedure to support the quality control in noble metal in-plant manufacturing. First, a ternary complex eluent (sodium tartrate–sodium citrate–sodium chloride) was used to separate the six heavy metal ions. The composition of the ternary eluent was optimized by the simplex method. As a result, the elution order was changed to Cu^{2+}, Ni^{2+}, Zn^{2+}, Pb^{2+}, Co^{2+} and Cd^{2+}. Nickel that eluted between zinc and lead in earlier work [4,5] now eluted before zinc, and the last ion, cadmium, eluted at about 20 min. The resolutions between each adjacent ion pair were larger than 1.17. This result was even better than that in ref. 6. Second, an on-line pre-enrichment column was used to remove the noble metal matrix from heavy metals and to enrich trace heavy metal impurities in a single operation based on the same principle as in earlier work [1–3]. The enriched heavy metals were separated on an analytical column and detected with a coulometric detector after the eluent flow pattern was switched. A few real samples were analysed and satisfactory results were obtained.

EXPERIMENTAL

Apparatus

This work was performed on a Model SY 202 high-performance ion-exchange chromatograph (Sichuan Analytical Instrument Factory, Chongqing, China) [7]. An on-line pre-enrichment column and related equipment were installed. A schematic diagram of the chromatographic system is shown in Fig. 1.

Column

The analytical column was a glass column (100 mm × 8 mm I.D.) jacketed by a Plexiglas tube. The enrichment column was specially designed in the laboratory and consisted of a Plexiglas tube (20 mm × 5 mm I.D.) with both ends sealed with Teflon screws.

Column resin

The resin packed in the analytical column was a polystyrene-based strongly acidic cation exchanger, YSG–SO_3Na (15–20 μm), obtained from the Tianjin Second Reagent Factory (Tianjin, China). The same resin but of particle size 25–30 μm was used for the enrichment column. The resins were washed with 2 *M* hydrochloric acid, water, 2 *M* sodium hydroxide solution and water before use.

Mobile phase

The mobile phase was prepared by dissolving certain amounts of sodium tartrate, sodium

citrate and sodium chloride in distilled, ion-exchanged water and then adjusting the pH to 4.1 with 2 *M* nitric acid.

Detector

The detector in this work was a flow coulometric detector [7]. Carbon cloth was used for both working and auxiliary electrodes. The detection potential was −0.75 V for all heavy metal ions *vs.* 0.1 *M* $Fe(CN)_6^{3-}$–0.1 *M* $Fe(CN)_6^{4-}$–0.4 *M* NH_3 solution.

Electrolyte for working electrode reaction

The secondary coulometric method was used to detect the eluted heavy metal ions. The principle is as follows:

$$M^{2+} + CuDTPA \rightarrow MDTPA + Cu^{2+} \quad (1)$$

$$Cu^{2+} + 2e \rightarrow Cu \quad (2)$$

Instead of direct reduction, the eluted ion M^{2+} replaced Cu^{2+} in CuDTPA (DTPA = diethylenetriaminepentaacetate) and then the Cu^{2+} was reduced on the working electrode. The composition of the electrolyte for the working electrode reaction was 0.01 *M* DTPA–0.01 *M* copper (II) sulphate–0.1 *M* ammonium nitrate–1.0 *M* ammonia solution.

Electrolyte for auxiliary electrode reaction

The electrolyte for the auxiliary electrode reaction was 0.1 *M* potassium hexacyanoferrate(III)–0.1 *M* potassium hexacyanoferrate(II)–0.4 *M* ammonia solution.

Standard solutions of heavy metal ions

Individual 0.5 *M* stock standard solutions of the heavy metal ions were prepared by dissolving 0.25 mol of the nitrates in hydrochloric acid (pH 1.5) in a 500-ml volumetric flask and diluting to volume with the same acid. The concentrations was accurately determined by titration with EDTA. Working standard solutions were prepared by diluting the stock standard solutions to the required concentrations (single or mixed) with hydrochloric (pH 1.5) acid in a volumetric flask before use.

Purified noble metal solutions

The calculated amounts of $PtCl_4$, $PdCl_2$ and $IrCl_4$ were dissolved in 6 *M* hydrochloric acid and the solutions were evaporated to dryness on a boiling water-bath. Then residues were dissolved in hydrochloric acid (pH 1.5) to give concentrations of 30.0 mg/ml of noble metals. The solutions were passed through a conventional cation-exchange column (100 mm × 15 mm I.D.) packed with YSG–SO_3Na resin (30–40 μm) to isolate any associated heavy metal impurities. These solutions were used for mixing with standard heavy metal solutions for investigating the effects of the base noble metals on the enrichment efficiency of the heavy metals.

Real samples of noble metals

Three platinum and one palladium metal solution samples and one iridium intermediate solution sample prepared during in-plant manufacturing were obtained from the central laboratory of the Northwestern Nonferrous Metal Company of China. These samples had already been pretreated and dissolved in 1.0 *M* hydrochloric acid at concentrations of 100.0 mg/ml for platinum and palladium and 50.0 mg/ml for iridium, and contained labelled concentrations of copper and nickel impurities based on pure noble metals. They were evaporated to dryness on a boiling water-bath and the residues were dissolved in hydrochloric acid (pH 1.5) with the original noble metal concentration and pH of the solutions was adjusted with sodium hydroxide to exactly 1.5 before use. A volume of 10 ml of each noble metal sample solution was pumped through the enrichment column and the residue was washed three times with a total of 10 ml (4 + 3 + 3 ml) of hydrochloric acid (pH 1.5) (the enrichment procedure is discussed in detail later).

Enrichment procedure

A schematic diagram of the chromatographic system is presented in Fig. 1. The enrichment column (4) was connected on the position normally used for the sample loop of the first six

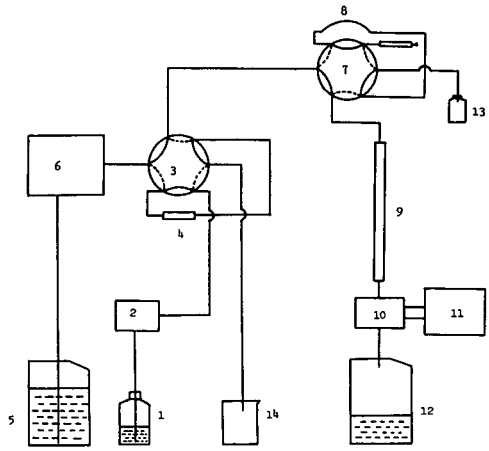

Fig. 1. Schematic diagram of the chromatographic system. 1 = Solution to be enriched; 2 = enrichment pump; 3 = first six-port valve; 4 = enrichment column; 5 = eluent; 6 = elution pump; 7 = second six-port valve; 8 = sample loop (10 μl); 9 = analytical column; 10 = detector; 11 = recorder; 12 and 13 = waste solution; 14 = collected noble metal solution.

port valve (3). The eluent was led by means of the elution pump (6) to the first six port valve, where it could flow in either of two directions, one via the six-port valve (solid line) directly to the second six-port valve (7) and then the analytical column (9), and the other via the enrichment column (dotted line). When the enrichment operation was carried out, the first valve was set at the position such that the eluent did not pass through the enrichment column. Volumes of 10–100 ml of noble metal solution with heavy metal impurities in hydrochloric acid (pH 1.5) were pumped through the enrichment column continuously by the enrichment pump (2). In this procedure, the trace heavy metal impurities were retained on the enrichment column in the form of cations while the base noble metals were drained out of the column in the form of chloro complex anions. The residue was washed with a total of 10 ml (4 + 3 + 3 ml) hydrochloric acid (pH 1.5). Then 15 ml of 0.1 *M* sodium nitrate solution were pumped through the column to convert the ion exchanger from the H^+ to the Na^+ form. The reason for this additional ion-exchange conversion will be discussed later. When the enrichment was finished, the eluent flow pattern was switched from the solid line to the dotted line and the eluent was passed through the enrichment column so that the retained heavy metal ions were eluted into the analytical column to be separated and determined.

This procedure maintained all the merits of the traditional method but was more convenient, rapid and effective because of the on-line pre-enrichment column and the high-performance ion chromatographic system.

Evaluation of enrichment efficiency

A 10-μl volume of a mixed standard solution of the six heavy metal ions with a concentration of $5.00 \cdot 10^{-2}$ *M* of each ion was injected directly into the analytical column by the second six-port valve (10-μl sample loop) and the eluted peak area for each heavy metal ion, $A_{i(\text{inject})}$, was measured. The same amount of the heavy metal ions, $5.00 \cdot 10^{-7}$ mol absolute amount, diluted in 10–100 ml hydrochloric acid (pH 1.5), was enriched by the enrichment procedure and the eluted peak area for each heavy metal ion, $A_{i(\text{enrich})}$, was measured. The enrichment efficiency (*EE*) of the heavy metal ions was given by:

$$EE = [A_{i(\text{enrich})}/A_{i(\text{inject})}] \cdot 100\%$$

Because the base noble metals did not interfere (see *Interference from associated noble metals*), they were not added to the solutions during the investigation of the enrichment efficiency.

Optimization procedure

A 10-μl volume of mixed standard solution of the six heavy metal ions with a concentration of $5.00 \cdot 10^{-2}$ *M* of each ion was injected by the second six-port valve (10-μl sample loop) and separated in the analytical column using a certain composition of the ternary eluent (sodium tartrate–sodium citrate–sodium chloride). The separation results were evaluated by the chromatographic optimization function (*COF*) [8], which will be discussed later. The new composition of the ternary eluent was calculated by the simplex method [9,10], which will also be discussed later. This procedure was repeated until satisfactory separation conditions were obtained.

Chemicals

All chemicals were of analytical-reagent grade from the Tianjin Second Reagent Factory (Tianjin, China) and the Shanghai Chemical Reagent Factory (Shanghai, China) and were used as received.

RESULTS AND DISCUSSIONS

Optimization of separation conditions

The equation for chromatographic resolution (R_s) is

$$R_S = \frac{1}{4} \cdot \frac{(\alpha - 1)}{\alpha} \cdot n^{1/2} \cdot \frac{k'}{k' + 1} \quad (3)$$

An increase in the separation factor, α, will result in an improvement in R_S. In ion-exchange chromatography, $\alpha = K_2/K_1$, where K_1 and K_2 are the partition coefficients of the first and second eluted ions, respectively on ion exchanger.

When n kinds of complex anions are present in solution, the partition coefficient on ion exchanger for any eluted ion is

$$\log K = \log K_x + Z \log Q - Z \log[M] - \log\left(\sum \alpha_{M(L_i)} - n + 1\right) \quad (4)$$

where K_x is the equilibrium constant of ion exchange, Z is the electric charge of the ion, Q is the exchange capacity of the resin, [M] is the concentration of the ion and $\alpha_{M(L_i)}$ is the side-effect coefficient of the metal ion coordinated by the ith complex anion (in this paper, it could be sodium tartrate, sodium citrate or sodium chloride). $\alpha_{M(L_i)}$ is given by the following equation:

$$\alpha_{M(L_i)} = 1 + \beta_{i1}[L_i] + \beta_{i2}[L_i]^2 + \cdots + \beta_{in}[L_i]^n \quad (5)$$

where β_{ij} is the overall formation constant of the coordination complex between metal ion and the ith complex anion.

According to eqns. 4 and 5, a larger value of the separation factor α may be obtained by choosing different complex anions and/or changing their concentrations if the increments of $\alpha_{M(L_i)}$ and then K are different for the various heavy metal ions. By evaluating the β_{ij} of various complex agents with the six heavy ions, we realized that the application of a ternary eluent composed of sodium tartrate, sodium citrate and sodium chloride would improve the separation of the six heavy metals because citrate anion has a relatively higher overall formation constant with Ni^{2+}. This was verified by experiments.

In order to obtain the optimum composition of the eluent, instead of the conventional single-factor method, the simplex method [8,9] was used and a satisfactory eluent composition was reached after ten experiments. During optimization, the chromatographic optimization function (*COF*) [7] was used as an objective function to evaluate the result of the optimization after each experiment. *COF* was given by

$$COF = \sum A_i \ln (R_i/R_{id}) - B(t_M - t_L) \quad (6)$$

where R_i is the measured resolution between any adjacent peaks on the chromatogram and R_{id} is the required resolution in a certain application. If $R_i \leqslant R_{id}$, the measured value is used; if $R_i > R_{id}$, let $R_i = R_{id}$. t_M is the retention time of the last-eluted peak on chromatogram and t_L is an acceptable analytical time in a certain application. If $t_M \geqslant t_L$, the measured value is used; if $t_M < t_L$, let $t_M = t_L$. A_i and B are weight factors. In this work, $R_{id} = 1.25$, $t_M = 20$ min, $A_i = 1$ and $B = 0.05$ were selected.

Among the different simplex methods, the modified simplex method (MSM) [8,9] was used in this work. The results of MSM are given in Table I. From Table I, the composition of the eluent in No. 10, *i.e.*, 0.100 *M* sodium tartrate–$1.55 \cdot 10^{-2}$ *M* sodium citrate–0.150 *M* sodium chloride (pH 4.1), was considered to be the optimum. The chromatogram obtained with this optium eluent is shown in Fig. 2.

Investigation of enrichment conditions

Flow-rate. The experimental results showed that the enrichment efficiency of various heavy metal ions decrease slightly with increase in flow-rate (Table II). This indicated that the ion-exchange equilibrium needed time to be completed. Although a higher enrichment efficiency could be obtained at low flow-rates, a longer enrichment time was required. When the flow-

TABLE I

RESULTS OF MODIFIED SIMPLEX METHOD

No.	Na tartrate (M)	Na citrate (10^{-2} M)	NaCl (M)	Type of point[a]	No. of apex	Resolution[b]					$t_{R\,max}$ (min:s)[c]	COF
						R_1	R_2	R_3	R_4	R_5		
1	0.100	1.40	0.150	Apex	1, 2, 3, 4	3.84	1.02	1.67	1.34	2.01	21:27	−0.276
2	0.110	1.40	0.150	Apex	1, 2, 3, 4	3.71	0.79	1.57	1.55	1.95	18:32	−0.459
3	0.100	1.60	0.150	Apex	1, 2, 3, 4	3.50	1.17	1.65	1.05	2.05	21:23	−0.310
4	0.100	1.40	0.160	Apex	1, 2, 3, 4	3.72	0.95	1.53	1.27	1.68	20:22	−0.293
	0.100	1.47	0.153	c.g.	1, 2, 3, 4							
5	0.090	1.55	0.155	Reflect	1, 3, 4, 5	3.71	1.45	1.69	0.8	2.19	23:57	−0.644
6	0.105	1.45	0.150	Shrink	1, 3, 4, 6	3.56	0.99	1.55	1.29	2.05	20:08	−0.240
	0.102	1.48	0.150	c.g.	1, 3, 4, 6							
7	0.105	1.55	0.140	Reflect	1, 3, 6, 7	3.62	1.10	1.68	1.25	2.51	20:33	−0.155
8	0.105	1.60	0.135	Amplify	1, 3, 6, 8	3.55	1.15	1.33	0.95	2.22	21:27	−0.430
	0.103	1.47	0.147	c.g.	1, 3, 6, 7							
9	0.105	1.35	0.150	Reflect	1, 6, 7, 9	3.87	0.91	1.63	1.49	1.95	20:17	−0.332
10	0.100	1.55	0.150	Shrink	1, 6, 7, 10	3.58	1.17	1.60	1.23	2.42	20:42	−0.117

[a] c.g. is the centre of gravity of the simplex. The reflection coefficient $\alpha = 1$, the shrink coefficient $\beta = 0.5$ and the amplifying coefficient $\gamma = 1.5$ were used in this work.

[b] R_1, R_2, R_3, R_4 and R_5 are the resolutions between Cu^{2+} and Ni^{2+}, Ni^{2+} and Zn^{2+}, Zn^{2+} and Pb^{2+}, Pb^{2+} and Co^{2+}, and Co^{2+} and Cd^{2+}, respectively.

[c] $t_{R\,max}$ is the retention time of Cd^{2+}, the last-eluted ion.

rate was below 3.0 ml/min, the *EE* of all ions were more than 98.0%, without much sacrifice with regard to experimental error. Therefore, 3.0 ml/min was adopted in real enrichment operations.

Concentration of heavy metal ions. The six heavy metal ions ($5.00 \cdot 10^{-7}$ mol) in 10-, 50- and 100-ml volumes were enriched and the influence of the concentration of the heavy metal ions on *EE* is shown in Table III. It can be seen that the concentration had no significant effect on the enrichment efficiency.

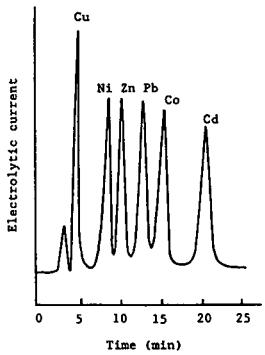

Fig. 2. Chromatogram of the six heavy metal ions. Sample size, $5.00 \cdot 10^{-7}$ mol of each heavy metal ion; resin, YSG-SO_3Na cation-exchange resin, 15–20 μm; column 100 mm × 8 mm I.D.; room temperature; eluent 0.100 M sodium tartrate–$1.55 \cdot 10^{-2}$ M sodium citrate–0.150 M sodium chloride (pH 4.1); flow-rate, 1.0 ml/min; electrolyte, 0.01 M CuDTPA–0.1 M NH_4N0_3–1.0 M NH_3 solution; detection potential −0.75 V *vs.* $Fe(CN)_6^{3-}$–$Fe(CN)_6^{4-}$.

Acidity of enrichment solution. The experimental results showed that *EE* for all the heavy metal ions was larger than 97.0% if the pH of the metal ion solution to be enriched was between 1.0 and 7.0 in hydrochloric acid medium. However, *EE* decreased rapidly when the pH was lower than 1.0 (Table IV). The reason was thought to be that part of the heavy metal ions also formed chloro complex anions at high acidity and could not be retained on the enrichment column. As noble metals could form chloro complex anions completely and *EE* for all the heavy metal ions was larger than 98.0% in hydrochloric acid of pH 1.5, we chose pH 1.5 as the acidity of the enrichment solution (hydrochloric acid medium).

Amount of sodium nitrate. When investigating the effects of acidity, we observed that *EE* for Cu^{2+} was as high as 140% at pH 3.0 and even

TABLE II

EFFECT OF ENRICHMENT FLOW-RATE ON ENRICHMENT EFFICIENCY

10 ml of $5.00 \cdot 10^{-5}$ *M* of the mixed heavy metal ions in hydrochloric acid (pH 1.5) were used.

Flow-rate (ml/min)	Enrichment efficiency (%)					
	Cu^{2+}	Ni^{2+}	Zn^{2+}	Pb^{2+}	Co^{2+}	Cd^{2+}
1.0	101.0	99.6	100.4	99.2	99.5	99.8
2.0	99.6	99.2	99.3	98.6	99.1	98.2
3.0	98.5	98.3	98.4	98.3	98.5	98.0
4.0	97.6	97.3	97.2	97.3	97.5	96.8
5.0	95.8	96.0	95.3	95.5	95.7	94.4

TABLE III

EFFECT OF CONCENTRATION OF HEAVY METALS ON ENRICHMENT EFFICIENCY

The flow-rate was 3.0 ml/min, the pH of the solution was 1.5 in hydrochloric acid and the amount of each heavy metal ion was $5 \cdot 10^{-7}$ mol.

Volume (ml)	Enrichment efficiency (%)					
	Cu^{2+}	Ni^{2+}	Zn^{2+}	Pb^{2+}	Co^{2+}	Cd^{2+}
10	99.7	98.9	100.1	98.7	99.1	99.0
50	99.2	99.4	99.6	99.2	98.8	98.5
100	98.6	98.5	98.8	98.2	98.5	98.7

higher at pH < 3.0. The signal at the elution position of Cu^{2+} was so large that the determination of the other ions was seriously affected. We suggest that the reason might be as follows.

As mentioned under Experimental, the secondary coulometric detection method was used in this work. Instead of direct reduction, the eluted ion M^{2+} replaced Cu^{2+} in CuDTPA and then the Cu^{2+} was reduced on the working electrode. When the acidic heavy metal solution

TABLE IV

EFFECT OF ACIDITY ON ENRICHMENT EFFICIENCY

A 10-ml volume of $5.00 \cdot 10^{-5}$ *M* of the mixed heavy metal ions was enriched at a flow-rate of 3.0 ml/min.

pH	Enrichment efficiency (%)					
	Cu^{2+}	Ni^{2+}	Zn^{2+}	Pb^{2+}	Co^{2+}	Cd^{2+}
7.0	99.4	100.0	100.6	99.4	99.2	99.4
3.0	99.7	99.6	101.2	98.8	100.4	98.6
1.5	99.5	100.8	100.3	98.5	99.4	98.5
1.0	98.9	98.2	98.6	97.2	98.9	97.3
0.0	22.1	49.7	44.6	9.6	37.7	6.5

was introduced into the enrichment column, a large amount of H^+ was retained on the exchanger so that the resin was converted from the Na^+ to the H^+ form. When the eluent flow pattern was switched after completion of enrichment, the retained H^+ entered the eluent in the analytical step and caused the mobile phase to be sectionally acidified. When the acidified section of the eluent reached the detector, H^+ combined with DTPA and a large amount of Cu^{2+} was released from CuDTPA. These extra Cu^{2+} ions were electrolysed and the above-mentioned phenomenon appeared.

In order to solve this problem, $NaNO_3$ solution was pumped through the enrichment column after enrichment to convert the exchanger back from the H^+ into the Na^+ form. After this treatment, the detector worked normally, However, the optimum amount of $NaNO_3$ should be considered. If the amount of $NaNO_3$ was insufficient, the conversion of the enrichment column was incomplete. On the other hand, too much $NaNO_3$ would lead to the risk of the enriched heavy metal ions being partially eluted from the enrichment column, mainly because of Na^+ replacing the enriched heavy metal ions. Throughout the experiments, a suitable amount was found to be 15 ml of 0.1 *M* $NaNO_3$ solution. *EE* for all the heavy metal ions was larger than 98% under this condition (Table V).

Interference from associated noble metals

A solution containing absolute amounts of 30.0 mg of noble metals (platinum, palladium and iridium) and $5.00 \cdot 10^{-7}$ mol of each heavy metal ion in 10 ml of hydrochloric acid (pH 1.5) was used to investigate the effects of associated noble metals on the enrichment efficiency of trace heavy metals. *EE* for all the heavy metal ions was larger than 98%. Hence base noble metals would not affect the enrichment under the experimental conditions used.

Interference from other ions

The coulometric detector is a selective detector. Under the experimental conditions it did not respond to Li^+, Na^+, K^+, Fe^{3+}, Fe^{2+}, Al^{3+} and Sn^{4+}, and the retention times of Mn^{2+}, Ca^{2+} and Mg^{2+} were 38, 45 and 56 min respectively. The six heavy metal ions of interest were not interfered with by any of these common ions.

Analysis of real samples

Mixed standard solutions containing various amounts of copper, nickel and lead in 10 ml of hydrochloric acid were passed through the enrichment column to obtain a calibration graph. The single peak area on the chromatogram was used in quantitative analysis. The calibration graphs were obtained by plotting the peak area of a certain heavy metal ion against the absolute mass of the ion in 10.0 ml of solution. As base noble metals did not interfere with *EE* for the trace heavy metals, they were not added to the solution used to obtain the calibration graph. Three heavy metals, copper, nickel and lead, were measured because they were the only

TABLE V

THE EFFECT OF CONCENTRATION OF $NaNO_3$ ON ENRICHMENT EFFICIENCY

A 15-ml volume of $NaNO_3$ solution was used.

$NaNO_3$ (*M*)	Enrichment efficiency (%)					
	Cu^{2+}	Ni^{2+}	Zn^{2+}	Pb^{2+}	Co^{2+}	Cd^{2+}
0.05	114.8	101.2	100.4	99.2	100.0	98.8
0.10	100.1	99.7	100.7	98.3	99.2	99.6
0.15	95.6	96.4	94.7	94.3	95.4	96.1
0.20	82.4	85.2	83.6	84.3	83.2	80.8
0.30	72.9	76.3	75.1	70.5	73.8	71.4

impurities in the available real samples. The calibration graphs can be expressed as follows, where y is peak area and x is amount (μg):

$$Cu^{2+}: y = 0.70 + 11.70x \quad (r = 0.9999) \tag{7}$$

$$Ni^{2+}: y = -1.05 + 19.70x \quad (r = 0.9998) \tag{8}$$

$$Pb^{2+}: y = 1.30 + 6.84x \quad (r = 0.9998) \tag{9}$$

Several real noble metal samples were analysed by the developed method. The results are given in Table VI. The palladium and platinum samples were pure noble metals. No lead was indicated for the platinum samples but it was detected by this method. Because the amounts of the platinum samples were limited, only two measurements were made. A certain amount of lead was added to the palladium sample owing to the absence of lead impurity in this sample. The iridium sample was an intermediate prepared during in-plant production. All three heavy metals were added as they did not exist in the original sample. From Table VI, the relative standard deviations were less than 3.5%, the recoveries of the added heavy metal impurities were higher than 97% and the relative error of the determination was less than ±6.0%. As this error range is acceptable in trace analysis, the results are considered satisfactory.

TABLE VI

RESULTS OF THE DETERMINATION OF HEAVY METAL IMPURITIES IN REAL NOBLE METAL SAMPLES

HM = Heavy metal elements determined in the noble metal samples, Standard value = labelled heavy metal impurity concentration in the noble metal samples. AD = Added standard heavy metal ions which were absent in the noble metal samples supplied. X = Mean. R.S.D. = relative standard deviation (σ_{n-1}/X). RE = relative Error. Recovery of the added heavy metal ions in the noble metal samples X/AD. All concentrations of the heavy metals in this table were based on the form of pure noble metals in the real samples.

Sample	HM	Standard value (10^{-3}%)	AD (10^{-3}%)	Found (10^{-3}%)	X (10^{-3}%)	R.S.D. (%)	RE (%)	Recovery (%)
Pd	Cu	1.25	–	1.24, 1.22, 1.30, 1.22, 1.22, 1.18, 1.44	1.22	3.3	−2.4	–
	Ni	1.23	–	1.28, 1.24, 1.30, 1.26, 1.25, 1.20, 1.20	1.25	3.0	1.6	–
	Pb	–	1.50	1.45, 1.49, 1.53, 1.52, 1.47, 1.53, 1.43	1.47	2.8	−2.0	98
Pt (1)	Cu	1.50	–	1.51, 1.58	1.55	–	3.3	–
	Ni	1.00	–	1.03, 1.08	1.06	–	6.0	–
	Pb	–	–	2.27, 2.33	2.30	–	–	–
Pt (2)	Cu	2.10	–	2.09, 2.05	2.07	–	−1.4	–
	Ni	0.20	–	0.21, 0.20	0.21	–	5.0	–
	Pb	–	–	1.78, 1.81	1.80	–	–	–
Pt (3)	Cu	1.80	–	1.87, 1.81	1.84	–	2.2	–
	Ni	0.55	–	0.60, 0.56	0.58	–	5.5	–
	Pb	–	–	2.11, 2.05	2.08	–	–	–
Ir	Cu	0.00	2.00	1.88, 1.94, 1.96, 2.02, 1.96	1.96	2.6	−2.0	98
	Ni	0.00	2.00	1.90, 1.96, 2.02, 2.04, 1.96	1.98	2.8	−1.0	99
	Pb	–	3.00	2.82, 2.90, 2.98, 3.00, 2.92	2.92	2.4	−2.7	97

CONCLUSIONS

A sensitive, rapid and continuous ion chromatographic method was developed for the determination of trace heavy metal impurities in noble metals, in which a three-component eluent was used to improve the chromatographic resolution and the simplex method was used to optimize the composition of the eluent. An on-line pre-enrichment column was used to remove the noble metal matrix and to enrich trace heavy metal impurities in a single operation. The resolution between each adjacent pair of the six heavy metal ions was larger than 1.17 and the enrichment efficiency of the ions was above 98% under the experimental conditions. The method was applied to real samples and the results were satisfactory.

ACKNOWLEDGEMENT

The authors are grateful to D.Y. Chang for helpful discussions and for providing the real samples studied.

REFERENCES

1 F.E. Beamish, *The Analytical Chemistry of the Noble Metals*, Pergamon Press, London, 1966, pp. 141–144.
2 F.E. Beamish and J.C. Van Loon, *Analysis of Noble Metals*, Academic Press, New York, 1977, pp. 247–250.
3 D.Y. Chang, Northwestern Nonferrous Metal Company of China, personal communication.
4 M.C. Liu, B.W. Fan and Z.D. Hu, *Chem. J. Chin. Univ.*, 1 (1980) 61.
5 L.R. Chen, Z.Y. Hu, Q. Wang, M.C. Liu, B.W. Fan and Z.D. Hu, in P.C. Lu and E. Bayer (Editors), *Proceedings of Sino–West German Symposium on Chromatography, Dalian, China, 1983*, p. 560.
6 Y. Takata and G. Muto, *Anal. Chem.*, 45 (1973) 1864.
7 Research Group 101, Lanzhou Institute of Chemical Physics, Chinese Academy of Sciences, *Huaxue Tongbao*, 2 (1981) 134.
8 J.L. Glajch, J.J. Kirkland, K.M. Squire and J.M. Minor, *J. Chromatogr.*, 199 (1980) 57.
9 M.L. Xu, *Fenxi Huaxue*, 12 (1984) 151.
10 J.A. Nelder and R. Mead, *Comput. J.*, 7 (1965) 308.

Journal of Chromatography, 644 (1993) 83–94
Elsevier Science Publishers B.V., Amsterdam

CHROM. 25 090

Use of thermal field flow fractionation for the fractionation of polybutadiene in various organic solvents

A.C. van Asten, E. Venema, W.Th. Kok and H. Poppe*

Laboratory for Analytical Chemistry, University of Amsterdam, Nieuwe Achtergracht 166, 1018 WV Amsterdam (Netherlands)

(First received February 3rd, 1993; revised manuscript received March 19th, 1993)

ABSTRACT

It is shown that thermal field flow fractionation (ThFFF) can be a valuable tool for the fractionation of polybutadiene (PB). The thermal diffusivity of four PB standards of different molecular mass was determined in six organic solvents. The results indicate that for this polymer species, the thermal diffusion coefficient varies significantly with the choice of the solvent but seems to be independent of the molecular mass. The highest retention for a given molecular mass was found with toluene and ethylbenzene as solvents. With respect to the speed of separation of polybutadiene, the best results were obtained with toluene. The influence of the temperature drop across the channel and the polymer concentration on retention was also studied. The use of an evaporative light-scattering detector made it possible to work with polymer sample concentrations as low as 0.1 mg/ml. The unique separation possibilities offered by ThFFF are demonstrated with the separation of polybutadiene, polyisoprene and polystyrene standards of the same molecular mass using tetrahydrofuran as solvent.

INTRODUCTION

After its introduction by Giddings [1] in 1966, field flow fractionation (FFF) has steadily developed and it now covers a fairly broad ensemble of separation methods. Retention and separation are accomplished by the use of an external field perpendicular to the direction of the laminar flow of a carrier liquid through an open channel [2]. FFF techniques are especially suited to the separation and characterization of macromolecules, colloids and particles.

Thermal field flow fractionation (ThFFF) is a variety of FFF in which a temperature gradient is used as the field. Over the years it has been shown that ThFFF is a valuable tool for the analysis of synthetic polymers in various organic solvents [3–8]. Only very recently has it been demonstrated that ThFFF is also useful for the separation of particles in aqueous and non-aqueous solutions [9,10]. In ThFFF, retention is determined by the ratio of the ordinary and thermal diffusion coefficients. This ratio is also expressed as α/T, where α is the Soret coefficient and T is the temperature.

Although studied for over a century [11], thermal diffusion in liquids is still a poorly understood process. Various theories have been developed that vary widely in conceptual basis [12–16]. However, Schimpf and Giddings [3] demonstrated that none of the existing theories is able to describe accurately the phenomenon of thermal diffusion of polymers in solution. In order to gain more knowledge of and insight into the effect of thermal diffusion, it is necessary to measure thermal diffusion coefficients for various polymer–solvent systems. In combination with another technique for the measurement of

* Corresponding author.

0021-9673/93/$06.00

diffusion coefficients, ThFFF will yield highly accurate data on thermal diffusion coefficients.

Schimpf and Giddings [3] found for polystyrene (PS), poly-α-metastyrene (PαMS), poly(methyl methacrylate) (PMMA) and polyisoprene (PI) in different organic solvents that the thermal diffusion coefficient is independent of the molecular mass of the polymer. However, thermal diffusion was found to be related to the chemical composition of both the polymer and the solvent. An empirical relationship linked the thermal diffusion coefficient to the thermal conductivity of the polymer and the solvent and the activation energy of viscous flow. In other studies by the same group it was found that the thermal diffusion of polystyrene in ethylbenzene is independent of the branching configuration of the polymer [17]. ThFFF studies of random and block copolymers [4] demonstrated that for random copolymers a linear relationship exists between the thermal diffusion coefficient and the mole fraction of one of the monomers. However, for block copolymers it was found that the monomer species in the outer regions of the solvated polymer predominantly determines the extent of thermal diffusion. Further complications arise from the fact that the thermal diffusion coefficient is strongly temperature dependent. Brimhall *et al.* [18] found for polystyrene in ethylbenzene a linear relationship between the thermal diffusion coefficient and the temperature in the centre of the solute zone.

The use of ThFFF for the analysis of water-soluble macromolecules has been very limited because only for very few polymer species [poly(ethylene oxide), polyvinylpyrrolidone and poly(styrene sulphonate)] has thermal diffusion in aqueous environments been observed [19].

In comparison with other polymer fractionation methods, ThFFF offers unique separation possibilities. Polymer species are separated not only according to size but also according to thermal diffusion. Because thermal diffusion depends on the chemical nature of the polymer, ThFFF can be used for the separation of macromolecules which are equal in size but differ in chemical composition [20].

In this paper, the use of ThFFF for the fractionation of polybutadiene (PB) is demonstrated. Values for α/T, which we believe are accurate, for four PB standards of different molecular mass were determined in six organic solvents. The effects of the polymer concentration and the temperature drop across the channel were investigated. Further, the unique separation capabilities of ThFFF are demonstrated with the separation of three different polymer species of the same molecular mass.

THEORY

Conversion of retention ratios into α/T values

The retention ratio in FFF, which is equal to the ratio of the void volume and the retention volume, can be expressed as [21]

$$R = \frac{\langle C(x)v(x)\rangle}{\langle C\rangle\langle v\rangle} \tag{1}$$

where x is the coordinate in the direction of the channel thickness, $\langle\ \rangle$ denotes values averaged over the cross-section of the channel and $C(x)$ and $v(x)$ are the concentration of the solute and the linear carrier fluid velocity, respectively, as functions of the position across the channel thickness.

The retention ratio can easily be obtained from the fractogram. When no temperature and concentration effects are considered, eqn. 1 leads to the following well known expression:

$$R \approx 6\lambda\left[\coth\left(\frac{1}{2\lambda}\right) - 2\lambda\right] \tag{2}$$

where the dimensionless parameter λ represents the mean layer thickness of the compressed solute zone. For ThFFF the λ value can be approximated by

$$\lambda \approx \frac{D}{D_T\,\Delta T} = \frac{1}{\frac{\alpha}{T}\Delta T} \tag{3}$$

where D and D_T are the ordinary and the thermal diffusion coefficient of the polymer species in the given solvent, respectively, ΔT is the temperature drop across the channel thickness and α is the Soret coefficient. With the use of eqns. 2 and 3 it is possible to convert retention data into α/T values. When diffusion data for the polymer–solvent system are available these α/T

values can be used to determine thermal diffusion coefficients.

However, theoretical complications arise from the fact that a number of important parameters are temperature dependent. Because of the temperature gradient used in ThFFF, these parameters will vary across the channel thickness. Gunderson *et al.* [22] showed that the temperature dependence of the viscosity and the thermal conductivity of the solvent can be accounted for by using empirical relationships. For the solvent viscosity η, the temperature dependence is expressed as

$$\frac{1}{\eta} = a_0 + a_1 T + a_2 T^2 + a_3 T^3 \quad (4)$$

where T is the temperature and a_i are empirical constants.

For the solvent thermal conductivity κ, the following equation is used to describe the temperature dependence:

$$\kappa = b_0 + b_1(T - T_c) \quad (5)$$

where b_0 and T_c are the thermal conductivity and the temperature at the cold wall, respectively. The term b_1, often expressed as $d\kappa/dT$, is considered to be constant in the temperature range of interest. In previous work [23] we have shown that the temperature dependence of the solvent viscosity has a significant effect on the shape of the velocity profile of the carrier liquid. The effect of the temperature dependence of the thermal conductivity on the velocity profile is negligible. However, it is important to consider the temperature dependence of this latter parameter because it has a significant effect on the concentration profile of the solute. As was shown by Brimhall *et al.* [18], α/T itself is also strongly temperature dependent. The temperature dependence of α/T can be expressed empirically with a second-degree polynomial function. To account for the influence of the temperature gradient across the solute zone on α/T, retention data should therefore be available for at least three different cold wall temperatures [23]. In this work this latter effect was neglected because the corresponding systematic error is only small. Using a numerical integration routine the temperature dependence of the solvent viscosity and thermal conductivity has been accounted for. The α/T values have been directly assigned to the temperature in the centre of gravity of the corresponding solute zones [18].

Effect of solvent and polymer type on time optimization in ThFFF

As was demonstrated by Giddings *et al.* [24], theoretical considerations of time optimization in FFF are largely equivalent to those in chromatography. The number of plates N needed to achieve a separation with a resolution R_s of two discrete polymer fractions is given by

$$N = 16R_s^2\left(\frac{M}{\Delta M}\right)^2\left(\frac{d\ln M}{d\ln V_r}\right)^2 \quad (6)$$

where ΔM is the difference in molecular mass of two polymer fractions having a mean molecular mass M and V_r is the retention volume.

The time required to generate one plate can be expressed as

$$t_p = \frac{H}{R\langle v\rangle} \quad (7)$$

where H is the plate height and $\langle v\rangle$ is the mean velocity of the carrier liquid. Combining eqns. 6 and 7 yields the following expression for the analysis time t_a necessary to obtain a separation with resolution R_s:

$$t_a = 16R_s^2 \cdot \left(\frac{M}{\Delta M}\right)^2 \cdot \frac{H}{R\langle v\rangle} \cdot \left(\frac{d\ln M}{d\ln V_r}\right)^2 \quad (8)$$

The first two factors on the right-hand side of eqn. 8 do not need any further consideration because they only reflect the demands put on the separation. The third factor reflects the efficiency and the last factor corresponds to the molecular mass selectivity of the separation mechanism.

Using this last equation, Giddings *et al.* [24] concluded that substantial improvements in separation speed and analysis time could be obtained with decreasing channel thickness and increasing temperature drop. However, when eqn. 8 is studied it can be expected that also the choice of the polymer and the solvent will have a signifi-

cant effect on the analysis time. In order to examine the influence of the solvent and polymer type on the separation speed in ThFFF, the analysis time has to be evaluated for a fixed channel thickness and temperature drop.

In the following discussion it has been neglected that the use of a temperature gradient in ThFFF disturbs both the velocity profile of the carrier liquid and the concentration profile of the solute. Although it is known that these temperatures effects have a significant effect on retention and plate height [22], we shall assume that the conclusions regarding time optimization will retain their validity.

The plate height in FFF is dominated by non-equilibrium effects [25]. The polydispersity of the polymer sample is also an important factor to consider in practice. However, polydispersity is not taken into account here, because only the separation power of the fractionation method is discussed. If only the non-equilibrium contribution is considered, the plate height in FFF is given by [26]

$$H = \chi \cdot \frac{w^2 \langle v \rangle}{D} \tag{9}$$

where w is the channel thickness and χ is a complicated function of the parameter λ. The influence of the diffusion coefficient on the plate height in ThFFF is not straightforward. The diffusion coefficient will influence λ (see eqn. 3) and thereby χ. In the limit of $\lambda \rightarrow 0$, χ can be approximated by $24\lambda^3$ [26]. As λ is proportional to D, the plate height will in this case be proportional to D^2, indicating that the efficiency will increase dramatically with increasing molecular mass of the polymer.

The parameter S, describing the molecular mass selectivity of a polymer fractionation method, is generally defined as [5]

$$S = \left| \frac{\mathrm{d} \ln V_r}{\mathrm{d} \ln M} \right| \tag{10}$$

This can be rearranged to

$$S = \left| \frac{\mathrm{d} \ln R}{\mathrm{d} \ln \lambda} \frac{\mathrm{d} \ln \lambda}{\mathrm{d} \ln M} \right| \tag{11}$$

Using eqn. 2 the term d ln R/d ln λ can be evaluated. For all polymer–solvent systems studied so far it has been found that the thermal diffusion coefficient is independent of the molecular mass. Therefore, M will influence λ only through its effect on the diffusion coefficient. The correlation between the diffusion coefficient and the molecular mass of a polymer is often expressed using the following empirical relationship:

$$D = A/M^b \tag{12}$$

where A and b are constants which are determined by both the solvent and the polymer.

With the use of eqn. 12 it can easily be found that the term d ln λ/d ln M equals b. In systems in which retention is high ($\lambda < 0.05$), the retention ratio can be approximated by 6λ [27]. In this case the term d ln R/d ln λ equals 1 and the mass selectivity is therefore equal to b. However, if the retention is lower the value of S will be significantly lower. This is demonstrated in Fig. 1, where d ln R/d ln λ is plotted as a function of λ.

In the limit of $\lambda \rightarrow 0$, when R is equal to 6λ, χ can be expressed as $24\lambda^3$ and S is equal to b, the analysis time will be proportional to

$$t_a \sim \frac{1}{b^2} \cdot \left(\frac{w}{\Delta T} \right)^2 \cdot \frac{D}{D_T^2} \tag{13}$$

The constant b is in the range 0.5–0.6 for most polymer–solvent systems. The second factor on the right-hand side of eqn. 13 corresponds to the experimental parameters of the ThFFF set-up. As Giddings *et al.* [24] concluded, a gain in

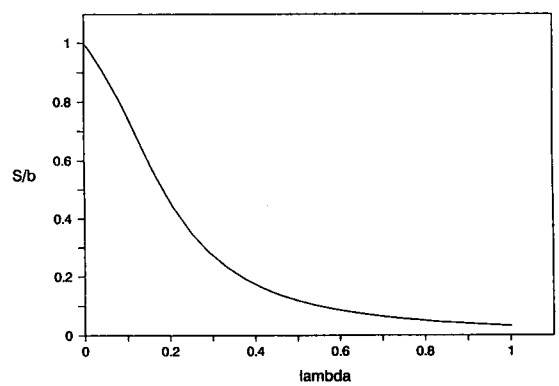

Fig. 1. S/b (d ln R/d ln λ) as a function of λ.

separation speed can be obtained when the temperature drop and channel thickness are increased and decreased, respectively. The last factor is determined by the mean molecular mass of the two polymer fractions and the polymer–solvent system that is considered. Decreasing diffusion and increasing thermal diffusion will improve the separation speed of ThFFF. To demonstrate the effect of the polymer–solvent system and the molecular mass of the polymer fractions on the analysis time in ThFFF under normal working conditions, eqn. 8 was fully evaluated for a fixed ThFFF set-up. Nowadays a channel thickness of 76 μm with a temperature drop across the channel of 80 K can be used routinely, and these values were therefore used in the calculations.

By combining eqns. 8 and 9, it can be seen that the analysis time is independent of the flow-rate of the carrier liquid. Therefore, with w and ΔT regarded as constants, the analysis time is only a function of M, A, b and D_T. The last three parameters are all dependent on the chemical nature of both the solvent and the polymer. If these three parameters are known it is possible to plot the analysis time as a function of the molecular mass for a given polymer–solvent system. This is illustrated in Fig. 2, from which it can be concluded that the separation

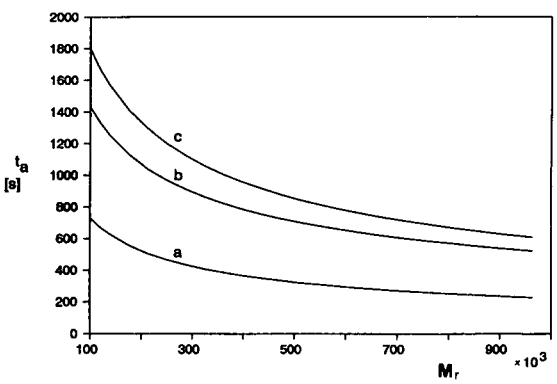

Fig. 2. Analysis time as a function of the molecular mass (M_r) for polystyrene in (a) THF and (b) cyclohexane and for (c) polyisoprene in THF. $w = 76$ μm; $\Delta T = 80$°C; $R_s = 1$; $M/\Delta M = 3$. Polystyrene in THF: $A = 3.861 \cdot 10^{-4}$, $b = 0.571$, $D_T = 1.0 \cdot 10^{-7}$ cm^2/s·K. Polyisoprene in THF: $A = 3.371 \cdot 10^{-4}$, $b = 0.570$, $D_T = 0.57 \cdot 10^{-7}$ cm^2/s·K. Polystyrene in cyclohexane: $A = 1.061 \cdot 10^{-4}$, $b = 0.497$, $D_T = 0.66 \cdot 10^{-7}$ cm^2/s·K.

speed in ThFFF varies significantly with the choice of the polymer and the solvent. Further, it can be seen that the use of ThFFF becomes more advantageous when samples of high molecular mass have to be analysed. However, these conclusions must be adjusted for ultra-high molecular masses for which lift forces will play a dominant role at high flow-rates [28].

A computer program was developed based on eqns. 2 and 9 to simulate fractograms for specific polystyrene samples with THF and cyclohexane as solvents. Fig. 3 shows the results obtained using data for ordinary and thermal diffusion coefficients given by Schimpf and Giddings [3]. For the three simulations shown, a constant temperature drop and channel thickness were chosen. The flow-rate was adjusted in such a way that for all three fractograms the analysis time was the same. In this way, differences in separation speed are illustrated by means of differences in resolution.

When the fractograms in Fig. 3a and b are compared, the effect of the molecular mass of the polymer fractions can be clearly seen. Higher molecular masses will result in lower λ values and therefore will allow a higher separation speed to be obtained by adjusting the flow-rate of the carrier liquid. Note that the standards in both fractograms have the same relative difference in molecular mass. For the fractograms in Fig. 3b and c the molecular mass of the three standards is the same. The difference in resolution, which is fairly large, is the result of the use of different solvents. For the fractogram in Fig. 3b THF was selected as the solvent, whereas for that in Fig. 3c cyclohexane was chosen. Although the thermal diffusion of polystyrene is much lower in cyclohexane than in THF, the λ values are comparable, because the diffusion coefficients for polystyrene standards are also much lower in cyclohexane than in THF. From the literature a general trend can be observed that high thermal diffusion is accompanied by relatively high ordinary diffusion. Because of the relatively higher diffusion without the loss of retention, the use of THF leads to much better resolution of the PS standards in the same analysis time.

One of the aims of this work was to find the

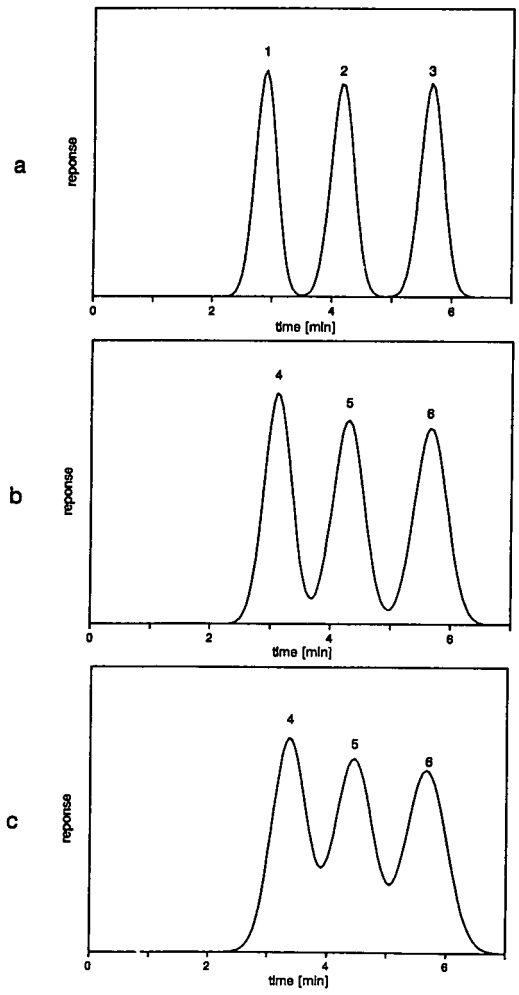

Fig. 3. Simulated ThFFF fractograms for polystyrene in (a, b) THF and (c) cyclohexane. Molecular mass: 1 = 250 000, 2 = 500 000, 3 = 875 000, 4 = 50 000, 5 = 100 000, 6 = 175 000. $w = 76$ μm; $\Delta T = 80$°C; flow-rate, (a) 0.942 ml/min, (b) 0.4 ml/min and (c) 0.394 ml/min; no polydispersity effects were considered. Values for A, b and D_T as in Fig. 2.

best solvent for the ThFFF analysis of polybutadiene. From eqn. 8 it can be seen that the solvent for which lowest λ values are obtained for a given molecular mass will yield the highest separation speed. However, if for two or more solvents comparable λ values are found, additional measurements have to be made to determine which solvent can best be used. In this case the solvent in which the polymer species has the highest diffusion coefficient (and highest thermal diffusion coefficient) will give the shortest analysis time.

EXPERIMENTAL

Instrumentation

A T100 thermal polymer fractionator was obtained from FFFractionation (Salt Lake City, UT, USA). A Mylar spacer (thickness 127 μm) was cut out and clamped between the two chrome-plated copper bars to form the channel. The tip-to-tip length of the channel was 46 cm and the channel breadth was 2 cm. The channel ends were tapered to allow a smooth fluid flow at the channel inlet and outlet. The void volume was 0.98 ml. For the determination of the α/T values a temperature drop of 60°C was used. The cold wall temperature ranged from 30 to 35°C. For some of the fractograms a higher ΔT value of 80°C was used; the accompanying cold wall temperature in this instance was 36°C. In all experiments the solvent flow was stopped for 5 min after injection to allow relaxation. A constant-flow pump (Spectroflow 400; ABI, Ramsey, NJ, USA) was used to deliver the solvents. Prior to use all solvents were filtered by vacuum suction over a 0.5-μm filter (Model FH; Millipore, Bedford, MA, USA). During the experiments the organic solvents were continuously degassed with helium. A small, laboratory-made column packed with silica particles and a pulse damper (Model 812; Tegimenta, Rotkreuz, Switzerland) were used to obtain a reliable solvent flow with minimum pulsation. The injection valve had a loop volume of 20 μl. Detection was performed with an evaporative light-scattering detector (Model 2A; Varex, Burtonsville, MD, USA). The outlet of the channel was connected to the detector by means of a fused-silica capillary of I.D. 100 μm and O.D. 360 μm (Polymicro Technologies, Phoenix, AZ, USA). A capillary length of 1 m was chosen to combine a small dead volume (0.008 ml) with a sufficiently large back-pressure (*ca.* 7 bar at a flow-rate of 0.2 ml/min) to elevate the boiling points of the organic solvents in the ThFFF channel.

Materials

All solvents were of analytical-reagent grade. THF and toluene were obtained from Janssen Chimica (Geel, Belgium), ethylbenzene, cyclohexane and dioxane from Merck (Darmstadt, Germany), benzene from Baker (Deventer, Netherlands) and polybutadiene, polyisoprene and polystyrene standards from Polymer Laboratories (Church Stretton, Shropshire, UK).

Data handling

Data from the fractograms were collected using the FFFractionation data acquisition board in combination with a personal computer. The data were analysed using the manufacturer's analysis software (version 2.0). Lotus 123 and Lotus Freelance Plus (Lotus Development, Cambridge, MA, USA) were used to create the fractograms from the data files. To correct for the temperature dependence of the solvent viscosity and solvent thermal conductivity, a computer program, which has been described in detail previously [23], was used for the conversion of the measured retention ratios into α/T values. This program, together with the computer program for the fractogram simulations, was written using Turbo Pascal 6.0 (Borland International, Scotts Valley, CA, USA). The empirical constants, needed to account for the temperature dependence of the viscosity and thermal conductivity of the various organic solvents, are given in Table I. Data concerning the temperature dependence of these two parameters were taken from the literature [18,22,29–31].

RESULTS AND DISCUSSION

To test the ThFFF set-up, retention measurements were made for three different polystyrene standards of different molecular mass (68 000, 310 000 and 700 000) in toluene. A temperature drop of 60°C was used and the polymer concentration of the injected samples was 0.2 mg/ml for each standard. Using diffusion data from Schimpf and Giddings [3], a thermal diffusion coefficient of 0.98 10^{-7} $cm^2/s \cdot K$ was found for all three standards. This value is in good agreement with other reported measurements.

Next the retention was determined of four polybutadiene standards (120 000, 330 000, 500 000 and 950 000) in six organic solvents. The results are shown in Fig. 4, where the λ values are plotted as a function of $M^{-1/2}$. The linear dependence indicates that the thermal diffusion coefficient is independent of the molecular mass (this follows from eqns. 3 and 12, bearing in mind that $b \approx 0.5$ for most polymer–solvent systems). This is in agreement with the results obtained for other polymer species. However, diffusion measurements have to be made to verify these preliminary conclusions. The highest retention for a given molecular mass was found in toluene and ethylbenzene. In contrast to other

TABLE I

EMPIRICAL CONSTANTS NEEDED TO DESCRIBE THE TEMPERATURE DEPENDENCE OF THE VISCOSITY AND THERMAL CONDUCTIVITY OF THE FIVE GIVEN SOLVENTS

Solvent	a_0	a_1	a_2	a_3 ($\times 10^5$)	κ (293 K) (W/s·K)	b_1 ($\times 10^5$) (W/s·K^2)
Benzene	6445.30	−80.057	0.2936	−26.477	0.1477	−35.00
Cyclohexane	4081.22	−40.278	0.1094	−25.481	0.1209	−25.19
Ethylbenzene	2892.92	−35.176	0.1284	−8.395	0.1321	−24.37
THF	7622.73	−88.933	0.3344	−32.587	0.1398	−19.89
Toluene	3109.76	−45.318	0.1818	−15.078	0.1320	−27.24

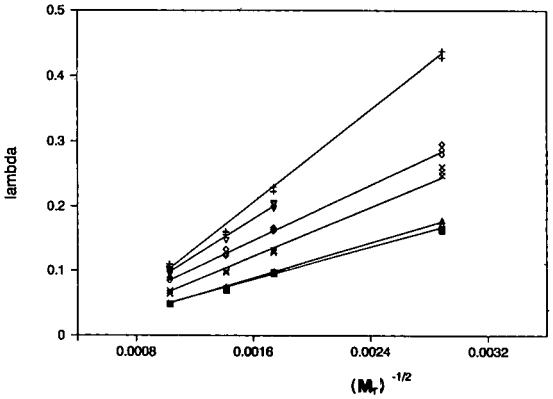

Fig. 4. λ Values for the four PB standards in six organic solvents. $w = 127$ μm; $\Delta T = 60$°C; $T_c = 32$°C; flow-rate, 0.2 ml/min; polymer concentration, 0.2 mg/ml. ■ = Toluene; + = THF; ◇ = cyclohexane; △ = ethylbenzene; × = dioxane; ▽ = benzene.

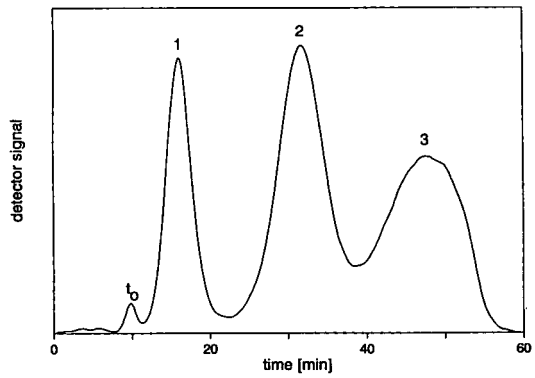

Fig. 5. ThFFF separation of three PB standards in toluene. Molecular mass: 1 = 120 000 ($\mu < 1.03$); 2 = 500 000 ($\mu < 1.03$); 3 = 950 000 ($\mu < 1.03$). $w = 127$ μm; $\Delta T = 60$°C; $T_c = 32$°C; flow-rate, 0.1 ml/min; polymer concentration, 0.2 mg/ml. Evaporative light-scattering detection.

polymer species, low retention was found when THF was used as the solvent. The corresponding α/T values are given in Table II. In the determination of the α/T values, the temperature dependence of the solvent viscosity and thermal conductivity was accounted for. The effect of the temperature drop across the solute zone on α/T was neglected and α/T values were directly assigned to the temperature in the centre of gravity of the solute zones.

The use of ThFFF for the fractionation of polybutadiene is demonstrated in Fig. 5. As was stated earlier, the solvent that gives rise to the highest retention for a certain molecular mass can best be used for the ThFFF analysis. Fig. 6 shows the separation of two PB standards in toluene, ethylbenzene and THF. The flow-rate

TABLE II

α/T VALUES FOR THE PB STANDARDS IN THE DIFFERENT ORGANIC SOLVENTS

For experimental conditions see Fig. 1. Numbers given are mean values of four different measurements; R.S.D. = standard deviation. The temperature in the centre of gravity of the solute zones ranged from 37°C (PB of molecular mass 950 000 in toluene) to 53°C (PB of molecular mass 120 000 in THF). For dioxane no parameters were found describing the temperature dependence of the viscosity and thermal conductivity. The empirical parameters of toluene were taken to calculate the α/T values for this solvent.

Solvent	Molecular mass of PB							
	120 000		330 000		500 000		950 000	
	α/T	R.S.D. (%)	α/T	R.S.D. (%)	α/T	R.S.D. (%)	α/T	R.S.D. (%)
THF	0.0387	0	0.0762	1.5	0.1080	1.3	0.1616	2.2
Benzene	–	–	0.0899	1.9	0.1198	0	0.1730	2.1
Cyclohexane	0.0595	2.7	0.1064	1.5	0.1380	3.4	0.2049	2.4
Dioxane	0.0678	2.1	0.1336	1.3	0.1786	1.5	0.2657	3.1
Toluene	0.1003	1.6	0.1795	1.3	0.2374	0.4	0.3667	0.7
Ethylbenzene	0.1015	1.3	0.1732	1.1	0.2343	1.7	0.3425	1.0

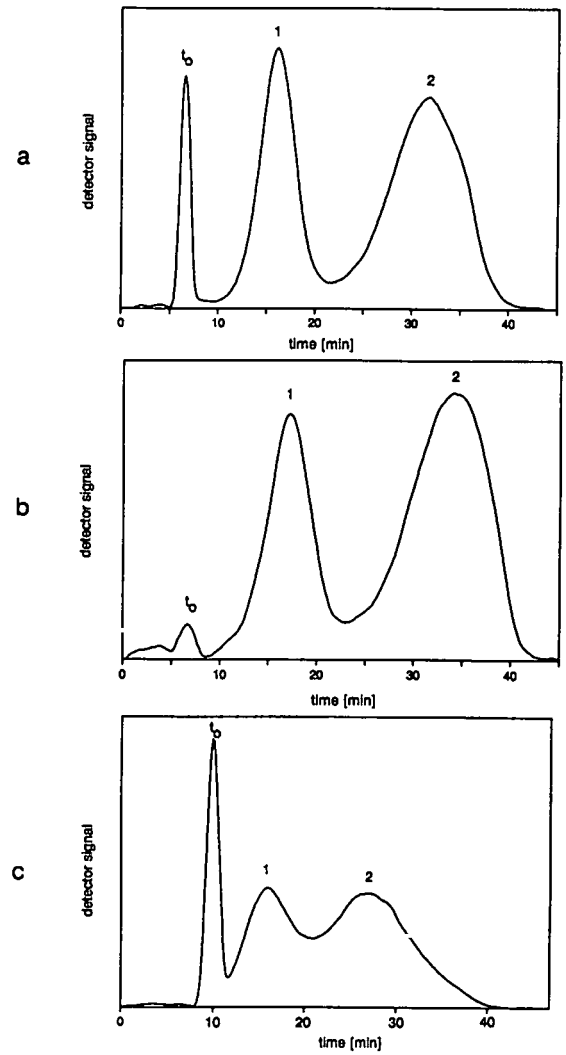

Fig. 6. Separation of two PB standards in (a) toluene, (b) ethylbenzene and (c) THF. Molecular mass: 1 = 330 000 (μ < 1.04); 2 = 950 000 (μ < 1.03). w = 127 μm. For THF: ΔT = 80°C; T_c = 36°C; flow-rate, 0.1 ml/min. For toluene and ethylbenzene: ΔT = 60°C; T_c = 31°C; flow-rate, 0.15 ml/min. Polymer concentration, 0.3 mg/ml. Evaporative light-scattering detection.

was adjusted in such a way that for all solvents the analysis time was the same. Even though for THF a higher temperature drop was used, it can be seen that the resolution is much smaller than that obtained with the other two solvents. This is caused by the fact that in THF relatively high λ values were found (see Fig. 4). For toluene and ethylbenzene the λ values were about equal for the different PB standards. As was pointed out in the theoretical section, a large difference in the separation speed of a given polymer species can still exist for solvents for which comparable λ values are found. When for a constant temperature drop and channel thickness the λ values are equal, this only indicates that the ratios of ordinary and thermal diffusion coefficients are the same in both situations. When fractograms a and b in Fig. 6 are compared, it can be seen that the use of toluene leads to slightly better resolution. This indicates that the ordinary and the thermal diffusion coefficient of PB are both higher in toluene than in ethylbenzene. The fact that the difference in resolution is only very small is mainly caused by the large contribution of the polydispersity of the PB standards to the plate height. From the fractograms in Fig. 6 it can be concluded that toluene is the best solvent to use for the ThFFF analysis of polybutadiene. The measurement of the peak width in ThFFF in combination with retention data provides in principle a route to the determination of ordinary diffusion coefficients. Therefore, if truly monodisperse standards (or standards for which the polydispersity is exactly known) could be used, the measurement of the retention ratio and the plate height in ThFFF could yield thermal diffusion coefficients without the need for additional diffusion measurements.

The effect of the temperature drop on retention was studied for PB of molecular mass 330 000 and 950 000 in toluene. The results are given in Fig. 7; the linear relationship between λ and $1/\Delta T$ is in good agreement with eqn. 3. This again indicates that the retention measurements are free from systematic errors caused by the ThFFF set-up.

Schimpf [32] and Caldwell *et al.* [33] stated that for high molecular masses the effect of polymer concentration on retention in ThFFF can be profound. When accurate retention measurements are made for the determination of thermal diffusion coefficients, it is important that the effect of polymer concentration is negligible. With the use of the evaporative light-scattering detector, polymer sample concentrations as low as 0.1 mg/ml can be used. To study the effect of polymer concentration, the retention ratio for

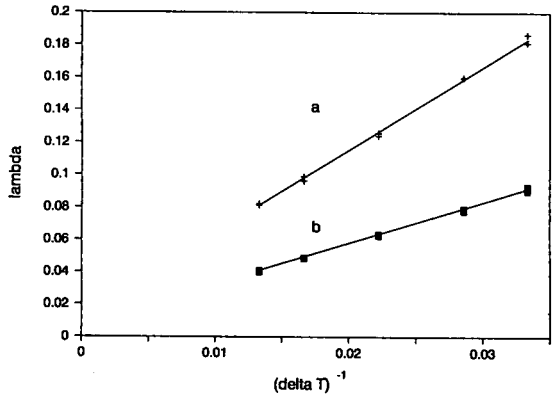

Fig. 7. Effect of ΔT on λ for PB of molecular mass (a) 330 000 and (b) 950 000 in toluene. $w = 127$ μm; $T_c = 26$–32°C; flow-rate, 0.2 ml/min; polymer concentration, 0.2 mg/ml.

PB of molecular mass 950 000 in toluene was measured for different sample concentrations; this system was chosen because the lowest λ values were obtained. The polymer concentration at the cold wall was in this instance equal to approximately twenty times the concentration of the injected sample ($\lambda \approx 0.05$). The results, shown in Fig. 8, indicate that significant effects are observed even if the polymer concentration is well below 1 mg/ml. The influence of the polymer concentration can in this instance only be neglected if concentrations of 0.2 mg/ml or lower are used. A systematic error of 10% in the determination of λ was found when the polymer concentration was 1 mg/ml. Because all retention measurements were made with a polymer concentration of 0.2 mg/ml, it can be concluded that the determined α/T values are virtually free from systematic errors due to concentration effects.

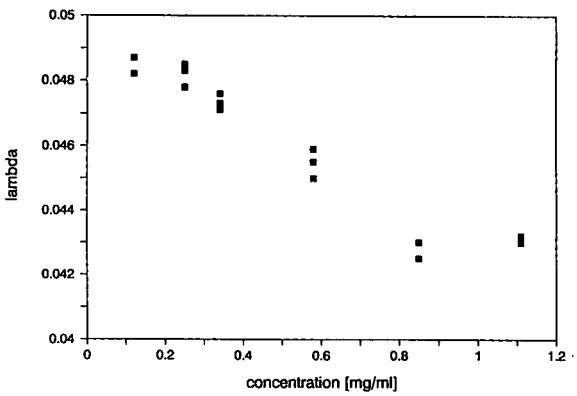

Fig. 8. Effect of polymer concentration on λ for PB of molecular mass 950 000 in toluene. $w = 127$ μm; $\Delta T = 60$°C; $T_c = 30$°C; flow-rate, 0.2 ml/min.

Compared with other polymer fractionation methods such as size-exclusion chromatography [34] and hydrodynamic chromatography (HDC) [35], ThFFF becomes more interesting when polymers of high molecular mass have to be analysed. An additional advantage is that in ThFFF retention is not only determined by the ordinary diffusion coefficient but also by the thermal diffusion coefficient. Because the thermal diffusion coefficient depends on the chemical nature of the polymer, ThFFF can separate polymer species according to both size and chemical characteristics. This unique feature, which was demonstrated for the first time by Gunderson and Giddings [20], makes it possible to perform separations of particle and polymer species that are equal in size but differ in chemical nature.

Fig. 9 shows a packed-column HDC separation of polystyrene, polyisoprene and polybutadiene standards of the same molecular mass in THF. Packed-column HDC is a very efficient

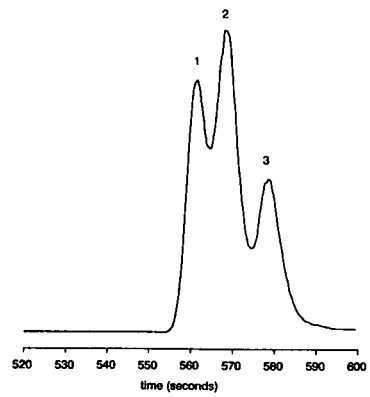

Fig. 9. Packed-column HDC separation of (1) PB of molecular mass 330 000, (2) PI of molecular mass 295 000 and (3) PS of molecular mass 336 000 in THF (courtesy of Mr. G. Stegeman, Laboratory of Analytical Chemistry, University of Amsterdam). (1) $\mu < 1.04$; (2) $\mu < 1.04$; (3) $\mu < 1.05$. Column, 150 × 4.6 mm I.D.; packing, 1.5-μm non-porous silica; flow-rate, 0.1 ml/min; pressure, 31 bar; polymer concentration, 0.11–0.15 mg/ml. Evaporative light-scattering detection.

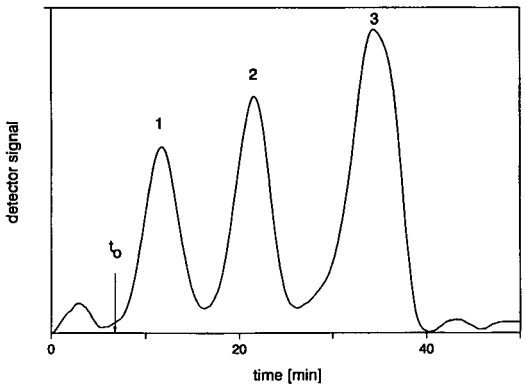

Fig. 10. ThFFF separation of (1) PB of molecular mass 330 000, (2) PI of molecular mass 295 000 and (3) PS of molecular mass 336 000 in THF. $w = 127$ μm; $\Delta T = 80$°C; $T_c = 28$°C; flow-rate, 0.15 ml/min; polymer concentration, 0.1–0.3 mg/ml. Evaporative light-scattering detection. For polydispersity of the standards, see Fig. 9.

polymer fractionation method. For sufficiently high molecular masses, the plate height, which is about 2.1 μm for a column packed with 1.5-μm particles, is independent of the velocity of the carrier liquid [36]. This indicates that the resolution for a given column length is constant, regardless of the mobile phase velocity. Because the size difference between the three standards is only very small, no baseline separation was obtained using this technique. However, because these three standards possess different thermal diffusion coefficients in THF, a baseline separation was easily obtained using ThFFF, as illustrated in Fig. 10. This ThFFF separation clearly demonstrates how the thermal diffusion effect can be employed to separate polymer species according to chemical characteristics. Note that again the highest thermal diffusion coefficient is accompanied by the highest ordinary diffusion coefficient (in HDC the largest polymers elute first).

CONCLUSIONS

Thermal field flow fractionation can be used effectively for the fractionation of polybutadiene samples. For a given set of experimental parameters and molecular mass, the highest α/T values were found when toluene was used as the solvent. For optimum fractionation conditions this solvent should be used for the ThFFF analysis of polybutadiene. Retention measurements of standards of different molecular mass indicate size independence of the thermal diffusion coefficient for polybutadiene in all six organic solvents. However, the effect of thermal diffusion seems to be dependent on the chemical nature of the solvent. Accurate diffusion measurements are currently being made to verify these preliminary conclusions. When samples of high molecular mass are used, special attention should be given to the polymer concentration. For PB of molecular mass 950 000 in toluene ($\lambda \approx 0.05$), a significant increase in retention was found for samples with a polymer concentration of 0.3 mg/ml or higher. The use in this instance of a polymer concentration of 1 mg/ml led to a systematic error of 10% in the determination of the corresponding α/T value.

ThFFF offers unique separation possibilities because retention is determined by both the size and the thermal diffusion coefficient of the polymer in solution. Because the thermal diffusion coefficient depends on the chemical nature of the polymer, ThFFF can be used for the separation of polymers that are identical in size but possess different chemical properties. This feature, which is unique to ThFFF, has been demonstrated with the separation of polybutadiene, polyisoprene and a polystyrene standards of the same molecular mass in THF. This and many other studies demonstrate that high thermal diffusion is often accompanied by high ordinary diffusion. Therefore, it may be possible to use the diffusion coefficient for a given molecular mass as an indicator of the magnitude of the thermal diffusion effect.

SYMBOLS

α	Soret coefficient	
C	Concentration	mol/m^3
C_0	Concentration at the cold wall	mol/m^3
D	Diffusion coefficient	m^2/s

D_T	Thermal diffusion coefficient	$m^2/s \cdot K$
H	Plate height	m
η	Solvent viscosity	Pa s
κ	Thermal conductivity	$J/m \cdot s \cdot K$
λ	Dimensionless mean layer thickness	
l	Mean layer thickness	m
M	Molecular mass	g/mol
N	Number of plates	
R	Retention ratio	
R_s	Resolution	
S	Selectivity	
T	Temperature	K
T_c	Cold wall temperature	K
ΔT	Temperature drop across channel thickness	K
t_0	Unretained time	s
t_p	Time needed to generate one plate	s
t_a	Analysis time	s
μ	Polydispersity	
v	Linear fluid velocity	m/s
$\langle v \rangle$	Mean linear fluid velocity	m/s
V_r	Retention volume	m^3
w	Channel thickness	m

ACKNOWLEDGEMENTS

This research was supported by Akzo Research Laboratories (Arnhem, Netherlands) and Shell Research (Amsterdam, Netherlands). Mr. G. Stegeman is thanked for helpful discussions and for providing the packed-column HDC separation shown in Fig. 9.

REFERENCES

1 J.C. Giddings, *Sep. Sci.*, 1 (1966) 123.
2 K.D. Caldwell, *Anal. Chem.*, 53 (1981) 1170A.
3 M.E. Schimpf and J.C. Giddings, *J. Polym. Sci., Part B*, 27 (1989) 1317.
4 M.E. Schimpf and J.C. Giddings, *J. Polym. Sci., Part B*, 28 (1990) 2673.
5 J.C. Giddings, M.N. Myers and J. Janča, *J. Chromatogr.*, 186 (1979) 37.
6 M.N. Martin and R. Reynaud, *Anal. Chem.*, 52 (1980) 2293.
7 J. Kirkland and S.W. Rementer, *Anal. Chem.*, 64 (1992) 904.
8 M.N. Myers, P. Chen and J.C. Giddings, in T. Provder (Editor), *Size Exclusion Chromatography, Field Flow Fractionation and Related Chromatographic Methods of Polymer Analysis (ACS Symposium Series)*, American Chemical Society, Washington, DC, in press.
9 G. Liu and J.C. Giddings, *Anal. Chem.*, 63 (1991) 296.
10 G. Liu and J.C. Giddings, *Chromatographia*, 34 (1992) 483.
11 C. Ludwig, *S. B. Akad. Wiss. Wien*, 20 (1859) 539.
12 F.S. Gaeta, *Phys. Rev.*, 182 (1969) 289.
13 H.J.V. Tyrell, *Diffusion and Heat Flow in Liquids*, Butterworths, London, 1961.
14 J.S. Ham, *J. Appl. Phys.*, 31 (1960) 1853.
15 A.H. Emery and H.G. Drickamer, *J. Chem. Phys.*, 23 (1955) 2252.
16 P.S. Epstein, *Z. Phys.*, 54 (1929) 537.
17 M.E. Schimpf and J.C. Giddings, *Macromolecules*, 20 (1987) 1561.
18 S.L. Brimhall, M.N. Myers, K.D. Caldwell and J.C. Giddings, *J. Polym. Sci., Polym. Phys. Ed.*, 23 (1985) 2443.
19 J.J. Kirkland and W.W. Yau, *J. Chromatogr.*, 353 (1986) 95.
20 J.J. Gunderson and J.C. Giddings, *Macromolecules*, 19 (1986) 2618.
21 J.C. Giddings, *Unified Separation Science*, Wiley, New York, 1991.
22 J.J. Gunderson, K.D. Caldwell and J.C. Giddings, *Sep. Sci. Technol.*, 19 (1984) 667.
23 A.C. van Asten, H.F.M. Boelens, W.Th. Kok, H. Poppe, P.S. Williams and J.C. Giddings, *Sep. Sci. Technol.*, submitted for publication.
24 J.C. Giddings, M. Martin and M.N. Myers, *J. Chromatogr.*, 158 (1978) 419.
25 M.E. Schimpf, M.N. Myers and J.C. Giddings, *J. Appl. Polym. Sci.*, 33 (1987) 117.
26 J.C. Giddings, Y.H. Yoon, K.D. Caldwell, M.N. Myers and M.E. Hoving, *Sep. Sci.*, 10 (1975) 447.
27 J.C. Giddings, K.D. Caldwell and L.F. Kesner, *Determination of Molecular Weight*, Wiley, New York, 1989, Ch. 12.
28 J.C. Giddings, S. Li, P.S. Williams and M.E. Schimpf, *Makromol. Chem., Rapid Commun.*, 9 (1988) 817.
29 R.C. Reid, J.M. Prausnitz and T.K. Sherwood, *Properties of Gases and Liquids*, McGraw-Hill, New York, 3rd ed., 1977.
30 D.S. Viswanath and G. Natarajan, *Databook on the Viscosity of Liquids*, Hemisphere, New York, 1990.
31 J.C. Giddings, K.D. Caldwell and M.N. Myers, *Macromolecules*, 9 (1976) 108.
32 M.E. Schimpf, *J. Chromatogr.*, 517 (1990) 405.
33 K.D. Caldwell, S.L. Brimhall, Y. Gao and J.C. Giddings, *J. Appl. Polym. Sci.*, 36 (1988) 703.
34 W.W. Yau and J.J. Kirkland, *Modern Size Exclusion Chromatography*, Wiley, New York, 1975.
35 G. Stegeman, R. Oostervink, J.C. Kraak, H. Poppe and K.K. Unger, *J. Chromatogr.*, 505 (1990) 547.
36 G. Stegeman, J.C. Kraak and H. Poppe, *J. Chromatogr.*, 634 (1993) 149.

Journal of Chromatography, 644 (1993) 95–139
Elsevier Science Publishers B.V., Amsterdam

CHROM. 25 120

Hydrogen bonding

XXVII. Solvation parameters for functionally substituted aromatic compounds and heterocyclic compounds, from gas–liquid chromatographic data

Michael H. Abraham

Department of Chemistry, University College London, 20 Gordon Street, London WC1H 0AJ (UK)

(Received January 22nd, 1993)

ABSTRACT

The truncated solvation equation log $SP = c + rR_2 + l \log L^{16}$ has been applied to a very large number of sets of gas–liquid chromatographic data on non-polar stationary phases. Here, log SP can be log V_G or can be the retention index I. R_2 is the excess molar refraction of the solute and c, r and l are constants. A set of solutes of known log L^{16} values is used to construct the equation, and then further values of log L^{16} can be obtained for any solute of known log SP value. In this way, new log L^{16} values for over 1000 solutes have been obtained. Then knowing log L^{16}, and R_2, the equation log $SP = c + rR_2 + s\pi_2^H + l \log L^{16}$ (s is a constant) can be applied to GLC data on polar non-acidic stationary phases, and the dipolarity/polarisability parameter, π_2^H determined similarly. Values of π_2^H for over 700 compounds are reported, including those for functionally substituted aromatic compounds and heterocyclic compounds. It is shown that π_2^H is a blend of dipolarity/polarisability, and cannot simply be calculated from solute dipole moments.

INTRODUCTION

We have recently shown [1–8] that the general solvation equation,

$$\log SP = c + rR_2 + s\pi_2^H + a\alpha_2^H + b\beta_2^H + l \log L^{16} \quad (1)$$

can be used to describe numerous processes in which a series of solutes are distributed between the gas phase and some condensed phase. These processes include gas–liquid chromatography (GLC) [1–5], gas–solid chromatography [6], the solubility of gases and vapours in polymers [7], and the solubility of gases and vapours in soya-bean oil [8]. The dependent variable in eqn. 1 can be log L or log K, where L (or K) is the Ostwald solubility coefficient or gas–liquid partition coefficient, or log V_G where V_G is the specific retention volume at the column temperature, or log V_G^0 the specific retention volume corrected to 273 K, or even log τ where τ is the adjusted relative retention time. All these dependent variables will give rise to the same coefficients in eqn. 1 except for the constant term, c. The retention index, I, can also be used in place of log SP, but now all the characteristic constants c, r, s, a, b and l will alter. Thus values of I cannot be used to characterise GLC stationary phases, but are very useful in the determination of descriptors, as we shall see later.

The explanatory variables, or descriptors, in eqn. 1 have been described before [1–10]. In brief they are: R_2 the solute excess molar refraction [9], π_2^H the solute dipolarity/polarisability, α_2^H the effective or summation solute hydrogen-bond acidity, β_2^H the effective or summation

0021-9673/93/$06.00

solute hydrogen-bond basicity, and log L^{16} where L^{16} is the solute gas–liquid partition coefficient on hexadecane at 298 K [1–5,9]. How general is the application of eqn. 1 depends in part on the availability of the descriptors, or solute parameters, used in the equation. There is no problem with R_2, which can be obtained from refractive index measurements on liquids at 293 K [10], or which can be calculated for solutes that are solid at 293 K, since R_2 is very nearly an additive property. However, the other four descriptors in eqn. 1 must be obtained by experiment, or by comparison to closely related compounds where possible. We have previously described the determination of π_2^H and log L^{16} for a wide variety of mostly aliphatic solutes [1], and for alkylaromatic solutes [5], and we now consider the very important class of functionally substituted aromatic compounds. During the course of this work we have also obtained π_2^H and log L^{16} values for a number of other compounds, and so we give these results as well.

The GLC stationary phases we shall consider are all either neutral or hydrogen-bond bases, so that the $b\beta_2^H$ term in eqn. 1 is redundant. Note that the b constant refers to the stationary phase acidity, the complementary property to solute hydrogen-bond basicity. Hence eqn. 1 will be reduced to eqn. 2

$$\log SP = c + rR_2 + s\pi_2^H + a\alpha_2^H + l \log L^{16} \quad (2)$$

For rather non-polar phases, such as squalane or apiezon, the π_2^H term is not significant, leaving

$$\log SP = c + rR_2 + a\alpha_2^H + l \log L^{16} \quad (3)$$

Now the a constant for such phases will be small or not significant, and so if α_2^H is known or can be estimated, then knowing R_2 and the constants in eqn. 3 it is possible to calculate log L^{16} for solutes with a known log SP value. Our method, as before [1,5] is thus to set up equations of the type of eqn. 3, to obtain the constants c, r, a and l, and then to obtain log L^{16} values by back-calculation. Retention index values can be used as log SP, leading to equations of the form,

$$I = c' + r'R_2 + a'\alpha_2^H + l' \log L^{16} \quad (4)$$

but the procedure is identical to that using eqn. 3.

If now GLC phases are chosen that are polar (but still non-acidic) such as Carbowax or esters, eqn. 1 will take the form of eqn. 2 or, in the case of log $SP = I$

$$I = c' + r'R_2 + s'\pi_2^H + a'\alpha_2^H + l' \log L^{16} \quad (5)$$

Once the constants in eqn. 2 or eqn. 5 have been established with solutes of known descriptors [1–5], then knowing R_2, α_2^H and log L^{16} (as above), the π_2^H parameter can be calculated for a variety of solutes of known log SP or of known I value.

RESULTS

There is a large amount of literature data on retention volumes or retention indices of aromatic compounds, including the extensive work of Korhonen and co-workers [11–19] the work of De Ligny *et al.* [20] and much other work on non-polar and polar stationary phases [21–97]. In addition there is an extensive compilation of GLC data that was also used [98].

A start was made on data obtained with rather non-polar stationary phases, for which eqn. 3 or eqn. 4 could be applied to calculate new values of log L^{16}. Some restrictions were placed on the data sets that were used. Generally, for sets that covered a wide range of compound type, at least some fifteen solutes were needed in the set. A few exceptions were made when solutes of similar compound type were involved. Secondly, data sets that yielded regression equations with poor fits were excluded. An estimate of the expected error in any calculated log L^{16} value can be obtained from the ratios S.D./l or S.D./l', where l and l' are the constants in eqn. 3 and eqn. 4, and S.D. is the overall standard deviation in the regression equation. In the event, some 75 data sets that conformed to eqn. 3 or eqn. 4 were considered. Once these data sets had been analyzed, the calculated log L^{16} values were averaged, and the entire analysis repeated. This had the effect of including more data points in a number of regressions, but the overall quality of the regression equations remained practically the same. Thus for the data of Bark and Clarke [38] on phenols chromatographed on OV-1 at 403 K, the successive equations were,

$$\log \tau = -1.901 + 0.453R_2 + 0.422 \log L^{16} \quad (6)$$
$$n = 11 \quad \rho = 0.9964 \quad \text{S.D.} = 0.039$$

$$\log \tau = -1.931 + 0.483R_2 + 0.427 \log L^{16} \quad (7)$$
$$n = 16 \quad \rho = 0.9967 \quad \text{S.D.} = 0.031$$

In these equations, n is the number of data points, ρ is the overall correlation constant, and S.D. is the standard deviation in the independent variable. The ratio S.D./l is 0.073 in eqn. 7, this being the estimate of the average error in the log L^{16} back-calculated values. For many data sets this ratio was rather smaller. Thus for the extensive results of Dutoit [95], the second round of analysis gave,

$$I/10 = 6.669 + 8.918R_2 + 20.002 \log L^{16} \quad (8)$$
$$n = 138 \quad \rho = 0.9995 \quad \text{S.D.} = 0.449$$

so that S.D./l' = 0.025 units. In eqn. 8 $I/10$ is used only for computing convenience. The only extensive set of literature data for which little use could be made was that of Peng *et al.* [81], yielding the regression equation,

$$I/10 = 6.317 + 9.129\pi_2^H + 9.596\alpha_2^H + 20.018 \log L^{16} \quad (9)$$
$$n = 156 \quad \rho = 0.9988 \quad \text{S.D.} = 1.524$$

Although Peng *et al.*'s results are for non-polar stationary phases, the present analysis suggests that a significant amount of polarity is associated with the phase. Furthermore, the quite large S.D./l' value of 0.076 (when combined with the necessity of requiring both π_2^H and a_2^H parameters) precluded any considerable use of Peng *et al.*'s results.

In Table I are given calculated log L^{16} values for over 1000 compounds, together with the number of values that have been averaged (No.), the average itself, the standard deviation in the log L^{16} value (S.D.) and the maximum and minimum calculated log L^{16} values. Also in Table I are values of the solute parameter R_2 needed for the calculation of log L^{16} via eqn. 3 or eqn. 4. A reasonable number of log L^{16} values in Table I are averages of three or more determinations: these can be regarded as reasonably firm values, since further experimental results will not be expected to alter the log L^{16} values to any extent. However, log L^{16} values for which only one datum is available, Table I, must be regarded, for the moment, as provisional. The experimental error in log L^{16} can be assessed from results on solutes for which (say) ten or more values have been averaged. There are 39 such solutes for which S.D. averages out as 0.057 log units, and for the functionally substituted benzenes only, there are 10 solutes for which S.D. averages as 0.038 log units. This is in accord with typical regression equations, where S.D./l or S.D./l' is around 0.04 or 0.05 log units.

It is of some interest to test whether or not the log L^{16} values can be calculated by a simple additive scheme. In Table II are functional group increments as $\Delta \log L^{16}$ obtained as,

$$\Delta \log L^{16} = \log L^{16}(\text{PhX}) - 2.786 \quad (10)$$

where 2.786 is log L^{16} for benzene itself. These substituent values, together with the value for benzene can then be used to calculate log L^{16} for a variety of disubstituted benzenes. For non-interacting substituents, the log L^{16} values are reasonably additive, for example in the case of the following *m*- and *p*-substituted benzenes; Me/Me, Me/Et, Et/Et, Me/F, F/F, Me/Cl, Cl/Cl, Me/Br, Br/Br, Me/I, I/I, Me/OMe, F/OMe, Cl/OMe, OMe/OMe, Me/CHO, Me/$COCH_3$, Me/NH_2, Me/NO_2, and Me/OH. However for *o*-substituted benzenes, additivity does not usually apply, and for *m*- and *p*-substituted benzenes with interacting substituents, additivity does not apply either, *e.g.*: NO_2/NH_2, CN/NH_2, Cl/OH, NO_2/OH, etc. Hence the additivity principle can be used to predict log L^{16} values for *m*- and *p*-methyl derivatives of functional groups, and for some halogen derivatives as well, but cannot be used as a general method for the prediction of log L^{16} values.

However, our previous conclusion, that log L^{16} increases regularly along an homologous series, except possibly for the first one or two members, applies to the *n*-alkyl benzoates, see Table I. For the ten solutes from *n*-propyl benzoate to *n*-dodecyl benzoate,

$$\log L^{16} = 4.1733 + 0.51005n(\text{C}) \quad (11)$$
$$n = 10 \quad r = 0.9999 \quad \text{S.D.} = 0.0067$$

TABLE I

CALCULATED VALUES OF LOG L^{16}

Solute	R_2	No.	Average	S.D.	Max	Min
Cyclopentane	0.263	5	2.477	0.030	2.515	2.433
Cyclohexane	0.305	14	2.964	0.106	3.202	2.734
Methylcyclohexane	0.244	5	3.323	0.046	3.395	3.278
Ethylcyclohexane	0.263	3	3.877	0.062	3.936	3.812
Cyclohexylcyclohexane	0.531	1	6.434			
Cycloheptane	0.350	6	3.704	0.040	3.778	3.659
Cyclooctane	0.413	6	4.329	0.065	4.460	4.279
Cyclononane	0.432	1	4.829			
Cyclodecane	0.474	4	5.340	0.014	5.353	5.322
Cycloundecane	0.517	1	5.761			
Cyclododecane	0.559	1	6.190			
Cyclotetradecane	0.644	1	7.363			
trans-Hydrindane	0.439	3	4.467	0.015	4.479	4.450
cis-Hydrindane	0.439	4	4.635	0.023	4.662	4.610
Adamantane	0.667	4	5.095	0.069	5.186	5.040
trans-Decalin	0.467	9	4.984	0.066	5.120	4.915
cis-Decalin	0.544	7	5.156	0.050	5.237	5.095
cis-2-Methyldecalin	0.540	1	5.550			
2-Methylbut-2-ene	0.159	2	2.226	0.051	2.262	2.190
2-Methylpent-2-ene	0.156	2	2.588	0.029	2.608	2.567
Cyclohexene	0.359	1	3.021			
1-Methylcyclohexene	0.391	1	3.483			
3-Methylcyclohexene	0.360	1	3.379			
4-Methylcyclohexene	0.347	1	3.372			
Cycloheptene	0.414	1	3.626			
Cyclooctene	0.460	1	4.119			
Cyclohexa-1,3-diene	0.515	1	2.917			
Cyclohexa-1,4-diene	0.501	1	3.132			
Cyclohepta-1,3-diene	0.615	1	3.607			
Cycloocta-1,5-diene	0.603	1	4.300			
Cyclohepta-1,3,5-triene	0.764	1	3.442			
Cycloocta-1,3,5,7-tetraene	0.804	1	3.884			
α-Pinene	0.446	1	4.200			
Dicyclopentadiene	0.712	1	4.651			
1-Fluorohexane	0.000	1	2.951			
1-Fluorooctane	−0.020	1	3.850			
Fluorocyclohexane	0.232	1	3.215			
1-Chlorooctane	0.191	2	4.772	0.058	4.813	4.731
Chlorocyclohexane	0.448	3	4.016	0.034	4.047	3.980
Bromocyclohexane	0.615	3	4.395	0.015	4.413	4.386
Iodocyclohexane	0.904	2	4.785	0.018	4.798	4.772
1-Chlorocyclohexene	0.530	1	3.990			
1-Bromocyclohexene	0.700	1	4.350			
1-Bromo-4-methylcyclohexene	0.650	1	4.669			
1-Iodocyclohexene	1.000	1	4.838			
Dibromomethane	0.714	3	2.886	0.027	2.905	2.855
Tribromomethane	0.974	3	3.784	0.056	3.816	3.719
Fluorotrichloromethane	0.207	2	1.995	0.091	2.059	1.930
1,1-Difluorotetrachloroethane	0.230	1	2.970			
1,2-Difluorotetrachloroethane	0.227	2	2.929	0.100	3.000	2.858
Methyl cyclohexyl ether	0.296	1	3.861			
1,2-Dimethoxyethane	0.116	1	2.565			

TABLE I *(continued)*

Solute	R_2	No.	Average	S.D.	Max	Min
2,5-Diethoxytetrahydrofuran	0.126	1	3.335			
1,8-Cineole	0.383	1	4.290			
Propenal	0.324	1	1.656			
trans-But-2-ene-1-al	0.387	1	2.570			
trans-Hex-2-ene-1-al	0.404	1	3.400			
trans-Hept-2-ene-1-al	0.400	1	3.897			
Carvone	0.674	1	5.330			
Butan-2,3-dione	0.220	1	1.639			
Acetylacetone	0.401	2	2.918	0.206	3.064	2.772
Ethyl trimethylacetate	0.000	1	3.481			
2-Methoxyethyl acetate	0.166	1	3.290			
2-Ethoxyethylacetate	0.099	1	3.747			
Diethylmalonate	0.112	1	4.472			
Cyanocyclohexane	0.410	1	4.333			
Isopentylamine	0.194	1	3.058			
Cyclohexylamine	0.326	2	3.796	0.057	3.836	3.755
3-Methylcyclohexylamine	0.383	1	4.125			
Di-*n*-propylamine	0.124	2	3.351	0.030	3.372	3.329
Di-isobutylamine	0.046	1	3.901			
Di-*n*-pentylamine	0.099	1	4.570			
Triethylamine	0.101	2	3.040	0.052	3.077	3.003
Tri-*n*-propylamine	0.066	1	4.229			
1-Nitrohexane	0.203	4	4.416	0.008	4.426	4.409
Nitrocyclohexane	0.441	3	4.826	0.108	4.951	4.762
Dimethylformamide	0.367	1	3.173			
Diethylformamide	0.305	1	3.995			
Dibutylformamide	0.255	1	5.927			
Dimethylacetamide	0.363	1	3.717			
Dimethylpropanamide	0.340	1	3.720			
Dimethylisobutanamide	0.310	1	4.371			
Dimethylpivalamide	0.270	1	4.623			
Heptan-2-ol	0.188	4	3.838	0.050	3.886	3.768
2-Ethoxyethanol	0.237	1	2.815			
trans-Hex-2-ene-1-ol	0.294	1	3.510			
trans-Hept-2-ene-1-ol	0.281	1	4.010			
trans-Oct-2-ene-1-ol	0.270	1	4.520			
Dodecafluoroheptan-1-ol	−0.640	1	3.089			
Dimethylsulphoxide	0.522	2	3.459	0.031	3.481	3.437
Tetramethylsilicon	0.000	2	1.778	0.021	1.793	1.763
Cyclopropylbenzene	0.806	1	4.479			
Diphenylmethane	1.220	8	6.313	0.044	6.364	6.218
2-Methyldiphenylmethane	1.220	3	6.812	0.013	6.823	6.797
3-Methyldiphenylmethane	1.220	3	6.771	0.001	6.772	6.770
4-Methyldiphenylmethane	1.220	3	6.864	0.008	6.873	6.858
1,1-Diphenylethane	1.289	3	6.506	0.006	6.512	6.501
1,2-Diphenylethane	1.200	8	6.764	0.031	6.797	6.702
1,4-Diphenylbutane	1.200	3	7.882	0.011	7.894	7.872
Biphenyl	1.360	17	6.014	0.106	6.128	5.647
2-Methylbiphenyl	1.330	5	6.058	0.088	6.188	5.939
3-Methylbiphenyl	1.370	7	6.591	0.046	6.666	6.551
4-Methylbiphenyl	1.370	9	6.612	0.048	6.666	6.522

(Continued on p. 100)

TABLE I *(continued)*

Solute	R_2	No.	Average	S.D.	Max	Min
2-Ethylbiphenyl	1.270	4	6.403	0.109	6.567	6.341
3-Ethylbiphenyl	1.370	3	6.954	0.008	6.961	6.945
4-Ethylbiphenyl	1.370	3	7.098	0.005	7.102	7.093
2,3-Dimethylbiphenyl	1.405	3	6.632	0.010	6.641	6.621
2,4-Dimethylbiphenyl	1.354	3	6.576	0.012	6.587	6.563
2,5-Dimethylbiphenyl	1.354	3	6.519	0.018	6.537	6.502
2,6-Dimethylbiphenyl	1.405	3	6.139	0.016	6.151	6.121
3,4-Dimethylbiphenyl	1.434	3	7.235	0.003	7.238	7.232
3,5-Dimethylbiphenyl	1.406	3	7.030	0.010	7.040	7.020
2,2′-Dimethylbiphenyl	1.286	4	6.168	0.087	6.298	6.117
2,3′-Dimethylbiphenyl	1.330	3	6.491	0.016	6.506	6.474
2,4′-Dimethylbiphenyl	1.342	3	6.588	0.012	6.600	6.576
3,3′-Dimethylbiphenyl	1.380	4	7.080	0.046	7.148	7.049
3,4′-Dimethylbiphenyl	1.380	3	7.126	0.006	7.132	7.120
4,4′-Dimethylbiphenyl	1.380	6	7.159	0.069	7.228	7.070
2-Isopropylbiphenyl	1.270	3	6.407	0.009	6.413	6.397
3-Isopropylbiphenyl	1.370	3	7.152	0.006	7.159	7.148
4-Isopropylbiphenyl	1.370	3	7.362	0.002	7.365	7.361
Triphenylmethane	1.830	2	8.545	0.208	8.692	8.398
o-Terphenyl	2.000	2	8.244	0.221	8.400	8.088
m-Terphenyl	2.040	1	9.530			
p-Terphenyl	2.040	1	9.689			
o-Quaterphenyl	2.700	1	11.145			
m-Quaterphenyl	2.740	1	12.584			
p-Quaterphenyl	2.740	1	13.039			
1,3,5-Triphenylbenzene	2.440	4	12.787	0.074	12.882	12.702
trans-Stilbene	1.700	5	7.469	0.148	7.650	7.238
cis-Stilbene	1.600	2	6.474	0.015	6.484	6.463
α-Methylstilbene (*cis*, *trans*?)	1.650	2	7.402	0.013	7.411	7.393
1-Ethylnaphthalene	1.371	2	6.136	0.041	6.165	6.107
2-Ethylnaphthalene	1.331	3	6.140	0.030	6.168	6.108
1-Propylnaphthalene	1.370	1	6.495			
2-Propylnaphthalene	1.330	1	6.563			
2-Isopropylnaphthalene	1.330	1	6.400			
1-Butylnaphthalene	1.370	1	6.977			
2-Butylnaphthalene	1.330	1	7.065			
1-Isobutylnaphthalene	1.370	1	6.653			
2-Isobutylnaphthalene	1.330	1	6.764			
2-*sec*.-Butylnaphthalene	1.330	1	6.797			
2-*tert*.-Butylnaphthalene	1.330	1	6.703			
1,3,7-Trimethylnaphthalene	1.390	1	6.733			
2,3,5-Trimethylnaphthalene	1.469	3	6.935	0.019	6.951	6.914
2,3,6-Trimethylnaphthalene	1.430	4	6.871	0.014	6.892	6.862
1-Phenylnaphthalene	1.950	1	8.217			
2-Phenylnaphthalene	1.950	2	8.717	0.022	8.732	8.701
2-Benzylnaphthalene	1.950	3	8.562	0.065	8.621	8.493
1,4-Dihydronaphthalene	1.096	1	5.040			
5-Methyltetralin	0.940	2	5.860	0.033	5.883	5.836
6-Methyltetralin	0.900	2	5.751	0.017	5.763	5.739
2,6-Dimethyltetralin	0.900	2	5.997	0.013	6.006	5.987
Acenaphthene	1.604	9	6.469	0.034	6.541	6.415
Acenaphthylene	1.750	5	6.175	0.067	6.241	6.069
1,2,2*a*,3,4,6-Hexahydroacenaphthylene	1.340	1	6.005			

TABLE I *(continued)*

Solute	R_2	No.	Average	S.D.	Max	Min
1-Methylacenaphthylene	1.750	2	6.818	0.004	6.821	6.815
Fluorene	1.588	14	6.922	0.152	7.162	6.512
1-Methylfluorene	1.588	4	7.443	0.191	7.578	7.162
2-Methylfluorene	1.588	4	7.426	0.180	7.554	7.162
9-Methylfluorene	1.588	2	7.090	0.005	7.093	7.086
9-Ethylfluorene	1.588	1	7.459			
9-Propylfluorene	1.588	1	8.435			
9-Butylfluorene	1.588	1	8.760			
9-Hexylfluorene	1.588	1	9.338			
Azulene	1.340	9	5.707	0.124	5.844	5.415
1-Methylazulene	1.340	1	6.379			
5-Methylazulene	1.340	1	6.385			
6-Methylazulene	1.340	1	6.442			
4,6,8-Trimethylazulene	0.340	1	7.641			
Anthracene	2.290	13	7.568	0.086	7.692	7.391
9,10-Dihydroanthracene	1.400	1	7.526			
1,2,3,4,5,6,7,8-Octahydroanthracene	1.188	1	7.687			
Decahydroanthracene	0.705	2	7.073	0.187	7.205	6.940
1-Methylanthracene	2.290	1	8.332			
2-Methylanthracene	2.290	3	8.184	0.114	8.280	8.058
9-Methylanthracene	2.290	3	8.438	0.120	8.512	8.299
9,10-Dimethylanthracene	2.290	1	9.283			
9-Phenylanthracene	2.900	1	10.265			
Phenanthrene	2.055	13	7.632	0.091	7.759	7.463
9,10-Dihydrophenanthrene	1.690	1	7.483			
1,2,3,4-Tetrahydrophenanthrene	1.606	1	7.813			
1,2,3,4,5,6,7,8-Octahydrophenanthrene	1.145	3	7.842	0.062	7.909	7.787
1-Methylphenanthrene	2.055	4	8.408	0.104	8.525	8.274
2-Methylphenanthrene	2.055	2	8.307	0.027	8.326	8.288
3-Methylphenanthrene	2.055	2	8.286	0.028	8.305	8.266
4-Methylphenanthrene	2.055	2	8.394	0.029	8.414	8.373
9-Methylphenanthrene	2.055	2	8.392	0.027	8.411	8.373
2-Ethylphenanthrene	2.055	1	8.838			
9-Ethylphenanthrene	2.055	1	8.825			
1,8-Dimethylphenanthrene	2.055	1	9.097			
2,7-Dimethylphenanthrene	2.055	1	8.889			
3,6-Dimethylphenanthrene	2.055	1	8.848			
9-Methyl-10-ethylphenanthrene	2.055	1	9.500			
9-Propylphenanthrene	2.055	1	9.216			
9-Isopropylphenanthrene	2.055	1	9.083			
9,10-Diethylphenanthrene	2.055	1	9.739			
1-Methyl-7-isopropylphenanthrene	2.055	1	9.759			
9,10-Dimethyl-3-ethylphenanthrene	2.055	1	10.149			
1-Phenylphenanthrene	2.665	1	11.100			
9-Phenylphenanthrene	2.665	1	10.663			
9-Methyl-10-phenylphenanthrene	2.665	1	10.967			
4H-Cyclopenta[*def*]phenanthrene	2.417	6	8.126	0.106	8.248	8.002
7-Benz[*de*]anthrene	2.530	1	10.758			
Fluoranthene	2.377	11	8.827	0.083	8.962	8.739
1,2,3,10*b*-Tetrahydrofluoranthene	1.900	1	8.271			
Benzo[*a*]fluorene	2.622	11	9.404	0.073	9.504	9.308

(Continued on p. 102)

TABLE I *(continued)*

Solute	R_2	No.	Average	S.D.	Max	Min
11-Methylbenzo[*a*]fluorene	2.622	1	9.501			
Benzo[*b*]fluorene	2.622	5	9.520	0.069	9.590	9.435
Benzo[*c*]fluorene	2.622	2	9.525	0.092	9.590	9.460
Pyrene	2.808	14	8.833	0.068	8.964	8.746
4,5-Dihydropyrene	2.360	1	8.503			
4,5,9,10-Tetrahydropyrene	1.970	1	8.639			
1,2,3,6,7,8-Hexahydropyrene	1.950	1	8.932			
1-Methylpyrene	2.808	5	9.541	0.073	9.624	9.462
2-Methylpyrene	2.808	2	9.502	0.031	9.524	9.480
3-Methylpyrene	2.808	6	9.510	0.047	9.597	9.473
4-Methylpyrene	2.808	2	9.493	0.018	9.506	9.480
1-Ethylpyrene	2.808	1	9.973			
1-Butylpyrene	2.808	1	10.846			
2,7-Dimethylpyrene	2.808	1	10.002			
Cyclopenta[*cd*]pyrene	3.200	2	10.150	0.013	10.159	10.141
Benz[*a*]anthracene	2.992	10	10.291	0.063	10.376	10.162
4,5,6-Trihydrobenz[*de*]anthracene	2.360	1	9.711			
1-Methylbenz[*a*]anthracene	2.992	1	10.763			
2-Methylbenz[*a*]anthracene	2.992	1	10.745			
3-Methylbenz[*a*]anthracene	2.992	1	10.830			
4-Methylbenz[*a*]anthracene	2.992	2	10.909	0.016	10.920	10.898
5-Methylbenz[*a*]anthracene	2.992	1	10.891			
7-Methylbenz[*a*]anthracene	2.992	4	11.096	0.117	11.256	10.997
6-Methylbenz[*a*]anthracene	2.992	1	10.857			
8-Methylbenz[*a*]anthracene	2.992	1	10.857			
9-Methylbenz[*a*]anthracene	2.992	1	10.826			
11-Methylbenz[*a*]anthracene	2.992	1	10.714			
12-Methylbenz[*a*]anthracene	2.992	2	10.905	0.009	10.911	10.898
1,12-Dimethylbenz[*a*]anthracene	2.992	1	11.427			
7,12-Dimethylbenz[*a*]anthracene	2.992	4	11.753	0.154	11.960	11.621
Benzo[*c*]phenanthrene	3.000	4	10.020	0.066	10.081	9.930
Naphthacene	2.847	4	10.748	0.338	11.236	10.458
5,12-Dihydronaphthacene	2.255	1	10.066			
Chrysene	3.027	11	10.334	0.097	10.466	10.129
1-Methylchrysene	3.027	2	10.993	0.012	11.001	10.984
2-Methylchrysene	3.027	2	10.884	0.004	10.886	10.881
3-Methylchrysene	3.027	2	10.849	0.016	10.860	10.837
4-Methylchrysene	3.027	2	10.937	0.006	10.941	10.933
5-Methylchrysene	3.027	2	10.905	0.004	10.907	10.902
6-Methylchrysene	3.027	2	10.934	0.001	10.934	10.933
Triphenylene	3.000	6	10.355	0.078	10.454	10.235
Dodecahydrotriphenylene	1.537	1	10.475			
1-Methyltriphenylene	3.000	1	10.818			
1,3-Dimethyltriphenylene	3.000	1	11.291			
1,6,11-Trimethyltriphenylene	3.000	1	11.702			
1,3,6,11-Tetramethyltriphenylene	3.000	1	12.160			
Perylene	3.256	12	12.053	0.113	12.294	11.902
Benz[*a*]fluoranthene	3.194	1	11.608			
Benz[*b*]fluoranthene	3.194	8	11.609	0.088	11.719	11.479
Benz[*j*]fluoranthene	3.194	2	11.496	0.033	11.519	11.473
Benzo[*k*]fluoranthene	3.194	4	11.607	0.093	11.723	11.521
Benz[*mno*]fluoranthene	3.194	4	9.913	0.031	9.932	9.866
Benzo[*ghi*]fluoranthene	3.194	4	9.879	0.084	9.956	9.802

TABLE I *(continued)*

Solute	R_2	No.	Average	S.D.	Max	Min
Benzofluoranthene 2,3	3.194	2	11.654	0.060	11.696	11.611
3-Methylcholanthrene	3.264	4	12.482	0.155	12.604	12.261
20-Methylcholanthrene	3.264	3	12.503	0.148	12.604	12.333
Indeno[1,2,3-*cd*]pyrene	3.610	2	12.690	0.227	12.850	12.529
Benzo[*a*]pyrene	3.625	10	11.715	0.082	11.828	11.526
3,4-Benzpyrene	3.625	7	11.765	0.094	11.896	11.590
Benz[*e*]pyrene	3.625	4	11.656	0.148	11.865	11.519
Dibenz[*ac*]anthracene	4.000	5	12.998	0.209	13.223	12.773
Pentacene	4.000	1	12.531			
Dibenz[*ah*]anthracene	4.000	5	12.960	0.174	13.202	12.786
Dibenz[*aj*]anthracene	4.000	1	13.028			
Picene	4.000	4	13.068	0.217	13.376	12.910
Benzo[*b*]chrysene	4.000	2	12.865	0.019	12.878	12.851
Benzo[*ghi*]perylene	4.073	5	13.264	0.484	14.070	12.892
1,2,3,4-Dibenzpyrene	4.621	2	14.347	0.416	14.641	14.053
1,2,4,5-Dibenzpyrene	4.621	1	15.077			
3,4,8,9-Dibenzpyrene	4.621	1	15.236			
3,4,9,10-Dibenzpyrene	4.621	1	15.236			
Dibenz[*cd,jk*]pyrene Anthanthrene	4.621	1	13.234			
Dibenz[*def,mno*]chrysene	4.621	2	12.807	0.002	12.808	12.805
2,3-Dihydrodibenz[*def,mno*]chrysene	4.000	1	13.036			
Coronene	4.236	2	14.712	0.636	15.161	14.262
1,1′-Binaphthyl	2.680	1	10.110			
1,2′-Binaphthyl	2.680	1	10.612			
2,2′-Binaphthyl	2.680	1	11.161			
Fluorobenzene	0.477	10	2.788	0.014	2.810	2.759
1,2-Difluorobenzene	0.390	1	3.620			
1,4-Difluorobenzene	0.384	1	2.766			
1,2,4,5-Tetrafluorobenzene	0.234	1	2.637			
Pentafluorobenzene	0.154	1	2.578			
Hexafluorobenzene	0.088	2	2.515	0.018	2.528	2.502
2-Fluorotoluene	0.491	2	3.338	0.021	3.352	3.323
3-Fluorotoluene	0.485	2	3.332	0.023	3.348	3.315
4-Fluorotoluene	0.488	2	3.366	0.026	3.384	3.347
Benzotrifluoride	0.225	2	2.894	0.008	2.899	2.888
Chlorobenzene	0.718	15	3.657	0.047	3.742	3.515
1,2-Dichlorobenzene	0.872	5	4.518	0.020	4.544	4.498
1,3-Dichlorobenzene	0.847	6	4.410	0.027	4.434	4.374
1,4-Dichlorobenzene	0.825	5	4.435	0.030	4.455	4.383
1,2,3-Trichlorobenzene	1.030	5	5.419	0.067	5.462	5.302
1,2,4-Trichlorobenzene	0.980	5	5.248	0.032	5.282	5.198
1,3,5-Trichlorobenzene	0.980	5	5.045	0.026	5.083	5.020
1,2,3,4-Tetrachlorobenzene	1.180	4	6.171	0.020	6.200	6.154
1,2,3,5-Tetrachlorobenzene	1.160	5	5.922	0.057	5.980	5.839
1,2,4,5-Tetrachlorobenzene	1.160	5	5.926	0.053	5.980	5.851
Pentachlorobenzene	1.330	4	6.716	0.109	6.852	6.599
Hexachlorobenzene	1.490	3	7.624	0.078	7.674	7.534
2-Chlorotoluene	0.762	5	4.173	0.014	4.185	4.150
3-Chlorotoluene	0.736	5	4.179	0.011	4.195	4.166
4-Chlorotoluene	0.705	5	4.205	0.016	4.225	4.188
2,4-Dichlorotoluene	0.921	2	4.951	0.018	4.963	4.938

(Continued on p. 104)

TABLE I *(continued)*

Solute	R_2	No.	Average	S.D.	Max	Min
2,5-Dichlorotoluene	0.888	2	4.984	0.021	4.999	4.969
2,6-Dichlorotoluene	0.919	2	4.948	0.018	4.961	4.935
3,4-Dichlorotoluene	0.900	1	5.089			
2,3,4-Trichlorotoluene	1.080	2	5.980	0.033	6.003	5.957
2,3,5-Trichlorotoluene	1.060	2	5.772	0.004	5.774	5.769
2,3,6-Trichlorotoluene	1.100	1	5.759			
2,4,5-Trichlorotoluene	1.060	2	5.805	0.033	5.828	5.781
2,4,6-Trichlorotoluene	1.060	2	5.605	0.031	5.627	5.583
2,3,4,5-Tetrachlorotoluene	1.230	2	6.744	0.031	6.766	6.722
2,3,4,6-Tetrachlorotoluene	1.230	1	6.729			
2,3,5,6-Tetrachlorotoluene	1.230	2	6.513	0.018	6.526	6.500
Pentachlorotoluene	1.390	2	7.391	0.011	7.398	7.383
2-Chloro-*p*-xylene	0.775	4	4.700	0.047	4.733	4.630
2,3-Dichloro-*p*-xylene	0.949	3	5.646	0.056	5.710	5.605
2,5-Dichloro-*p*-xylene	0.949	3	5.485	0.039	5.519	5.442
2,3,5-Trichloro-*p*-xylene	1.117	3	6.371	0.046	6.408	6.320
Benzyl chloride	0.821	4	4.384	0.115	4.557	4.320
4-Methylbenzyl chloride	0.830	1	4.840			
2-Chlorobenzyl chloride	0.931	1	5.101			
4-Chlorobenzyl chloride	0.920	1	5.640			
2-Chloro-4-methylbenzyl chloride	0.931	1	5.651			
3-Chloro-4-methylbenzyl chloride	0.944	1	5.692			
1,4-Bis(chloromethyl)benzene	1.032	1	5.857			
Benzal chloride	0.916	1	5.151			
4-Chlorobenzal chloride	1.024	1	5.978			
Benzotrichloride	1.005	1	5.450			
4-Chlorobenzotrichloride	1.113	1	6.101			
2-Chlorostyrene	0.983	1	4.785			
Bromobenzene	0.882	14	4.041	0.033	4.077	3.965
1,2-Dibromobenzene	1.190	1	5.456			
1,3-Dibromobenzene	1.170	1	5.327			
1,4-Dibromobenzene	1.150	1	5.324			
1,3,5-Tribromobenzene	1.450	1	6.307			
2-Bromotoluene	0.923	3	4.559	0.014	4.575	4.548
3-Bromotoluene	0.896	3	4.577	0.016	4.589	4.559
4-Bromotoluene	0.879	3	4.586	0.007	4.593	4.579
Benzyl bromide	1.014	4	4.672	0.013	4.689	4.660
2-Bromo-1-phenylethane	0.974	3	5.170	0.013	5.181	5.156
2-Bromobiphenyl	1.592	1	6.435			
1-Bromonaphthalene	1.326	1	6.682			
2-Bromonaphthalene	1.286	1	6.678			
Iodobenzene	1.188	9	4.502	0.038	4.558	4.460
1,2-Diiodobenzene	1.860	1	6.395			
1,3-Diiodobenzene	1.830	1	6.377			
1,4-Diiodobenzene	1.800	1	6.255			
2-Iodotoluene	1.223	1	5.043			
3-Iodotoluene	1.210	1	5.036			
4-Iodotoluene	1.190	1	5.048			
Methylphenylether	0.708	15	3.890	0.054	4.000	3.769
Ethylphenylether	0.681	4	4.242	0.021	4.260	4.218
2-Methylanisole	0.725	2	4.339	0.063	4.383	4.294
3-Methylanisole	0.709	1	4.393			
4-Methylanisole	0.699	1	4.406			

TABLE I *(continued)*

Solute	R_2	No.	Average	S.D.	Max	Min
2,3-Dimethylanisole	0.775	1	5.084			
2,4-Dimethylanisole	0.739	1	4.913			
2,5-Dimethylanisole	0.739	1	4.859			
2,6-Dimethylanisole	0.674	1	4.641			
3,4-Dimethylanisole	0.757	1	5.208			
3,5-Dimethylanisole	0.728	1	5.053			
2-Ethylanisole	0.741	1	4.656			
3-Ethylanisole	0.717	1	4.920			
4-Ethylanisole	0.728	1	4.963			
2-Propylanisole	0.740	1	5.200			
3-Propylanisole	0.720	1	5.524			
4-Propylanisole	0.720	1	5.614			
4-Allylanisole	0.815	1	5.475			
2-Fluoroanisole	0.600	1	3.887			
3-Fluoroanisole	0.571	1	3.865			
4-Fluoroanisole	0.571	2	3.904	0.054	3.942	3.865
2-Chloroanisole	0.883	4	4.847	0.108	5.009	4.787
3-Chloroanisole	0.825	3	4.685	0.052	4.741	4.637
4-Chloroanisole	0.838	5	4.802	0.099	4.955	4.702
2,3-Dichloroanisole	1.000	3	5.901	0.059	5.953	5.836
2,4-Dichloroanisole	1.000	4	5.734	0.068	5.787	5.639
2,5-Dichloroanisole	1.000	4	5.685	0.064	5.734	5.596
2,6-Dichloroanisole	1.030	4	5.273	0.017	5.287	5.252
3,4-Dichloroanisole	0.960	3	5.762	0.032	5.793	5.729
3,5-Dichloroanisole	0.940	3	5.544	0.027	5.570	5.516
2,3,4-Trichloroanisole	1.130	3	6.720	0.027	6.751	6.703
2,3,5-Trichloroanisole	1.120	3	6.506	0.050	6.548	6.451
2,3,6-Trichloroanisole	1.150	3	6.153	0.040	6.177	6.107
2,4,5-Trichloroanisole	1.120	4	6.499	0.051	6.541	6.428
2,4,6-Trichloroanisole	1.150	4	5.929	0.066	5.982	5.844
3,4,5-Trichloroanisole	1.080	3	6.563	0.025	6.591	6.543
2,3,4,5-Tetrachloroanisole	1.280	3	7.318	0.068	7.396	7.268
2,3,4,6-Tetrachloroanisole	1.310	4	6.790	0.040	6.835	6.748
2,3,5,6-Tetrachloroanisole	1.300	3	6.798	0.035	6.830	6.760
Pentachloroanisole	1.420	4	7.566	0.105	7.696	7.441
2-Chloro-5-methylanisole	0.880	2	5.438	0.016	5.450	5.426
4-Chloro-3-methylanisole	0.840	2	5.343	0.004	5.345	5.340
4-Bromoanisole	0.992	2	5.187	0.023	5.203	5.170
4-Iodoanisole	1.286	1	5.616			
Methyl benzyl ether	0.645	3	4.238	0.008	4.246	4.231
Ethyl benzyl ether	0.629	1	4.524			
Dibenzyl ether	1.210	2	7.316	0.016	7.327	7.305
Diphenyl ether	1.216	3	6.287	0.028	6.315	6.259
1,2-Dimethoxybenzene	0.832	2	4.925	0.054	4.963	4.887
1,3-Dimethoxybenzene	0.816	1	5.022			
4-Methylveratrole	0.830	1	5.588			
3-Chloroveratrole	0.960	1	5.580			
4-Chloroveratrole	0.960	1	5.775			
3,4-Dichloroveratrole	1.090	1	6.506			
3,5-Dichloroveratrole	1.080	1	6.305			
3,6-Dichloroveratrole	1.090	1	5.956			

(Continued on p. 106)

TABLE I *(continued)*

Solute	R_2	No.	Average	S.D.	Max	Min
4,5-Dichloroveratrole	1.090	1	6.662			
3,4,5-Trichloroveratrole	1.240	1	7.291			
3,4,6-Trichloroveratrole	1.240	1	6.725			
Tetrachloroveratrole	1.380	1	7.647			
Benzaldehyde	0.820	9	4.008	0.039	4.083	3.967
2-Methylbenzaldehyde	0.870	2	4.559	0.030	4.580	4.538
3-Methylbenzaldehyde	0.840	4	4.548	0.015	4.565	4.528
4-Methylbenzaldehyde	0.862	4	4.592	0.042	4.654	4.564
2,4-Dimethylbenzaldehyde	0.929	2	5.170	0.028	5.189	5.150
2,5-Dimethylbenzaldehyde	0.900	2	5.106	0.018	5.118	5.093
3,4-Dimethylbenzaldehyde	0.890	2	5.367	0.042	5.397	5.337
4-Isopropylbenzaldehyde	0.859	1	5.294			
Furfural	0.690	1	3.262			
Phthalaldehyde	0.990	2	5.542	0.334	5.778	5.305
Terephthalaldehyde	1.030	2	5.500	0.379	5.768	5.232
Phenylacetaldehyde	0.755	2	4.344	0.004	4.346	4.341
3-Phenylpropanal	0.750	2	4.913	0.007	4.918	4.908
Acetophenone	0.818	7	4.501	0.020	4.540	4.483
4-Methylacetophenone	0.842	1	5.081			
2-Methoxyacetophenone	0.892	1	5.992			
3-Methoxyacetophenone	0.902	1	6.153			
4-Methoxyacetophenone	0.916	1	6.500			
Ethylphenylketone	0.804	2	4.971	0.009	4.977	4.964
n-Propylphenylketone	0.797	2	5.343	0.017	5.355	5.331
Benzylmethylketone	0.748	3	4.726	0.077	4.815	4.679
1-Phenylbutan-2-one	0.746	2	5.138	0.011	5.146	5.130
4-Phenylbutan-2-one	0.746	2	5.245	0.013	5.254	5.235
1,4-Naphthoquinone	1.080	1	6.341			
2-Methyl-1,4-naphthoquinone	1.080	1	6.886			
Anthraquinone	1.405	2	8.593	0.000	8.593	8.593
Phenanthraquinone	1.410	2	9.395	0.010	9.402	9.388
Anthrone	1.372	2	8.879	0.009	8.885	8.872
Methyl benzoate	0.733	7	4.704	0.088	4.835	4.634
Ethyl benzoate	0.689	4	5.075	0.091	5.211	5.014
Propyl benzoate	0.675	1	5.718			
Butyl benzoate	0.668	1	6.210			
Pentyl benzoate	0.663	1	6.718			
Hexyl benzoate	0.657	1	7.230			
Heptyl benzoate	0.653	1	7.739			
Octyl benzoate	0.647	1	8.248			
Nonyl benzoate	0.640	1	8.763			
Decyl benzoate	0.632	1	9.276			
Undecyl benzoate	0.630	1	9.786			
Dodecyl benzoate	0.627	1	10.299			
Methyl 2-methylbenzoate	0.772	3	5.053	0.022	5.076	5.032
Methyl 3-methylbenzoate	0.754	3	5.204	0.023	5.218	5.178
Methyl 4-methylbenzoate	0.730	3	5.248	0.013	5.260	5.234
Methyl 2,4-dimethylbenzoate	0.770	2	5.620	0.021	5.634	5.605
Methyl 2,5-dimethylbenzoate	0.800	2	5.559	0.025	5.576	5.541
Methyl 3,4-dimethylbenzoate	0.760	2	5.959	0.078	6.014	5.904
Methyl 4-isopropylbenzoate	0.760	2	5.977	0.038	6.004	5.950
Methyl 2-fluorobenzoate	0.576	1	4.719			
Methyl 3-fluorobenzoate	0.556	1	4.620			

TABLE I *(continued)*

Solute	R_2	No.	Average	S.D.	Max	Min
Methyl 4-fluorobenzoate	0.556	1	4.620			
Methyl 2-chlorobenzoate	0.817	2	5.702	0.102	5.774	5.630
Methyl 4-chlorobenzoate	0.797	1	5.620			
Methyl 2,4-dichlorobenzoate	0.950	1	6.353			
Methyl 2,5-dichlorobenzoate	0.950	1	6.372			
Methyl 2,3,6-trichlorobenzoate	1.050	1	6.923			
Methyl 4-methoxybenzoate	0.830	1	5.848			
Methyl 2-methoxy-3,6-dichlorobenzoate	1.050	1	6.917			
Benzyl benzoate	1.264	1	7.873			
Phenyl acetate	0.661	1	4.414			
2-Methylphenyl acetate	0.661	2	4.924	0.110	5.002	4.846
3-Methylphenyl acetate	0.660	1	4.871			
4-Methylphenyl acetate	0.660	1	4.900			
Benzyl acetate	0.798	1	5.012			
2-Methylbenzyl acetate	0.840	2	5.413	0.185	5.543	5.282
4-Methylbenzyl acetate	0.800	1	5.318			
2,4-Dimethylbenzyl acetate	0.840	2	5.934	0.170	6.054	5.813
2,5-Dimethylbenzyl acetate	0.850	2	5.875	0.182	6.003	5.746
3,4-Dimethylbenzyl acetate	0.810	2	6.077	0.203	6.220	5.933
2-Phenylethyl acetate	0.788	1	5.364			
Methyl phenylacetate	0.700	2	4.879	0.023	4.895	4.862
Ethyl phenylacetate	0.660	1	5.522			
Ethyl cinnamate	1.107	1	6.322			
Dimethyl phthalate	0.780	1	6.051			
Dimethyl isophthalate	0.830	1	6.482			
Dimethyl terephthalate	0.850	1	6.453			
Dimethyl methylterephthalate	0.850	1	6.856			
Benzonitrile	0.742	9	4.039	0.045	4.141	3.990
2-Methylbenzonitrile	0.780	1	4.478			
3-Methylbenzonitrile	0.762	1	4.561			
4-Methylbenzonitrile	0.740	1	4.600			
2-Chlorobenzonitrile	0.890	1	4.847			
3-Chlorobenzonitrile	0.870	1	4.712			
4-Chlorobenzonitrile	0.850	1	4.757			
Phenylacetonitrile	0.751	5	4.700	0.055	4.779	4.639
cis-Cinnamonitrile	1.098	1	5.339			
trans-Cinnamonitrile	1.186	1	5.597			
2-Methyl-*cis*-cinnamonitrile	1.140	1	5.768			
2-Methyl-*trans*-cinnamonitrile	1.230	1	6.025			
2-Chloro-*cis*-cinnamonitrile	1.250	1	5.941			
2-Chloro-*trans*-cinnamonitrile	1.330	1	6.352			
2-Bromo-*cis*-cinnamonitrile	1.410	1	6.364			
2-Bromo-*trans*-cinnamonitrile	1.500	1	6.745			
2-Methoxy-*cis*-cinnamonitrile	1.220	1	6.304			
2-Methoxy-*trans*-cinnamonitrile	1.300	1	6.640			
4-Methyl-*cis*-cinnamonitrile	1.100	1	5.936			
4-Methyl-*trans*-cinnamonitrile	1.190	1	6.193			
4-Chloro-*cis*-cinnamonitrile	1.210	1	6.234			
4-Chloro-*trans*-cinnamonitrile	1.290	1	6.545			
4-Methoxy-*cis*-cinnamonitrile	1.200	1	6.537			
4-Methoxy-*trans*-cinnamonitrile	1.280	1	6.849			

(Continued on p. 108)

TABLE I *(continued)*

Solute	R_2	No.	Average	S.D.	Max	Min
4-Trifluoromethyl-*cis*-cinnamonitrile	0.710	1	5.222			
4-Trifluoromethyl-*trans*-cinnamonitrile	0.800	1	5.504			
Aniline	0.955	13	3.934	0.032	3.993	3.866
o-Toluidine	0.966	8	4.442	0.042	4.494	4.364
m-Toluidine	0.946	8	4.463	0.043	4.536	4.417
p-Toluidine	0.923	8	4.452	0.040	4.510	4.404
2-Ethylaniline	0.962	3	4.829	0.083	4.921	4.761
3-Ethylaniline	0.940	2	4.840	0.064	4.885	4.794
4-Ethylaniline	0.942	3	4.895	0.099	4.986	4.789
2,3-Dimethylaniline	1.010	2	5.088	0.009	5.094	5.081
2,4-Dimethylaniline	0.950	4	4.983	0.016	4.997	4.961
2,5-Dimethylaniline	0.962	3	4.966	0.049	5.006	4.912
2,6-Dimethylaniline	0.972	6	5.028	0.019	5.049	4.998
3,4-Dimethylaniline	0.960	3	5.089	0.063	5.161	5.047
3,5-Dimethylaniline	0.956	2	5.072	0.001	5.072	5.071
2,6-Diethylaniline	0.987	1	6.342			
2-Vinylaniline	1.230	1	4.783			
3-Vinylaniline	1.210	1	4.975			
4-Vinylaniline	1.210	1	4.908			
2-Fluoroaniline	0.744	3	3.771	0.085	3.861	3.693
3-Fluoroaniline	0.749	2	3.988	0.090	4.051	3.924
4-Fluoroaniline	0.760	3	4.007	0.028	4.032	3.977
2-Chloroaniline	1.033	3	4.674	0.016	4.692	4.660
3-Chloroaniline	1.053	3	4.909	0.016	4.924	4.893
4-Chloroaniline	1.060	2	4.889	0.015	4.899	4.878
2-Bromoaniline	1.070	3	5.104	0.011	5.115	5.093
3-Bromoaniline	1.128	3	5.304	0.009	5.314	5.298
4-Bromoaniline	1.190	3	5.276	0.011	5.288	5.268
2-Iodoaniline	1.290	3	5.574	0.020	5.591	5.552
3-Iodoaniline	1.414	3	5.739	0.011	5.747	5.726
4-Iodoaniline	1.530	3	5.695	0.033	5.731	5.665
2-Cyanoaniline	1.067	1	5.018			
3-Cyanoaniline	1.077	1	5.380			
4-Cyanoaniline	1.087	1	5.639			
2-Methoxyaniline	0.988	3	4.818	0.066	4.865	4.742
3-Methoxyaniline	1.027	3	5.023	0.036	5.049	4.982
4-Methoxyaniline	1.050	3	4.949	0.049	4.984	4.893
2-Ethoxyaniline	0.888	1	5.203			
3-Ethoxyaniline	0.927	1	5.430			
4-Ethoxyaniline	0.950	2	5.357	0.001	5.357	5.356
2-Nitroaniline	1.180	3	5.627	0.022	5.652	5.609
3-Nitroaniline	1.200	1	5.880			
4-Nitroaniline	1.220	1	6.343			
o-Phenylenediamine	1.260	2	4.845	0.005	4.848	4.841
m-Phenylenediamine	1.280	1	4.893			
3-Fluoro-4-methylaniline	0.717	2	4.509	0.026	4.527	4.490
4-Fluoro-2-methylaniline	0.771	2	4.533	0.024	4.550	4.516
2,4-Difluoroaniline	0.549	2	3.843	0.043	3.873	3.812
2,5-Difluoroaniline	0.538	2	3.898	0.049	3.932	3.863
2,3-Dichloroaniline	1.136	2	5.652	0.006	5.656	5.647
2,4-Dichloroaniline	1.140	2	5.650	0.006	5.654	5.645
3,4-Dichloroaniline	1.160	2	5.944	0.015	5.954	5.933
2-Bromo-4-methylaniline	1.084	1	5.579			

TABLE I *(continued)*

Solute	R_2	No.	Average	S.D.	Max	Min
3-Bromo-4-methylaniline	1.142	1	5.541			
2,5-Dimethoxyaniline	1.065	2	5.954	0.012	5.962	5.945
2-Methoxy-5-aminoaniline	1.318	1	5.948			
N-Methylaniline	0.948	8	4.478	0.024	4.508	4.448
N-Ethylaniline	0.945	4	4.811	0.042	4.846	4.752
N-Propylaniline	0.921	3	5.324	0.013	5.338	5.313
N-Butylaniline	0.908	2	5.836	0.007	5.841	5.831
N-Isopentylaniline	0.890	2	6.183	0.015	6.193	6.172
2-Methyl-N-methylaniline	0.959	3	4.885	0.027	4.915	4.861
3-Methyl-N-methylaniline	0.939	3	4.917	0.066	4.993	4.870
4-Methyl-N-methylaniline	0.916	2	4.983	0.041	5.012	4.954
2-Methyl-N-ethylaniline	0.956	2	5.213	0.008	5.219	5.207
3-Methyl-N-ethylaniline	0.936	2	5.322	0.006	5.326	5.317
4-Methyl-N-ethylaniline	0.913	2	5.346	0.005	5.349	5.342
2-Chloro-N-methylaniline	1.026	2	5.025	0.010	5.032	5.018
4-Chloro-N-methylaniline	1.053	2	5.445	0.002	5.446	5.443
N,N-Dimethylaniline	0.957	8	4.701	0.037	4.748	4.644
N,N-Diethylaniline	0.953	5	5.287	0.074	5.392	5.207
N-Methyl-N-ethylaniline	0.955	2	4.953	0.012	4.961	4.944
2-Methyl-N,N-dimethylaniline	1.090	4	4.608	0.069	4.708	4.559
3-Methyl-N,N-dimethylaniline	0.993	4	5.144	0.116	5.228	4.978
4-Methyl-N,N-dimethylaniline	0.940	5	5.188	0.028	5.211	5.146
2,4-Dimethyl-N,N-dimethylaniline	0.970	1	5.070			
2,6-Dimethyl-N,N-dimethylaniline	0.990	1	4.921			
4-*tert.*-Butyl-N,N-dimethylaniline	0.944	1	6.337			
3-Methyl-N,N-diethylaniline	0.936	2	5.804	0.006	5.808	5.800
4-Methyl-N,N-diethylaniline	0.989	2	5.759	0.008	5.764	5.753
2-Chloro-N,N-dimethylaniline	1.035	2	5.110	0.007	5.115	5.105
4-Bromo-N,N-dimethylaniline	1.230	2	6.046	0.018	6.059	6.033
1-Naphthylamine	1.670	1	6.490			
2-Naphthylamine	1.670	1	6.540			
2-Aminoanthracene	2.635	4	9.300	0.103	9.452	9.225
Benzylamine	0.829	1	4.319			
Dibenzylamine	1.316	1	7.596			
Diphenylamine	1.700	2	7.086	0.006	7.090	7.082
2,2′-Bipyridyl	1.384	5	6.385	0.025	6.428	6.366
Nitrobenzene	0.871	9	4.557	0.032	4.618	4.524
2-Nitrotoluene	0.866	3	4.878	0.027	4.900	4.848
3-Nitrotoluene	0.874	3	5.097	0.028	5.122	5.067
4-Nitrotoluene	0.870	3	5.154	0.025	5.178	5.128
2-Nitrobiphenyl	1.580	3	7.452	0.115	7.582	7.365
3-Nitrobiphenyl	1.680	3	8.031	0.093	8.132	7.949
4-Nitrobiphenyl	1.680	3	8.190	0.103	8.265	8.072
4-Nitro-*p*-terphenyl	2.300	1	11.583			
1-Nitronaphthalene	1.600	1	6.991			
2-Nitronaphthalene	1.600	1	7.176			
2-Nitrofluorene	1.850	1	9.126			
1-Fluoro-3-nitrobenzene	0.737	1	4.441			
1-Chloro-2-nitrobenzene	1.020	2	5.235	0.011	5.243	5.227
1-Chloro-3-nitrobenzene	1.000	2	5.206	0.051	5.242	5.170
1-Chloro-4-nitrobenzene	0.980	2	5.220	0.002	5.221	5.218

(Continued on p. 110)

TABLE I *(continued)*

Solute	R_2	No.	Average	S.D.	Max	Min
2,3-Dichloronitrobenzene	1.180	1	5.837			
2,4-Dichloronitrobenzene	1.130	1	5.752			
2,5-Dichloronitrobenzene	1.130	1	5.726			
2,6-Dichloronitrobenzene	1.180	1	5.650			
3,4-Dichloronitrobenzene	1.130	1	5.843			
3,5-Dichloronitrobenzene	1.130	1	5.575			
2,3,4-Trichloronitrobenzene	1.330	1	6.432			
2,3,5-Trichloronitrobenzene	1.310	1	6.156			
2,3,6-Trichloronitrobenzene	1.330	1	6.189			
2,4,5-Trichloronitrobenzene	1.310	1	6.247			
2,4,6-Trichloronitrobenzene	1.310	1	5.978			
3,4,5-Trichloronitrobenzene	1.310	1	6.333			
2,3,4,5-Tetrachloronitrobenzene	1.480	1	6.875			
2,3,4,6-Tetrachloronitrobenzene	1.480	1	6.637			
2,3,5,6-Tetrachloronitrobenzene	1.480	1	6.606			
Pentachloronitrobenzene	1.640	1	7.261			
Benzamide	0.990	1	5.767			
Dimethyl phenylacetamide	0.920	1	6.899			
Phenol	0.805	12	3.766	0.059	3.885	3.682
o-Cresol	0.840	11	4.218	0.051	4.293	4.112
m-Cresol	0.822	10	4.310	0.036	4.348	4.240
p-Cresol	0.820	10	4.312	0.038	4.387	4.271
2-Ethylphenol	0.831	6	4.612	0.076	4.726	4.509
3-Ethylphenol	0.810	5	4.741	0.085	4.873	4.652
4-Ethylphenol	0.800	6	4.737	0.080	4.862	4.632
2,3-Dimethylphenol	0.850	6	4.952	0.023	4.977	4.919
2,4-Dimethylphenol	0.843	6	4.770	0.020	4.795	4.742
2,5-Dimethylphenol	0.840	5	4.774	0.022	4.796	4.739
2,6-Dimethylphenol	0.860	4	4.680	0.062	4.753	4.605
3,4-Dimethylphenol	0.830	6	4.980	0.032	5.019	4.935
3,5-Dimethylphenol	0.820	6	4.856	0.053	4.947	4.798
2-*n*-Propylphenol	0.822	3	4.951	0.062	4.996	4.880
3-*n*-Propylphenol	0.789	3	5.117	0.025	5.143	5.094
4-*n*-Propylphenol	0.793	3	5.185	0.034	5.221	5.153
2-Isopropylphenol	0.842	4	4.816	0.090	4.921	4.733
3-Isopropylphenol	0.811	2	4.951	0.066	4.998	4.904
4-Isopropylphenol	0.791	3	4.984	0.055	5.042	4.933
2-Methyl-3-ethylphenol	0.850	1	5.228			
2-Methyl-4-ethylphenol	0.843	2	5.161	0.011	5.168	5.153
2-Methyl-5-ethylphenol	0.840	1	5.149			
3-Methyl-4-ethylphenol	0.830	1	5.295			
3-Methyl-5-ethylphenol	0.820	2	5.215	0.046	5.247	5.182
3-Methyl-6-ethylphenol	0.840	1	5.030			
4-Methyl-2-ethylphenol	0.843	2	5.052	0.026	5.070	5.033
4-Methyl-3-ethylphenol	0.830	1	5.419			
2,3,4-Trimethylphenol	0.860	1	5.544			
2,3,5-Trimethylphenol	0.860	2	5.334	0.042	5.363	5.304
2,3,6-Trimethylphenol	0.870	2	5.270	0.063	5.314	5.225
2,4,5-Trimethylphenol	0.850	1	5.386			
2,4,6-Trimethylphenol	0.860	5	5.133	0.039	5.185	5.091
3,4,5-Trimethylphenol	0.830	1	5.568			
2-*n*-Butylphenol	0.806	1	5.473			
3-*n*-Butylphenol	0.800	1	5.590			

TABLE I *(continued)*

Solute	R_2	No.	Average	S.D.	Max	Min
4-*n*-Butylphenol	0.796	2	5.640	0.055	5.679	5.601
2-*sec.*-Butylphenol	0.819	2	5.050	0.086	5.111	4.989
4-*sec.*-Butylphenol	0.800	2	5.332	0.161	5.445	5.218
2-*tert.*-Butylphenol	0.823	2	5.021	0.195	5.159	4.883
4-*tert.*-Butylphenol	0.810	3	5.264	0.097	5.340	5.155
2,4-Diethylphenol	0.840	1	5.375			
2,5-Diethylphenol	0.820	1	5.440			
2,6-Diethylphenol	0.860	1	5.199			
3,5-Diethylphenol	0.820	1	5.500			
2-Methyl-6-propylphenol	0.860	1	5.524			
4-Methyl-2-propylphenol	0.820	1	5.419			
3-Methyl-5-propylphenol	0.810	1	5.634			
2-Methyl-4-isopropylphenol	0.824	1	5.464			
3-Methyl-5-isopropylphenol	0.810	1	5.429			
4-Methyl-2-isopropylphenol	0.822	1	5.198			
3,4-Dimethyl-6-ethylphenol	0.850	1	5.678			
2,3,4,5-Tetramethylphenol	0.870	1	6.099			
2,3,5,6-Tetramethylphenol	0.880	2	5.788	0.172	5.909	5.666
2(1-Methylbutyl)phenol	0.820	1	5.524			
4(1-Methylbutyl)phenol	0.790	1	5.921			
4-*tert.*-Pentylphenol	0.810	1	5.775			
2-Ethyl-5-propylphenol	0.810	1	5.880			
4-Methyl-2,6-diethylphenol	0.860	1	5.722			
Pentamethylphenol	0.900	1	6.725			
2(1-Methylpentyl)phenol	0.820	1	5.965			
4(1-Methylpentyl)phenol	0.790	1	6.383			
2,6-Dipropylphenol	0.820	1	5.910			
2,6-Di-isopropylphenol	0.860	1	5.637			
2,4-Dimethyl-6-*tert.*-butylphenol	0.860	1	5.859			
2(1-Methylhexyl)phenol	0.820	1	6.479			
4(1-Methylhexyl)phenol	0.790	1	6.914			
2(1-Methylheptyl)phenol	0.820	1	6.935			
4(1-Methylheptyl)phenol	0.790	1	7.377			
4-Methyl-2,6-di-*tert.*-butylphenol	0.860	1	6.255			
Thymol	0.822	2	5.381	0.134	5.476	5.286
Carvacrol	0.824	1	5.369			
4-Cyclohexylphenol	1.110	1	7.226			
2-Phenylphenol	1.550	1	7.227			
5,6,7,8-Tetrahydro-1-naphthol	1.043	1	6.624			
5,6,7,8-Tetrahydro-2-naphthol	1.020	1	6.747			
4-Indanol	0.980	1	5.820			
5-Indanol	0.960	1	5.879			
5-Methyl-4-indanol	0.990	1	6.236			
6-Methyl-4-indanol	0.980	1	6.280			
7-Methyl-4-indanol	0.990	1	6.328			
4-Methyl-5-indanol	1.000	1	6.230			
6-Methyl-5-indanol	0.980	1	6.280			
7-Methyl-5-indanol	0.960	1	6.355			
2-Fluorophenol	0.660	1	3.453			
3-Fluorophenol	0.667	2	3.842	0.004	3.844	3.839
4-Fluorophenol	0.670	2	3.844	0.016	3.855	3.833

(Continued on p. 112)

TABLE I *(continued)*

Solute	R_2	No.	Average	S.D.	Max	Min
2-Chlorophenol	0.853	2	4.178	0.023	4.194	4.162
3-Chlorophenol	0.909	5	4.773	0.090	4.893	4.650
4-Chlorophenol	0.915	5	4.775	0.105	4.917	4.667
2-Bromophenol	1.037	1	4.526			
3-Bromophenol	1.060	2	5.144	0.083	5.202	5.085
4-Bromophenol	1.080	2	5.135	0.117	5.218	5.052
2-Iodophenol	1.360	1	4.964			
3-Iodophenol	1.370	1	5.528			
4-Iodophenol	1.380	1	5.492			
2,3-Dichlorophenol	0.960	2	4.989	0.049	5.024	4.954
2,4-Dichlorophenol	0.969	2	4.943	0.066	4.989	4.896
2,5-Dichlorophenol	0.960	2	4.939	0.059	4.980	4.897
2,6-Dichlorophenol	0.900	2	5.086	0.048	5.120	5.052
3,4-Dichlorophenol	1.020	2	5.708	0.182	5.837	5.579
3,5-Dichlorophenol	1.020	2	5.653	0.261	5.837	5.468
2,3,4-Trichlorophenol	1.070	2	5.772	0.221	5.928	5.615
2,3,5-Trichlorophenol	1.070	2	5.609	0.190	5.743	5.475
2,3,6-Trichlorophenol	1.010	2	5.718	0.140	5.817	5.619
2,4,5-Trichlorophenol	1.070	2	5.725	0.226	5.885	5.565
2,4,6-Trichlorophenol	1.010	2	5.664	0.204	5.808	5.519
3,4,5-Trichlorophenol	1.130	2	6.351	0.684	6.835	5.867
2,3,4,5-Tetrachlorophenol	1.170	2	6.353	0.573	6.758	5.947
2,3,4,6-Tetrachlorophenol	1.110	1	6.740			
2,3,5,6-Tetrachlorophenol	1.110	2	6.294	0.561	6.690	5.897
Pentachlorophenol	1.220	2	6.822	1.107	7.604	6.039
2-Chloro-5-methylphenol	0.930	1	4.354			
4-Chloro-2-methylphenol	0.890	1	5.246			
4-Chloro-3-methylphenol	0.920	1	5.290			
2,4-Dibromophenol	1.310	1	5.282			
2,6-Dibromophenol	1.270	1	5.608			
2-Methoxyphenol	0.837	3	4.449	0.096	4.548	4.356
3-Methoxyphenol	0.879	1	4.803			
4-Methoxyphenol	0.900	1	4.773			
2-Hydroxybenzaldehyde	0.962	1	4.539			
4-Hydroxybenzaldehyde	1.010	1	5.533			
2-Chloro-4-hydroxybenzaldehyde	1.130	1	6.495			
3-Chloro-4-hydroxybenzaldehyde	1.140	1	5.528			
2,3-Dichloro-4-hydroxybenzaldehyde	1.180	1	6.374			
2,5-Dichloro-4-hydroxybenzaldehyde	1.180	1	6.300			
2,6-Dichloro-4-hydroxybenzaldehyde	1.250	1	7.589			
3,5-Dichloro-4-hydroxybenzaldehyde	1.110	1	6.363			
2,3,5-Trichloro-4-hydroxybenzaldehyde	1.230	1	7.144			
2,3,6-Trichloro-4-hydroxybenzaldehyde	1.300	1	7.265			
Tetrachloro-4-hydroxybenzaldehyde	1.340	1	8.051			
Catechol	0.970	2	5.060	0.152	5.168	4.952
Resorcinol	0.980	6	6.216	0.276	6.585	5.750
Hydroquinone	1.000	6	5.937	0.253	6.296	5.585
4-Allyl-2-methoxyphenol	0.928	1	5.992			
4-Propyl-2-methoxyphenol	0.820	1	6.069			
2-*tert.*-Butyl-4-methoxyphenol	0.920	1	6.603			
2,6-Dimethoxyphenol	0.870	1	6.287			
4-Methyl-2,6-dimethoxyphenol	0.870	1	6.826			
4-Ethyl-2,6-dimethoxyphenol	0.870	1	7.127			

TABLE I *(continued)*

Solute	R_2	No.	Average	S.D.	Max	Min
4-Propyl-2,6-dimethoxyphenol	0.870	1	7.451			
2-Cyanophenol	0.920	1	4.531			
3-Cyanophenol	0.930	1	5.181			
4-Cyanophenol	0.940	1	5.420			
2-Nitrophenol	1.015	3	4.760	0.091	4.861	4.684
3-Nitrophenol	1.050	2	5.692	0.028	5.711	5.672
4-Nitrophenol	1.070	2	5.876	0.116	5.958	5.794
3-Methyl-2-nitrophenol	1.030	1	5.274			
2-Methyl-4-nitrophenol	1.100	1	6.324			
2-Methyl-5-nitrophenol	1.080	1	6.222			
2-Methyl-6-nitrophenol	1.050	1	5.300			
2,5-Dimethyl-4-nitrophenol	1.120	1	6.620			
2,6-Dimethyl-4-nitrophenol	1.120	1	6.605			
2,4-Dinitrophenol	1.280	1	6.041			
2,5-Dinitrophenol	1.260	1	5.959			
2,6-Dinitrophenol	1.220	1	6.189			
3,4-Dinitrophenol	1.320	1	5.953			
1-Naphthol	1.520	1	6.130			
2-Naphthol	1.520	1	6.200			
Benzyl alcohol	0.803	10	4.221	0.016	4.249	4.193
2-Methylbenzyl alcohol	0.850	2	4.659	0.117	4.742	4.576
3-Methylbenzyl alcohol	0.815	2	4.581	0.113	4.661	4.501
4-Methylbenzyl alcohol	0.810	2	4.584	0.136	4.680	4.488
2,4-Dimethylbenzyl alcohol	0.857	2	5.117	0.088	5.179	5.055
2,5-Dimethylbenzyl alcohol	0.868	2	5.119	0.080	5.175	5.062
3,4-Dimethylbenzyl alcohol	0.830	2	5.190	0.112	5.269	5.111
4-Isopropylbenzyl alcohol	0.804	2	5.119	0.189	5.252	4.985
1-Phenylethanol	0.784	2	4.394	0.007	4.399	4.389
2-Phenylethanol	0.811	6	4.628	0.043	4.713	4.601
3-Phenylpropan-1-ol	0.821	1	5.180			
2-Phenylpropan-2-ol	0.848	2	4.520	0.003	4.522	4.518
Phenylmethylsulphide	1.068	1	4.659			
Furan	0.369	1	1.830			
Benzofuran	0.888	3	4.355	0.024	4.378	4.330
Dibenzofuran	1.407	8	6.716	0.018	6.745	6.694
Dinaphtho[1,2-*b*;1′,2′-*d*]furan	3.230	1	11.734			
Xanthene	1.220	1	7.462			
Benzo[*kl*]xanthene	1.830	1	9.627			
Dibenzo[*c*,*kl*]xanthene	2.440	1	12.068			
Benzodioxane	0.874	1	4.971			
4-Phenyl-1,3-dioxane	0.857	1	6.081			
9-Fluorenone	1.342	1	7.840			
11-Benzo[*a*]fluorenone	1.950	1	10.323			
9-Xanthenone	1.430	2	8.116	0.004	8.118	8.113
Dibenzo-*p*-dioxin	1.290	1	7.045			
Trioxan	0.100	1	2.650			
Paraldehyde	0.136	1	3.169			
Pyridine	0.631	20	3.022	0.046	3.131	2.899
2-Methylpyridine	0.598	16	3.422	0.034	3.471	3.324
3-Methylpyridine	0.631	17	3.631	0.030	3.724	3.592
4-Methylpyridine	0.630	16	3.640	0.033	3.718	3.593

(Continued on p. 114)

TABLE I *(continued)*

Solute	R_2	No.	Average	S.D.	Max	Min
2-Ethylpyridine	0.613	13	3.844	0.027	3.900	3.801
3-Ethylpyridine	0.640	12	4.093	0.034	4.170	4.025
4-Ethylpyridine	0.634	13	4.124	0.030	4.207	4.095
2,3-Dimethylpyridine	0.657	10	4.045	0.028	4.086	3.988
2,4-Dimethylpyridine	0.634	13	4.006	0.045	4.132	3.963
2,5-Dimethylpyridine	0.633	11	3.986	0.030	4.050	3.927
2,6-Dimethylpyridine	0.607	14	3.760	0.052	3.856	3.656
3,4-Dimethylpyridine	0.676	10	4.317	0.037	4.385	4.257
3,5-Dimethylpyridine	0.659	10	4.214	0.024	4.250	4.176
2-*n*-Propylpyridine	0.604	6	4.288	0.028	4.330	4.249
3-*n*-Propylpyridine	0.632	1	4.546			
4-*n*-Propylpyridine	0.627	6	4.597	0.030	4.632	4.555
4-Isopropylpyridine	0.625	1	4.449			
2-Methyl-4-ethylpyridine	0.639	3	4.442	0.015	4.459	4.432
2-Methyl-5-ethylpyridine	0.629	4	4.467	0.051	4.541	4.427
2-Methyl-6-ethylpyridine	0.613	5	4.102	0.063	4.156	3.994
3-Methyl-2-ethylpyridine	0.662	1	4.392			
3-Methyl-4-ethylpyridine	0.681	2	4.728	0.011	4.736	4.720
3-Methyl-5-ethylpyridine	0.664	1	4.622			
3-Methyl-6-ethylpyridine	0.638	1	4.398			
4-Methyl-2-ethylpyridine	0.639	3	4.376	0.009	4.384	4.366
4-Methyl-3-ethylpyridine	0.689	1	4.989			
2,3,4-Trimethylpyridine	0.703	4	4.688	0.018	4.706	4.664
2,3,5-Trimethylpyridine	0.687	5	4.524	0.081	4.613	4.394
2,3,6-Trimethylpyridine	0.674	6	4.308	0.070	4.376	4.178
2,4,5-Trimethylpyridine	0.686	4	4.630	0.042	4.687	4.592
2,4,6-Trimethylpyridine	0.634	13	4.324	0.065	4.513	4.246
3,4,5-Trimethylpyridine	0.690	1	4.939			
2-*n*-Butylpyridine	0.600	1	4.790			
4-*tert.*-Butylpyridine	0.631	3	4.742	0.008	4.750	4.734
2,5-Diethylpyridine	0.640	1	4.822			
2,6-Diethylpyridine	0.619	1	4.428			
3,4-Diethylpyridine	0.690	1	5.116			
3,5-Diethylpyridine	0.670	1	4.873			
2-Methyl-4-propylpyridine	0.600	1	4.889			
2-Methyl-5-propylpyridine	0.600	1	4.879			
2-Methyl-6-propylpyridine	0.620	1	4.571			
4-Methyl-2-propylpyridine	0.600	1	4.818			
4-Methyl-3-propylpyridine	0.680	1	5.128			
5-Methyl-2-propylpyridine	0.600	1	4.830			
4-Methyl-3-isopropylpyridine	0.680	1	4.995			
2,3-Dimethyl-4-ethylpyridine	0.703	2	5.078	0.070	5.127	5.028
2,3-Dimethyl-6-ethylpyridine	0.674	1	4.690			
2,4-Dimethyl-5-ethylpyridine	0.686	2	5.030	0.048	5.064	4.996
2,4-Dimethyl-6-ethylpyridine	0.634	2	4.646	0.004	4.648	4.643
2,5-Dimethyl-4-ethylpyridine	0.686	2	5.043	0.009	5.049	5.036
2,5-Dimethyl-6-ethylpyridine	0.674	2	4.672	0.045	4.704	4.640
2,6-Dimethyl-3-ethylpyridine	0.674	2	4.756	0.021	4.771	4.741
2,6-Dimethyl-4-ethylpyridine	0.634	2	4.736	0.019	4.749	4.722
3,4-Dimethyl-6-ethylpyridine	0.686	1	4.996			
3,5-Dimethyl-6-ethylpyridine	0.687	1	4.904			
2,3,4,5-Tetramethylpyridine	0.770	1	5.339			
2,3,4,6-Tetramethylpyridine	0.727	4	4.988	0.066	5.079	4.935

TABLE I *(continued)*

Solute	R_2	No.	Average	S.D.	Max	Min
2,3,5,6-Tetramethylpyridine	0.730	2	4.876	0.006	4.880	4.871
2-*n*-Pentylpyridine	0.600	2	5.270	0.014	5.280	5.260
4-*n*-Pentylpyridine	0.620	1	5.980			
2-Methyl-6-butylpyridine	0.620	1	5.042			
2-Ethyl-6-propylpyridine	0.620	1	4.924			
2-Methyl-4,5-diethylpyridine	0.690	1	5.443			
2-Methyl-4,6-diethylpyridine	0.640	2	5.078	0.023	5.094	5.061
2-Methyl-5,6-diethylpyridine	0.680	1	5.023			
4-Methyl-2,6-diethylpyridine	0.640	1	5.004			
2,6-Dimethyl-4-propylpyridine	0.630	1	5.200			
2-Isopropyl-3,6-dimethylpyridine	0.670	1	4.901			
2,3,6-Trimethyl-4-ethylpyridine	0.730	1	5.346			
2,4,6-Trimethyl-3-ethylpyridine	0.730	2	5.327	0.002	5.328	5.325
2,3,4-Triethylpyridine	0.710	1	5.726			
2,3,5-Triethylpyridine	0.700	1	5.458			
2,4,6-Triethylpyridine	0.640	1	5.463			
2,3-Dimethyl-4,6-diethylpyridine	0.740	1	5.659			
2,5-Dimethyl-4,6-diethylpyridine	0.740	1	5.614			
3,4-Dimethyl-2,6-diethylpyridine	0.750	1	5.643			
2(5-Nonyl)pyridine	0.570	1	6.560			
4(5-Nonyl)pyridine	0.600	1	7.380			
2-Benzylpyridine	1.222	1	7.250			
4-Benzylpyridine	1.244	1	7.730			
3,5-Diphenylpyridine	1.851	2	9.956	0.045	9.987	9.924
Cyclopenteno[*b*]pyridine	1.020	1	4.628			
2-Methylcyclopenteno[*b*]pyridine	1.020	1	4.813			
4-Methylcyclopenteno[*b*]pyridine	1.020	1	4.968			
7-Methylcyclopenteno[*b*]pyridine	1.020	1	4.769			
Cyclopenteno[*c*]pyridine	1.020	1	4.818			
3-Methylthiopyridine	1.040	1	4.760			
2-Fluoropyridine	0.489	2	3.106	0.076	3.159	3.052
3-Fluoropyridine	0.504	2	2.991	0.057	3.031	2.950
4-Fluoropyridine	0.500	1	2.934			
2-Chloropyridine	0.738	3	3.875	0.118	3.946	3.739
3-Chloropyridine	0.732	4	3.783	0.046	3.840	3.729
4-Chloropyridine	0.740	2	3.728	0.037	3.754	3.701
2-Bromopyridine	0.921	2	4.386	0.065	4.432	4.340
3-Bromopyridine	0.905	2	4.185	0.001	4.186	4.184
4-Bromopyridine	0.900	2	4.027	0.140	4.126	3.928
2-Iodopyridine	1.210	1	4.712			
3-Iodopyridine	1.210	1	4.635			
4-Iodopyridine	1.210	1	4.553			
3-Methoxypyridine	0.680	1	4.290	0.000	4.290	4.290
4-Methoxypyridine	0.680	1	4.279			
2-Acetylpyridine	0.730	1	4.478			
3-Acetylpyridine	0.795	1	4.880			
4-Acetylpyridine	0.771	1	4.660			
2-Cyanopyridine	0.734	2	4.441	0.213	4.591	4.290
3-Cyanopyridine	0.750	2	4.164	0.159	4.276	4.051
4-Cyanopyridine	0.750	3	4.033	0.121	4.155	3.913
2-Formylpyridine	0.768	1	4.031			

(Continued on p. 116)

TABLE I *(continued)*

Solute	R_2	No.	Average	S.D.	Max	Min
3-Formylpyridine	0.817	1	4.258			
β-Methylnicotinate	0.710	1	5.095			
2-Nitropyridine	0.890	1	4.667			
3-Nitropyridine	0.890	1	4.548			
4-Nitropyridine	0.890	1	4.327			
2-Chloro-5-nitropyridine	1.000	1	5.609			
2-Methoxy-5-nitropyridine	0.900	1	5.875			
2-Methoxy-3-nitropyridine	0.920	1	5.913			
Piperidine	0.422	2	3.304	0.008	3.310	3.298
N-Methylpiperidine	0.318	2	3.330	0.099	3.400	3.260
N-Ethylpiperidine	0.300	2	3.729	0.069	3.778	3.680
Quinoline	1.268	13	5.457	0.069	5.608	5.331
1,2,3,4-Tetrahydroquinoline	1.221	2	5.665	0.262	5.850	5.480
2-Methylquinoline	1.287	9	5.791	0.050	5.879	5.707
3-Methylquinoline	1.317	1	5.969			
4-Methylquinoline	1.335	8	6.126	0.055	6.242	6.060
6-Methylquinoline	1.309	9	5.988	0.049	6.057	5.897
7-Methylquinoline	1.305	7	5.992	0.026	6.017	5.941
8-Methylquinoline	1.313	10	5.801	0.061	5.862	5.683
2,3-Dimethylquinoline	1.370	1	6.330			
2,4-Dimethylquinoline	1.352	4	6.371	0.076	6.456	6.305
2,6-Dimethylquinoline	1.320	6	6.294	0.057	6.355	6.219
2,7-Dimethylquinoline	1.320	1	6.310			
2,4,6-Trimethylquinoline	1.390	1	6.854			
2,4,6,8-Tetramethylquinoline	1.440	1	6.860			
6-Phenylquinoline	1.878	2	9.010	0.057	9.050	8.969
Isoquinoline	1.211	11	5.595	0.062	5.708	5.466
1,2,3,4-Tetrahydroisoquinoline	1.016	1	5.170			
1-Methylisoquinoline	1.275	2	5.941	0.074	5.993	5.888
3-Methylisoquinoline	1.230	3	5.931	0.034	5.960	5.893
Benzo[*c*]quinoline	1.878	7	7.978	0.079	8.073	7.878
Benzo[*f*]quinoline	1.878	7	7.974	0.080	8.068	7.872
2-Methylbenzo[*f*]quinoline	1.878	1	8.373			
3-Methylbenzo[*f*]quinoline	1.878	4	8.314	0.097	8.409	8.184
Benzo[*h*]quinoline	1.878	7	7.797	0.045	7.861	7.759
Indeno[1,2,3-*ij*]isoquinoline	2.180	1	9.089			
Benzo[*lmn*]phenanthridine	2.488	1	9.299			
Acridine	2.356	8	7.644	0.089	7.751	7.462
9,10-Dihydroacridine	1.600	2	7.959	0.042	7.988	7.929
2-Methylacridine	2.356	4	8.252	0.095	8.341	8.130
3-Methylacridine	2.356	2	8.064	0.053	8.101	8.026
9-Methylacridine	2.356	1	8.512			
Benz[*a*]acridine	2.970	3	10.285	0.025	10.309	10.260
10-Methylbenz[*a*]acridine	2.970	1	10.782			
5,7-Dimethylbenz[*a*]acridine	2.970	1	11.459			
7,10-Dimethylbenz[*a*]acridine	2.970	1	11.491			
Benz[*c*]acridine	2.970	3	10.036	0.135	10.124	9.880
10-Methylbenz[*c*]acridine	2.970	1	10.668			
1,10-Dimethylbenz[*c*]acridine	2.970	1	10.945			
2,10-Dimethylbenz[*c*]acridine	2.970	1	11.490			
7,9-Dimethylbenz[*c*]acridine	2.970	1	11.457			
2,2′-Biquinoline	2.540	2	11.138	0.011	11.146	11.130
Pyrrole	0.613	1	2.865			

TABLE I *(continued)*

Solute	R_2	No.	Average	S.D.	Max	Min
N-Methylpyrrole	0.559	1	2.923			
Pyrrolidine	0.406	2	2.893	0.014	2.903	2.883
N-Methylpyrrolidine	0.303	1	2.808			
Indole	1.200	8	5.505	0.161	5.675	5.209
N-Methylindole	1.206	2	5.765	0.305	5.980	5.549
2-Methylindole	1.200	3	6.180	0.019	6.197	6.160
3-Methylindole	1.200	5	6.114	0.060	6.170	6.024
5-Methylindole	1.200	3	6.121	0.080	6.212	6.067
7-Methylindole	1.200	2	6.081	0.047	6.114	6.048
2,N-Dimethylindole	1.206	1	6.362			
2,3-Dimethylindole	1.200	2	6.693	0.001	6.694	6.692
2,5-Dimethylindole	1.200	1	6.673			
2,7-Dimethylindole	1.200	1	6.459			
2,3,5-Trimethylindole	1.200	2	7.187	0.018	7.199	7.174
2,3,7-Trimethylindole	1.200	2	7.140	0.150	7.246	7.034
2-Phenylindole	1.810	5	8.966	0.168	9.187	8.819
Indoline	1.076	1	5.254			
5H-Indeno[1,2-*b*]pyridine	1.350	1	7.379			
Carbazole	1.787	9	7.982	0.093	8.149	7.836
1,2,3,4-Tetrahydrocarbazole	1.310	1	8.183			
1-Methylcarbazole	1.787	1	8.461			
2-Methylcarbazole	1.787	2	8.586	0.040	8.614	8.558
3-Methylcarbazole	1.787	1	8.590			
4-Methylcarbazole	1.787	1	8.681			
1,2-Dimethylcarbazole	1.787	1	9.137			
1,3-Dimethylcarbazole	1.787	1	9.170			
1,4-Dimethylcarbazole	1.787	1	9.014			
9-Ethylcarbazole	1.787	1	8.242			
9-Phenylcarbazole	2.400	2	10.033	0.069	10.082	9.984
Benzo[*a*]carbazole	2.400	2	10.556	0.024	10.573	10.539
Benzo[*b*]carbazole	2.400	2	10.788	0.042	10.818	10.758
Benzo[*c*]carbazole	2.400	1	10.824			
4-H-Benzo[*def*]carbazole	2.397	1	9.462			
Quinoxaline	1.304	1	5.654			
Pyrazole	0.620	1	3.151			
3-Methylpyrazole	0.586	1	3.672			
4-Methylpyrazole	0.586	1	3.674			
Imidazole	0.710	1	4.018			
N-Methylimidazole	0.589	1	3.805			
Pyrazine	0.629	1	2.920			
2-Methylpyrazine	0.629	1	3.254			
Chloropyrazine	0.727	1	3.867			
Pyrimidine	0.606	1	2.837			
Pyridazine	0.670	1	3.426			
3-Methylpyridazine	0.650	1	3.841			
Piperazine	0.570	1	3.400			
Thiophene	0.687	2	2.819	0.044	2.850	2.788
2-Methylthiophene	0.688	2	3.308	0.008	3.314	3.302
3-Methylthiophene	0.690	1	3.388			
2,5-Dimethylthiophene	0.690	2	3.769	0.053	3.806	3.731
2,3,5-Trimethylthiophene	0.690	1	4.511			

(Continued on p. 118)

TABLE I *(continued)*

Solute	R_2	No.	Average	S.D.	Max	Min
2,3,4,5-Tetramethylthiophene	0.690	1	5.158			
Benzo[*b*]thiophene	1.323	5	5.174	0.105	5.314	5.052
2-Methylbenzo[*b*]thiophene	1.323	2	5.610	0.016	5.621	5.598
3-Methylbenzo[*b*]thiophene	1.323	2	5.677	0.016	5.688	5.666
4-Methylbenzo[*b*]thiophene	1.323	1	5.692			
5-Methylbenzo[*b*]thiophene	1.323	1	5.661			
6-Methylbenzo[*b*]thiophene	1.323	1	5.661			
7-Methylbenzo[*b*]thiophene	1.323	1	5.574			
3,5-Dimethylbenzo[*b*]thiophene	1.323	1	6.295			
5-Ethylbenzo[*b*]thiophene	1.323	2	6.129	0.074	6.181	6.076
Dibenzothiophene	1.959	6	7.575	0.043	7.641	7.520
1,2,3,4-Tetrahydrodibenzothiophene	1.628	1	7.719			
trans-Hexahydrodibenzothiophene	1.300	1	7.113			
cis-Hexahydrodibenzothiophene	1.300	1	7.164			
1-Methyldibenzthiophene	1.959	1	8.316			
2-Methyldibenzothiophene	1.959	1	8.212			
3-Methyldibenzothiophene	1.959	1	8.216			
4-Methyldibenzothiophene	1.959	1	8.110			
1,7-Dimethyldibenzothiophene	1.959	1	8.897			
2,6-Dimethyldibenzothiophene	1.959	1	8.692			
2,8-Dimethyldibenzothiophene	1.959	1	8.794			
3,6-Dimethyldibenzothiophene	1.959	1	8.705			
3,7-Dimethyldibenzothiophene	1.959	1	8.798			
3,8-Dimethyldibenzothiophene	1.959	1	8.800			
4,6-Dimethyldibenzothiophene	1.959	1	8.596			
2-Ethyldibenzothiophene	1.959	1	8.698			
3-Ethyldibenzothiophene	1.959	1	8.571			
Benzo[*b*]naphtho[2,1-*d*]thiophene	2.570	2	10.162	0.021	10.177	10.147
2,[2′-Naphthyl)benzo[*b*]thiophene	2.660	2	11.317	0.035	11.342	11.292
Thianthrene	2.315	4	8.407	0.079	8.524	8.354

where $n(C)$ is number of carbon atoms in the alkyl group.

Once log L^{16} values were available, it then became possible to apply eqn. 2 or eqn. 5 to data sets, and then to calculate the π_2^H parameter, as described above. Again, data sets were restricted to those that included a reasonable number of solutes, around 15 as the minimum, and which led to regression equations of the required quality. For the determination of π_2^H values, the rations S.D./s or S.D./s' should now be as low as possible, and only equations where these ratios were less than or equal to 0.03 units were considered. Some 120 data sets were then left to be analyzed using eqn. 2 or eqn. 5. As for the log L^{16} values, once π_2^H values had been calculated, they were averaged and the entire process repeated. For a few regression equations a third round of calculations was carried out, but mostly this was not needed. A typical final regression equation is that for phenols on OV-1701 at 423 K [82],

$$I/10 = 2.991 - 22.683R_2 + 52.865\pi_2^H + 21.692\alpha_2^H + 20.579 \log L^{16} \quad (12)$$

$$n = 30 \quad \rho = 0.9987 \quad \text{S.D.} = 0.849$$

where S.D./s' = 0.016 units. Once again we could make little use of the very large data set of Peng *et al.* [94] on polar columns because of the very large S.D./l' value of 0.073 units, as shown in eqn. 13

TABLE II

SUBSTITUTENT VALUES FOR LOG L^{16} AND π_2^H IN PhX SOLUTES

Substituent X	$\Delta \log L^{16}$	$\Delta\pi_2^H$	μ (D)
H	0.000[a]	0.00[a]	0.00
Me	0.539[a]	0.00[a]	0.36
Et	0.992[a]	−0.01[a]	0.59
Pr	1.444[a]	−0.02[a]	0.35
Ph	3.228	0.47	0.00
F	0.002	0.05	1.66
Cl	0.871	0.13	1.75
Br	1.255	0.21	1.52
I	1.716	0.30	1.70
OMe	1.104	0.23	1.38
CHO	1.222	0.48	2.75
COMe	1.715	0.49	3.00
CO_2Me	1.918	0.33	1.80
CN	1.253	0.59	4.18
NH_2	1.148	0.44	1.57
NO_2	1.771	0.59	3.93
OH	0.980	0.37	1.55
SH	1.325	0.28	1.20
NHMe	1.692	0.38	1.67
NMe_2	1.915	0.32	1.57

[a] From ref. 5; log L^{16} for benzene is 2.786 and π_2^H for benzene is 0.52 units.

$$I/10 = 1.084 + 11.938R_2 + 57.217\pi_2^H + 94.986\alpha_2^H + 20.911 \log L^{16} \quad (13)$$

$n = 269 \quad \rho = 0.9956 \quad \text{S.D.} = 4.186$

The final calculated values of π_2^H for over 700 solutes are in Table III with the number of averaged values and the maximum and minimum values in the calculated π_2^H values. Also given are the α_2^H values that are needed to solve eqn. 2 or eqn. 5 for log π_2^H. Again, where π_2^H values are averages of three or more determinations, they can be regarded as reasonably firm values, but π_2^H values from a single determination must be only provisional. There are 52 π_2^H values in Table III that are averages of ten or more determinations; for these, S.D. values themselves average as 0.019 units. For the 41 π_2^H values that refer to functionally substituted aromatic compounds, as a subset, the average S.D. is 0.020 units. These error values agree well with the various S.D./s or S.D./s' values obtained in the regression equations, and so the estimated error in π_2^H can be set at 0.02 units.

Our estimated error in π_2^H, and in log L^{16} above, must be viewed in the light of the analysis of Poole *et al.* [99] who has shown that interfacial adsorption can make a significant contribution to the net retention of solutes. The effects of interfacial adsorption are particularly pronounced for less polar compounds such as alkanes on polar stationary phases at lower temperatures [99]. Since nearly all the data we have used, except for the excellent results of Poole and co-workers [86,87], is uncorrected for interfacial adsorption, it is necessary to consider possible errors from this source. First of all, most of the data we have used has been collected at temperatures of around 390 K or higher, where interfacial adsorption is not so pronounced. Secondly, we have concentrated on aromatic compounds, where again interfacial adsorption is much less significant than for aliphatic compounds. Finally, results in Table III may be compared with π_2^H values calculated only from the data of Poole and co-workers [86,87], see Table IV. It may be concluded that the present results are perfectly compatible with those derived from the corrected retention data of Poole and co-workers [86,87], and hence do not suffer from effects due to interfacial adsorption.

Estimation of π_2^H values

Before attempting any estimation of π_2^H values for multisubstituted benzenes, it is useful to dissect π_2^H values into contributions from dipolarity and polarisability. A plot of π_2^H for the monosubstituted benzenes in Table II against solute dipole moment is a quite scattered diagram, see Fig. 1, showing the dipole moment cannot make any very large contribution. An analysis of π_2^H values for all the chlorobenzenes (13, including benzene itself) is instructive, and a regression of π_2^H against the number of chlorine atoms in the solute, nCl, and the overall solute dipole moment, μ in D, yields eqn. 14,

$$\pi_2^H = 0.538 + 0.0743n\text{Cl} + 0.0353\mu \quad (14)$$

$n = 13 \quad \rho = 0.977 \quad \text{S.D.} = 0.030$

TABLE III

CALCULATED VALUES OF π_2^H

Solute	α_2^H	No.	Average	S.D.	Max	Min	Taken
Cyclohexane	0.00	9	0.104	0.022	0.140	0.071	0.10
Methylcyclohexane	0.00	13	0.106	0.034	0.142	0.036	0.10
Cycloheptane	0.00	2	0.102	0.009	0.108	0.095	0.10
Cyclooctane	0.00	2	0.120	0.018	0.132	0.107	0.10
cis-Hydrindane	0.00	2	0.247	0.016	0.258	0.236	0.25
trans-Decalin	0.00	3	0.230	0.014	0.246	0.221	0.23
cis-Decalin	0.00	3	0.250	0.038	0.278	0.206	0.25
Cyclohexene	0.00	2	0.188	0.006	0.192	0.183	0.20
1-Methylcyclohexene	0.00	2	0.203	0.006	0.207	0.198	0.20
3-Methylcyclohexene	0.00	2	0.135	0.007	0.140	0.130	0.14
4-Methylcyclohexene	0.00	2	0.145	0.006	0.149	0.140	0.14
Cycloheptene	0.00	2	0.222	0.006	0.226	0.218	0.22
Cyclooctene	0.00	2	0.243	0.006	0.247	0.239	0.24
Cyclohexa-1,3-diene	0.00	3	0.302	0.015	0.318	0.289	0.30
Cyclohexa-1,4-diene	0.00	3	0.349	0.018	0.363	0.329	0.35
Cyclohepta-1,3-diene	0.00	3	0.381	0.007	0.387	0.374	0.38
Cycloocta-1,5-diene	0.00	2	0.359	0.005	0.362	0.355	0.36
Cyclohepta-1,3,5-triene	0.00	3	0.459	0.008	0.467	0.451	0.46
Cycloocta-1,3,5,7-tetraene	0.00	3	0.518	0.025	0.536	0.489	0.52
α-Pinene	0.00	1	0.185				0.20
Fluorocyclohexane	0.00	4	0.421	0.076	0.529	0.365	0.42
Chlorocyclohexane	0.00	5	0.478	0.028	0.519	0.455	0.48
Trichloroethene	0.00	1	0.367				0.37
Tetrachloroethene	0.00	1	0.442				0.44
1-Chlorocyclohexene	0.00	1	0.472				0.47
Bromocyclohexane	0.00	5	0.540	0.019	0.567	0.521	0.54
1-Bromocyclohexene	0.00	1	0.566				0.57
1-Bromo-4-methylcyclohexene	0.00	1	0.528				0.53
Iodocyclohexane	0.00	5	0.582	0.016	0.601	0.557	0.58
1-Iodocyclohexene	0.00	1	0.608				0.61
1,1-Difluorotetrachloroethane	0.00	1	0.334				0.33
1,2-Difluorotetrachloroethane	0.00	1	0.344				0.34
Methyl cyclohexyl ether	0.00	1	0.404				0.40
1,2-Dimethoxyethane	0.00	1	0.661				0.66
1,8-Cineole	0.00	1	0.497				0.50
Propenal	0.00	1	0.721				0.72
trans-But-2-ene-1-al	0.00	1	0.800				0.82
trans-Hex-2-ene-1-al	0.00	1	0.842				0.82
trans-Hept-2-ene-1-al	0.00	1	0.833				0.82
Carvone	0.00	1	0.934				0.93
Butan-2,3-dione	0.00	1	0.939				0.94
2-Methoxyethyl acetate	0.00	1	0.864				0.86
2-Ethoxyethyl acetate	0.00	2	0.819	0.041	0.848	0.790	0.82
Cyanocyclohexane	0.00	1	0.939	0.000	0.939	0.939	0.94
Cyclohexylamine	0.05	2	0.558	0.054	0.596	0.519	0.56
3-Methylcyclohexylamine	0.05	1	0.473				0.47
Nitrocyclohexane	0.00	1	0.971				0.97
Dimethylformamide	0.00	1	1.314				1.31
Dibutylformamide	0.00	1	1.114				1.11
Dimethylacetamide	0.00	1	1.332				1.33
2-Ethoxyethanol	0.30	1	0.501				0.50
trans-Hex-2-ene-1-ol	0.33	1	0.513				0.53

TABLE III *(continued)*

Solute	α_2^H	No.	Average	S.D.	Max	Min	Taken
trans-Hept-2-ene-1-ol	0.33	1	0.538				0.53
trans-Oct-2-ene-1-ol	0.33	1	0.539				0.53
Dodecafluoroheptan-1-ol	0.65	1	0.500				0.50
Dimethylsulphoxide	0.00	1	1.744				1.74
Cyclopropylbenzene	0.00	1	0.647				0.65
Diphenylmethane	0.00	2	1.038	0.001	1.038	1.037	1.04
2-Methyldiphenylmethane	0.00	2	1.009	0.002	1.010	1.007	1.01
3-Methyldiphenylmethane	0.00	2	1.019	0.020	1.033	1.005	1.01
4-Methyldiphenylmethane	0.00	2	1.001	0.001	1.002	1.000	1.01
1,1-Diphenylethane	0.00	2	0.984	0.036	1.009	0.958	0.98
1,2-Diphenylethane	0.00	2	1.029	0.008	1.035	1.023	1.03
1,4-Diphenylbutane	0.00	2	1.045	0.013	1.054	1.036	1.04
Biphenyl	0.00	5	0.985	0.049	1.050	0.933	0.99
2-Methylbiphenyl	0.00	2	0.875	0.011	0.882	0.867	0.88
3-Methylbiphenyl	0.00	2	0.951	0.045	0.982	0.919	0.95
4-Methylbiphenyl	0.00	2	0.980	0.038	1.007	0.953	0.98
2-Ethylbiphenyl	0.00	2	0.828	0.011	0.835	0.820	0.83
3-Ethylbiphenyl	0.00	2	0.960	0.018	0.972	0.947	0.96
4-Ethylbiphenyl	0.00	2	0.962	0.026	0.980	0.943	0.96
2,3-Dimethylbiphenyl	0.00	2	0.890	0.020	0.904	0.876	0.89
2,4-Dimethylbiphenyl	0.00	2	0.858	0.015	0.868	0.847	0.86
2,5-Dimethylbiphenyl	0.00	2	0.855	0.018	0.867	0.842	0.86
2,6-Dimethylbiphenyl	0.00	2	0.767	0.037	0.793	0.741	0.77
3,4-Dimethylbiphenyl	0.00	2	0.988	0.035	1.012	0.963	0.99
3,5-Dimethylbiphenyl	0.00	2	0.950	0.013	0.959	0.940	0.95
2,2′-Dimethylbiphenyl	0.00	2	0.747	0.028	0.767	0.727	0.75
2,3′-Dimethylbiphenyl	0.00	2	0.864	0.032	0.886	0.841	0.86
2,4′-Dimethylbiphenyl	0.00	2	0.863	0.024	0.880	0.846	0.86
3,3′-Dimethylbiphenyl	0.00	2	0.931	0.035	0.955	0.906	0.93
3,4′-Dimethylbiphenyl	0.00	2	0.942	0.030	0.963	0.920	0.94
4,4′-Dimethylbiphenyl	0.00	2	0.960	0.028	0.979	0.940	0.96
2-Isopropylbiphenyl	0.00	2	0.823	0.062	0.867	0.779	0.82
3-Isopropylbiphenyl	0.00	2	0.906	0.003	0.908	0.904	0.91
4-Isopropylbiphenyl	0.00	2	0.930	0.005	0.933	0.926	0.93
o-Terphenyl	0.00	1	1.181				1.18
p-Terphenyl	0.00	1	1.483				1.48
trans-Stilbene	0.00	2	1.184	0.089	1.247	1.121	1.18
cis-Stilbene	0.00	2	0.982	0.013	0.991	0.972	0.98
α-Methylstilbene (*cis*, *trans*?)	0.00	2	1.065	0.009	1.071	1.058	1.06
1-Ethylnaphthalene	0.00	2	0.870	0.012	0.878	0.861	0.88
2-Ethylnaphthalene	0.00	2	0.904	0.011	0.912	0.896	0.90
1-*n*-Propylnaphthalene	0.00	1	0.880				0.88
2-*n*-Propylnaphthalene	0.00	1	0.870				0.87
2-Isopropylnaphthalene	0.00	1	0.865				0.86
1-*n*-Butylnaphthalene	0.00	1	0.882				0.88
2-*n*-Butylnaphthalene	0.00	1	0.874				0.87
1-Isobutylnaphthalene	0.00	1	0.851				0.85
2-Isobutylnaphthalene	0.00	1	0.848				0.85
2-*sec*.-Butylnaphthalene	0.00	1	0.842				0.84
2-*tert*.-Butylnaphthalene	0.00	1	0.842				0.84
1,3,7-Trimethylnaphthalene	0.00	1	0.919				0.91

(Continued on p. 122)

TABLE III *(continued)*

Solute	α_2^H	No.	Average	S.D	Max	Min	Taken
2,3,5-Trimethylnaphthalene	0.00	1	0.856				0.86
2,3,6-Trimethylnaphthalene	0.00	1	0.863				0.86
2-Phenylnaphthalene	0.00	1	1.198				1.20
2-Benzylnaphthalene	0.00	1	1.198				1.20
Acenaphthene	0.00	3	1.048	0.016	1.064	1.032	1.05
Acenaphthylene	0.00	2	1.141	0.009	1.147	1.134	1.14
Fluorene	0.00	3	1.059	0.084	1.122	0.963	1.06
9-Methylfluorene	0.00	1	1.487				1.50
Azulene	0.00	1	1.171				1.17
1-Methylazulene	0.00	1	0.965				0.97
5-Methylazulene	0.00	1	0.974				0.97
6-Methylazulene	0.00	1	0.979				0.97
4,6,8-Trimethylazulene	0.00	1	1.010				1.01
Anthracene	0.00	5	1.340	0.104	1.459	1.239	1.34
9,10-Dihydroanthracene	0.00	1	1.009				1.01
Phenanthrene	0.00	5	1.295	0.090	1.402	1.215	1.29
9,10-Dihydrophenanthrene	0.00	1	1.045				1.05
Fluoranthene	0.00	2	1.551	0.011	1.559	1.543	1.55
Benzo[*a*]fluorene	0.00	2	1.588	0.009	1.594	1.581	1.59
Benzo[*b*]fluorene	0.00	2	1.565	0.010	1.572	1.558	1.57
3,4-Benzfluorene	0.00	1	1.586				1.59
Pyrene	0.00	3	1.716	0.030	1.744	1.684	1.72
Benz[*a*]anthracene	0.00	2	1.699	0.011	1.707	1.691	1.70
Benz[*c*]phenanthrene	0.00	1	1.683				1.68
Chrysene	0.00	2	1.729	0.006	1.733	1.725	1.73
Triphenylene	0.00	2	1.713	0.007	1.718	1.708	1.71
Benz[*b*]fluoranthene	0.00	1	1.824				1.82
Benz[*j*]fluoranthene	0.00	1	1.909				1.91
Benz[*k*]fluoranthene	0.00	1	1.912				1.91
Benz[*ghi*]fluoranthene	0.00	1	1.834				1.83
Perylene	0.00	2	1.794	0.016	1.805	1.783	1.79
3-Methylcholanthrene	0.00	1	1.570				1.57
Dibenz[*ac*]anthracene	0.00	2	1.927	0.008	1.933	1.921	1.93
Dibenz[*ah*]anthracene	0.00	1	2.044				2.04
Benz[*a*]pyrene	0.00	2	1.980	0.028	2.000	1.960	1.98
3,4-Benzpyrene	0.00	1	1.917				1.92
Benz[*e*]pyrene	0.00	1	1.994				1.99
Benz[*b*]chrysene	0.00	1	2.189				2.19
Pentacene	0.00	1	2.714				2.71
Benz[*ghi*]perylene	0.00	2	1.897	0.013	1.906	1.887	1.90
Picene	0.00	2	2.041	0.035	2.066	2.016	2.04
Fluorobenzene	0.00	32	0.571	0.016	0.617	0.536	0.57
1,2-Difluorobenzene	0.00	2	0.755	0.000	0.755	0.755	0.75
1,2,4,5-Tetrafluorobenzene	0.00	3	0.697	0.067	0.740	0.620	0.70
Pentafluorobenzene	0.00	3	0.680	0.113	0.750	0.550	0.68
Hexafluorobenzene	0.00	3	0.657	0.167	0.790	0.470	0.66
2-Fluorotoluene	0.00	4	0.572	0.027	0.600	0.536	0.57
3-Fluorotoluene	0.00	4	0.585	0.032	0.610	0.539	0.58
4-Fluorotoluene	0.00	5	0.548	0.038	0.590	0.493	0.55
Benzotrifluoride	0.00	16	0.485	0.026	0.540	0.438	0.48
Chlorobenzene	0.00	36	0.655	0.015	0.687	0.618	0.65
1,2-Dichlorobenzene	0.00	18	0.779	0.022	0.812	0.725	0.78
1,3-Dichlorobenzene	0.00	17	0.727	0.019	0.752	0.686	0.73

TABLE III *(continued)*

Solute	α_2^H	No.	Average	S.D.	Max	Min	Taken
1,4-Dichlorobenzene	0.00	17	0.752	0.021	0.771	0.698	0.75
1,2,3-Trichlorobenzene	0.00	5	0.858	0.019	0.888	0.840	0.86
1,2,4-Trichlorobenzene	0.00	5	0.810	0.031	0.856	0.771	0.81
1,3,5-Trichlorobenzene	0.00	5	0.728	0.053	0.795	0.653	0.73
1,2,3,4-Tetrachlorobenzene	0.00	4	0.919	0.012	0.933	0.904	0.92
1,2,3,5-Tetrachlorobenzene	0.00	5	0.845	0.042	0.894	0.780	0.85
1,2,4,5-Tetrachlorobenzene	0.00	5	0.859	0.033	0.899	0.808	0.86
Pentachlorobenzene	0.00	4	0.957	0.014	0.976	0.947	0.96
Hexachlorobenzene	0.00	4	0.990	0.015	1.006	0.971	0.99
2-Chlorotoluene	0.00	13	0.650	0.010	0.664	0.629	0.65
3-Chlorotoluene	0.00	14	0.672	0.014	0.703	0.646	0.67
4-Chlorotoluene	0.00	14	0.669	0.019	0.704	0.638	0.67
2,4-Dichlorotoluene	0.00	5	0.742	0.030	0.784	0.706	0.74
2,5-Dichlorotoluene	0.00	3	0.757	0.011	0.767	0.745	0.76
2,6-Dichlorotoluene	0.00	5	0.750	0.030	0.789	0.715	0.75
3,4-Dichlorotoluene	0.00	3	0.803	0.025	0.831	0.786	0.80
2,3,4-Trichlorotoluene	0.00	2	0.874	0.001	0.874	0.873	0.87
2,3,5-Trichlorotoluene	0.00	2	0.844	0.008	0.849	0.838	0.84
2,4,5-Trichlorotoluene	0.00	2	0.855	0.026	0.873	0.836	0.85
2,4,6-Trichlorotoluene	0.00	2	0.772	0.002	0.773	0.770	0.77
2,3,4,5-Tetrachlorotoluene	0.00	2	0.943	0.006	0.947	0.938	0.94
2,3,5,6-Tetrachlorotuluene	0.00	2	0.914	0.026	0.932	0.895	0.91
Pentachlorotoluene	0.00	2	0.996	0.052	1.033	0.959	1.00
2-Chloro-*p*-xylene	0.00	4	0.706	0.068	0.807	0.665	0.71
2,3-Dichloro-*p*-xylene	0.00	3	0.816	0.020	0.827	0.793	0.82
2,5-Dichloro-*p*-xylene	0.00	3	0.779	0.012	0.790	0.767	0.78
2,3,5-Trichloro-*p*-xylene	0.00	3	0.867	0.011	0.880	0.861	0.87
Benzyl chloride	0.00	6	0.818	0.062	0.879	0.731	0.82
2-Chlorobenzyl chloride	0.00	2	0.983	0.008	0.988	0.977	0.98
4-Chlorobenzyl chloride	0.00	3	0.879	0.020	0.892	0.856	0.88
2-Chloro-4-methylbenzyl chloride	0.00	1	1.038				1.03
3-Chloro-4-methylbenzyl chloride	0.00	1	1.067				1.06
1,4-Bis(chloromethyl)benzene	0.00	1	1.338				1.34
Benzal chloride	0.10	3	0.788	0.019	0.806	0.769	0.79
Benzotrichloride	0.00	1	0.843				0.84
2-Chlorostyrene	0.00	2	0.669	0.018	0.681	0.656	0.67
Bromobenzene	0.00	30	0.732	0.016	0.766	0.691	0.73
1,2-Dibromobenzene	0.00	2	0.960	0.003	0.962	0.958	0.96
1,3-Dibromobenzene	0.00	2	0.878	0.004	0.880	0.875	0.88
1,4-Dibromobenzene	0.00	1	0.861	0.000	0.861	0.861	0.86
2-Bromotoluene	0.00	3	0.723	0.003	0.725	0.720	0.72
3-Bromotoluene	0.00	4	0.746	0.005	0.752	0.741	0.75
4-Bromotoluene	0.00	4	0.737	0.006	0.744	0.732	0.74
Benzyl bromide	0.00	1	0.978				0.98
2-Bromo-1-phenylethane	0.00	1	0.937				0.94
1-Bromonaphthalene	0.00	1	1.037				1.04
Iodobenzene	0.00	29	0.823	0.024	0.878	0.764	0.82
1,2-Diiodobenzene	0.00	2	1.208	0.004	1.210	1.205	1.21
1,3-Diiodobenzene	0.00	2	1.071	0.004	1.074	1.068	1.07
1,4-Diiodobenzene	0.00	2	1.150	0.004	1.153	1.147	1.15
2-Iodotoluene	0.00	3	0.822	0.021	0.846	0.807	0.82

(Continued on p. 124)

TABLE III *(continued)*

Solute	α_2^H	No.	Average	S.D.	Max	Min	Taken
3-Iodotoluene	0.00	3	0.838	0.022	0.863	0.823	0.84
4-Iodotoluene	0.00	1	0.850				0.85
Methylphenylether	0.00	30	0.745	0.026	0.778	0.659	0.75
2-Methylanisole	0.00	3	0.745	0.003	0.748	0.742	0.75
3-Methylanisole	0.00	3	0.779	0.006	0.784	0.772	0.78
4-Methylanisole	0.00	3	0.773	0.002	0.776	0.772	0.77
2,3-Dimethylanisole	0.00	2	0.793	0.001	0.794	0.792	0.79
2,4-Dimethylanisole	0.00	2	0.774	0.014	0.784	0.764	0.77
2,5-Dimethylanisole	0.00	2	0.795	0.016	0.806	0.784	0.79
2,6-Dimethylanisole	0.00	2	0.781	0.012	0.789	0.772	0.78
3,4-Dimethylanisole	0.00	2	0.807	0.010	0.814	0.800	0.81
3,5-Dimethylanisole	0.00	2	0.783	0.029	0.803	0.762	0.78
2-Ethylanisole	0.00	2	0.796	0.006	0.800	0.792	0.80
3-Ethylanisole	0.00	2	0.813	0.004	0.816	0.810	0.80
4-Ethylanisole	0.00	2	0.798	0.006	0.802	0.794	0.80
2-Propylanisole	0.00	2	0.806	0.014	0.816	0.796	0.80
3-Propylanisole	0.00	2	0.813	0.001	0.814	0.812	0.80
4-Propylanisole	0.00	2	0.797	0.004	0.800	0.794	0.80
4-Allylanisole	0.00	2	0.830	0.017	0.842	0.818	0.83
2-Fluoroanisole	0.00	4	0.790	0.042	0.836	0.744	0.79
3-Fluoroanisole	0.00	4	0.718	0.033	0.760	0.682	0.72
4-Fluoroanisole	0.00	6	0.735	0.035	0.772	0.680	0.74
2-Chloroanisole	0.00	3	0.915	0.018	0.936	0.904	0.91
3-Chloroanisole	0.00	1	0.860				0.86
4-Chloroanisole	0.00	5	0.862	0.023	0.890	0.832	0.86
2,3-Dichloroanisole	0.00	1	1.021				1.02
2,4-Dichloroanisole	0.00	3	0.943	0.025	0.960	0.915	0.94
2,5-Dichloroanisole	0.00	3	0.950	0.010	0.959	0.939	0.95
2,6-Dichloroanisole	0.00	3	0.863	0.012	0.870	0.850	0.86
3,4-Dichloroanisole	0.00	1	0.946				0.95
3,5-Dichloroanisole	0.00	1	0.868				0.87
2,3,4-Trichloroanisole	0.00	1	1.118				1.12
2,3,5-Trichloroanisole	0.00	1	1.007				1.01
2,3,6-Trichloroanisole	0.00	1	0.906				0.91
2,4,5-Trichloroanisole	0.00	3	1.006	0.014	1.021	0.993	1.01
2,4,6-Trichloroanisole	0.00	3	0.846	0.034	0.884	0.818	0.85
3,4,5-Trichloroanisole	0.00	1	0.988				0.99
2,3,4,5-Tetrachloroanisole	0.00	1	1.146				1.15
2,3,4,6-Tetrachloroanisole	0.00	3	0.953	0.033	0.983	0.917	0.95
2,3,5,6-Tetrachloroanisole	0.00	1	0.915				0.92
Pentachloroanisole	0.00	3	1.055	0.051	1.099	0.999	1.05
4-Bromoanisole	0.00	2	0.902	0.008	0.907	0.896	0.90
4-Iodoanisole	0.00	2	0.991	0.021	1.005	0.976	0.99
Methyl benzyl ether	0.00	1	0.771				0.77
Ethyl benzyl ether	0.00	1	0.710				0.71
Diphenyl ether	0.00	2	1.084	0.089	1.147	1.021	1.08
1,2-Dimethoxybenzene	0.00	2	0.965	0.070	1.014	0.915	0.97
1,3-Dimethoxybenzene	0.00	1	1.011				1.01
4-Methylveratrole	0.00	2	0.949	0.001	0.950	0.948	0.95
3-Chloroveratrole	0.00	1	0.959				0.96
4-Chloroveratrole	0.00	1	1.027				1.03
3,4-Dichloroveratrole	0.00	1	1.051				1.05
3,5-Dichloroveratrole	0.00	1	0.979				0.98

TABLE III *(continued)*

Solute	α_2^H	No.	Average	S.D.	Max	Min	Taken
3,6-Dichloroveratrole	0.00	1	0.895				0.90
4,5-Dichloroveratrole	0.00	1	1.114				1.11
3,4,5-Trichloroveratrole	0.00	1	1.102				1.10
3,4,6-Trichloroveratrole	0.00	1	0.925				0.93
Tetrachloroveratrole	0.00	1	1.004				1.00
Benzaldehyde	0.00	22	0.999	0.013	1.020	0.967	1.00
2-Methylbenzaldehyde	0.00	2	0.959	0.010	0.966	0.952	0.96
3-Methylbenzaldehyde	0.00	2	0.973	0.018	0.986	0.960	0.97
4-Methylbenzaldehyde	0.00	2	1.004	0.020	1.018	0.990	1.00
2,4-Dimethylbenzaldehyde	0.00	2	0.932	0.001	0.932	0.931	0.93
2,5-Dimethylbenzaldehyde	0.00	2	0.927	0.012	0.935	0.918	0.93
3,4-Dimethylbenzaldehyde	0.00	2	0.923	0.025	0.940	0.905	0.92
4-Isopropylbenzaldehyde	0.00	2	0.968	0.001	0.968	0.967	0.97
Furfural	0.00	1	1.134				1.13
Phthalaldehyde	0.00	2	1.291	0.052	1.327	1.254	1.29
Terephthalaldehyde	0.00	2	1.294	0.059	1.335	1.252	1.29
Acetophenone	0.00	18	1.007	0.023	1.074	0.978	1.01
2-Methoxyacetophenone	0.00	2	0.993	0.001	0.994	0.992	0.99
3-Methoxyacetophenone	0.00	2	0.970	0.006	0.974	0.966	0.97
4-Methoxyacetophenone	0.00	2	0.971	0.010	0.978	0.964	0.97
4-Phenylbutan-2-one	0.00	1	1.144				1.14
Methyl benzoate	0.00	23	0.851	0.032	0.939	0.779	0.85
Ethyl benzoate	0.00	2	0.854	0.006	0.858	0.850	0.85
Propyl benzoate	0.00	1	0.794				0.80
Butyl benzoate	0.00	1	0.797				0.80
Pentyl benzoate	0.00	1	0.786				0.79
Hexyl benzoate	0.00	1	0.787				0.79
Heptyl benzoate	0.00	1	0.788				0.79
Octyl benzoate	0.00	1	0.786				0.79
Nonyl benzoate	0.00	1	0.784				0.78
Decyl benzoate	0.00	1	0.783				0.78
Undecyl benzoate	0.00	1	0.784				0.78
Dodecyl benzoate	0.00	1	0.782				0.78
Methyl 2-methylbenzoate	0.00	3	0.866	0.054	0.926	0.821	0.87
Methyl 3-methylbenzoate	0.00	3	0.878	0.048	0.929	0.833	0.88
Methyl 4-methylbenzoate	0.00	3	0.881	0.045	0.930	0.842	0.88
Methyl 2,4-dimethylbenzoate	0.00	2	0.760	0.052	0.797	0.723	0.80
Methyl 2,5-dimethylbenzoate	0.00	2	0.776	0.040	0.804	0.747	0.80
Methyl 3,4-dimethylbenzoate	0.00	2	0.854	0.040	0.882	0.825	0.85
Methyl 4-isopropylbenzoate	0.00	2	0.785	0.024	0.802	0.768	0.80
Methyl 2-fluorobenzoate	0.00	4	0.888	0.042	0.928	0.832	0.89
Methyl 3-fluorobenzoate	0.00	4	0.883	0.071	0.974	0.816	0.88
Methyl 4-fluorobenzoate	0.00	4	0.885	0.070	0.971	0.819	0.89
Methyl 2-chlorobenzoate	0.00	3	0.989	0.024	1.015	0.968	0.99
Methyl 4-chlorobenzoate	0.00	1	0.917				0.92
Methyl 2,4-dichlorobenzoate	0.00	2	0.976	0.026	0.994	0.957	0.98
Methyl 2,5-dichlorobenzoate	0.00	2	0.986	0.027	1.005	0.967	0.99
Methyl 2,3,6-trichlorobenzoate	0.00	2	1.077	0.020	1.091	1.063	1.08
Methyl 2-MeO-3,6-dichlorobenzoate	0.00	2	1.038	0.019	1.051	1.024	1.04
Methyl 4-methoxybenzoate	0.00	1	1.313				1.31
Phenyl acetate	0.00	1	1.131				1.13

(Continued on p. 126)

TABLE III *(continued)*

Solute	α_2^H	No.	Average	S.D.	Max	Min	Taken
2-Methylphenyl acetate	0.00	1	1.039				1.04
3-Methylphenyl acetate	0.00	1	1.132				1.13
4-Methylphenyl acetate	0.00	3	1.006	0.121	1.144	0.920	1.01
Benzyl acetate	0.00	2	1.065	0.050	1.100	1.029	1.06
2-Methylbenzyl acetate	0.00	2	0.957	0.013	0.966	0.947	0.96
4-Methylbenzyl acetate	0.00	2	1.003	0.024	1.020	0.986	1.00
2,4-Dimethylbenzyl acetate	0.00	2	0.913	0.025	0.931	0.895	0.91
2,5-Dimethylbenzyl acetate	0.00	2	0.914	0.018	0.926	0.901	0.91
3,4-Dimethylbenzyl acetate	0.00	2	0.909	0.042	0.939	0.879	0.91
2-Phenylethyl acetate	0.00	1	1.096				1.10
Benzyl benzoate	0.00	2	1.355	0.136	1.451	1.258	1.35
Methyl phenylacetate	0.00	1	1.134				1.13
Ethyl phenylacetate	0.00	1	1.008				1.01
Ethyl cinnamate	0.00	1	1.237				1.24
Dimethyl phthalate	0.00	2	1.407	0.035	1.432	1.382	1.41
Dimethyl isophthalate	0.00	2	1.256	0.027	1.275	1.237	1.26
Dimethyl terephthalate	0.00	2	1.219	0.025	1.236	1.201	1.22
Dimethyl methylterephthalate	0.00	2	1.172	0.006	1.176	1.167	1.17
Benzonitrile	0.00	21	1.110	0.019	1.157	1.078	1.11
2-Methylbenzonitrile	0.00	2	1.056	0.015	1.066	1.045	1.06
3-Methylbenzonitrile	0.00	1	1.075				1.08
4-Methylbenzonitrile	0.00	1	1.097				1.10
2-Chlorobenzonitrile	0.00	1	1.236				1.24
3-Chlorobenzonitrile	0.00	1	1.139				1.14
4-Chlorobenzonitrile	0.00	1	1.180				1.18
4-Nitrobenzonitrile	0.00	1	1.331				1.33
Phenylacetonitrile	0.00	1	1.152				1.15
Aniline	0.26	29	0.960	0.023	1.005	0.907	0.96
o-Toluidine	0.23	9	0.923	0.022	0.955	0.880	0.92
m-Toluidine	0.23	10	0.950	0.018	0.978	0.928	0.95
p-Toluidine	0.23	11	0.948	0.027	0.987	0.902	0.95
2-Ethylaniline	0.23	3	0.853	0.021	0.875	0.834	0.85
3-Ethylaniline	0.23	2	0.946	0.006	0.950	0.942	0.95
4-Ethylaniline	0.23	4	0.910	0.034	0.959	0.885	0.91
2,3-Dimethylaniline	0.20	5	0.962	0.024	0.981	0.922	0.96
2,4-Dimethylaniline	0.20	5	0.951	0.006	0.958	0.945	0.95
2,5-Dimethylaniline	0.20	4	0.931	0.023	0.964	0.912	0.93
2,6-Dimethylaniline	0.20	7	0.891	0.018	0.912	0.860	0.89
3,4-Dimethylaniline	0.20	6	0.971	0.020	0.995	0.954	0.97
3,5-Dimethylaniline	0.20	2	0.949	0.004	0.952	0.946	0.95
2,6-Diethylaniline	0.20	1	0.556				0.56
2-Vinylaniline	0.25	1	0.984				0.98
3-Vinylaniline	0.26	1	1.120				1.12
4-Vinylaniline	0.25	1	1.100				1.10
2-Fluoroaniline	0.28	3	0.879	0.024	0.907	0.864	0.88
3-Fluoroaniline	0.30	5	1.075	0.081	1.185	0.979	1.08
4-Fluoroaniline	0.28	8	1.095	0.073	1.175	1.004	1.09
2-Chloroaniline	0.30	6	0.923	0.016	0.940	0.903	0.92
3-Chloroaniline	0.33	7	1.099	0.041	1.146	1.050	1.10
4-Chloroaniline	0.30	5	1.127	0.040	1.167	1.073	1.13
2-Bromoaniline	0.31	5	0.979	0.025	1.001	0.942	0.98
3-Bromoaniline	0.33	6	1.186	0.028	1.215	1.155	1.19
4-Bromoaniline	0.31	6	1.189	0.035	1.229	1.145	1.19

TABLE III *(continued)*

Solute	α_2^H	No.	Average	S.D.	Max	Min	Taken
2-Iodoaniline	0.31	1	1.000				1.00
3-Iodoaniline	0.33	5	1.258	0.025	1.282	1.229	1.26
4-Iodoaniline	0.31	3	1.278	0.014	1.294	1.266	1.28
2-Cyanoaniline	0.35	1	1.374				1.37
3-Cyanoaniline	0.38	1	1.594				1.59
4-Cyanoaniline	0.40	1	1.779				1.78
2-Methoxyaniline	0.23	5	1.027	0.051	1.083	0.982	1.00
3-Methoxyaniline	0.25	6	1.216	0.026	1.241	1.168	1.22
4-Methoxyaniline	0.23	5	1.194	0.039	1.231	1.148	1.10
2-Nitroaniline	0.37	2	1.365	0.034	1.389	1.341	1.36
3-Nitroaniline	0.40	3	1.713	0.102	1.823	1.623	1.71
4-Nitroaniline	0.42	3	1.906	0.019	1.928	1.895	1.91
2-Ethoxyaniline	0.23	1	1.111				1.10
3-Ethoxyaniline	0.25	1	1.090				1.10
4-Ethoxyaniline	0.23	3	1.173	0.084	1.224	1.076	1.17
3-Fluoro-4-methylaniline	0.27	2	1.160	0.001	1.161	1.159	1.16
4-Fluoro-2-methylaniline	0.25	2	1.140	0.001	1.141	1.139	1.14
2,4-Difluoroaniline	0.30	2	1.021	0.001	1.021	1.020	1.02
2,5-Difluoroaniline	0.32	2	1.149	0.001	1.150	1.148	1.15
N-Methylaniline	0.17	10	0.898	0.020	0.934	0.881	0.90
N-Ethylaniline	0.17	5	0.851	0.042	0.887	0.784	0.85
N-Propylaniline	0.17	4	0.853	0.014	0.867	0.840	0.85
N-Butylaniline	0.17	4	0.855	0.006	0.860	0.847	0.85
N-Isopentylaniline	0.17	2	0.845	0.002	0.846	0.843	0.84
2-Methyl-N-methylaniline	0.17	2	0.977	0.000	0.977	0.977	0.98
3-Methyl-N-methylaniline	0.17	2	1.004	0.001	1.004	1.003	1.00
4-Methyl-N-methylaniline	0.17	2	0.977	0.040	1.005	0.949	0.98
2-Methyl-N-ethylaniline	0.17	4	0.842	0.038	0.878	0.807	0.84
3-Methyl-N-ethylaniline	0.17	4	0.898	0.014	0.912	0.885	0.90
4-Methyl-N-ethylaniline	0.17	4	0.886	0.023	0.907	0.865	0.90
2-Chloro-N-methylaniline	0.19	2	0.961	0.002	0.962	0.959	0.96
4-Chloro-N-methylaniline	0.21	2	1.011	0.001	1.011	1.010	1.01
N,N-Dimethylaniline	0.00	11	0.842	0.016	0.869	0.817	0.84
N,N-Diethylaniline	0.00	7	0.799	0.026	0.834	0.772	0.80
2-Methyl-N,N-dimethylaniline	0.00	5	0.651	0.051	0.740	0.620	0.65
3-Methyl-N,N-dimethylaniline	0.00	5	0.861	0.016	0.889	0.851	0.86
4-Methyl-N,N-dimethylaniline	0.00	6	0.827	0.015	0.849	0.811	0.83
4-Bromo-N,N-dimethylaniline	0.00	4	0.968	0.050	1.012	0.924	0.97
3-Methyl-N,N-diethylaniline	0.00	4	0.793	0.032	0.822	0.764	0.79
4-Methyl-N,N-diethylaniline	0.00	4	0.797	0.040	0.833	0.761	0.80
1-Naphthylamine	0.20	2	1.257	0.001	1.258	1.256	1.26
2-Naphthylamine	0.22	2	1.276	0.000	1.276	1.276	1.28
Benzylamine	0.10	2	0.879	0.058	0.920	0.838	0.88
Nitrobenzene	0.00	20	1.108	0.019	1.153	1.064	1.11
2-Nitrotoluene	0.00	2	1.114	0.021	1.129	1.099	1.11
3-Nitrotoluene	0.00	2	1.101	0.011	1.108	1.093	1.10
4-Nitrotoluene	0.00	1	1.114				1.11
1-Fluoro-3-nitrobenzene	0.00	4	1.108	0.172	1.330	0.930	1.11
1-Chloro-2-nitrobenzene	0.00	3	1.253	0.005	1.256	1.248	1.25
1-Chloro-3-nitrobenzene	0.00	3	1.133	0.032	1.169	1.108	1.13
1-Chloro-4-nitrobenzene	0.00	3	1.168	0.020	1.184	1.145	1.17

(Continued on p. 128)

TABLE III *(continued)*

Solute	α_2^H	No.	Average	S.D.	Max	Min	Taken
1-Methoxy-4-nitrobenzene	0.00	1	1.213				1.21
Phenol	0.60	46	0.892	0.020	0.942	0.839	0.89
o-Cresol	0.52	32	0.862	0.018	0.895	0.821	0.86
m-Cresol	0.57	33	0.879	0.014	0.902	0.847	0.88
p-Cresol	0.57	33	0.873	0.016	0.906	0.843	0.87
2-Ethylphenol	0.52	11	0.841	0.039	0.919	0.776	0.84
3-Ethylphenol	0.55	16	0.906	0.017	0.930	0.871	0.91
4-Ethylphenol	0.55	16	0.899	0.020	0.935	0.867	0.90
2,3-Dimethylphenol	0.53	23	0.808	0.022	0.870	0.763	0.81
2,4-Dimethylphenol	0.53	24	0.797	0.013	0.830	0.770	0.80
2,5-Dimethylphenol	0.54	18	0.789	0.012	0.807	0.761	0.79
2,6-Dimethylphenol	0.86	22	0.787	0.031	0.846	0.702	0.79
3,4-Dimethylphenol	0.56	19	0.865	0.031	0.947	0.818	0.86
3,5-Dimethylphenol	0.57	23	0.840	0.020	0.872	0.792	0.84
2-*n*-Propylphenol	0.52	6	0.859	0.019	0.888	0.833	0.86
3-*n*-Propylphenol	0.55	5	0.896	0.020	0.913	0.864	0.90
4-*n*-Propylphenol	0.55	6	0.875	0.014	0.895	0.864	0.88
2-Isopropylphenol	0.52	7	0.885	0.051	0.985	0.834	0.89
3-Isopropylphenol	0.55	7	0.917	0.024	0.971	0.905	0.92
4-Isopropylphenol	0.55	7	0.894	0.027	0.952	0.872	0.89
2-Methyl-4-ethylphenol	0.53	4	0.787	0.015	0.805	0.774	0.79
2-Methyl-5-ethylphenol	0.54	3	0.782	0.009	0.791	0.773	0.78
3-Methyl-4-ethylphenol	0.56	2	0.886	0.030	0.907	0.864	0.89
3-Methyl-5-ethylphenol	0.57	4	0.854	0.020	0.880	0.834	0.85
3-Methyl-6-ethylphenol	0.54	3	0.870	0.053	0.931	0.834	0.87
4-Methyl-2-ethylphenol	0.53	4	0.789	0.040	0.818	0.730	0.79
2,3,4-Trimethylphenol	0.52	3	0.821	0.025	0.849	0.800	0.82
2,3,5-Trimethylphenol	0.52	12	0.840	0.012	0.852	0.819	0.84
2,3,6-Trimethylphenol	0.37	7	0.808	0.046	0.864	0.719	0.81
2,4,5-Trimethylphenol	0.52	3	0.791	0.027	0.817	0.764	0.79
2,4,6-Trimethylphenol	0.37	11	0.791	0.033	0.824	0.724	0.78
3,4,5-Trimethylphenol	0.55	6	0.881	0.027	0.920	0.842	0.88
2-*n*-Butylphenol	0.52	4	0.839	0.019	0.855	0.812	0.84
3-*n*-Butylphenol	0.55	4	0.909	0.028	0.924	0.867	0.91
4-*n*-Butylphenol	0.55	4	0.879	0.007	0.886	0.870	0.88
2-*sec.*-Butylphenol	0.52	5	0.905	0.032	0.947	0.868	0.91
4-*sec.*-Butylphenol	0.55	5	0.907	0.007	0.916	0.899	0.91
2-*tert.*-Butylphenol	0.52	7	0.924	0.034	0.977	0.886	0.92
4-*tert.*-Butylphenol	0.56	7	0.888	0.010	0.906	0.876	0.89
2,4-Diethylphenol	0.53	3	0.833	0.022	0.858	0.817	0.83
2,5-Diethylphenol	0.54	2	0.857	0.033	0.880	0.834	0.86
2,6-Diethylphenol	0.39	1	0.847				0.85
2-Methyl-6-propylphenol	0.39	3	0.703	0.024	0.725	0.677	0.70
4-Methyl-2-propylphenol	0.53	3	0.796	0.017	0.812	0.779	0.80
2-Methyl-4-isopropylphenol	0.53	1	0.844				0.84
3-Methyl-5-isopropylphenol	0.57	1	0.736				0.74
3,4-Dimethyl-6-ethylphenol	0.52	1	0.794				0.79
2,3,4,5-Tetramethylphenol	0.52	3	0.873	0.058	0.940	0.835	0.87
2,3,5,6-Tetramethylphenol	0.35	7	0.860	0.028	0.885	0.807	0.86
2-Ethyl-5-propylphenol	0.54	3	0.829	0.025	0.856	0.807	0.83
Pentamethylphenol	0.35	4	0.852	0.028	0.879	0.816	0.85
2,6-Diisopropylphenol	0.38	2	0.750	0.059	0.791	0.708	0.75
4-Methyl-2,6-di-*tert.*-butylphenol	0.37	2	0.706	0.042	0.735	0.676	0.71

TABLE III *(continued)*

Solute	α_2^H	No.	Average	S.D.	Max	Min	Taken
Thymol	0.52	6	0.791	0.031	0.850	0.763	0.79
Carvacrol	0.54	4	0.814	0.033	0.860	0.789	0.81
4-*tert.*-Pentylphenol	0.56	4	0.885	0.012	0.903	0.874	0.89
2-Phenylphenol	0.56	1	1.030				1.03
4-Phenylphenol	0.59	1	1.482				1.48
5,6,7,8-Tetrahydro-1-naphthol	0.53	3	0.715	0.019	0.728	0.693	0.72
5,6,7,8-Tetrahydro-2-naphthol	0.56	2	0.758	0.006	0.762	0.754	0.76
4-Indanol	0.53	5	0.802	0.019	0.823	0.778	0.80
5-Indanol	0.56	5	0.834	0.016	0.855	0.813	0.83
5-Methyl-4-indanol	0.37	2	0.803	0.093	0.869	0.737	0.80
6-Methyl-4-indanol	0.52	3	0.778	0.005	0.784	0.774	0.78
7-Methyl-4-indanol	0.52	3	0.791	0.010	0.803	0.784	0.79
7-Methyl-5-indanol	0.55	2	0.839	0.006	0.843	0.834	0.84
2-Fluorophenol	0.61	3	0.687	0.004	0.691	0.684	0.69
3-Fluorophenol	0.68	3	0.976	0.012	0.990	0.967	0.98
4-Fluorophenol	0.63	7	0.954	0.053	1.014	0.861	0.95
2-Chlorophenol	0.32	3	0.884	0.026	0.913	0.854	0.86
3-Chlorophenol	0.69	11	1.058	0.014	1.075	1.040	1.06
4-Chlorophenol	0.67	12	1.076	0.011	1.105	1.064	1.08
2-Bromophenol	0.35	1	0.901				0.55
3-Bromophenol	0.70	7	1.153	0.031	1.200	1.112	1.15
4-Bromophenol	0.67	7	1.169	0.015	1.198	1.156	1.17
2-Iodophenol	0.40	1	1.000				0.65
3-Iodophenol	0.70	1	1.204				1.20
4-Iodophenol	0.68	4	1.332	0.108	1.486	1.250	1.33
3,4-Dichlorophenol	0.74	2	1.202	0.076	1.256	1.148	1.20
3,5-Dichlorophenol	0.77	4	1.166	0.031	1.210	1.143	1.17
3,4,5-Trichlorophenol	0.82	2	1.465	0.057	1.505	1.425	1.46
4-Chloro-2-methylphenol	0.63	1	0.907				0.91
4-Chloro-3-methylphenol	0.65	4	1.022	0.044	1.067	0.964	1.02
2-Methoxyphenol	0.26	9	0.910	0.039	0.950	0.852	0.91
3-Methoxyphenol	0.59	7	1.174	0.025	1.196	1.124	1.17
4-Methoxyphenol	0.57	9	1.170	0.011	1.193	1.153	1.17
2,6-Dimethoxyphenol	0.25	2	0.900	0.057	0.940	0.860	0.90
4-Allyl-2-methoxyphenol	0.26	3	0.796	0.035	0.819	0.756	0.80
4-Propyl-2-methoxyphenol	0.26	3	0.755	0.020	0.773	0.733	0.76
2-Cyanophenol	0.74	2	1.328	0.049	1.363	1.293	1.33
3-Cyanophenol	0.77	3	1.548	0.014	1.559	1.533	1.55
4-Cyanophenol	0.79	3	1.626	0.014	1.642	1.614	1.63
2-Nitrophenol	0.05	5	1.048	0.080	1.093	0.907	0.82
3-Nitrophenol	0.79	5	1.569	0.007	1.576	1.560	1.57
4-Nitrophenol	0.82	5	1.720	0.029	1.759	1.693	1.72
3-Methyl-2-nitrophenol	0.05	1	1.082				1.08
2-Methyl-4-nitrophenol	0.78	1	1.614				1.61
2-Methyl-5-nitrophenol	0.75	1	1.520				1.52
2-Methyl-6-nitrophenol	0.05	1	1.064				1.06
2,5-Dimethyl-4-nitrophenol	0.79	1	1.551				1.55
2,6-Dimethyl-4-nitrophenol	0.79	1	1.536				1.54
Catechol	0.85	3	1.065	0.027	1.081	1.034	1.07
Resorcinol	1.10	8	1.001	0.055	1.062	0.833	1.00
Hydroquinone	1.16	9	0.999	0.127	1.154	0.705	1.00

(Continued on p. 130)

TABLE III *(continued)*

Solute	α_2^H	No.	Average	S.D.	Max	Min	Taken
Methyl paraban	0.69	1	1.366				1.37
1-Naphthol	0.61	6	1.046	0.014	1.066	1.024	1.05
2-Naphthol	0.61	6	1.079	0.014	1.098	1.060	1.08
Benzyl alcohol	0.39	18	0.867	0.019	0.903	0.832	0.87
2-Methylbenzyl alcohol	0.39	2	0.897	0.016	0.908	0.885	0.90
3-Methylbenzyl alcohol	0.39	2	0.904	0.006	0.908	0.900	0.90
4-Methylbenzyl alcohol	0.39	2	0.885	0.006	0.889	0.880	0.89
2,4-Dimethylbenzyl alcohol	0.39	2	0.878	0.002	0.879	0.876	0.88
2,5-Dimethylbenzyl alcohol	0.39	2	0.878	0.008	0.883	0.872	0.88
3,4-Dimethylbenzyl alcohol	0.39	2	0.896	0.004	0.899	0.893	0.90
1-Phenylethanol	0.33	1	0.831				0.83
2-Phenylethanol	0.33	2	0.908	0.011	0.915	0.900	0.91
Thiophenol	0.09	16	0.802	0.028	0.899	0.777	0.80
Benzylthiol	0.00	1	0.788				0.79
Phenylmethylsulphide	0.00	1	0.918				0.92
Furan	0.00	1	0.525				0.53
Benzofuran	0.00	1	0.830				0.83
Dibenzofuran	0.00	3	1.018	0.033	1.043	0.980	1.02
Benzodioxane	0.00	3	1.073	0.049	1.128	1.035	1.07
Benzo[*kl*]xanthene	0.00	1	1.261				1.26
Trioxan	0.00	1	1.031				1.03
Pyridine	0.00	16	0.836	0.017	0.862	0.800	0.84
2-Methylpyridine	0.00	15	0.754	0.014	0.772	0.715	0.75
3-Methylpyridine	0.00	15	0.814	0.006	0.827	0.804	0.81
4-Methylpyridine	0.00	15	0.824	0.006	0.837	0.816	0.82
2-Ethylpyridine	0.00	13	0.708	0.009	0.723	0.694	0.71
3-Ethylpyridine	0.00	12	0.792	0.012	0.818	0.780	0.79
4-Ethylpyridine	0.00	14	0.804	0.010	0.826	0.789	0.80
2,3-Dimethylpyridine	0.00	9	0.769	0.007	0.778	0.757	0.77
2,4-Dimethylpyridine	0.00	10	0.759	0.008	0.776	0.748	0.76
2,5-Dimethylpyridine	0.00	8	0.743	0.005	0.753	0.737	0.74
2,6-Dimethylpyridine	0.00	10	0.696	0.034	0.767	0.636	0.70
3,4-Dimethylpyridine	0.00	8	0.854	0.015	0.877	0.830	0.85
3,5-Dimethylpyridine	0.00	6	0.794	0.007	0.804	0.786	0.79
2-*n*-Propylpyridine	0.00	7	0.699	0.008	0.714	0.692	0.70
3-*n*-Propylpyridine	0.00	3	0.785	0.018	0.803	0.767	0.78
4-*n*-Propylpyridine	0.00	7	0.767	0.005	0.774	0.760	0.77
4-Isopropylpyridine	0.00	3	0.757	0.008	0.766	0.752	0.76
2-Methyl-4-ethylpyridine	0.00	7	0.751	0.016	0.775	0.728	0.75
2-Methyl-5-ethylpyridine	0.00	6	0.705	0.035	0.754	0.663	0.71
2-Methyl-6-ethylpyridine	0.00	8	0.644	0.018	0.675	0.617	0.64
3-Methyl-2-ethylpyridine	0.00	2	0.717	0.013	0.726	0.708	0.72
3-Methyl-4-ethylpyridine	0.00	5	0.851	0.020	0.876	0.825	0.85
3-Methyl-5-ethylpyridine	0.00	3	0.807	0.013	0.820	0.794	0.81
3-Methyl-6-ethylpyridine	0.00	4	0.710	0.015	0.724	0.690	0.71
4-Methyl-2-ethylpyridine	0.00	5	0.725	0.009	0.738	0.713	0.73
4-Methyl-3-ethylpyridine	0.00	2	0.785	0.048	0.819	0.751	0.79
2,3,4-Trimethylpyridine	0.00	8	0.801	0.065	0.849	0.641	0.80
2,3,5-Trimethylpyridine	0.00	8	0.785	0.016	0.821	0.767	0.79
2,3,6-Trimethylpyridine	0.00	10	0.717	0.011	0.730	0.699	0.72
2,4,5-Trimethylpyridine	0.00	8	0.800	0.018	0.826	0.780	0.80
2,4,6-Trimethylpyridine	0.00	9	0.690	0.014	0.703	0.669	0.69
3,4,5-Trimethylpyridine	0.00	2	0.924	0.018	0.937	0.911	0.92

TABLE III *(continued)*

Solute	α_2^H	No.	Average	S.D.	Max	Min	Taken
2-*n*-Butylpyridine	0.00	1	0.693				0.69
4-*tert.*-Butylpyridine	0.00	2	0.763	0.003	0.765	0.761	0.76
2,5-Diethylpyridine	0.00	2	0.699	0.008	0.704	0.693	0.70
2,6-Diethylpyridine	0.00	3	0.617	0.038	0.651	0.576	0.62
3,4-Diethylpyridine	0.00	2	0.814	0.004	0.816	0.811	0.81
3,5-Diethylpyridine	0.00	3	0.806	0.009	0.815	0.797	0.81
2-Methyl-4-propylpyridine	0.00	2	0.733	0.014	0.743	0.723	0.73
2-Methyl-5-propylpyridine	0.00	2	0.722	0.015	0.732	0.711	0.72
2-Methyl-6-propylpyridine	0.00	2	0.612	0.008	0.618	0.606	0.61
4-Methyl-2-propylpyridine	0.00	2	0.706	0.014	0.716	0.696	0.71
4-Methyl-3-propylpyridine	0.00	2	0.800	0.037	0.826	0.774	0.80
5-Methyl-2-propylpyridine	0.00	2	0.694	0.006	0.698	0.689	0.69
4-Methyl-3-isopropylpyridine	0.00	2	0.812	0.001	0.812	0.811	0.81
2,3-Dimethyl-4-ethylpyridine	0.00	3	0.757	0.158	0.875	0.578	0.76
2,3-Dimethyl-6-ethylpyridine	0.00	2	0.677	0.013	0.686	0.668	0.68
2,4-Dimethyl-5-ethylpyridine	0.00	4	0.805	0.030	0.831	0.778	0.80
2,4-Dimethyl-6-ethylpyridine	0.00	4	0.658	0.009	0.669	0.649	0.66
2,5-Dimethyl-4-ethylpyridine	0.00	4	0.789	0.025	0.816	0.763	0.79
2,5-Dimethyl-6-ethylpyridine	0.00	4	0.668	0.026	0.689	0.630	0.67
2,6-Dimethyl-3-ethylpyridine	0.00	4	0.695	0.008	0.706	0.686	0.69
2,6-Dimethyl-4-ethylpyridine	0.00	4	0.702	0.020	0.718	0.674	0.70
3,4-Dimethyl-6-ethylpyridine	0.00	2	0.773	0.014	0.783	0.763	0.77
3,5-Dimethyl-6-ethylpyridine	0.00	3	0.724	0.022	0.741	0.700	0.72
2,3,4,5-Tetramethylpyridine	0.00	1	0.845	0.000	0.845	0.845	0.84
2,3,4,6-Tetramethylpyridine	0.00	5	0.755	0.012	0.767	0.737	0.76
2,3,5,6-Tetramethylpyridine	0.00	4	0.768	0.058	0.852	0.721	0.77
2-*n*-Pentylpyridine	0.00	2	0.635	0.081	0.692	0.578	0.64
4-*n*-Pentylpyridine	0.00	2	0.568	0.010	0.575	0.561	0.57
2-Methyl-6-butylpyridine	0.00	2	0.545	0.024	0.562	0.528	0.55
2-Ethyl-6-propylpyridine	0.00	2	0.547	0.004	0.550	0.544	0.55
2-Methyl-4,5-diethylpyridine	0.00	2	0.849	0.021	0.864	0.834	0.83
2-Methyl-4,6-diethylpyridine	0.00	4	0.646	0.013	0.663	0.635	0.65
2-Methyl-5,6-diethylpyridine	0.00	2	0.659	0.032	0.681	0.636	0.66
4-Methyl-2,6-diethylpyridine	0.00	2	0.593	0.002	0.594	0.591	0.59
2,6-Dimethyl-4-propylpyridine	0.00	2	0.656	0.004	0.658	0.653	0.66
2-Isopropyl-3,6-dimethylpyridine	0.00	2	0.579	0.010	0.586	0.572	0.58
2,3,6-Trimethyl-4-ethylpyridine	0.00	2	0.696	0.011	0.703	0.688	0.70
2,4,6-Trimethyl-3-ethylpyridine	0.00	4	0.742	0.053	0.804	0.689	0.74
2,4,6-Triethylpyridine	0.00	2	0.531	0.020	0.545	0.517	0.54
2,3-Dimethyl-4,6-diethylpyridine	0.00	2	0.769	0.029	0.789	0.748	0.77
2,5-Dimethyl-4,6-diethylpyridine	0.00	2	0.778	0.030	0.799	0.757	0.78
3,4-Dimethyl-2,6-diethylpyridine	0.00	2	0.605	0.032	0.627	0.582	0.61
2-(5-Nonyl)pyridine	0.00	2	0.486	0.034	0.510	0.462	0.49
4-(5-Nonyl)pyridine	0.00	2	0.487	0.024	0.504	0.470	0.49
2-Benzylpyridine	0.00	1	0.809				0.81
4-Benzylpyridine	0.00	1	0.797				0.80
Cyclopenteno[*b*]pyridine	0.00	2	0.905	0.007	0.910	0.900	0.90
2-Methylcyclopenteno[*b*]pyridine	0.00	2	0.774	0.012	0.782	0.765	0.77
4-Methylcyclopenteno[*b*]pyridine	0.00	1	0.844				0.84
7-Methylcyclopenteno[*b*]pyridine	0.00	2	0.802	0.001	0.803	0.801	0.80
Cyclopenteno[*c*]pyridine	0.00	2	0.942	0.013	0.951	0.933	0.94

(Continued on p. 132)

TABLE III *(continued)*

Solute	α_2^H	No.	Average	S.D.	Max	Min	Taken
3-Methylthiopyridine	0.00	2	1.135	0.030	1.156	1.113	1.13
2-Fluoropyridine	0.00	1	0.890				0.89
3-Fluoropyridine	0.00	1	0.739				0.74
4-Fluoropyridine	0.00	1	0.773				0.77
2-Chloropyridine	0.00	1	1.026				1.03
3-Chloropyridine	0.00	1	0.834				0.83
4-Chloropyridine	0.00	1	0.848				0.85
2-Bromopyridine	0.00	1	1.056				1.06
3-Bromopyridine	0.00	1	0.895				0.90
4-Bromopyridine	0.00	1	0.931				0.93
2-Iodopyridine	0.00	1	1.105				1.10
3-Iodopyridine	0.00	1	0.978				0.98
4-Iodopyridine	0.00	1	0.968				0.97
3-Methoxypyridine	0.00	1	0.945				0.95
4-Methoxypyridine	0.00	1	0.932				0.93
2-Cyanopyridine	0.00	1	1.437				1.44
3-Cyanopyridine	0.00	1	1.264				1.26
4-Cyanopyridine	0.00	1	1.207				1.21
2-Nitropyridine	0.00	1	1.421				1.42
3-Nitropyridine	0.00	1	1.280				1.28
4-Nitropyridine	0.00	1	1.211				1.21
Piperidine	0.10	2	0.463	0.004	0.466	0.460	0.46
N-Methylpiperidine	0.00	3	0.386	0.081	0.480	0.334	0.39
N-Ethylpiperidine	0.00	2	0.315	0.004	0.318	0.312	0.32
Quinoline	0.00	9	0.965	0.032	1.027	0.916	0.97
1,2,3,4-Tetrahydroquinoline	0.00	1	0.943				0.94
2-Methylquinoline	0.00	3	0.877	0.035	0.917	0.854	0.88
4-Methylquinoline	0.00	4	0.978	0.020	0.999	0.951	0.98
6-Methylquinoline	0.00	5	0.948	0.017	0.974	0.931	0.95
7-Methylquinoline	0.00	1	0.949				0.95
8-Methylquinoline	0.00	5	0.867	0.033	0.911	0.829	0.87
2,3-Dimethylquinoline	0.00	1	1.009				1.01
2,4-Dimethylquinoline	0.00	4	0.957	0.020	0.983	0.939	0.96
2,6-Dimethylquinoline	0.00	4	0.898	0.012	0.912	0.882	0.90
2,4,6-Trimethylquinoline	0.00	1	0.995				1.00
2,4,6,8-Tetramethylquinoline	0.00	1	0.941				0.94
Isoquinoline	0.00	9	0.998	0.034	1.056	0.953	1.00
1,2,3,4-Tetrahydroisoquinoline	0.00	1	0.904				0.90
1-Methylisoquinoline	0.00	1	1.025				1.02
3-Methylisoquinoline	0.00	6	0.897	0.050	0.970	0.822	0.90
Benzo[*c*]quinoline	0.00	4	1.254	0.046	1.295	1.212	1.25
Benzo[*f*]quinoline	0.00	2	1.252	0.008	1.257	1.246	1.25
3-Methylbenzo[*f*]quinoline	0.00	1	0.979				0.98
Benzo[*h*]quinoline	0.00	2	1.215	0.019	1.228	1.201	1.22
Acridine	0.00	4	1.325	0.030	1.370	1.304	1.32
2-Methylacridine	0.00	1	1.055				1.06
3-Methylacridine	0.00	1	1.108				1.11
Benz[*a*]acridine	0.00	2	1.577	0.009	1.583	1.570	1.58
10-Methylbenz[*a*]acridine	0.00	1	1.700				1.70
Benz[*c*]acridine	0.00	3	1.516	0.030	1.537	1.481	1.52
10-Methylbenz[*c*]acridine	0.00	1	1.689				1.69
1,10-Dimethylbenz[*c*]acridine	0.00	1	1.568				1.57
2,10-Dimethylbenz[*c*]acridine	0.00	1	1.583				1.58

TABLE III *(continued)*

Solute	α_2^H	No.	Average	S.D.	Max	Min	Taken
Pyrrole	0.41	2	0.731	0.049	0.766	0.696	0.73
N-Methylpyrrole	0.00	1	0.792				0.79
N-Methylpyrrolidine	0.00	1	0.497				0.50
Indole	0.44	7	1.125	0.047	1.178	1.047	1.12
N-Methylindole	0.00	1	0.922				0.92
2-Methylindole	0.44	2	1.054	0.011	1.061	1.046	1.05
3-Methylindole	0.44	5	1.058	0.015	1.076	1.037	1.06
5-Methylindole	0.44	4	1.082	0.024	1.115	1.060	1.08
7-Methylindole	0.44	1	1.049				1.05
2,N-Dimethylindole	0.00	2	0.961	0.008	0.967	0.955	0.96
2,3-Dimethylindole	0.44	1	1.005				1.01
2,5-Dimethylindole	0.44	1	1.029				1.03
2,7-Dimethylindole	0.44	2	1.050	0.068	1.098	1.002	1.05
2,3,7-Trimethylindole	0.44	2	1.106	0.059	1.148	1.064	1.11
Carbazole	0.47	4	1.423	0.028	1.447	1.388	1.42
2-Methylcarbazole	0.47	2	1.384	0.006	1.388	1.379	1.38
Pyrazole	0.54	1	0.995				1.00
3-Methylpyrazole	0.54	1	0.876				0.88
4-Methylpyrazole	0.54	1	0.991				0.99
Thiophene	0.00	1	0.565				0.57
2-Methylthiophene	0.00	1	0.561				0.56
2,5-Dimethylthiophene	0.00	1	0.538				0.54
Tetrahydrothiophene	0.00	1	0.528				0.53
Benzo[*b*]thiophene	0.00	2	0.881	0.039	0.908	0.853	0.88
Dibenzothiophene	0.00	1	1.308				1.31
Benz[*b*]naphtho[2,1-*d*]thiophene	0.00	1	1.561				1.56

TABLE IV

COMPARISON OF π_2^H VALUES WITH THOSE FROM RESULTS OF POOLE AND CO-WORKERS [86,87]

Solute	Table III			Poole and co-workers π_2^H
	π_2^H	S.D.	No.	
Anisole	0.745	0.026	30	0.768
Benzonitrile	1.110	0.019	21	1.125
Aniline	0.960	0.023	29	0.972
N-Methylaniline	0.898	0.020	10	0.892
N,N-Dimethylaniline	0.842	0.016	11	0.829
Nitrobenzene	1.108	0.019	20	1.113
Phenol	0.892	0.020	46	0.909
2,4,6-Trimethylphenol	0.791	0.033	11	0.820

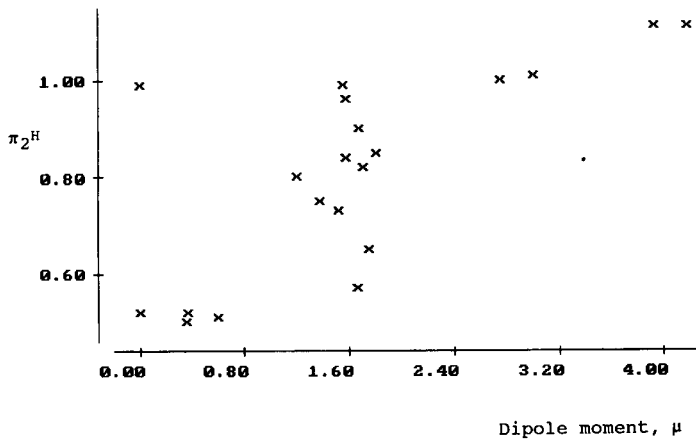

Fig. 1. Plot of π_2^H *vs.* dipole moment, μ, for solutes in Table II.

If μ is replaced by the calculated dipole moment, μ^c, *i.e.* calculated by vectorial summation taking μ for chlorobenzene as 1.72 D, then eqn. 15 results,

$$\pi_2^H = 0.541 + 0.0750nCl + 0.0252\mu^c$$
$$n = 13 \quad \rho = 0.982 \quad \text{S.D.} = 0.027 \qquad (15)$$

In both eqn. 14 and eqn. 15 the major contribution is made by the term in nCl, suggesting that polarisability is a much larger factor than dipole moment. A similar equation results from an analysis of the chloroanisoles, provided that all 2,6-dichloroanisoles are left out,

$$\pi_2^H = 0.717 + 0.0856nCl + 0.0375\mu^c$$
$$n = 14 \quad \rho = 0.965 \quad \text{S.D.} = 0.030 \qquad (16)$$

If the number of chlorine substituents is the major factor affecting π_2^H, as in eqns. 14–16, then simple summation of substituent constants might yield reasonable estimates of π_2^H, at least for disubstituted solutes. Results are in Table V, using the substituent constants in Table II, $\Delta\pi_2^H$, together with an adjustment for *meta*-substituted compounds by a factor of 0.94 and one for para-substituted compounds by a factor of 0.96. For halogen substituted compounds, except those of aniline and phenol, there is reasonable agreement between calculated and observed π_2^H values. Hence the calculated values for the substituents Br/OMe, I/OMe, Cl/CO_2Me, F/NO_2, Br/NMe_2 and probably also Cl/NHMe can be taken as reasonable estimates of π_2^H. There seems no reason why π_2^H values for the substituents Br/CO_2Me, I/CO_2Me, Br/NO_2, I/NO_2, Br/NHMe (*m* and *p* only) and I/NMe_2 cannot be similarly calculated.

For polyhalogenated compounds a rather more elaborate treatment is required, based on equations such as eqn. 15. Analysis of the various π_2^H values for halogen substituents leads to the $n(n\text{X})$ and $m(\mu^c)$ values in Table VI that correspond to equations like that of eqn. 15. The π_2^H value for any polyhalogenated compound is given by

$$\pi_2^H = 0.52 + n \cdot n'(\text{X}) + n'(\text{Y}) + m'\mu^c \qquad (17)$$

where n is the number of halogen substituents, n'(X) is the value listed in Table VI for the halogen concerned, n'(Y) is the value listed in Table VI for the other (single) substituent, μ^c is the calculated overall dipole moment, and m' is the average of the *m*-values in Table VI. For example, in 2,5-dichloro methylbenzoate[a] $n = 2$, $n'(\text{X}) = 0.0750$, $n'(\text{Y}) = 0.2940$, $\mu^c = 1.80$ D using the dipole moments in Table II, and $m' = (2 \times 0.0252 + 0.0200)/3 = 0.023$ units. In Table VII are results on these lines. There is good agreement with experiment, except for 3-chloroveratrole and 3,4–dichloroveratrole where there are substituents in the 1,2,3-positions (cf. the exceptions to eqn. 16). Agreement is possibly even better if a correction factor is again used for the case of meta substituted com-

[a] Listed as methyl 2,5-dichlorobenzoate in Tables II and III.

TABLE V

OBSERVED AND CALCULATED π_2^H VALUES FOR DIFUNCTIONAL BENZENES WITH ONE OR TWO HALOGEN SUBSTITUENTS

First line observed, second line calculated.

Substituents	*Ortho*[a]	*Meta*	*Para*	Substituents	*Ortho*[a]	*Meta*	*Para*
F/F	0.75			Cl/NO_2	1.25	1.13	1.17
	0.62	0.58[b]	0.60[c]		1.24	1.17[b]	1.19[c]
Cl/Cl	0.78	0.73	0.75	Cl/NHMe	0.96		1.01
	0.78	0.73[b]	0.75[c]		1.03	0.97[b]	0.99[c]
Br/Br	0.96	0.88	0.86	Br/NMe_2			0.97
	0.94	0.88[b]	0.90[c]		1.05	0.99[b]	1.01[c]
I/I	1.21	1.07	1.15	F/NH_2	0.88	1.08	1.09
	1.12	1.05[b]	1.08[c]		1.01		
F/OMe	0.79	0.72	0.74	Cl/NH_2	0.92	1.10	1.13
	0.80	0.75[b]	0.77[c]		1.09		
Cl/OMe	0.91	0.86	0.86	Br/NH_2	0.98	1.19	1.19
	0.88	0.83[b]	0.85[c]		1.17		
Br/OMe			0.90	I/NH_2	1.00	1.26	1.28
	0.96	0.90[b]	0.92[c]		1.26		
I/OMe			0.99	F/OH	0.69	0.98	0.95
	1.05	0.99[b]	1.01[c]		0.94		
F/CO_2Me	0.89	0.88	0.89	Cl/OH	0.86	1.06	1.08
	0.90	0.85[b]	0.86[c]		1.04		
Cl/CO_2Me	0.99		0.92	Br/OH	0.90	1.15	1.17
	0.98	0.92[b]	0.94[c]		1.10		
Cl/CN	1.24	1.14	1.18	I/OH	1.00	1.20	1.33
	1.24	1.16[b]	1.19[c]		1.19		
F/NO_2		1.11					
	1.16	1.09[b]	1.11[c]				

[a] All *ortho* values calculated by simple summation.
[b] Taken as 94% of the calculated *ortho* value.
[c] Taken as 96% of the calculated *ortho* value.

TABLE VI

VALUES OF n' AND m' IN EQN. 17

Substituent	n'	m'
F	0.0241	0.0132
Cl	0.0750	0.0252
Br	0.1670	0.0349
I	0.2710	0.0128
OMe	0.2028	0.0158
COMe	0.4300	0.0200
CO_2Me	0.2940	0.0200
CN	0.5064	0.0200
NO_2	0.5114	0.0200
CHO	0.4250	0.0200
NMe_2	0.2886	0.0200

pounds. For these calculations a factor of 0.96 for *meta*-substituted C_6H_5XY compounds seems appropriate. A rather large number of π_2^H values for halogeno-substituted derivatives of PhY where Y = (F), Cl, Br, I, OMe (in part), CHO, COMe, CO_2Me, CN, NO_2 and NMe_2 can be estimated using eqn. 17.

Halogeno derivatives of phenol and aniline behave quite differently to those of the above compounds, as shown quite clearly by results in Table V. Not only do the *ortho*-halogeno compounds have π_2^H lower than calculated by simple summation, but the *meta*- and *para*-derivatives have π_2^H values larger than calculated. For both series, π_2^H values are known for all the isomers

TABLE VII

CALCULATION OF π_2^H FOR HALO-AROMATICS VIA EQN. 17

Solute	π_2^H	
	Observed	Calculated
3-Chloroveratrole	0.96	1.06
4-Chloroveratrole	1.03	1.02
3,4-Dichloroveratrole	1.05	1.13
4,5-Dichloroveratrole	1.11	1.08
2-Chloro methylbenzoate	0.96	0.99
4-Chloro methylbenzoate	0.89	0.92
2,4-Dichloro methylbenzoate	0.98	1.01
2,5-Dichloro methylbenzoate	0.99	1.01
2-Fluoro methylbenzoate	0.89	0.89
3-Fluoro methylbenzoate	0.88	0.87
4-Fluoro methylbenzoate	0.89	0.84
2-Chlorobenzonitrile	1.24	1.22
3-Chlorobenzonitrile	1.14	1.19(1.14)[a]
4-Chlorobenzonitrile	1.16	1.11
2-Chloronitrobenzene	1.24	1.22
3-Chloronitrobenzene	1.14	1.18(1.13)[a]
4-Chloronitrobenzene	1.18	1.16
4-Bromoanisole	0.90	0.89
4-Iodoanisole	0.99	0.99
4-Bromo-N,N-dimethylamine	0.97	0.98

[a] Using a factor of 0.96 for *m*-substituents, see text.

of all the halogens in the monohalogenated derivatives, so no estimations here are needed. It would be helpful to be able to estimate π_2^H values for the polyhalogenated compounds, but there are not enough data to attempt this.

Such is the case also with disubstituted (and polysubstituted) compounds where neither substituent is halogen. Again, there are not enough data to come to any general conclusion as to how π_2^H varies with di- and poly-substitution. Further results are needed, and it is hoped that data will be obtained in the near future.

There is a reasonable amount of data, however, for substituted pyridines, especially the monosubstituted ones. In Table VIII are collected π_2^H values for 2-, 3- and 4-substituted pyridines, taken from Table III, together with the aromatic $\Delta\pi_2^H$ substituent constants from Tables II and III. If the aromatic $\Delta\pi_2^H$ constants are applied to the substituted pyridine, with π_2^H equal to 0.84 for pyridine itself, the calculated π_2^H values for the pyridine are as given also in Table VIII. The trends in these calculated values can be seen more clearly by setting out values of π_2^H (calculated – observed), again given in Table VIII. There is a clear separation between the alkyl substituents and the others. In the former case, π_2^H for the 2-alkylpyridines is always lower than for the corresponding 3- and 4-alkylpyridines, leading to π_2^H (calculated – observed) around 0.12 units for the higher alkyl groups. The π_2^H (calculated – observed) values seem quite regular, and allow the estimation of further values, given in parentheses in Table VIII.

For the other substituents shown in Table VIII, there are again general trends, but now π_2^H for the 2-substituent is usually larger than for the 3- or 4-substituents. If the remaining 2-substituents in Table VIII show the same trend, then π_2^H values for various 2-substituted pyridine can be found by simple addition using the aromatic substituent constants in Table II. Note that for the six nonalkyl 2-substituted pyridines in Table VIII, π_2^H(observed – calculated) averages as −0.01 unit, so when the estimated π_2^H (observed – calculated) values are taken as zero (*i.e.* simple addition obtains), the corresponding π_2^H values themselves can be calculated.

In the case of the (nonalkyl) 3- and 4-substituted pyridines in Table VIII, the value of π_2^H (calculated – observed) depends slightly on π_2^H itself. Estimated values of π_2^H (calculated – observed) are given, taking into account this dependency, and from these values, then π_2^H values for 3- and 4-substituted pyridine can be obtained as shown. There is not enough data available to estimate π_2^H values for polysubstituted pyridines, other than for polyalkylated ones, but at least there are now available π_2^H values or estimated π_2^H values for a quite wide range of 2-, 3- and 4-substituted pyridines.

Finally, we note that Li *et al.* [100] have constructed a scale of π_2^C values using a similar equation to eqn. 1 except that the old-fashioned δ_2 parameter [101] is retained instead of the R_2 parameter. Because the defining equation for π_2^C is not the same as the defining equation for π_2^H, these two parameters are not interchangeable, and cannot simply be transformed into each other. The π_2^H parameter must be used in combi-

TABLE VIII

CALCULATION OF π_2^H FOR MONOSUBSTITUTED PYRIDINES

Calculated π_2^H obtained using π_2^H of 0.84 for pyridine, and the aromatic substituent constants in Table II or from ref. 5. Estimated π_2^H (calculated – observed) and estimated π_2^H values are in parentheses.

Substituent	π_2^H (observed)			π_2^H (calculated)	π_2^H (calculated – observed)		
	2	3	4		2	3	4
Me	0.75	0.81	0.82	0.84	0.09	0.03	0.02
Et	0.70	0.79	0.80	0.83	0.13	0.04	0.03
Pr	0.70	0.79	0.77	0.82	0.12	0.03	0.05
Pr^{iso}	(0.68)	(0.78)	0.76	0.81	(0.13)	(0.03)	0.05
Bu	0.69	(0.80)	(0.78)	0.83	0.14	(0.03)	(0.05)
$Bu^{tert.}$	(0.67)	(0.78)	0.76	0.81	(0.14)	(0.03)	0.05
Pe	0.64		0.57	0.83	0.19		0.26
F	0.89	0.74	0.77	0.89	0.00	0.15	0.12
Cl	1.03	0.83	0.85	0.97	−0.06	0.14	0.12
Br	1.06	0.90	0.93	1.05	−0.01	0.15	0.12
I	1.11	0.98	0.97	1.14	0.03	0.16	0.17
MeO		0.94	0.93	1.07		0.13	0.14
CN	1.44	1.26	1.21	1.43	−0.01	0.17	0.22
NO_2	1.42	1.28	1.21	1.43	0.01	0.15	0.22
CO_2Me	(1.17)	(1.07)	(1.01)	1.17	(0.00)	(0.15)	(0.16)
CO_2H	(1.22)	(1.07)	(1.05)	1.22	(0.00)	(0.15)	(0.17)
HCO	(1.32)	(1.16)	(1.12)	1.32	(0.00)	(0.16)	(0.20)
CH_3CO	(1.33)	(1.17)	(1.13)	1.33	(0.00)	(0.16)	(0.20)
$CONH_2$	(1.82)	(1.65)	(1.60)	1.82	(0.00)	(0.17)	(0.22)
NH_2	–	(1.13)	(1.10)	1.28	–	(0.15)	(0.18)
NMe_2	–	(1.01)	(1.00)	1.16	–	(0.15)	(0.16)
CH_2OH	–	(1.04)	(1.02)	1.19	–	(0.15)	(0.17)

nation with R_2, as in the general solvation eqn. 1, whereas the π_2^C parameter must be used together with δ_2.

As far as the generality of eqn. 1 is concerned, this lack of transferability is not a problem since there are now available, from this work and previous work [1,5], around 1000 values of π_2^H. The π_2^H scale can now be regarded as reasonably well-established, and further values for, *e.g.* multifunctional aromatic compounds can in principle be obtained by the methods outlined in the present work.

REFERENCES

1 M.H. Abraham, G.S. Whiting, R.M. Doherty and W.J. Shuely, *J. Chromatogr.*, 587 (1991) 213.
2 M.H. Abraham, G.S. Whiting, R.M. Doherty and W.J. Shuely, *J. Chromatogr.*, 587 (1991) 229.
3 M.H. Abraham, I. Hamerton, J.B. Rose and J.W. Grate, *J. Chem. Soc., Perkin Trans. 2*, (1990) 1451.
4 M.H. Abraham, G.S. Whiting, J. Andonian-Haftvan and J.W. Steed, *J. Chromatogr.*, 588 (1991) 361.
5 M.H. Abraham and G.S. Whiting, *J. Chromatogr.*, 594 (1992) 229.
6 M.H. Abraham and D.V. Walsh, *J. Chromatogr.*, 627 (1992) 294.
7 M.H. Abraham, G.S. Whiting, R.M. Doherty, W.J. Shuely and P. Sakellariou, *Polymer*, 33 (1992) 2163.
8 M.H. Abraham and G.S. Whiting, *J. Am. Oil. Chem. Assoc.*, 69 (1992) 1236.
9 M.H. Abraham, P.L. Grellier and R.A. McGill, *J. Chem. Soc., Perkin Trans. 2*, (1987) 797.
10 M.H. Abraham, G.S. Whiting, R.M. Doherty and W.J. Shuely, *J. Chem. Soc., Perkin Trans. 2*, (1990) 1451.
11 I.O.O. Korhonen and J. Knuutinen, *J. Chromatogr.*, 292 (1984) 345.
12 I.O.O. Korhonen, J. Knuutinen and R. Jaaskelainen, *J. Chromatogr.*, 287 (1984) 293.
13 I.O.O. Korhonen, *J. Chromatogr.*, 294 (1984) 99.
14 I.O.O. Korhonen, *J. Chromatogr.*, 315 (1984) 185.

15 I.O.O. Korhonen and M.A. Lind, *J. Chromatogr.*, 322 (1985) 71.
16 I.O.O. Korhonen and M.A. Lind, *J. Chromatogr.*, 322 (1985) 83.
17 I.O.O. Korhonen and M.A. Lind, *J. Chromatogr.*, 328 (1985) 325.
18 I.O.O. Korhonen, *J. Chromatogr.*, 356 (1986) 285.
19 I.O.O. Korhonen, *J. Chromatogr.*, 363 (1986) 277.
20 G.H.E. Nieuwdorp, C.L. de Ligny and N.G. van der Veen, *J. Chromatogr.*, 154 (1978) 133.
21 A.T. James, *Anal. Chem.*, 28 (1956) 1564.
22 J. Janak and R. Komers, in D.H. Desty (Editor), *Gas Chromatography 1958*, Butterworths, London, 1958, p. 343.
23 A. Wehrli and E. Kováts, *Helv. Chim. Acta*, 42 (1959) 2709.
24 D.H. Desty and C.L.A. Harbourn, *Anal. Chem.*, 31 (1959) 1965.
25 J. Janák and M. Hrivnac, *J. Chromatogr.*, 3 (1960) 297.
26 S.H. Langer, C. Zahn and G. Pantazoplos, *J. Chromatogr.*, 3 (1960) 154.
27 S.H. Langer and J.H. Purnell, *J. Phys. Chem.*, 67 (1963) 263.
28 J. Ratusky and L. Bastar, *Chem. Ind.*, (1964) 579.
29 V. Cantuti, G.P. Cartoni, A. Liberti and A.G. Torri, *J. Chromatogr.*, 17 (1965) 60.
30 A.C. Pronay, *J. Chromatogr.*, 18 (1965) 586.
31 E. Pillion, *J. Gas Chromatogr.*, 3 (1965) 239.
32 G. Alberini, V. Cantuti and G.P. Cartoni, in A.B. Littlewood (Editor), *Gas Chromatography 1966*, Butterworths, London, 1966, p. 258.
33 N. Carugno and S. Rossi, *J. Gas Chromatogr.*, 5 (1967) 103.
34 A.R. Cooper, C.W.P. Crowne and P.G. Farrell, *J. Chromatogr.*, 29 (1967) 1.
35 S.H. Langer, B.M. Johnson and J.R. Conder, *J. Phys. Chem.*, 72 (1968) 4020.
36 G.S. Giam, S.D. Abbott and W.B. Davis, *J. Chromatogr.*, 42 (1969) 457.
37 R.E. Poulson, *J. Chromatogr. Sci.*, 7 (1969) 152.
38 L.S. Bark and K.F. Clarke, *J. Chromatogr.*, 48 (1970) 418.
39 J. Hrivnak and J. Macak, *Anal. Chem.*, 43 (1971) 1039.
40 P.T. Mitchell and F. Vernon, *J. Chromatogr.*, 65 (1972) 487.
41 L.E. Cook and F.M Raushel, *J. Chromatogr.*, 65 (1972) 556.
42 V. Kusý, *Chemical Utilisation of Coal, Tar and Petroleum*, 11 (1971) 219.
43 J. Macak, P. Buryan and J. Hrivnak, *J. Chromatogr.*, 89 (1974) 309.
44 K. Tesarik and S. Ghyczy, *J. Chromatogr.*, 91 (1974) 723.
45 L.S. Bark and K.C. Wheatstone, *J. Chromatogr.*, 92 (1974) 281.
46 J. Kriz, M. Popl and J. Mostecky, *J. Chromatogr.*, 97 (1974) 3.
47 A.F. Shlyakhov, B.I. Anvaer, O.V. Zolotareva, N.N. Romina, N.V. Novikova and R.I. Koreshkova, *Zh. Anal. Khim.*, 30 (1975) 788.
48 S.D. West and R.C. Hall, *J. Chromatogr. Sci.*, 13 (1975) 5.
49 F. Vernon and G.T. Edwards, *J. Chromatogr.*, 110 (1975) 73.
50 G. Weissmann, *J. Chromatogr.*, 129 (1976) 431.
51 A.N. Korol, *J. Chromatogr.*, 129 (1976) 125.
52 I.L. Zhuravleva, Yu.P. Kapustin and R.V. Golovnya, *Zh. Anal. Khim.*, 31 (1976) 1378.
53 V.D. Shatts, A.A. Avots and V.A. Belikov, *Zh. Anal. Khim.*, 32 (1977) 797.
54 P. Buryan and J. Macak, *J. Chromatogr.*, 139 (1977) 69.
55 P. Buryan, J. Macak and J. Hrivnak, *J. Chromatogr.*, 139 (1977) 425
56 L.S. Lysyuk and A.N. Korol, *Chromatographia*, 10 (1977) 712.
57 L.G. Sednevets and A.G. Pankov, *Zh. Anal. Khim.*, 32 (1977) 1039.
58 A. Radecki and J. Grzybowski, *J. Chromatogr.*, 152 (1978) 211.
59 V.S. Kozlova and A.N. Korol, *Zh. Anal. Khim.*, 34 (1979) 2412.
60 V.M. Nabivarach and V.P. Dmitrikov, *Zh. Anal. Khim.*, 34 (1979) 2412.
61 M.L. Lee, D.L. Vassilaros, C.M. White and M. Novotny, *Anal. Chem.*, 51 (1979) 768.
62 A.N. Korol and N.V. Novorusskaya, *J. Chromatogr.*, 169 (1979) 73.
63 A. Radecki, J. Grzybowski, H. Lamparczyk and A. Nasal, *J. High Resolut. Chromatogr. Chromatogr. Commun.*, 2 (1979) 581.
64 W. Engewald, L. Wennrich and E. Ritter, *J. Chromatogr.*, 174 (1979) 315.
65 J. Grzybowski, H. Lamparczyk, A. Nasal and A. Radecki, *J. Chromatogr.*, 196 (1980) 217.
66 F. Sellier, G. Tersac and G. Guiochon, *J. Chromatogr.*, 219 (1981) 213.
67 V.A. Gerasimenko, A.V. Kirilenko and V.M. Nabivach, *J. Chromatogr.*, 208 (1981) 9.
68 C.M. White and N.C. Li, *Anal. Chem.*, 54 (1982) 1564.
69 F. Patte, M. Etcheto and P. Laffort, *Anal. Chem.*, 54 (1982) 2239.
70 D.L. Vassilaros, R.C. Kong, D.W. Later and M.L. Lee, *J. Chromatogr.*, 252 (1982) 1.
71 M. Novrocikova, J. Novrocik and J. Vymetal, *Collect. Czech. Chem. Commun.*, 48 (1983) 3270.
72 J.K Haken and I.O.O. Korhonen, *J. Chromatogr.*, 265 (1983) 323.
73 O. Buchman, G.-Y. Cao and C.T. Peng, *J. Chromatogr.*, 312 (1984) 75.
74 R. Fellous, L. Lizzani-Cuvelier and R. Luft, *Anal. Chim. Acta*, 174 (1985) 53.
75 K. Osmialowski, J. Halkiewicz and R. Kaliszan, *J. Chromatogr.*, 361 (1986) 63.
76 J. Oszczapowicz, K. Ciszkowski and J. Osek, *J. Chromatogr.*, 362 (1986) 383.
77 J. Bermeja, C.G. Blanco and M.D. Guillen, *J. Chromatogr.*, 351 (1986) 425.
78 J. Oszczapowicz, J. Osek, W. Krawczyk and B. Kielak, *J. Chromatogr.*, 357 (1986) 93.

79 U. Knecht and H.-J. Nitsch, *Fresenius' Z. Anal. Chem.*, 324 (1986) 142.
80 J.K. Haken and F. Vernon, *J. Chromatogr.*, 361 (1986) 57.
81 C.T. Peng, S.F. Ding, R.L. Hua and Z.C. Yang, *J. Chromatogr.*, 436 (1988) 137.
82 W. Engewald, U. Billing, I. Topalova and N. Petsev, *J. Chromatogr.*, 446 (1988) 71.
83 H.-B. Lee, *J. Assoc. Off. Anal. Chem.*, 71 (1988) 803.
84 C.G. Blanco, J. Blanco, J. Bermejo and M.D. Guillen, *J. Chromatogr.*, 465 (1989) 378.
85 N.R. Ayyangar, A.S. Tambe and S.S. Biswas, *J. Chromatogr.*, 483 (1989) 33.
86 B.R. Kersten, S.K. Poole and C.F. Poole, *J. Chromatogr.*, 468 (1989) 235.
87 C.F. Poole, R.M. Pomaville and T.A. Dean, *Anal. Chim. Acta*, 225 (1989) 193.
88 J. Krupcik, D. Repka, E. Benicka, T. Hevesi, J. Nolte, B. Paschold and H. Mayer, *J. Chromatogr.*, 448 (1988) 203.
89 I.L. Zhuraveleva, M.B. Terenina, V.V. Shenderyuk and R.V. Golovnya, *Zh. Anal. Khim.*, 45 (1990) 722.
90 G. Defayes, D.E. Fritz, T. Gorner, G. Huber, C. de Reyff and E. Kováts, *J. Chromatogr.*, 500 (1990) 139.
91 C.G. Blanco, J. Blanco, P. Bernard and M.D Guillen, *J. Chromatogr.*, 539 (1991) 157.
92 L.H. Wright and J.F. Walling, *J. Chromatogr.*, 540 (1991) 311.
93 D.T. Williams, Q. Tran, P. Fellin and K.A. Brice, *J. Chromatogr.*, 549 (1991) 297.
94 C.T. Peng, Z.C. Yang and S.F. Ding, *J. Chromatogr.*, 586 (1991) 85.
95 J.-C. Dutoit, *J. Chromatogr.*, 555 (1991) 191.
96 M.S. Vigdergauz and R.V. Vigalok, *Neftekhimiya*, 11 (1971) 144.
97 T. Toth, *Magy. Kém. Foly.*, 75 (1969) 245.
98 O.E. Schupp and J.S. Lewis (Editors), *Gas Chromatographia Data Compilation, Supplement 1*, American Society for Testing and Materials, Philadelphia, PA.
99 C.F. Poole, T.O. Kollie and S.K. Poole, *Chromatographia*, 34 (1992) 281.
100 J. Li, Y. Zhang, A.J. Dallas and P.W. Carr, *J. Chromatogr.*, 550 (1991) 101.
101 M.J. Kamlet, R.M. Doherty, J.-L.M. Abboud, M.H. Abraham and R.W. Taft, CHEMTECH, 16 (1986) 566.

Journal of Chromatography, 644 (1993) 141–151
Elsevier Science Publishers B.V., Amsterdam

CHROM. 25 187

Determination of anthropogenic and biogenic organic compounds on airborne particles: flash chromatographic fractionation and capillary gas chromatographic analysis

Euripides G. Stephanou* and Nicolaos E. Stratigakis

Division of Environmental Chemistry, Department of Chemistry, University of Crete, 71409 Heraklion (Greece) and Institute of Marine Biology of Crete, 71003 Heraklion (Greece)

(First received February 25th, 1993

ABSTRACT

n-Alkanes, polycyclic aromatic hydrocarbons, *n*-alkanals, 2-alkanones and *n*-alkanols were efficiently separated from alkanoic acids and then fractionated by flash chromatography on a silica gel column. These compounds were determined by capillary gas chromatography with flame ionization and/or mass spectrometric detection in the selected ion monitoring mode. The recoveries obtained for the whole analytical procedure were 82–91% for *n*-alkanes, 68–78% for polycyclic aromatic hydrocarbons, 70–75% for *n*-alkanals and 2-alkanones, 73–76% for *n*-alkanols and 80–84% for alkanoic acids. This analytical protocol was suitable for the determination of more than 140 compounds on aeolian particles collected on glass-fibre filters.

INTRODUCTION

The chemical composition of the lower troposphere in urban and non-urban environments is controlled, to a significant extent, by the marine and terrestrial biosphere and also the emission of various anthropogenic chemicals. Among these anthropogenic and biogenic compounds, many organic species are found, including a variety of naturally produced and synthetic organic compounds [1]. Long-chain *n*-alkanes, *n*-alkanols, *n*-alkanals, 2-alkanones, *n*-alkanoic acids, *n*-alkanoic acid salts, α,ω-dicarboxylic acids (or higher plant origin and/or photooxidation products of anthropogenic cyclic alkenes and biogenic unsaturated fatty acids), polycyclic aromatic hydrocarbons (PAHs) and chlorinated hydrocarbons from anthropogenic sources have been detected in urban, rural and in remote marine aerosols [2–8]. The study of the chemical composition of the atmosphere is of major importance not only because the anthropogenic compounds often represent a serious potential hazard to human health, but also because the atmosphere constitutes a "conveyor belt" for biogenic and anthropogenic compounds to the ocean. Atmospheric transport, and the relative importance of the aeolian input of continental material to the ocean, are subjects to intense research. Consequently, the reliable determination of organic compounds, which can be used as molecular markers, in air particulates is very important.

Some analytical methods [1,9] for the determination of organic compounds on airborne particles have been reported. The total organic extract is methylated to produce the corresponding fatty acid esters and then the compounds are separated by column liquid chromatography [9] into a non-polar fraction (aliphatic), a semi-polar fraction (aromatic) and a third fraction containing the polar compounds. The

* Corresponding author. Address for correspondence: Division of Environmental Chemistry, Department of Chemistry, University of Crete, 71409 Heraklion, Greece.

0021-9673/93/$06.00

same separation has also been achieved by using, instead of liquid column chromatography, a thin-layer chromatographic system [1]. Taking into consideration that the concentrations of various polar compounds often differ greatly from one another, we would expect problems if, after fractionation, they are found in the same fraction.

In this paper we present a method in which acids are first separated from neutral compounds by using a liquid chromatographic column containing specially prepared silica gel, and then the neutral compounds are fractionated by silica gel flash chromatography into very distinct non-polar, semi-polar and polar compound fractions. This method is very sensitive and selective, and allows the use of capillary gas chromatography with flame ionization detection (GC–FID) as a reliable identification and quantification method. A comparison of GC–FID with capillary gas chromatographic–mass spectrometric analysis in the selected ion monitoring mode (GC–MS-SIM) is also presented.

EXPERIMENTAL

Materials

All solvents were of Pestanal grade from Riedel-de Haën (Seelze, Germany). Standard compounds were purchased from Ehrenstorfer (Augsburg, Germany). *n*-Alkanals were prepared by oxidation of the corresponding alcohols [10]. Silica gel (70–230 and 230–400 mesh) was obtained from Merck (Darmstadt, Germany). Soxhlet cartridges were supplied by Schleicher and Schüll (Dassel, Germany). Glass-fibre filters were purchased from Whatman (Maidstone, UK).

All materials used (silica gel, glass- and cotton-wool, paper filters, anhydrous sodium sulphate, etc.) were Soxhlet extracted overnight and kept dry until use. Glass-fibre filters were extracted with methylene chloride for 72 h. Every 24 h a new portion of methylene chloride was used for the extraction. The extracted and dried glass-fibre filters were kept in a dedicated clean glass container with silica gel to avoid contamination and humidity.

Fractionation, derivatization and identification

The standard compounds, about 100 ng each, dissolved in methylene chloride, were applied on a glass-fibre filter (their concentration corresponds to an air concentration of 40 pg/m^3) and the methylene chloride was evaporated. The compounds were extracted from the filters, which has been cut into small pieces, in a flask by refluxing methylene chloride for 20 h. The extracts were vacuum evaporated and separated into individual compound classes. The alkanoic acids were separated from neutral compounds by using a McCarthy–Dutie column [11]. The alkanoic acids (fraction F I) were methylated with boron trifluoride etherate–methanol (1:2).

The neutral compounds were further fractionated by flash chromatography on silica gel (Merck) (230–400 mesh, activated at 150°C for 3 h). The compound mixture was dissolved in *n*-hexane and applied to the top of a 30×0.7 cm I.D. column containing silica gel in *n*-hexane. Nitrogen pressure was used in order to obtain a flow-rate of 1.4 ml/min at the bottom of the column. The following solvent systems were used to elute the different compound classes: (1) 15 ml of *n*-hexane (fraction F II1, aliphatics), (2) 15 ml of toluene–*n*-hexane (9.4:5.6) (fraction F II2, PAHs) (3) 15 ml of *n*-hexane–methylene chloride (7.5:7.5) (fraction F II3, carbonyl compounds such as *n*-alkanals and 2-alkanones) and (4) 20 ml of ethyl acetate–*n*-hexane (8:12) (fraction F II4, *n*-alkanols). The extracted filters were treated with 0.1 *M* hydrochloric acid–methanol to protonate all fatty acid salts. The acidified filter was further extracted with *n*-hexane and the liberated fatty acids (fraction F III) were methylated as above.

n-Alkanols were derivatised to the corresponding acetates, as follows. The fraction containing the *n*-alkanols was evaporated to dryness under a gentle stream of nitrogen, 1 ml of pyridine and 1 ml of acetic anhydride were added and the reaction mixture was shaken vigorously for 10 min and allowed to stand overnight at room temperature. A few drops of 3 *M* hydrochloric acid were added to adjust the pH to 2–3, 20 ml of water were added and the mixture was extracted with 3×15 ml of *n*-hexane. The *n*-hexane phase was dried with sodium

sulphate, filtered through a paper filter and evaporated in a rotary evaporator.

The individual fractions were spiked with internal standards (1-chlorohexadecane for *n*-alkanes, *n*-alkanals, 2-alkanones and *n*-alkanol acetates, hexamethylbenzene for PAHs and *n*-hexacosane for alkanoic acid methyl esters) for quantitative determinations.

Relative response factors, for both GC–FID and GC–MS-SIM, were calculated for 3–5 standard compounds, representing each compound class, of increasing molecular mass. Relative response factors for PAHs were calculated for each compound individually.

Control of procedural blanks were performed to assess possible contamination. The total blank mass never exceeded 2% of the individual sample extracts, except for the alkanoic acids fraction, where the maximum contamination represented 10% of the total fraction extract. The contaminants were characterized by GC–MS and comparison with standard mixtures. The most frequent contaminants were phthalate esters, *n*-alkanes ranging from C_{20} to C_{30} and alkanoic acids ranging from C_6 to C_{20}. All amounts given here were corrected by taking into consideration the application of the analytical methodology with standard compounds (column chromatographic performance and relative response factors in GC–FID and GC–MS-SIM).

Compound identification was performed by GC–MS and co-injection with authentic standard compounds or compound mixtures (PAHs).

GC–MS and GC–FID

GC–MS analyses were carried out on a Hewlett-Packard mass-selective detector with the appropriate data system. A Hewlett-Packard Model 5890 gas chromatograph, equipped with a Grob-type split–splitless injector, was directly coupled with the fused-silica capillary column (SE-54) (25 × 0.25 mm I.D.) to the ion source. Helium was used as the carrier gas with a back-pressure of 0.8 atm (1 atm = 101 325 Pa). The electron impact ionization conditions were ion energy 70 eV, ion source temperature 195°C, mass range m/z 35–590 or in the selected ion monitoring mode for quantitative determinations and electron multiplier voltage 1700–1800 V.

The GC–FID analyses were performed on a Hewlett-Packard Model 5890 gas chromatograph with a Hewlett-Packard Chemstation data system, equipped with the same fused-silica capillary column as above. Hydrogen was used as the carrier gas with a back-pressure of 1 atm. The chromatographic conditions were as follows: injector temperature, 270°C; detector temperature (FID), 290°C; temperature programme 1 (aliphatics, PAHs, *n*-alkanals, alkanoic acid methyl esters), 70°C (1 min), 70–150°C at 10°C/min, 150–290°C at 5°C/min, 290°C (30 min); temperature programme 2 (*n*-alkanol acetates), 80°C (2 min), 80–280°C at 4°C/min, 280°C (30 min). A 1-μl volume of each sample was injected, in the splitless mode (split closed for 30 s), and the hot needle technique was used.

Sampling of air particles and storage of glass-fibre filters

Particulate material was collected on a pre-extracted 20 × 25 cm glass-fibre filter, having a collection efficiency higher than 99% for particles with radius larger than 0.3 μm at the flow-rate of 90 m^3/h used. Filters were mounted in a high-volume air sampling system (Model GMWL-2000; General Metals Works, Cleves, OH, USA). Samples were collected for 24–36 hs (2500–3000 m^3 air sampled) on a 15-m high building situated in a urban coastal area of the Eastern Mediterranean (Heraklion, Island of Crete, Greece). The samples were stored frozen (−30°C) in precleaned glass flasks sealed with PTFE tape and covered with aluminium paper. Compound isolation from samples and determination were performed as described above.

RESULTS AND DISCUSSION

Table I gives the recoveries for each lipid class, with standard compounds used for the evaluation of extraction, separation and fractionation procedures.

A typical gas chromatogram of a methylated carboxylic acid fraction (F I) of an urban aerosol extract is presented in Fig. 1A. In Fig. 1B is shown a combined ion chromatogram for m/z 97, 111 and 112 (specific ions for ω-oxo- and α,ω-dicarboxylic acids [8]) of the same

TABLE I

RECOVERIES (TRIPLICATE MEASUREMENTS) FOR EACH LIPID CLASS, WITH STANDARD COMPOUNDS

Compound class	Recovery (%)	
	A[a]	B[b]
n-Alkanes		
n-$C_{19}H_{40}$	91.5 ± 1.5	78.4 ± 0.6
n-$C_{26}H_{54}$	82.0 ± 2.0	76.3 ± 1.0
PAHs		
Phenanthrene	78.0 ± 1.0	76.6 ± 2.0
Benzo[*a*]anthracene	68.5 ± 1.5	65.8 ± 0.2
n-Alkanals		
n-$C_{22}H_{44}O$	74.3 ± 1.0	71.4 ± 1.5
n-$C_{26}H_{52}O$	71.5 ± 1.5	67.2 ± 1.0
n-Alkanols[c]		
n-$C_{16}H_{33}OH$	76.1 ± 1.0	70.6 ± 2.3
n-$C_{22}H_{45}OH$	73.3 ± 1.0	68.4 ± 1.0
n-Alkanoic acid[c]		82.0 ± 2.0
n-$C_{18}H_{36}O_2$		

[a] After filter extraction and flash chromatography.
[b] After filter extraction and McCarthy–Dutie column.
[c] After derivatization.

methylated acidic fraction. In Fig. 2A is shown a representative GC–FID profile of an aliphatic hydrocarbon fraction (F II1), of the same aerosol sample as above, and Fig. 2B shows the ion chromatogram of the same fraction for the ion of m/z 191 (representative for the hopanes). Fig. 3A shows a typical GC–FID trace for a PAH fraction (F II2). The same fraction analysed by GC–MS-SIM (only molecular ions of the compounds of interest were selected) is presented in Fig. 3B. In Fig. 4 are given GC–FID traces for (A) n-alkanals and 2-alkanones (F II3) and (B) n-alkanols (F II4, as acetates), identified in the same as for the above aerosol extract.

In Table II are summarized the quantitative results of the analyses of airborne particles collected in the sampling area.

The recoveries obtained fro the representative standard compounds are generally higher if the McCarthy–Dutie column for the separation of acidic fraction is not used. When used, the corresponding recoveries are lower but still satisfactory if we consider the small amount (about 10 ng for each compound or 4 pg/m^3 if we take into consideration the sampling volume) of the compounds applied on the filter and the efficiency of fractionation. The efficiency of fractionation becomes obvious when the GC–FID traces of all fractions are examined (Figs. 1A, 2A, 3A and 4A and B). We obtained a reliable fractionation of the different compound classes, namely complete separation of the non-polar aliphatic fraction (Fig. 2A) from the semi-polar PAH fraction (Fig. 3A). Also carbonyl compounds, such as alkanals and alkanones (Fig. 4A), were cleanly separated from the more polar alkanols (Fig. 4B). The McCarthy–Dutie column proved to lead to very efficient separations of alkanoic acids from the neutral lipids (Fig. 1A). When larger amounts of standard compounds (1–10 μg) were applied on the glass-fibre filters, the recoveries obtained were 5–10% higher than those shown in Table I.

In Table II are given the concentration ranges measured for each compound class in the samples collected. These concentration ranges differ appreciably in the polar compounds, such as alkanoic acids, n-alkanols, n-alkanals and 2-alkanones. Whenever these compounds were collected in the same fraction and then derivatized, determination of compounds of lower concentration was very difficult. This may be one of the reasons why in most published studies n-alkanals and 2-alkanones are generally only tentatively identified, and rarely quantified.

The results of the analysis of the above fractions by GC–MS-SIM mode, shown in Figs. 1B, 2B and 3B, indicate that greater specificity can be obtained for some compound classes. We used the SIM mode, as being more specific, to determine the ω-oxo- and α,ω-dicarboxylic acids (Fig. 1B), although this could be also done by GC–FID . The SIM technique was very useful in detecting some molecular markers, such as hopanes in the aliphatic fraction (Fig. 2B), which are difficult to determine with FID alone. Especially for the PAH fraction, by eliminating the possible interferences from other compound classes, this technique gives a better resolved chromatogram (Fig. 3B) than the corresponding

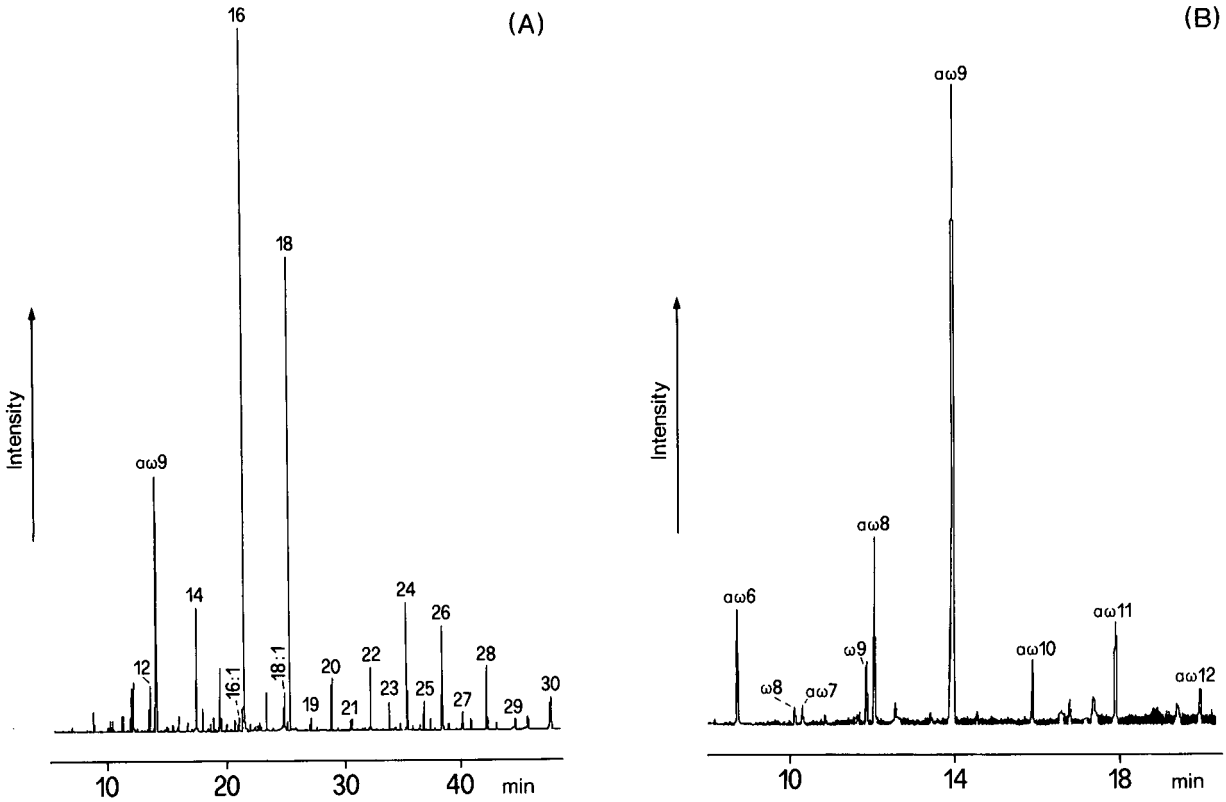

Fig. 1. (A) GC–FID trace of methylated alkanoic acid fraction (F I) identified in an urban aerosol (city of Heraklion); (B) selected ion (m/z 97, 111 and 112) GC–MS trace of the same fraction, specific for the α,ω-dicarboxylic ($\alpha\omega$ 6, 7, 8, 9, 10, 11, 12) and ω-oxocarboxylic (ω 8, 9) acids. Numbers on the peaks indicate the carbon number for each homologue.

FID trace (Fig. 3A). The GC–MS-SIM technique for the analysis of F I (carboxylic acids, selected ion m/z 74), F II3 (selected ions m/z 82 and 96 for n-alkanals and m/z 58 for 2-alkanones) and F II4 (selected ions m/z 61, 83 and 97), because of the efficiency of fractionation, did not offer any clear advantage over the FID technique.

Carboxylic compound fraction (F I)

The chromatographic profile of this fraction (Fig. 1A) shows that the compounds present range from C_{10} to C_{32}. The compound distribution, characterized by a strong even-to-odd carbon preference index (CPI) (Table II), indicates a definite biogenic origin of these compounds. The homologues of $<C_{20}$ are attributed to microbial sources, while those of $>C_{20}$ show a more pronounced plant origin [1].

In all samples analysed in this study, a series of α,ω-dicarboxylic acids and ω-oxocarboxylic acids were determined. It has been proposed that these compounds are photooxidation products of cyclic alkenes [12] and of unsaturated fatty acids [8]. The C_5 and C_6 homologues are formed by the oxidation of cyclic alkenes, whereas the C_8 and C_9 homologues, which are the most abundant, are formed by the photooxidation of unsaturated carboxylic acids such as oleic ($C_{18:1}$) and linoleic ($C_{18:2}$) acid. The latter compounds were either absent or found in very low concentrations in all the samples examined. It is interesting that the highest α,ω-dicarboxylic acid concentrations (summer), and at the same time the lowest concentrations of their precursors (oleic and linoleic acids), were related to high ozone concentrations (160 $\mu g/m^3$) determined in the sampling area [8].

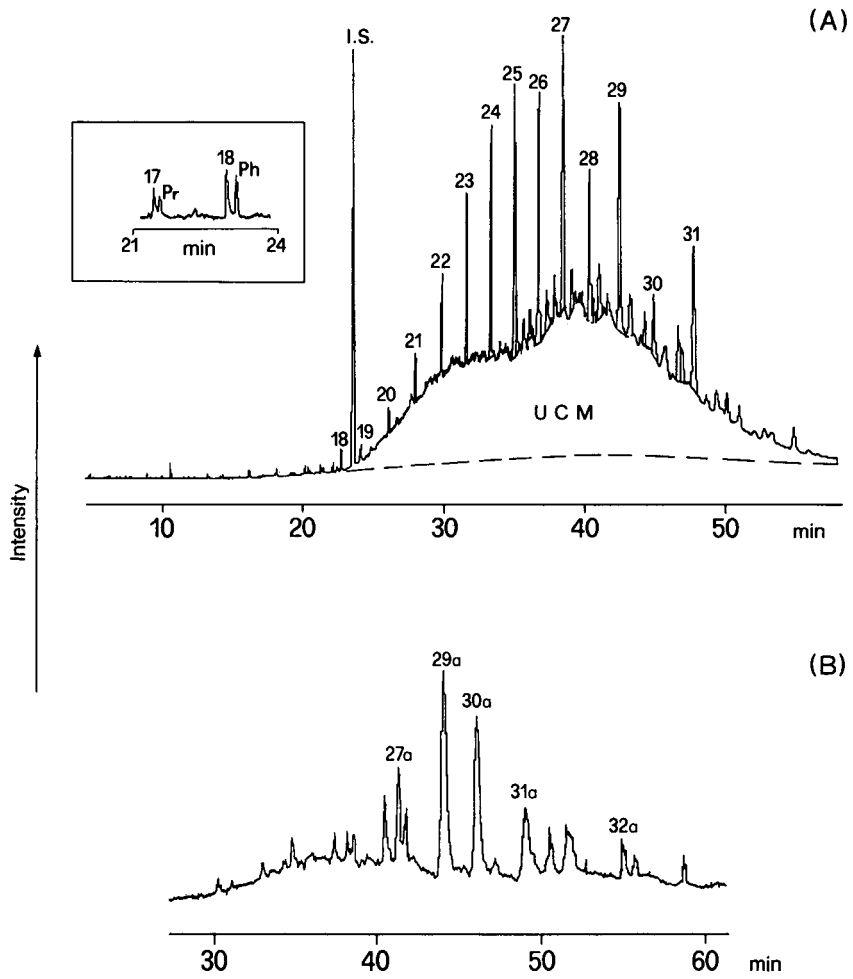

Fig. 2. (A) GC–FID trace of the aliphatic hydrocarbon fraction (F II1) present in airborne particles collected in Heraklion. UCM = unresolved complex mixture; Pr = pristane; Ph = phytane. (B) Ion chromatogram (m/z 191) of the same fraction, specific for the 17α(H),21β(H)-hopanes. The numbers on the peaks indicate the carbon number of each homologue.

Aliphatic hydrocarbon fraction (F III)

All gas chromatograms of the aliphatic fraction (Fig. 2A) exhibited an envelope of an unresolved complex mixture (UCM) of branched and cyclic hydrocarbons. Such traces are characteristic of petroleum residues. The carbon preference index (CPI), a measure of carbon number predominance in a homologous compound series, is a useful estimate of the relative contributions of biogenic *versus* anthropogenic sources. The *n*-alkanes of plant waxes show a pronounced odd carbon number predominance, or CPI > 1, while fossil fuel hydrocarbons exhibit CPI ≤ 1. In these aerosol samples the *n*-alkanes ranged from about C_{11} to C_{33} and had CPI varying from 0.6 to 1.3. Those *n*-alkanes in the range C_{22}–C_{33} had CPI values between 1.4 and 1.6. The homologues above C_{25} in all the samples, maximizing at C_{25}, C_{29} and C_{27}, suggest predominant vascular plant wax alkane inputs. Most of the oils contained isoprenoid hydrocarbons such as pristane (Pr) and phytane (Ph) and some molecular markers such as hopanes and steranes [13]. Pristane, phytane and hopanes were present in all the samples analysed. The ratio of unresolved complex mixture to the total

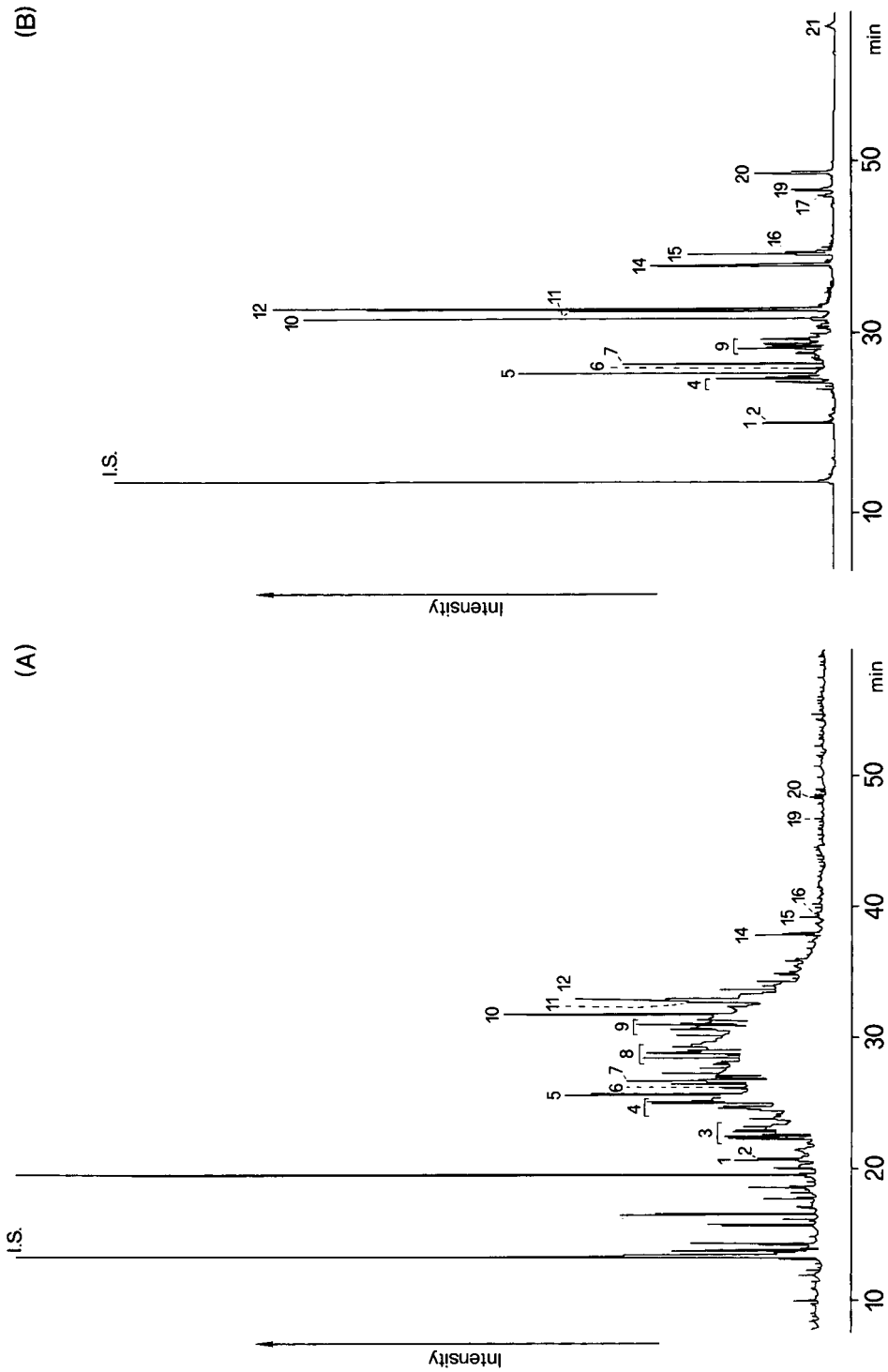

Fig. 3. (A) GC–FID trace of the PAH fraction (F II2) identified in an urban aerosol extract collected in Heraklion; (B) the same fraction analysed by GC–MS-SIM. The peak numbers are identified in Table III.

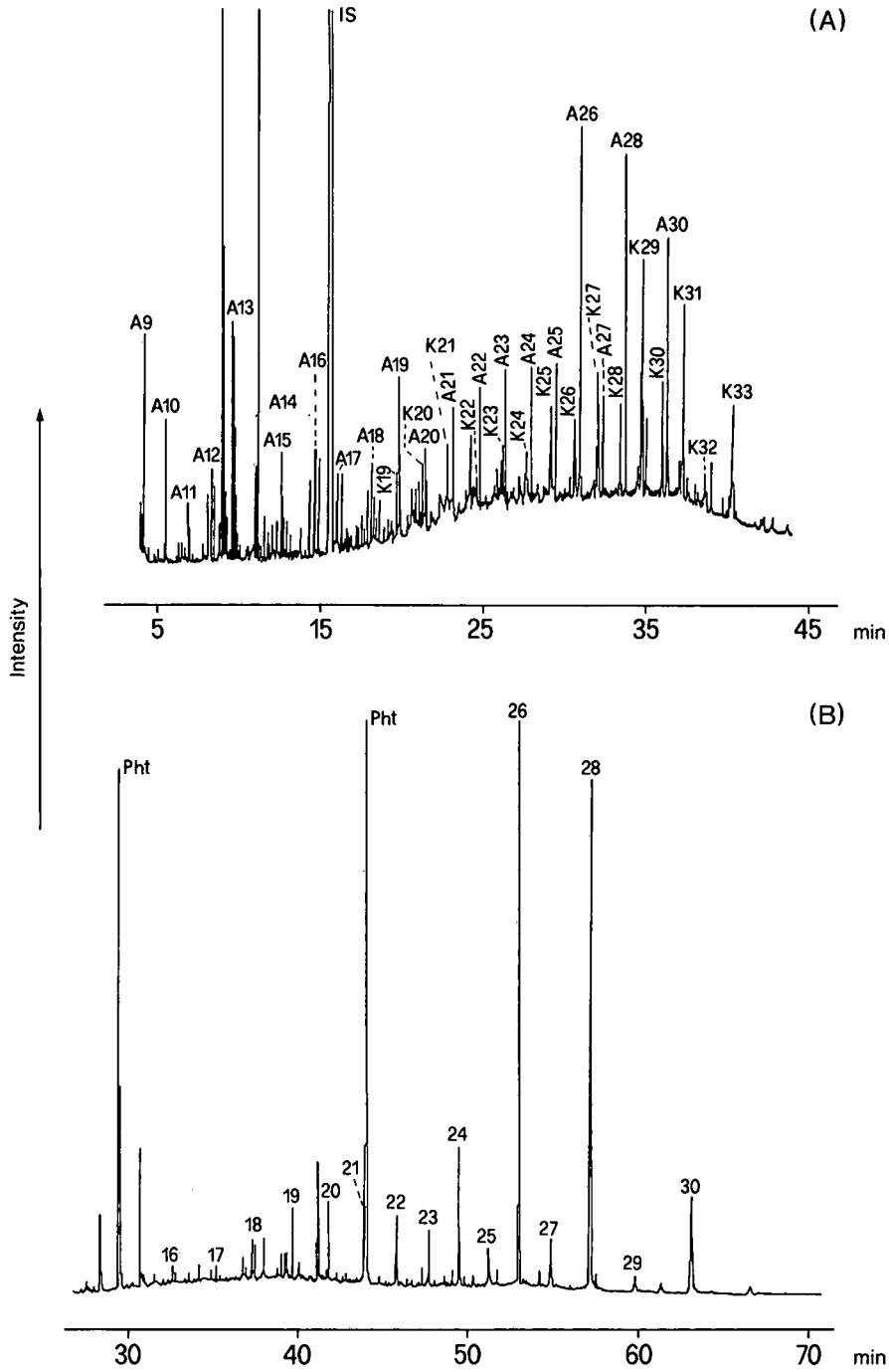

Fig. 4. (A) GC–FID trace of the *n*-alkanal and 2-alkanone fraction (F II3) present in Heraklion aerosol extract. The number of carbon atoms is indicated by A for the *n*-alkanal homologues and K for the 2-alkanone homologues. (B) GC–FID trace of the *n*-alkanol fraction (F II4) identified in an urban aerosol extract. The numbers on the peaks indicate the carbon number of each homologue identified; Pht: phthalate esters.

TABLE II

QUANTITATIVE RESULTS OF THE ANALYSES OF AIR PARTICLES COLLECTED IN THE SAMPLING AREA

CPI (carbon preference index), odd-to-even for *n*-alkanes and 2-alkanones and even-to-odd for *n*-alkanals, *n*-alkanols and *n*-alkanoic acids. Pr = pristane; Ph = phytane; UCM = unresolved complex mixture; TRA = total resolvable aliphatics; IP = indeno[1,2,3-*cd*]pyrene; BgP = benzo[*ghi*]perylene; BeP = benzo[*e*]pyrene; BaP = benzo[*a*]pyrene; MP = methylphenanthrenes; P = phenanthrene.

Compound class	Concentration range (ng/m^3)	CPI	C_{max}	Diagnostic ratio
Aliphatics				
C_{11}–C_{33}	76.6–323,1	0.6–1.3	C_{25}, C_{29}	
UCM	382.0–1277.0			
Pr	0.3–0.6			
Ph	0.2–0.9			
UCM/TRA				4.0–6.6
PAHs	8.8–48.4			
IP/BgP + IP				0.28–0.54
BeP/BeP + BaP				0.76–0.87
MP/P				1.3–8.6
n-Alkanals				
C_9–C_{32}	5.4–6.7	1.1–1.4	C_{26}, C_{28}	
C_{20}–C_{32}	3.6–4.6	1.5–2.3		
2-Alkanones				
C_{16}–C_{33}	1.8–2.6	1.1–1.8	C_{25}, C_{29}	
n-Alkanols				
C_{10}–C_{32}	17.2–100.7	6.6–11.9	C_{26}, C_{28}	
n-Alkanoic acids				
C_9–C_{32}	132.1–205.2	7.0–12.8	C_{16}	
n-Alkanoic acid salts				
C_{11}–C_{30}	39.4–48.9	2.2–4.8	C_{16}	
α,ω-Dicarboxylic acids				
C_6–C_{24}	19.2–45.8		C_9, C_8	
α,ω-Dicarboxylic acid salts				
C_6–C_{26}	16.8–35.0		C_9, C_8	

resolvable aliphatics (UCM/TRA, Table II) is consonant with an important anthropogenic contribution. Thus in the aliphatic fraction two main sources of compounds are reflected in the aeolian particulates of this coastal urban area: emmissions from higher plant waxes and petroleum residues.

Aromatic hydrocarbon fraction (F II2)

The gas chromatograms of the aromatic hydrocarbon fractions (Fig. 3A and B and Table III) contain mostly compounds of pyrolytic origin. In Table II are given the diagnostic ratios [4,9] (indeno[1,2,3-*cd*]pyrene)/(benzo[*ghi*]perylene + indeno[1,2,3-*cd*]pyrene) and (benzo[*e*]pyrene)/(benzo[*e*]pyrene + benzo[*a*]pyrene). These ratios should be interpreted with caution because the values obtained here cannot be attributed to specific sources with certainty. For example, the first ratio (0.28–0.54) indicates mixed combustion sources. The ratio values reported are 0.18 for cars, 0.37 for diesel fuel and 0.56 for coal [4]. The second ratio, between 0.76 and 0.87, corresponds to a faster decay of benzo[*a*]pyrene,

TABLE III

POLYCYCLIC AROMATIC HYDROCARBONS IDENTIFIED IN AN URBAN AEROSOL SAMPLE COLLECTED IN THE CITY OF HERAKLION

No.	Specific ion (*m/z*)	Compound
1	178	Phenanthrene
2	178	Anthracene
3	192	Methylphenanthrenes Methylanthracenes
4	206	Dimethyl-178
5	202	Fluoranthene
6	202	Acephenanthrylene
7	202	Pyrene
8	220	Trimethyl-178
9	216	Methylpyrene Benzo[*a*]fluorene
10	226	Cyclopenta[*cd*]pyrene
11	228	Benzo[*a*]anthracene
12	228	Chrysene/triphenylene
13	242	Methylchrysene
14	252	Benzo[*b,j,k*]fluoranthene
15	252	Benzo[*e*]pyrene
16	252	Benzo[*a*]pyrene
17	252	Perylene
18	276	Indeno[7,1,2,3-*cdef*]chrysene
19	276	Indeno[1,2,3-*cd*]pyrene
20	276	Benzo[*ghi*]perylene
21	300	Coronene

which indicates an origin from a more distant source. Petrogenic inputs also constitute important contributors of aromatic compounds in air particulates. The compositional difference, from combustion originates PAHs, is expressed as the relative abundance of total methylphenanthrenes to phenanthrene (MP/P). Values of MP/P measured in combustion mixtures are generally <1, whereas unburned, fossil PAH mixtures typically display a range of values from 2 to 8 [14]. In this study the MP/P values are between 1.3 and 8.6, thus indicating important unburned petrogenic inputs.

Carbonyl compound fraction (F II3)

n-Alkanals and 2-alkanones are the major compound classes dominating this fraction. Their concentration ranges are at least one order of magnitude lower than those of the other polar compounds, such as *n*-alkanols and alkanoic acids (Table II).

The *n*-alkanals, especially those $>C_{20}$, are of biogenic origin [15]. The chain length distribution of alkanals in the range C_{20}–C_{32} (Fig. 4A) is usually very similar to or identical with that of alkanols (Fig. 4B), suggesting a close relationship [15]. The CPI (even-to-odd) values for the alkanals (Table II), although >1, are not as high as expected for compounds of biogenic origin. The higher values found for these in the range C_{20}–C_{32} indicate more biogenic input, whereas the lower values of the homologues with lower carbon atoms number, C_9–C_{19}, indicate oxidation of alkanes as a possible origin [16].

2-Alkanones are considered to originate form *in situ* microbial formation from *n*-alkanes [17]. The homologue distribution and C_{max} (Fig. 4A) within the range C_{25}–C_{33} are very similar to those for the corresponding *n*-alkanes (Fig. 2A), supporting the above hypothesis.

Hydroxy compound fraction (F II4)

n-Alkanols constitute by far the most abundant compound class determined in this fraction. The homologues range from C_{11} to C_{33}, with a strong even carbon number preference (CPI 6.6–11.9) (Fig. 4B and Table II). This very strong even-to-odd carbon number predominance and the presence of major amounts of C_{26} and C_{28} suggest higher plant waxes as sources of these aerosol lipids. The homologues up to C_{20} are characteristic of vascular plant waxes [18], whereas those lower than C_{20} may originate from microbial sources [1]. The distributions obtained here are similar to those obtained in other areas, such as the north Pacific [19] or in many locations in the United States [1].

Alkanoic acid salt fraction (F III)

The alkanoic acid salts, ranging between C_{10} and C_{30}, show very similar GC profiles (Fig. 1A) and compound distributions to the free alkanoic acids. Their CPI values indicate a definite biogenic origin. The FAS fraction is dominated by the lower carbon number homologues, which are probably derived from a marine source,

although a terrestrial plant wax source may be a minor contributor.

Unsaturated fatty acids were also detected but in lower concentrations than in those detected in the free carboxylic acid fraction. In contrast, ω-oxocarboxylic and α,ω-dicarboxylic acids were found in higher concentrations in the salt form than in the free acid form (Table II). Considering these two pieces of evidence, we conclude that in air particulate samples unsaturated fatty acids undergo faster degradation when in the salt than when in the free acid form.

CONCLUSIONS

We have established a procedure for the determination of biogenic and anthropogenic compounds in airborne particulates. This method consists of separation of the acidic compounds from the neutrals, followed by a flash chromatographic fractionation technique, which allows the complete separation of compound classes into distinct fractions. The fractions obtained can be easily analysed, qualitatively and quantitatively, by capillary gas chromatography with flame ionization detection. The GC–MS technique in the selected ion monitoring method was advantageous over the GC–FID technique for the analysis of PAHs and for the detection of some molecular markers such as hopanes and dicarboxylic acids. More than 140 organic compounds were determined in aeolian particulates from a coastal urban area, using this procedure. Petrogenic and pyrolytic hydrocarbons dominated the anthropogenic compounds, whereas the biogenic compounds consisted mainly of fatty acids and their salts, alkanols, alkanals and 2-alkanones.

ACKNOWLEDGEMENTS

This research was supported by the European Community CT92-084 SCIENCE programme. We thank NATO for support with a Collaborative Travel Grant.

REFERENCES

1 R.B.T. Simoneit and M. Mazurec, *Atmos. Environ.*, 16 (1982) 2139.
2 E. Atlas and C.S. Giam, *Science*, 211 (1981) 163.
3 R.B.T. Simoneit, *Sci. Total Environ.*, 36 (1984) 61.
4 M.A. Sicre, J.C. Marty, A. Saliot, X. Aparicio, J. Grimalt and J. Albaiges, *Atmos. Environ.*, 21 (1987) 2247.
5 M.A. Sicre, J.C. Marty and A. Saliot, *J. Geophys. Res.*, 95 (1990) 3649.
6 M. Mazurec, G.R. Cass and R.B.T. Simoneit, *Environ. Sci. Technol.*, 25 (1991) 684.
7 E.G. Stephanou, *Atmos. Environ.*, 26A (1992) 2821.
8 E.G. Stephanou, *Naturwissenschaften*, 79 (1992) 128.
9 J.O. Grimalt and M. Aceves, *J. Chromatogr.*, 607 (1992) 261.
10 E.J. Corey and G. Schmidt, *Tetrahedron Lett.*, 5 (1979) 399.
11 R.D. McCarthy and A.H. Dutie, *J. Lipid. Res.*, 2 (1962) 117.
12 S. Hatakeyama, T. Tanokaka, J.H. Weng, H. Bandow, H. Takagi and H. Akimoto, *Environ. Sci. Technol.*, 19 (1985) 935.
13 J. Albaiges and P. Albrecht, *Int. J. Environ. Anal. Chem.*, 6 (1979) 171.
14 H. Takada, T. Onda and N. Ogura, *Environ. Sci. Technol.*, 24 (1990) 1179.
15 E.G. Stephanou, *Naturwissenschaften*, 76 (1989) 464.
16 P.M. Gschwend, O.C. Zafiriou, R.C. Mantoura, R.P. Schwarzenbach and R.B. Gagosian, *Environ. Sci. Technol.*, 16 (1982) 31.
17 A. Hollerbach, in *Grundlagen der Organischen Geochemie*, Springer, Berlin, 1985, p. 50.
18 G. Eglinton and R.J. Hamilton, in T. Swain (Editor), *Chemical Plant Taxonomy*, *Academic Press*, New York, 1963, p. 187.
19 R.B. Gagosian, E.T. Peltzer and O.C. Zafiriou, *Nature*, 291 (1981) 312.

Journal of Chromatography, 644 (1993) 153–160
Elsevier Science Publishers B.V., Amsterdam

CHROM. 25 174

Alkyltin speciation in sea water with on-line hydride conversion and gas chromatography–atomic emission detection

Thomas M. Dowling[☆] and Peter C. Uden*

Department of Chemistry, Lederle Graduate Research Tower A, The University of Massachusetts, Amherst, MA 01003 (USA)

(First received November 12th, 1992; revised manuscript received April 6th, 1993)

ABSTRACT

A method for the speciation of alkyltin pollutants in sea water combines solid phase extraction of organotin species from aqueous samples and an on-line hydride generation technique with gas chromatography, followed by element-specific detection for tin. Detection was performed using a microwave-induced plasma atomic emission detection system which provides a 0.5 pg detection limit for tin and a $3 \cdot 10^4$ tin-to-carbon selectivity ratio. Solid-phase extraction provides fast, simple analyte concentration while on-line hydride conversion improves chromatographic behavior and analyte recovery. This combination results in a method capable of measuring pg/ml levels of alkyltin species in the complex matrix of sea water.

INTRODUCTION

Alkyltin compounds have a wide range of uses and their consumption has grown to $50 \cdot 10^6$ kg world wide in 1986 [1]. The largest use of organotin compounds, such as di-*n*-octyl and di-*n*-butyl tins, is in the polymer industry, where there are used extensively as stabilizers in poly(vinyl chloride) (PVC), in products ranging from floor coverings and piping to food packaging.

Alkyltins are also used as herbicides, pesticides, and slimicides in cooling tower water and as antifoulants in boat paints [2]. The trialkyltins are most commonly used as biocides, tributyltin chloride being used as an additive in boat paints; this has led to aquatic environmental problems. These additives are toxic to barnacles and other aquatic species that accumulate on the bottoms of boats, but they are also toxic to other species, particularly shellfish. Levels of tributyltin of pg/ml have been shown to have detrimental effects on shellfish populations [3] and have been shown to be concentrated in oysters and mussels with concentration factors of 5000–50 000 [4]. The bioaccumulation of these toxic species could lead to their appearance in human food supply.

Tin toxicity varies widely, tetraalkyltins and trialkyltins being the most toxic and the inorganic forms less so. As the number of the alkyl substituents increases for alkyltins, the level of toxicity increases as illustrated below. To determine the level of toxic material in a sample containing tin, a total tin measurement is insufficient, and the levels of the different organic forms must be measured to gain an accurate assessment of toxicity.

Increasing toxicity of organotins from right to left: $R_4Sn = R_3SnX > R_2SnX_2 > RSnX_3 >>> SnX_4$.

* Corresponding author.
☆ Present address: Merck, Sharp and Dohme Research Laboratories, Rahway, NJ 07065, USA.

0021-9673/93/$06.00

MEASUREMENT STRATEGIES

Extremely sensitive and selective methods of analysis are required to determine the highly toxic alkyltins present in complex environmental matrices. Atomic spectroscopic methods provide high degrees of sensitivity and selectivity, but cannot differentiate the organic bonded forms of a metal that may be present. Since such different forms of tin must be determined individually, analytical separation of the tin-containing components is needed. The microwave induced plasma (MIP) provides sensitive and selective spectroscopic detection of tin and when combined with gas chromatography allows speciation of volatile or derivatizable alkyltins in complex matrices [5,6].

Extraction/concentration techniques for alkyltin species in aqueous samples include purge and trap after hydride generation, liquid–liquid extraction and solid-phase extraction (SPE) [7–9]. The latter requires no reagent solutions, large extractant solvent quantities or tedious separation of phases; it is fast, simple and easily automated. The possibility of contamination of samples is also reduced. SPE readily provides analyte concentration factors of 1000 or more in situations in which the SPE extract can be concentrated by evaporation.

Conversion of the alkyltin chlorides to their analogous hydrides has several advantages. The former are difficult to gas chromatograph directly at trace levels because they react with chromatographic active sites, causing poor peak shape and analyte recovery. Hydride conversion provides more volatile derivatives, increases stability, improves peak shape and increases sensitivity. Utilized with GC–atomic emission detection (AED) methods, on-line hydride conversion gives "chemical reaction selectivity" in addition to chromatographic and spectroscopic selectivity. Analysis of the same sample with or without hydride conversion may aid confirmation and identification analytes. Craig *et al.* have developed an on-line hydride conversion technique [10,11] in which a small amount of solid sodium borohydride ($NaBH_4$) is placed inside the gas chromatograph injection port and extracted tin chlorides are injected through it. This paper presents a method which combines SPE, on-line hydride conversion and GC–AED, for alkyltin speciation in sea water samples. It provides the sensitivity and selectivity to measure pg/ml levels of organotin species with little sample preparation and few possibilities for sample contamination.

EXPERIMENTAL

Instrumentation

A HP5921A GC–AED system (Hewlett-Packard, Avondale, PA, USA) [12–15] which features a thin walled, water cooled quartz discharge tube, a solvent venting system and a direct connection between the cavity and a nitrogen purged spectrometer, was used for all GC analyses. Wavelength dispersion in this system is with a fixed grating spectrometer with a flat focal plane, and detection is by a movable photodiode array. The photodiode array detector allows simultaneous multi-element monitoring within wavelength regions of about 20–30 nm, from 160 nm to 810 nm. Tin was detected at 303 nm, hydrogen and oxygen being added to the plasma gas as reagents. This system allows two different pre-set plasma make-up flow conditions, a "high" and "low" helium flow, the former providing better sensitivity and selectivity for tin.

A Model 5890 II gas chromatograph with a HP-7673A auto-injector and "Chem Station" (Hewlett-Packard) were used in combination with the AED system. GC columns used included: a 12 m × 0.32 mm I.D., 0.17 μm film thickness column HP-1 (Hewlett-Packard), a 25 m × 0.32 mm I.D., 0.25 μm film thickness DB-1 (J&W Scientific, Folsom, CA) and a 10 m × 0.53 mm I.D., 0.25 μm film thickness HP-1 (Hewlett-Packard).

Chemical and reagents

Tributyltin chloride and tripropyltin chloride (Aldrich, Milwaukee, WI, USA) standards were prepared in HPLC-grade dichloromethane or methanol (Fisher Scientific, Fair Lawn, NJ, USA). Sodium borohydride, consisting of crystalline material of mesh range *ca.* 40–100 was used as obtained (Fisher Scientific). Solid-phase

extractions were performed using C_{18} Sep-Paks (Millipore, Milford, MA, USA).

On-line hydride conversion

Hydrides were formed on-line by placing *ca.* 100 mg of solid sodium borohydride ($NaBH_4$) inside the injection port liner and injecting the extracted alkyltin chlorides through the solid material [10]. A cup-type liner was used, the distance from the septum to the top of the $NaBH_4$ bed was *ca.* 45 mm and the column end was *ca.* 13 mm below the bed. Hydrides which formed in the hot injection port were then carried by the carrier gas into the GC column. The optimum temperature for the complete conversion of chlorides to hydrides without redistribution reactions occurring was 240–250°C.

The solid $NaBH_4$ plug, which filled approximately 1 cm of the injection port liner, was held in place between plugs of glass wool. Initially the $NaBH_4$ was mixed in a ratio of approximately 4:1 with an inert material such as a molecular sieve in order to keep it from packing too tightly, thus causing non-uniform carrier gas glow patterns through the solid material. This procedure proved to be of small utility and was later eliminated for simplicity.

No problem was experienced with the $NaBH_4$ becoming inactive, even after 50–60 splitless injections, and so automated injections could proceed without interruption. Initially there was some concern that large splitless injections might dissolve some of the solid reagent and wash it onto the head of the column where it could precipitate and clog the column. This problem never occurred however, despite many 5-μl splitless injections.

Preparation of standards

Tripropyltin chloride and tributyltin chloride stock standards were prepared by dissolving the appropriate amount of the analyte in HPLC-grade methanol or dichloromethane. These stock solutions were stored under refrigeration in the dark, and were used to make fresh dilutions each day. Methanol stock solutions were used to spike water samples at the appropriate levels.

Sample collection

Water samples were collected at two sites, the Thames River at the State Pier in New London, CT, USA, and the end of Long Wharf in Newport, RI, USA. The samples were collected by placing 1-l bottles just beneath the water surface and allowing them to be filled. Each of these sites was a marine environment where a high level of commercial boat traffic was known to occur.

RESULTS AND DISCUSSION

The linear dynamic range, limits of detection and selectivity for tin over carbon were determined as was the linear range of the hydride generation technique and its performance in the splitless injection mode.

Tin response factors for tetraethyltin, tripropyltin hydride and tributyltin hydride were 251, 193 and 203 area counts/ng tin injected, respectively. The slightly lower response factors for the hydrides may indicate a slight loss of the chlorides prior to conversion or that conversion to the hydrides was incomplete.

Each of these calibrations were made using the 12 m × 0.32 mm I.D. HP-1 column at a split ratio of 100:1. The 1-μl injections were made at 250°C for all three calibrations. Standards ranging in concentration from $0.12 \cdot 10^{-9}$ g/ml to $120 \cdot 10^{-9}$ g/ml were prepared in chloromethane. Standards above $8 \cdot 10^{-8}$ g/ml were found to extend beyond the linear range for tetraethyltin itself and when hydride generation was performed. A greater split ratio could be used to analyze these higher concentrations if required.

The limit of detection was calculated at 0.5 pg of tin absolute and selectivity over carbon was calculated to be greater than 30 000. A splitless 5-μl injection of $1 \cdot 10^{-9}$ g/ml provides 5 pg to the detector, this being well above the detection limit for tin. These figures of merit illustrate that GC–AED provides the sensitivity and selectivity required to detect ng/ml levels of tin in complex matrices. Also, as shown subsequently, the hydride conversion technique was shown to be quantitative, giving uniform conversion of the alkyltin chlorides to their hydrides.

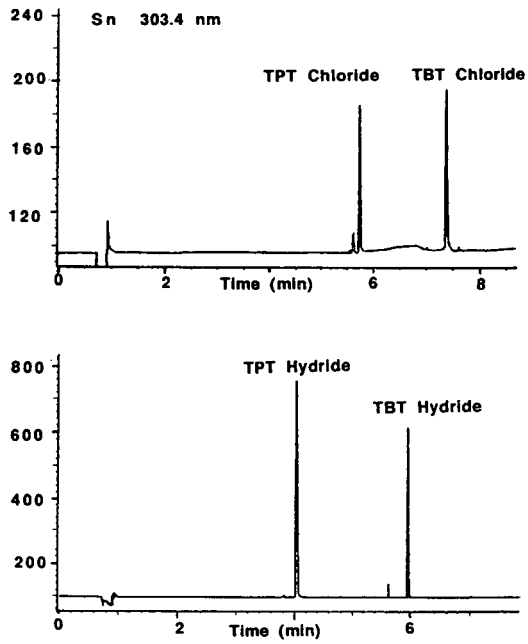

Fig. 1. Tin-specific chromatograms of (top) tripropyltin chloride (TPTCl) and tributyltin chloride (TBTCl) and (bottom) their corresponding hydrides (TPTH and TBTH) after hydride conversion with $NaBH_4$. Column 12 m × 0.32 mm I.D. HP-1, 250°C isothermal. Inlet split ratio 100:1.

The improvement in chromatography and recovery of injected material is illustrated in Fig. 1. In all GC–AED chromatograms, the *y* axis gives both indication of absolute response and also offset. A mixture of tripropyltin (TPT) and tributyltin (TBT) chlorides was injected with and without $NaBH_4$ in the injection port. The upper chromatogram shows the results when no $NaBH_4$ was used and the lower chromatogram shows the results with hydride conversion. The hydrides elute earlier than the corresponding chlorides and show less tailing. Increased response for the hydrides suggests better recovery of injected material.

Spiked water samples

Water samples were spiked at the 1 ng/ml and 0.1 ng/ml level with TPT and TBT chlorides. SPE of a 100-ml sample of 1 ng/ml solution and 500 ml of the 0.1 ng/ml solution were performed by pulling the samples through a Sep-Pak under a slight vacuum. Extracted components were eluted from the extraction cartridge with 25–30 ml of dichloromethane and concentrated by evaporation to 1 ml. The 1 ng/ml sample was chromatographed on the 25 m × 0.32 mm I.D. DB-1 column, and the 0.1 ng/ml sample was chromatographed on the 10 m × 0.53 mm I.D. (Megabore) HP-1 column. Splitless 1-μl injections were made with the 1 ng/ml standard, while 5-μl splitless injections were made with the 0.1 ng/ml sample. When splitless injections were made with the 0.32 mm I.D. column, the tripropyltin hydride showed poor peak shape due presumably to the injection volume exceeding the capacity of the column. Installation of a retention gap could remedy this problem, as could a modification in the initial column temperature.

A 0.53 mm I.D. column was then used in order to better evaluate the performance of the method for splitless injection. The peak shape of the tripropyltin hydride was improved, due to the greater column capacity and its ability to operate at higher carrier gas flow rates (Fig. 2). The higher carrier gas flow allows the large vapor cloud that forms in the injection port when splitless injections are made, to enter the column more quickly with less dispersion. This reduces peak tailing of early eluting components. The peak shape of the tributyltin hydride remained

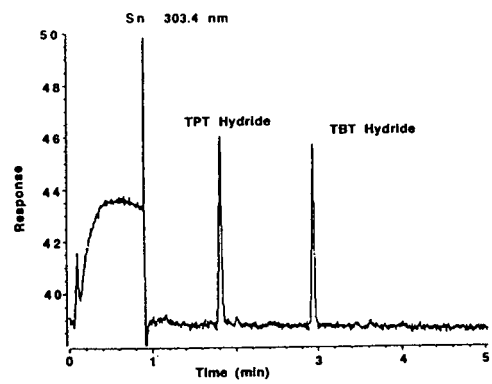

Fig. 2. Tin-specific chromatogram from 0.1 pg/ml aqueous trialkyltin chloride solution, extracted (Sep-Pak) and hydride converted to TPTH and TBTH. Column 10 m × 0.53 mm I.D. HP-1, 250°C isothermal, splitless injection.

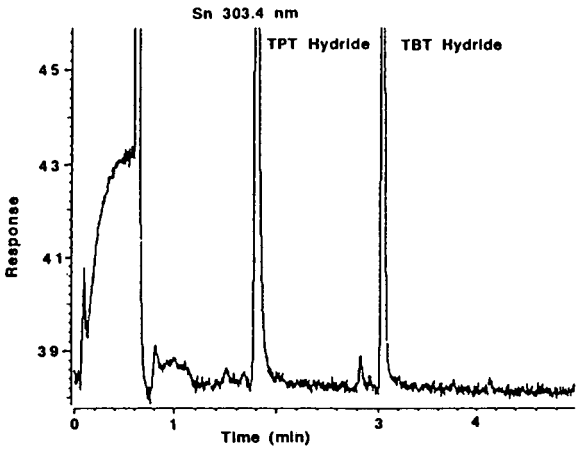

Fig. 3. Tin-specific chromatogram of converted trialkyltin chloride (as hydrides) standards. Column and conditions as in Fig. 2, 5-μl splitless injection, 200 pg tin levels on column.

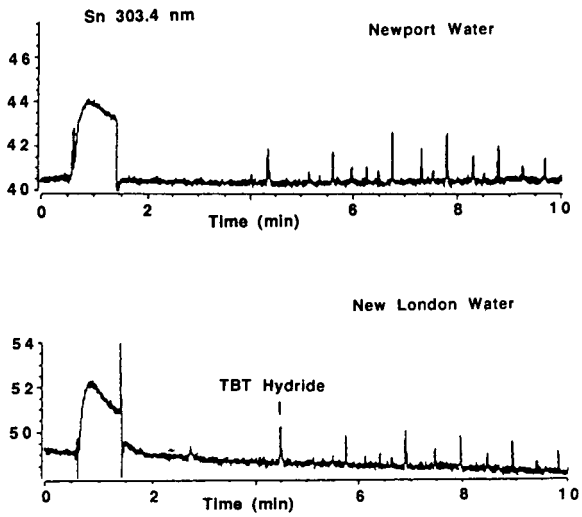

Fig. 4. Tin-specific chromatograms of Newport, RI, USA (top) and New London, CT, USA (bottom) water extracts (500-fold concentration). Column and conditions as in Fig. 2, 5-μl splitless injection.

sharp and symmetric. Fig. 3 illustrates the peak shapes obtained for a more concentrated sample, the response axis having been extended to emphasize the peak symmetry. The 0.53 mm I.D. column was clearly preferred, especially when splitless injections must be made.

Despite the different conditions under which the 1 ng/ml and 0.1 ng/ml samples were analyzed, the relative responses were very close to those predicted. After accounting for the different volumes of water extracted and the different injection volumes, the peak areas per unit mass of alkyltin for each of these samples should be similar. The peak areas for the tripropyltin hydride were 170 and 180 for the 0.1 ng/ml solution and the 1 ng/ml solution respectively, and those for the tributyltin hydride were 180 and 200 for the 0.1 ng/ml and 1 ng/ml solutions respectively. In each case recoveries were approximately 90%.

Sea water samples from New London, CT, USA and Newport, RI, USA were collected and solid phase extraction of 500-ml volumes was carried out as described earlier. Splitless 5-μl injections of the extracts were made, representative chromatograms being shown in Fig. 4, tributyltin hydride being expected at a retention time of approximately 4.5 min. Both samples show response at the expected retention time and based on the calibration for tributyl tin hydride, each was found to contain approximately 30 pg/ml tributyltin. In addition to the response seen at 4.5 min, several other peaks appear later in both chromatograms.

The responses seen for the analyte of interest were near the detection limit as were those for unexpected peaks. Therefore, confirmation of the identity of the analyte peak was necessary and the identification of the additional presumed tin containing peaks was also of interest. The source and removal of the additional peaks is discussed subsequently.

The combination of the photodiode array detector and software allows three-dimensional chromatograms to be plotted (retention time *versus* wavelength against emission intensity). These plots allow spectral regions to be viewed during a chromatographic peak and aid confirmation of the presence of an element in that peak. Tin shows characteristic atomic emission in the MIP at 301 nm and 303.4 nm. An indication of these lines can be seen in Fig. 5 which depicts the peak at 4.4 min in the New London water sample. However, the low level of the organotin species present, and the large amounts of inter-

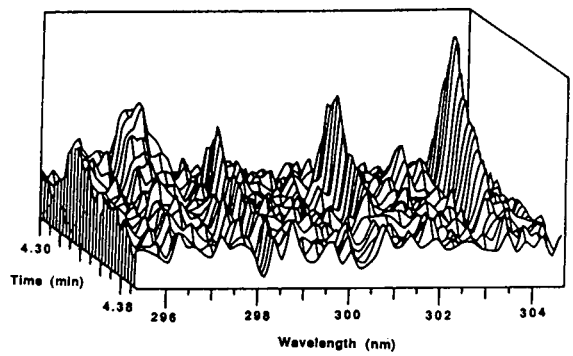

Fig. 5. Three-dimensional spectral–chromatographic snapshot of the peak at 4.4 min in the New London water extract chromatogram.

fering carbon species, make even this powerful feature of the GC-AED system inconclusive.

The added dimension of chemical selectivity provided by the on-line hydride conversion gave additional confirmation of the analyte peak. Fig. 6 compares the chromatograms obtained with and without hydride conversion. The sample injected with sodium borohydride shows the expected analyte peak at approximately 4.4 min in addition to the unidentified later eluting peaks. The sample injected without hydride conversion does not show response at 4.4 min but does show response for the other unidentified peaks. Also, in this sample at approximately 5.5 min there is a slight shift in the baseline, which is considered to correspond to tributyltin chloride which would elute in this region and show poor peak shape at this low level. The fact that this ill defined peak is not seen in the reacted sample chromatogram in which the hydride peak occurs, provides further evidence for the validity of the conversion reaction.

It is interesting to note that the interfering peaks did not change in retention time or peak shape in the presence or absence of the hydride conversion reaction. This suggests that if these were tin containing species, they are probably tetraalkyl species. Although each of these peaks showed some indication of the two tin emission lines expected (303 nm and 303.4 nm), its presence in these peaks could not be absolutely confirmed, as discussed above.

Tin-containing interferences

Initially it was thought that the additional peaks appearing in the tin chromatogram were due to non-selective response of carbon containing species. However, Fig. 7 shows that the major carbon response does not correspond with the pattern of peaks seen in the tin chromatogram. Most of the carbon response occurs later in the chromatogram and the unidentified peaks in the tin chromatogram were not due to carbon interference. Silicon, sulfur, phosphorus and

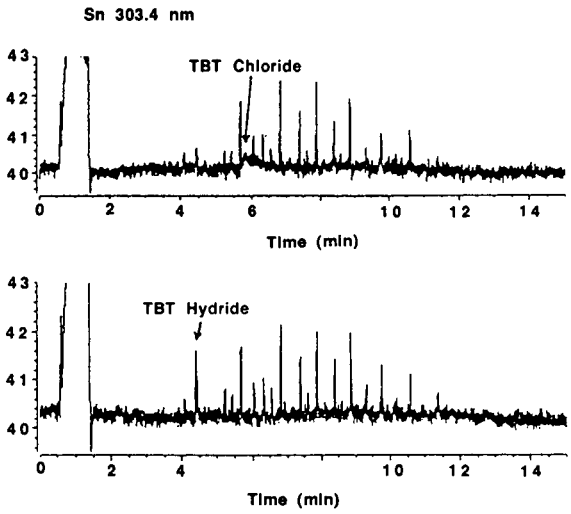

Fig. 6. Tin-specific chromatograms of the Newport, RI water extract with (bottom) and without (top) $NaBH_4$ conversion. Column and conditions as in Fig. 2, 5-μl splitless injection.

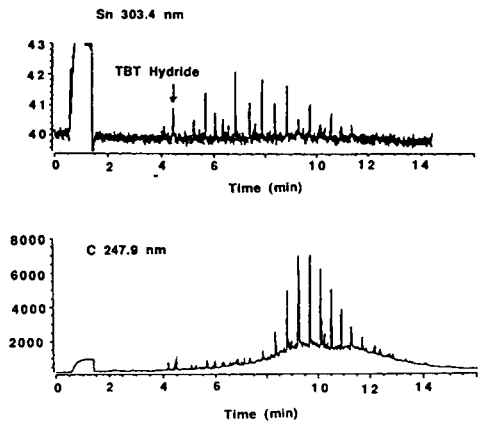

Fig. 7. Tin-specific (top) and carbon-specific (bottom) chromatograms of the Newport, RI water extract. Column and conditions as in Fig. 2, 5-μl splitless injection.

chlorine specific detection was performed, and none of these element specific chromatograms showed the same pattern of responses seen in the tin chromatogram. This indicates that these elements were not responsible for the unidentified peaks in the tin chromatograms.

Identification of the source and removal of interferences

Since the New London and Newport water extracts showed the same pattern of interfering species, it was hypothesized that they were being introduced during the sample preparation procedure. Each step of the procedure was thus examined.

Dichloromethane which had not been in contact with any of the sample preparation materials was injected and none of the interfering peaks were observed. Each piece of glassware and the syringes used in the sample preparation were washed with dichloromethane and these washes were injected, none giving response on the tin channel. Finally, a Sep-Pak that had not been used to extract any samples was washed with 15 ml of dichloromethane. This extract was condensed to 1 ml as for the sample extracts. Injection of this Sep-Pak wash showed the same response pattern for the interfering species seen in the previous water extracts but did not show response at the retention time expected for the TBT hydride (Fig. 8, top). This indicated that the interferents were being washed from the Sep-Pak. Extraction of a second aliquot of the New London water with the now "clean" Sep-Pak showed response for the analyte of interest, but none of the interfering species were observed (Fig. 8, bottom). Subsequent extractions were performed after washing each Sep-Pak with approximately 15 ml of dichloromethane.

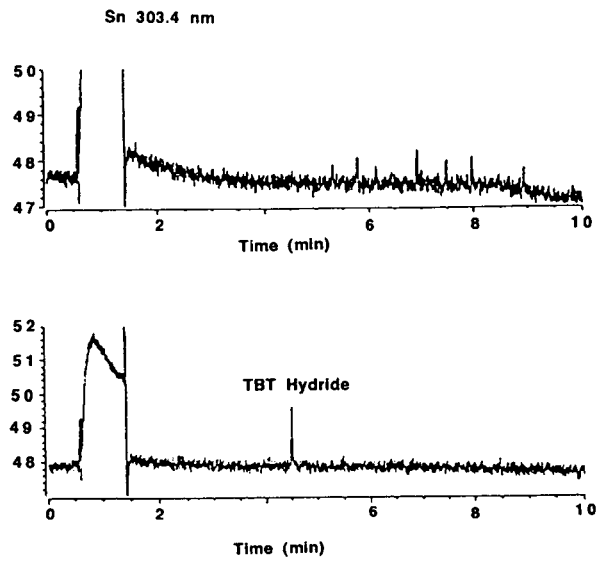

Fig. 8. Tin-specific chromatograms of Sep-Pak blank and the New London, CT water extracted with the "clean" Sep-Pak. Column and conditions as in Fig. 2, 5-μl splitless injection.

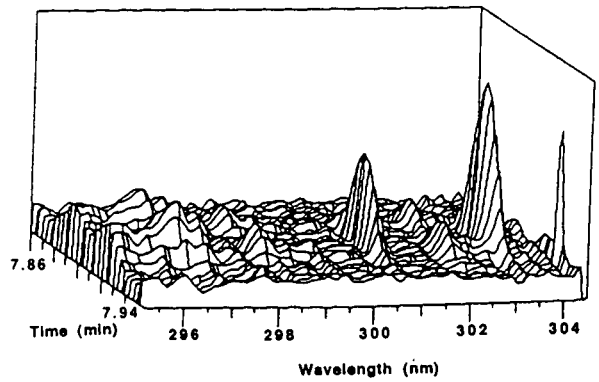

Fig. 9. Three-dimensional spectral-chromatographic snapshot of the peak at 7.84 min in the chromatogram of the five combined Sep-Pak washes.

In order to confirm that the interfering compounds were being washed from the Sep-Paks and that they did contain tin, five unused cartridges were washed with dichloromethane. These washes were then combined and condensed to 1 ml. Injection of the condensate showed the same pattern of response on the tin channel as was seen for the sea water extracts except for tributyltin. Three-dimensional plots for each of the major peaks showed characteristic emission of tin at 303 nm and 303.4 nm (Fig. 9). It was evident that the interferents were being washed from the Sep-Pak cartridges, and did contain tin. Pre-washing the Sep-Pak with 10–15 ml of dichloromethane before the extraction of samples removed these contaminants.

CONCLUSIONS

The use of toxic alkyltin compounds in boat paints has led to their appearance in aquatic

environments where extremely sensitive and selective methods of analysis are required for trace detection and analyte speciation.

The microwave-induced plasma atomic emission detector for GC provides a low detection limit for tin (0.5 pg of tin absolute or less than 1 ng/ml) and selectivity over carbon of greater than 30 000. SPE provides a fast simple method for the extraction and concentration (concentration factors of up to 1000 times are possible) of tin species. With a concentration factor of 1000 and the ability to detect ng/ml solutions directly, environmental levels of 10 pg/ml can be detected with the MIP after extraction. On-line hydride conversion allows the GC of alkyltin species without time-consuming sample preparation or sample loss in the chromatographic system. This combination results in a method capable of detecting pg/ml levels of alkyltin species in marine water samples with minimal sample preparation. This technique is robust, utilizes commercially available instrumentation and is capable of automation.

ACKNOWLEDGEMENTS

We thank Bruce Quimby, James Sullivan and the Hewlett-Packard Company for their interest and support. This work was supported in part by Merck, Sharp and Dohme Research Laboratories, the Union Carbide Corporation and Rhone Poulenc Rorer Company.

REFERENCES

1 S. Nicklin and M.W. Robson, *Appl. Organomet. Chem.*, 2 (1988) 487.
2 E.A. Clark, R.M. Sterrit and J.N. Lester, *Environ. Sci. Tech.*, 22 (1988) 600.
3 R.J. Carter, N.J. Juroczy and A.M. Bond, *Environ. Sci. Tech.*, 23 (1989) 615.
4 M.O. Stallard, S.Y. Cola and C.A. Dooley, *Appl. Organomet. Chem.*, 3 (1989) 105.
5 S.A. Estes, P.C. Uden and R.M. Barnes, *J. Chromatogr.*, 239 (1982) 239.
6 P.C. Uden, *Element-Specific Detection by Atomic Emission Spectroscopy*, (*American Chemical Society Symposium Series*, No. 479), American Chemical Society, Washington, DC, 1992.
7 V.F. Hodge, S.L. Seldel and E.D. Goldberg, *Anal. Chem.*, 51 (1979) 1256.
8 K.W. Siu, P.S. Maxwell and S.S. Berman, *J. Chromatogr.*, 475 (1989) 373.
9 M.D. Muller, *Anal. Chem.*, 59 (1987) 617.
10 S. Clark, H. Ashby and P.J. Craig, *Analyst*, 112 (1987) 1781.
11 S. Clark and P.J. Craig, *Appl. Organomet. Chem.*, 2 (1988) 33.
12 J.J. Sullivan and B.D. Quimby, *J. High Resolut. Chromatogr.*, 12 (1989) 282.
13 B.D. Quimby and J.J. Sullivan, *Anal. Chem.*, 62 (1990) 1027.
14 J.J. Sullivan and B.D. Quimby, *Anal. Chem.*, 62 (1990) 1034.
15 J.J. Sullivan and B.D. Quimby, *J. High Resolut. Chromatogr.*, 12 (1989) 813.

Journal of Chromatography, 644 (1993) 161–174
Elsevier Science Publishers B.V., Amsterdam

CHROM. 25 063

Axial temperature effects in electromigration

Bohuslav Gaš

Faculty of Science, Charles University, Albertov 2030, 128 40 Prague 2 (Czech Republic)

(First received August 10th, 1992; revised manuscript received March 12th, 1993)

ABSTRACT

A model of electrophoretic migration that is influenced by generated Joule heat is presented. The model takes into account the axial flux of the heat. It is shown that the mutual influence of non-equilibrium fluxes of mass and heat may lead to new phenomena: oscillation of the concentration profile on concentration boundaries and changes in concentration of the electrolytes (either an increase or a decrease) appearing at sites of jumps of the radial heat flux of the capillary tube. The theoretical results are supported by experiments.

INTRODUCTION

The production of heat is an inherent phenomenon accompanying all electromigration separation methods. The heat is generated by ohmic resistance of the electrolyte due to flow of the electric current and, in consequence, the temperature of the separation media is increased. The heat is generated in the whole volume of the separation media but it is transported outside by the walls of the column. It causes a non-homogeneous radial distribution of the temperature in the separation column. Electrophoretic mobility, which plays a significant role in electromigration methods, is strongly influenced by the temperature. Therefore, the temperature gradient causes radial variations in the migration velocity profile and, in consequence, a decrease in separation efficiency [1–9].

The loss of heat by the walls of the separation column is dependent on the overall heat transfer through the capillary walls. This heat transfer may vary in various parts of the column owing to different thermal conductivities and the heat transfer coefficient of the walls. Additionally, different electric conductivities of various sites of the solution in the capillary column (*e.g.*, in distinctive isotachophoretic zones or in any disturbances in the axial concentration profile) also cause different Joule heat powers and different temperatures of the sites. Both will cause an axial flux of the heat.

It should be emphasized that the axial variation of the heat transfer through the column walls can be distinguished, especially in junctions of non-thermostated column tubing. In consequence, the axial variation of temperature can reach several tens of degrees and can exceed the radial variation. In all studies [1–9] dealing with the effects of temperature gradients on the efficiency of electrophoretic separations, the axial flux of heat was omitted. This neglect may be acceptable in cases of thermal band broadening of peaks moving relatively quickly by electrophoretic or electroosmotic velocity in a homogenous and concentrated background buffer, but may fail in cases of concentration boundaries. Such a concentration boundary moves in a capillary relatively slowly owing to the concentration dependence of the transference numbers of ions on both sides of the boundary [10,11].

Generally, the transference numbers are also dependent on temperature. It will be shown in this paper that the temperature dependence of transference numbers gives rise to an interesting phenomenon, *i.e.*, moving oscillation of the

0021-9673/93/$06.00

concentration profile of the concentration boundary. Additionally, owing to the temperature dependence of the transference numbers, the axial jumps in the heat transfer coefficient of the capillary walls and consequent axial jumps in the temperature of the buffer will cause an increase or decrease in concentration at sites of the jumps.

The aim of this work was to obtain a theoretical description, computer solution and experimental support of a model of electromigration separation processes taking into account the mutual influence of the mass and heat fluxes. This paper is organized as follows: formulation of a general mathematical model of temperature-influenced electromigration; formulation of a simplified mathematical model of temperature influenced electromigration assuming a homogeneous radial distribution of temperature; numerical solution of both models; formulation of a linearized modification of the simplified model and both its analytical and numerical solution; and experimental verification.

MATHEMATICAL MODELS

General model of temperature-influenced electromigration

Let us consider a capillary tube as a separation column with length L and inner radius R filled by a solution of n strong ions. Let the axial x coordinate be the axis of the capillary and let an outer electric field act in the direction of x coordinate. Further, we do not consider bulk convection or electrosmotic flow in the column.

The system is cylindrically symmetrical, therefore it is possible to cope with only two spatial coordinates, namely x and r, where r is the radial coordinate of the capillary tube. The concentration $c_i = c_i(x, r, t)$ of the ith ion and the temperature $T = T(x, r, t)$ in the column will be functions of the three variables, *i.e.*, the spatial x and r coordinates, $x \in \langle 0, L \rangle$, $r \in \langle 0, R \rangle$, and the time t, $t \geq 0$.

Each ion inside the column is affected by two forces: the chemical potential gradient of the ion and the electric potential gradient. In a very dilute solution, eventual cross-effects between fluxes of different ions can be neglected [12] and a gradient of concentration can be used instead of the chemical potential gradient. The matter flux $\boldsymbol{J}_i(x, r, t)$ of the ith ion in the capillary tube is a vector composed of two components, $J_{i,x}(x, r, t)$ and $J_{i,r}(x, r, t)$. Assuming proportionality between fluxes and forces, the matter fluxes are [12]

$$\boldsymbol{J}_i = -D_i \operatorname{grad} c_i - \operatorname{sgn}(z_i) u_i c_i \operatorname{grad} \phi \,, \quad i = 1, \ldots, n \tag{1}$$

where z_i, D_i and u_i are the relative charge number, diffusion coefficient and ionic mobility of the ith ion, respectively, ϕ is the electric potential and grad is the gradient of a scalar function in cylindrical coordinates.

Fluxes of charged particles are related to the flow of the electric current. It must be realized that the current density $\boldsymbol{j}$ is also a vector, which is dependent on x, r and t coordinates:

$$\boldsymbol{j} = F \sum_{k=1}^{n} z_k \boldsymbol{J}_k \tag{2}$$

where F is the Faraday constant. Eliminating the potential gradient from eqn. 1 using eqn. 2, we have

$$\boldsymbol{J}_i = -D_i \operatorname{grad} c_i + \frac{\operatorname{sgn}(z_i) c_i u_i}{\kappa} \left(\boldsymbol{j} + F \sum_{k=1}^{n} z_k D_k \operatorname{grad} c_k \right) \tag{3}$$

where κ is the specific conductivity:

$$\kappa = F \sum_{k=1}^{n} |z_k| c_k u_k \tag{4}$$

The continuity equation, $\partial c_i / \partial t = -\operatorname{div} \boldsymbol{J}_i$ (where div is the divergence of a vector) expresses the mass balance at each point in the capillary tube. In our system it can be written as

$$\frac{\partial c_i}{\partial t} = \operatorname{div} \left[D_i \operatorname{grad} c_i - \frac{\operatorname{sgn}(z_i) c_i u_i}{\kappa} \left(\boldsymbol{j} + F \sum_{k=1}^{n} z_k D_k \operatorname{grad} c_k \right) \right] \tag{5}$$

The vector heat flux, $\boldsymbol{J}_T(x, r, t)$, in the capillary tube is composed of two components, $J_{T,x}(x, r, t)$ and $J_{T,r}(x, r, t)$, and, neglecting the Soret

effect [13], can be described by a phenomenological Fourier law [14,15]:

$$\boldsymbol{J}_T = -K \operatorname{grad} T \tag{6}$$

where K is the thermal conductivity. The relevance of the neglect of the Soret effect is discussed in the Appendix.

The Joule heat power, w_g, generated by the electric current density, j, in solution per unit volume is $w_g = |j|^2/\kappa$. This term appears as the source term in the following equation which can be written for temperature:

$$\rho_m c_h \frac{\partial T}{\partial t} = \operatorname{div}(K \operatorname{grad} T) + \frac{|j|^2}{\kappa} \tag{7}$$

where ρ_m is the mass density and c_h is the heat capacity of the solution.

It should be further considered that many physico-chemical properties depend on temperature and/or concentration. For the correct description of a real situation, these dependences should be taken into account.

Mobilities, u_i, depend strongly on concentrations and temperature, *i.e.*, $u_i = u_i(c_1, \ldots, c_n, T)$. The limiting ionic mobility, u_i^0, which is the mobility of an ion at infinite dilution, varies owing to changes in the interaction between solvent molecules and the ions, and between the solvent molecules themselves. The main part of this variation is caused by the change in viscosity of the solvent. This can be expressed as the Walden rule [16], which states that the product of the limiting mobility and the viscosity of the solvent is approximately constant. For practical reasons, the temperature dependence of the limiting mobility can be expressed as a polynomial function of the temperature. Constants of the polynomiai can easily be obtained by fitting from available experimental data.

The Debye–Hückel–Onsager theory [17] describes the temperature dependence of the electrophoretic and relaxation effects influencing the mobility in a finite concentration. The Onsager limiting law can be written in the form

$$u_i = u_i^0 - (Au_i^0 + B)\sqrt{I_S} \tag{8}$$

where I_S is the ionic strength and A and B are terms corresponding to the relaxation and electrophoretic effects, respectively. They are independent of concentration, but dependent on temperature, permittivity and viscosity of the solvent. The temperature dependence of the terms A and B may also be expressed, in a not very broad temperature interval, as a polynomial function.

The concentration dependence of the diffusion coefficients can be neglected with good precision. For example, the diffusion coefficient of NaCl in aqueous solution at 25°C increases by about 0.5% on changing the concentration from infinite dilution to 10 mol m^{-3} [16]. However, the diffusion coefficients of ions depend strongly on temperature, *i.e.*, $D_i = D_i(T)$. There is no theory describing the temperature dependence of diffusion coefficients in liquids precisely. Nevertheless, for our purposes the simplest hydrodynamic theory can be used. For diffusion of the large, spherically symmetrical ith ion with diameter r_i in a solvent with small molecules, the Stokes–Einstein equation [18] holds for the diffusion coefficient D_i:

$$D_i = \frac{k(T + 273)}{6\pi\eta r_i} \tag{9}$$

where k is the Boltzmann constant, T is the temperature expressed in °C and η is the viscosity coefficient of the solvent. As the temperature dependence of the viscosity of liquids is approximately exponential [18], it can be written in accordance with the Arrhenius relationship for the viscosity coefficient:

$$\eta = A_{visc} \exp\left[\frac{E_{visc}}{k(T + 273)}\right] \tag{10}$$

where A_{visc} and E_{visc} are constants of the solvent independent of temperature. Hence, taking into account eqns. 9 and 10, the temperature dependence of the diffusion coefficient of the ith ion is

$$D_i = K_{i,visc}(T + 273) \exp\left[-\frac{E_{visc}}{k(T + 273)}\right] \tag{11}$$

where $K_{i,visc}$ is a constant of the ith ion. Again, the parameters A_{visc}, E_{visc} and $K_{i,visc}$ can be obtained by fitting from available experimental data.

For a complete description of electromigration including the temperature effects, the equations

describing the temperature and/or concentration dependences of mobilities, diffusion coefficients and thermal conductivities must be added to eqns. 5 and 7. These equations, together with appropriate initial and boundary conditions, form the general model of temperature-influenced electromigration. The initial condition is an initial distribution of concentration and temperature in a column. It is natural to assume a homogeneous initial radial distribution of concentration of all ions in the tube and a constant initial temperature equal to the temperature of the surroundings T_S at time $t = 0$ in the whole column, *i.e.*,

$$c_i(x, r, 0) = C_i(x), \quad T(x, r, 0) = T_S,$$
$$x \in \langle 0, L \rangle, \quad r \in \langle 0, R \rangle \tag{12}$$

where $C_i(x)$ is the initial axial concentration distribution of the ith ion.

The boundary condition at the centre line $r = 0$ reflects a cylindrical symmetry of the problem; therefore,

$$\frac{\partial c_i}{\partial r}(x, 0, t) = 0 \quad \text{and} \quad \frac{\partial T}{\partial r}(x, 0, t) = 0,$$
$$x \in \langle 0, L \rangle, \quad t > 0 \tag{13}$$

At the capillary wall, where $r = R$, heat is transported outside the column. The overall radial heat flux will be proportional to the difference between the temperature of the inner wall and the temperature of the surroundings, hence the boundary condition is

$$-K \cdot \frac{\partial T}{\partial r}(x, R, t) = h_0[T(x, R, t) - T_S],$$
$$x \in \langle 0, L \rangle, \quad t > 0 \tag{14}$$

where h_0 is the overall heat transfer coefficient. If the column is formed of a simple capillary tube with an inner radius R and an outer radius R_0, the overall heat transfer coefficient is [19]

$$h_0 = \frac{1}{R} \cdot \frac{1}{[\ln (R/R_0)/K_W] + 1/R_0 h_S} \tag{15}$$

where K_W is the thermal conductivity of the capillary wall and h_S is the surface heat transfer coefficient. The surface heat transfer coefficient h_S is a function of the cooling properties of the surroundings and the surface temperature of the outer capillary wall. Gobie and Ivory [8] calculated its value for various cooling conditions and found $h_S \approx 130$ or $h_S \approx 3200$ W m^{-2} K^{-1} for an air-cooled or liquid-cooled capillary, respectively. Generally, it will be assumed that $h_S = h_S(x)$ and $h_0 = h_0(x)$.

The boundary conditions for concentrations at the boundary $r = R$ are

$$\frac{\partial c_i}{\partial r}(x, R, t) = 0, \quad x \in \langle 0, L \rangle, \quad t > 0 \tag{16}$$

which means that matter cannot be transported through the walls.

Boundary conditions at the boundaries $x = 0$ and $x = L$ should reflect the fact that here we are interested in phenomena taking place inside a capillary tube. Real boundaries originating at connections of the capillary column to electrode vessels would bring another complexity to modelling. Therefore, it will be convenient to adopt boundary conditions:

$$\frac{\partial c_i}{\partial x}(0, r, t) = 0 \quad \frac{\partial T}{\partial x}(0, r, t) = 0$$
$$\frac{\partial c_i}{\partial x}(L, r, t) = 0 \quad \frac{\partial T}{\partial x}(L, r, t) = 0$$
$$r \in \langle 0, R \rangle, \quad t > 0 \tag{17}$$

Analogous equations for transport of mass to the set of eqns. 5 can be written for electromigration of weak electrolytes. In this case, for the relevant description of temperature-influenced electromigration, the temperature dependence of the dissociation constants should also be known.

Simplified model of temperature influenced electromigration

The solution of the general eqns. 5 and 7, assuming the initial and boundary conditions 12–14, 16 and 17, is very complex, hence it would be beneficial to find a simplification of the model.

Owing to diverse thermal conductivity and the overall heat transfer coefficient of the various parts of the column walls, it can be expected that an axial temperature profile may vary considerably in different parts of the column. Especially in junctions of column tubing or in junc-

tions of liquid-cooled and air-cooled parts of a capillary tube the overall heat flux outside the column exhibits large jumps. The axial jumps in temperature may easily reach several tens of degrees. Other reasons for a non-constant axial temperature distribution are different conductivities or concentrations of solutions in various parts of the capillary.

On the other hand, the radial temperature gradient often hardly reaches a few degrees under working conditions typical in CZE or ITP.

From this point of view, if only axial effects are to be studied, it will be not too far from reality to assume uniform radial distributions of concentration and temperature, *i.e.*, $c_i = c_i(x, t)$ and $T = T(x, t)$. Hence eqns. 5 will have the form

$$\frac{\partial c_i}{\partial t} = \frac{\partial}{\partial x}\left[D_i \cdot \frac{\partial c_i}{\partial x} - \frac{\mathrm{sgn}(z_i) c_i u_i}{\kappa}\left(j + F\sum_{k=1}^{n} z_k D_k \cdot \frac{\partial c_k}{\partial x}\right)\right] \quad (18)$$

The current density j is now not a function of r and consequently not a function of x, hence $j = j(t)$. If the electric current is controlled by an electronic regulator to a constant value I, then $j = I/(\pi R^2)$.

In the simplest case of a uni–univalent electrolyte, $i = 1,2$ and the electroneutrality condition relates $c_1 = c_2$. Denoting $c = c_1 = c_2$, $z_1 = 1$ and $z_2 = -1$, the set of eqns. 18 is reduced to one equation:

$$\frac{\partial c}{\partial t} = \frac{\partial}{\partial x}\left\{D_1 \cdot \frac{\partial c}{\partial x} - \frac{u_1}{u_1 + u_2}\left[\frac{j}{F} + (D_1 - D_2)\frac{\partial c}{\partial x}\right]\right\} \quad (19)$$

which can be rewritten as

$$\frac{\partial c}{\partial t} = \frac{\partial}{\partial x}\left(D \cdot \frac{\partial c}{\partial x} - \frac{u_1}{u_1 + u_2} \cdot \frac{j}{F}\right) \quad (20)$$

denoting $D = (D_1 u_2 + D_2 u_1)/(u_1 + u_2)$.

Eqn. 14 can no longer be a boundary condition but an additional term describing a heat loss. Therefore, the analogy of eqn. 7 will now be (using the simple relationship between the surface and volume of a cylinder)

$$\rho_m c_h \cdot \frac{\partial T}{\partial t} = \frac{\partial}{\partial x}\left(K \cdot \frac{\partial T}{\partial x}\right) + \frac{j^2}{\kappa} - h_0 \cdot \frac{2}{R}(T - T_S) \quad (21)$$

The initial and boundary conditions can be analogous to eqns. 12 and 17:

$$c_i(x, 0) = c_i(x), \quad T(x, 0) = T_S, \quad x \in \langle 0, L \rangle \quad (22)$$

$$\frac{\partial c_i}{\partial x}(0, t) = 0, \quad \frac{\partial T}{\partial x}(0, t) = 0, \quad t > 0 \quad (23)$$

In fact, the isolated set of eqns. 18 gives a complete description of the migration of strong ions in an electric field at constant temperature. This set of equations was solved numerically by Dose and Guiochon [20] for several strong electrolytes.

It is evident that an analytical solution of eqns. 5 and 7 or even eqns. 20 and 21 can hardly be found, and therefore a numerical solution must be coped with.

EXPERIMENTAL

The numerical solution of the partial differential equations was performed by the method of lines. It consisted in discretizing spatial derivatives at a set of grid points to generate a set of ordinary differential equations with time as the independent variable. The finite-difference approximation is based on the first-order symmetrical difference approximation for both first and second derivatives. The Hamming's modification of the fourth-order predictor–corrector method [21] was used for the solution of the resulting set of ordinary differential equations.

The algorithm solving dynamics of electromigration was programmed in Pascal and can run on IBM PC computers. Simulation results can be displayed in graphical form.

The electromigration experiments were done on a one-column isotachophoretic analyser consisting of the hydraulic part from an Agrofor system (JZD, Odra Krmelín, Czech Republic) and a high-frequency contactless detector [22]. The capillaries were made of PTFE. Sodium chloride (Lachema, Brno, Czech Republic) was of analytical-reagent grade and bromophenol blue (Lachema) was of purum grade. No addi-

tives were added to solutions to decrease the electroosmotic flow.

RESULTS AND DISCUSSION

Further considerations will be limited to the temperature-influenced electromigration of binary uni–univalent electrolytes.

Stockmayer [11] derived that the concentration boundary of a binary electrolyte moves in an electric field in a capillary due to concentration dependence of the transference numbers. He showed that if this dependence is linear, the moving concentration boundary is simply shifted by a constant velocity and spread by diffusion. If the dependence is non-linear, additional distortion of the boundary shape takes place.

It will be further shown that if the temperature influence is considered, the moving concentration boundary can have a different character. From comparison with experiments, an available and well defined electrolyte system should be chosen. NaCl was considered as such an electrolyte because Na^+ and Cl^- ions have different mobilities and different temperature dependences of the mobility. Additionally, detailed data on the mobility and diffusion of these ions are readily available. In the following text, the subscripts 1 and 2 represent Na^+ and Cl^-, respectively. Assuming a polynomial temperature dependence of limiting mobilities and using published experimental data [16,23], the following concentration and temperature dependences of the mobilities in aqueous solution were obtained by fitting:

$$A = 0.2209 + 3.325 \cdot 10^{-4}T + 1.640 \cdot 10^{-6}T^2 \quad (24)$$

$$B = 31.45 + 0.6304T + 0.01428T^2 \quad (25)$$

$$L_1 = 25.58 + 0.9000T + 3.852 \cdot 10^{-3}T^2 \quad (26)$$

$$L_2 = 40.49 + 1.357T + 3.688 \cdot 10^{-3}T^2 \quad (27)$$

$$u_1 = [L_1 - (AL_1 + B)\sqrt{c/1000}]/10000F \quad (28)$$

$$u_2 = [L_2 - (AL_2 + B)\sqrt{c/1000}]/10000F \quad (29)$$

where c is the concentration in mol m^3, T is the temperature in °C and u_1 and u_2 are the mobilities in $m^2\ V^{-1}\ s^{-1}$.

Analogously, for the temperature dependence of the diffusion coefficients we obtained

$$D_1 = 4.195 \cdot 10^{-9}(T + 273)\exp\left(-\frac{2040}{T + 273}\right) \quad (30)$$

$$D_2 = 6.396 \cdot 10^{-9}(T + 273)\exp\left(-\frac{2040}{T + 273}\right) \quad (31)$$

where D_1 and D_2 are the diffusion coefficients in $m^2\ s^{-1}$.

For very dilute solutions, the heat is transported in a capillary column mainly by the solvent, and therefore values valid for water were taken as constants, namely $\rho_m = 1000$ kg m^{-3} and $c_h = 4187$ J K^{-1} kg^{-1}. The thermal conductivity of water varies slightly with temperature from 0.56 W K^{-1} m^{-1} at 0°C to 0.68 W K^{-1} m^{-1} at 100°C. In this work, an average value of $K = 0.6$ W K^{-1} m^{-1} was considered. The thermal conductivity of the PTFE wall of the capillary tube was assumed to be $K_w = 0.27$ W K^{-1} m^{-1}.

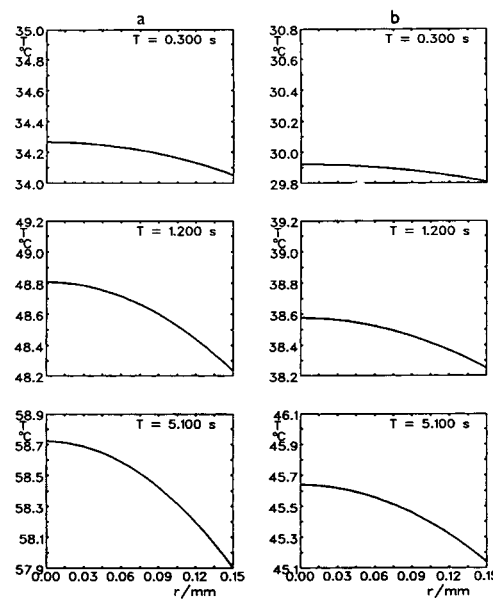

Fig. 1. Radial temperature profile in the capillary tube. Current density, −1373 A m^{-2}; temperature of surroundings, 25°C; PTFE capillary of I.D. 0.3 mm, O.D. 0.5 mm; thermal conductivity of the PTFE wall, 0.27 W K^{-1} m^{-1}; surface heat transfer coefficient, 130 W m^{-2} K^{-1}. T = temperature; r = radial coordinate of the capillary tube; t = time. (a) 1 mM NaCl; (b) 2 mM NaCl.

Computer solution of the general model

A general numerical solution of the set of eqns. 5 and 7 will be published elsewhere. For the purpose of this paper, the calculation will be limited to a uni–univalent electrolyte and cases of constant initial axial and radial distribution of concentration in the capillary, *i.e.*,

$$c(x, r, 0) = C\,, \quad T(x, r, 0) = T_S\,, \quad x \in \langle 0, L \rangle\,,$$

$$r \in \langle 0, R \rangle \tag{32}$$

where C is the initial concentration of the electrolyte.

Fig. 1 shows the radial temperature profile at various times attained by solution of eqns. 5 and 7 for two different concentrations of sodium chloride, namely 1 and 2 mol m^{-3}, and assuming the initial conditions in eqn. 32. At time $t = 5.1$ s, the radial temperature profile is almost in a steady state. It is seen that the temperature difference between the centre and the wall of the capillary is less than 1°C, whereas that between the two solutions is about 13°C.

Computer solution of the simplified model

The simplified model in eqns. 20 and 21 has the advantage of a fairly rapid numerical solution and less computer memory requirement, but nevertheless still seems to be able to describe main "axial features" of the general model.

The solution reveals the existence of two interesting effects: oscillation of the concentration profile on concentration boundaries and changes in concentration of the electrolytes (either an increase or a decrease) appearing at sites of jumps of the overall heat transfer coefficient h_0.

Oscillation of the concentration profile. The numerical solution of eqns. 20 and 21, with initial and boundary conditions in eqns. 22 and 23 and assuming a constant heat transfer coefficient along the capillary tube, is demonstrated in Fig. 2. In this and analogous figures, the initial distribution of concentration shown in (a) is the initial condition. The triad (a), (b) and (c) shows the time development of a moving concentration boundary between $c' = 2$ mol m^{-3} and $c'' = 4$ mol m^{-3} NaCl in an air-cooled PTFE capillary of I.D. 0.3 mm and O.D. 0.5 mm. The linear

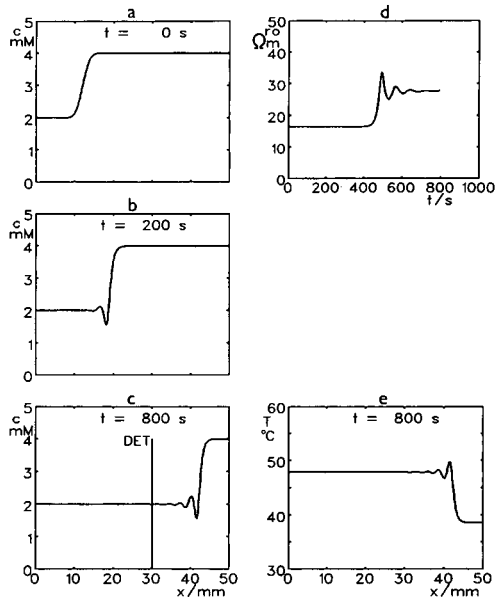

Fig. 2. Simulation of electromigration of the boundary between 2 and 4 mM NaCl. Current density, −1500 A m^{-2}; temperature of surroundings, 25°C; PTFE capillary of I.D. 0.3 mm, O.D. 0.5 mm; thermal conductivity of the PTFE wall, 0.27 W K^{-1} m^{-1}; surface heat transfer coefficient, 130 W m^{-2} K^{-1}. c = Concentration; r_0 = specific resistance; T = temperature; x = axial coordinate of the capillary tube; t = time; DET = position of the detector. (a), (b), (c) Distributions of concentration in the capillary tube; (d) time record of the specific resistance measured by the detector at a position 30 mm along the capillary tube; (e) distribution of temperature in the capillary tube.

velocity, v, of the boundary according to Stockmayer [11] is

$$v = \frac{j(N' - N'')}{F(c' - c'')} \tag{33}$$

where N' and N'' are the transference numbers of sodium in the two solutions with concentrations c' and c'' and the transference number N is expressed as $N = u_1/(u_1 + u_2)$. In Fig. 2, the transference numbers resulting from eqns. 28 and 29 are $N' = 0.40042$ and $N'' = 0.39544$ and, hence, the velocity of the concentration boundary calculated by eqn. 33 is $v = 38.7 \cdot 10^{-6}$ m/s. This value corresponds well with the velocity of the boundary deduced from Fig. 2. With the direction of the electric current used, $j = -1500$ A m^2, the temperature gradient facilitates main-

taining the boundary width in a steady state, *i.e.*, it has a sharpening effect. Additionally, moving dumped oscillations of the profile appear on the trailing edge of the boundary. Fig. 2 also shows the axial temperature profile (e) corresponding to a given time and the time record (d) of the signal of a conductivity detector placed at a position 30 mm along the capillary tube.

If the current is in the opposite direction towards the concentration boundary (Fig. 3), only small oscillations are observed and the moving boundary is spread more rapidly than in the case of free diffusion.

Both sharpening and spreading effects have been described previously [10,11] for electromigration not influenced by Joule heat evaluation. Nevertheless, they can be much more pronounced if the heat evaluation plays a significant role.

Eqns. 20 and 21 are non-linear, hence their solution depends non-linearly on the initial and boundary conditions. On changing the concentration of the solution and the electric current density (Figs. 4–6), further patterns of the concentration profile moving in the capillary can be seen. Fig. 4 reveals a slight irregularity in the oscillations, Fig. 5 shows a series of sharp per-

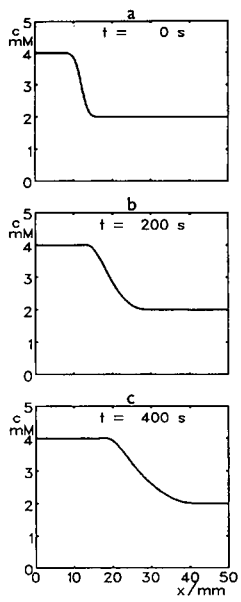

Fig. 3. Simulation of electromigration of the boundary between 4 and 2 m*M* NaCl. Current density, -1500 A m^{-2}; temperature of surroundings, 25°C; PTFE capillary of I.D. 0.3 mm, O.D. 0.5 mm; thermal conductivity of the PTFE wall, 0.27 W K^{-1} m^{-1}; surface heat transfer coefficient, 130 W m^{-2} K^{-1}. c = Concentration; x = axial coordinate of the capillary tube; t = time. (a), (b), (c) Distributions of concentration in the capillary tube.

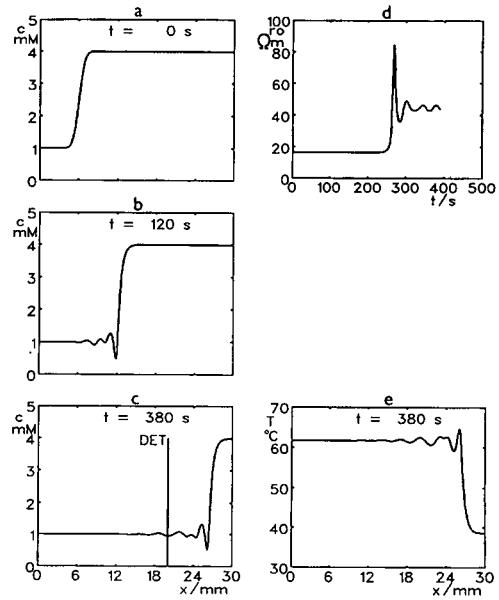

Fig. 4. Simulation of electromigration of the boundary between 1 and 4 m*M* NaCl. Details as in Fig. 2.

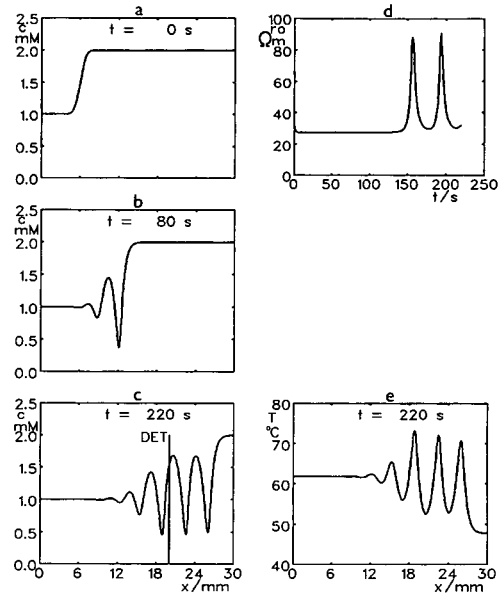

Fig. 5. Simulation of electromigration of the boundary between 1 and 2 m*M* NaCl. Details as in Fig. 2.

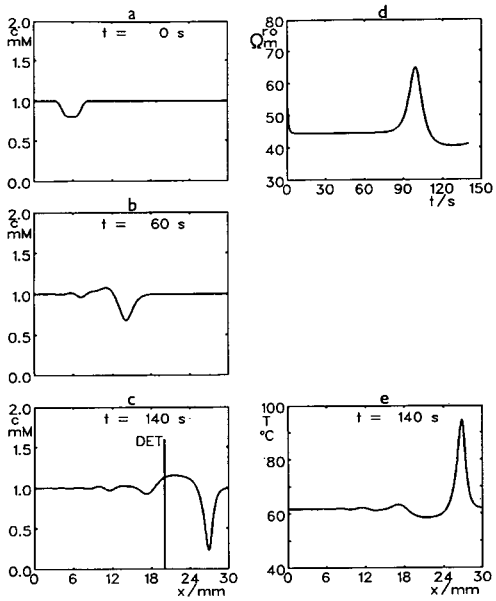

Fig. 6. Simulation of electromigration of a small concentration disturbance in 1 m*M* NaCl. Details as in Fig. 2.

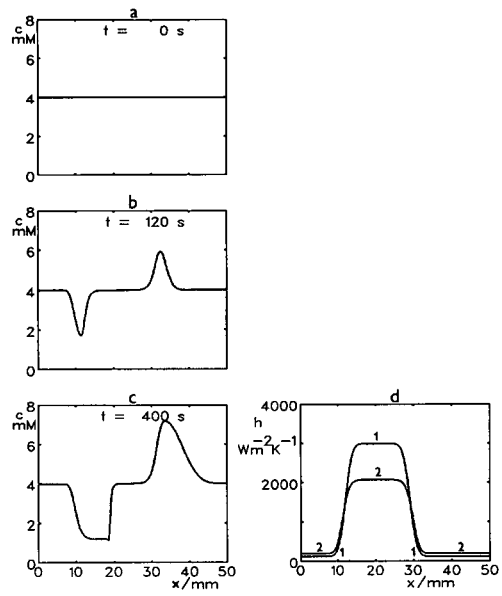

Fig. 7. Simulation of concentration development at the sites of two jumps in the radial heat transfer. Current density, -1500 A m^{-2}; temperature of surroundings, 25°C; PTFE capillary of I.D. 0.3 mm, O.D. 0.5 mm; thermal conductivity of the PTFE wall, 0.27 W K^{-1} m^{-1}. c = Concentration; x = axial coordinate of the capillary tube; t = time; h = heat transfer coefficient. (a), (b), (c) Distributions of concentration in the capillary tube; (d) axial profiles of the heat transfer coefficients. 1 = Surface heat transfer coefficient; 2 = overall heat transfer coefficient.

iodic dips that may move stably in a capillary tube and Fig. 6 demonstrates that if the current density is sufficiently high for a given concentration, even a small disturbance in the concentration profile is quickly amplified.

Changes in concentration at jumps of the overall heat transfer coefficient. The overall heat transfer coefficient h_0 may not be constant along the capillary, *i.e.*, it may be a function of the x-coordinate. Jumps of the heat flux through the capillary wall may often occur in practice at junctions of tubing.

Fig. 7 shows a simulation of the concentration development at the sites of two jumps of h_S (from 130 to 3200 W m^{-2} K^{-1} and *vice versa*). This corresponds to an illustrative situation where an air-cooled capillary tube is partly immersed in cooling water. The axial profiles of h_S and h_0 are shown in Fig. 7d for the PTFE capillary of I.D. 0.3 mm and O.D. 0.5 mm. A constant initial distribution of concentration in the capillary is assumed. The concentration decreases at the site of the left jump, whereas it increases at the site of the right jump. Both sites therefore generate concentration boundaries that move in the capillary as in previous cases and that can cause oscillations. This is shown in Fig. 8, where the jump in radial heat flux may be a source of moving sharp oscillations.

If the electric current exceeds a certain value, a decrease in concentration occurs and the temperature tends to exceed the boiling point of the solution. In reality, boiling of the solution at such a site leads immediately to the breaking of the electric current. It seems that this mechanism of breaking of the current will be more probable than the axial mechanism of autothermal runaway described by Gobie and Ivory [8]. This is supported by the practical observation that an occasional "trip" during electrophoretic experiments frequently occurs at one junction between a capillary tube and an electrode vessel where the radial heat flux exhibits a large jump. If the electric current is in the opposite direction, the trip takes place at the junction of the other electrode vessel (or on another jump of heat resistance).

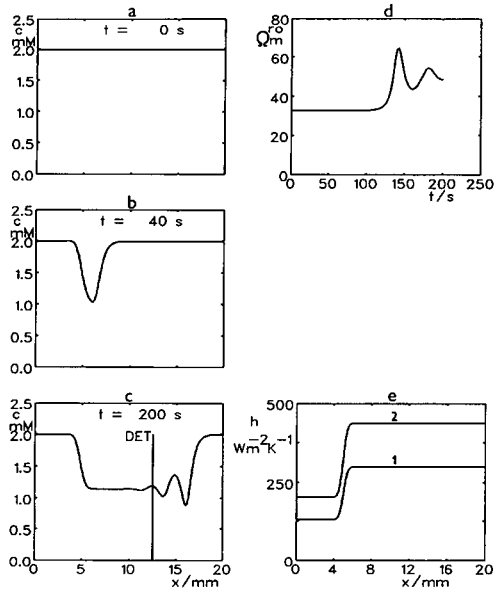

Fig. 8. Generation of oscillations at a jump in the radial heat transfer. Current density, −1500 A m^{-2}; temperature of surroundings, 25°C; PTFE capillary of I.D. 0.3 mm, O.D. 0.5 mm; thermal conductivity of the PTFE wall, 0.27 W K^{-1} m^{-1}. c = Concentration; x = axial coordinate of the capillary tube; t = time; h = heat transfer coefficient. (a), (b), (c) Distributions of concentration in the capillary tube; (d) time record of the specific resistance measured by the detector at a position 12.5 mm along the capillary tube; (e) axial profiles of the heat transfer coefficients. 1 = Surface heat transfer coefficient; 2 = overall heat transfer coefficient.

Linear model

For a better understanding of the origin of the oscillations, eqns. 20 and 21 can be converted into a linear form, which is of course only approximate but able to reveal substantial terms responsible for oscillations.

Assuming a constant current density j, diffusion coefficient D and thermal conductivity K, eqns. 20 and 21 can be rewritten accordingly:

$$\frac{\partial c}{\partial t} = D \cdot \frac{\partial^2 c}{\partial x^2} - \frac{j}{F} \cdot \frac{\partial}{\partial x}\left(\frac{u_1}{u_1 + u_2}\right) \tag{34}$$

$$\rho_m c_h \cdot \frac{\partial T}{\partial t} = K \cdot \frac{\partial^2 T}{\partial x^2} + \frac{j^2}{Fc(u_1 + u_2)} - h_0 \cdot \frac{2}{R}(T - T_S) \tag{35}$$

It can be shown that for every reasonable value of c there is a unique T satisfying

$$\frac{j^2}{F(u_1 + u_2)c} - h_0 \cdot \frac{2}{R}(T - T_S) = 0 \tag{36}$$

where u_1 and u_2 are given by eqns. 28 and 29. The value of T obtained by solving eqn. 36 is a function of c, say $T = T(c)$, and represents the value to which the temperature of a system with an axially homogenous concentration c stabilizes when t tends to infinity. If we took just the function $T(c)$ and inserted it in eqn. 34, we would reduce the pair of eqns. 34 and 35 to an equation for c but the phenomena found when studying the full system would not appear. This is a consequence of the maximum principle for parabolic equations. It proves the importance of eqn. 35 in the process. It seems that in the behaviour of the full system of eqns. 34 and 35 it is very important that, in some way, the temperature lags behind the concentration.

As the initial concentration profile we take $c(x,0) = \gamma(1000x - 8)$, where

$$\begin{aligned} \gamma(\xi) &= 1 && \text{for } \xi < -1 \\ &= \frac{1}{2}\left[\frac{\sin(\pi\xi)}{\pi} + \xi + 3\right] && \text{for } -1 \leq \xi \leq 1 \\ &= 2 && \text{for } \xi > 1 \end{aligned} \tag{37}$$

If $c = 1.5$, the "average" value of the initial concentration and $j = -1373$, $h_0 = 200$, $T_S = 25$, $R = 0.15 \cdot 10^{-3}$, we find from eqns. 36 and 24–29 that $T = T_S + 25$. These values will be used when arranging terms in eqns. 34 and 35. For $N(c, T) = u_1/(u_1 + u_2)$, the transference number, this means that

$$-\frac{j}{F} \cdot \frac{\partial N}{\partial x} = -\frac{j}{F}\left(\frac{\partial N}{\partial c} \cdot \frac{\partial c}{\partial x} + \frac{\partial N}{\partial T} \cdot \frac{\partial T}{\partial x}\right) = -V \cdot \frac{\partial c}{\partial x} + M \cdot \frac{\partial T}{\partial x} \tag{38}$$

where the values of V and M can be found from eqns. 24–29 and are $V = 1.910 \cdot 10^{-5}$ and $M = 4.476 \cdot 10^{-6}$.

Linearizing $1/c$ around $c = 3/2$, we obtain $1/c \approx (4/9)(3 - c)$ and the system of eqns. 34 and 35 changes to

$$\frac{\partial c}{\partial t} = D \cdot \frac{\partial^2 c}{\partial x^2} - V \cdot \frac{\partial c}{\partial x} + M \cdot \frac{\partial T}{\partial x} \tag{39}$$

$$\frac{\partial T}{\partial t} = \alpha \cdot \frac{\partial^2 T}{\partial x^2} + \beta\left[\frac{50}{3}(3 - c) - (T - T_S)\right] \tag{40}$$

where $D = 1.50 \cdot 10^{-9}$, $\alpha = 1.4 \cdot 10^{-7}$ and $\beta = 0.6274$. Finally, as the initial conditions are taken

$$c(x, 0) = \gamma(1000x - 8) \quad (41)$$

$$T(x, 0) = T_S + 50 - \frac{50}{3} c(x, 0) \quad (42)$$

Eqn. 42 gives the initial temperature distribution to which the temperature governed by eqn. 40 would stabilize if the concentration in the capillary were $c(x, 0)$.

The system of eqns. 39–42 was studied on the real line, *i.e.*, for $x \in (-\infty, \infty)$ by applying Fourier transformation. The solution of the transformed equation can be inverted numerically for any value of time and thus the evolution of the concentration profile governed by eqns. 39–42 can be obtained.

Fig. 9 presents the results of three different computations for comparison. Curve 1 is the result of the Fourier transform solution of the linear eqns. 39–42, curve 2 is the result of the numerical solution of the linear eqns. 39–42 and curve 3 is the result of the numerical solution of the original non-linear eqns. 20 and 21 using the initial conditions 41 and 42 and with $j = -1373$, $h_0 = 200$, $T_S = 25$ and $R = 0.15 \cdot 10^{-3}$. There is perfect agreement between both solutions of the linear problem and very good qualitative agreement with the non-linear solution.

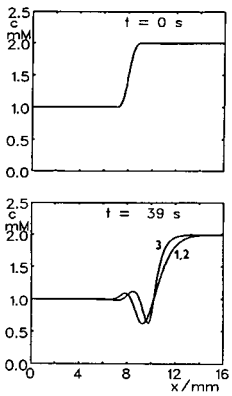

Fig. 9. Comparison of various solutions of differential equations. Current density, -1373 A m^{-2}; temperature of surroundings, 25°C; overall heat transfer coefficient, 200 W m^{-2} K^{-1}. x = Axial coordinate of the capillary tube; t = time. (a) Initial condition eqn. 41; (b) results. 1 = Result of the Fourier transform solution of the linear eqns. 39–42; 2 = result of the numerical solution of the linear eqns. 39–42; 3 = result of the numerical solution of the non-linear eqns. 21 and 22 using the initial conditions 41 and 42.

On the basis of the results, it can be stated that the phenomena found when studying the full non-linear system are also found in the linearized problem.

It can be concluded, that, according to Stockmayer [11], the concentration boundary moves if the transference number depends on concentration. Additionally, the moving oscillations of the concentration profile can appear if the transference number is dependent on temperature, even if this dependence is linear.

Similarly, a non-linear nature of the system is not essential for the increase and decrease in concentration on jumps in the overall heat transfer coefficient. They can appear whenever a transference number is dependent on temperature, even if this dependence is linear.

Experimental verification

The theoretically predicted phenomena were supported experimentally.

Oscillation phenomena frequently occur in practice and are often misinterpreted as artifacts of contact conductivity detectors. Fig. 10 shows the records of a high-frequency contactless conductivity detector, revealing examples of such oscillations. The oscillations appear several minutes after switching an electric current. The high-frequency detector has the advantage of contactless conductivity measurement, hence electrode reactions that would disturb measurements are prevented. On the other hand, it should be emphasized that most construction designs of conductivity detectors alter the radial flux of the capillary wall, which therefore causes the above-mentioned jumps in the radial heat flux and, consequently, sites where a decrease or increase in concentration may occur. The measuring cell of the high-frequency contactless conductivity detector used (similar to that described previously [22]) is formed by a brass cylinder with measuring electrodes. A PTFE capillary tube is fed through the axial hole in the cylinder. It implies the origination of two jumps in the heat flux at both ends of the cylinder. In addition, other sites of such jumps are at every junction of tubing. Apparently, these jumps are sources of the observed oscillations.

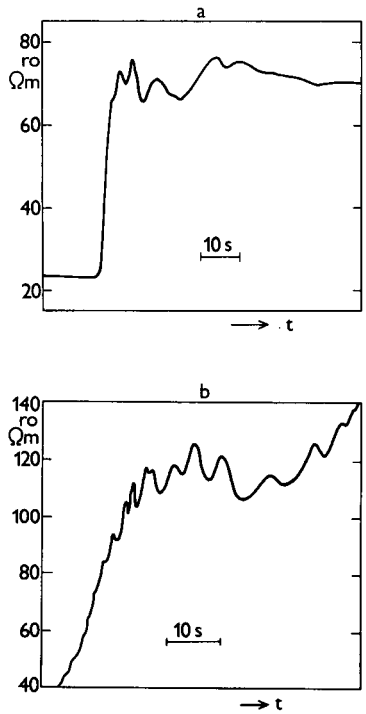

Fig. 10. Experimental record of the conductivity detector. Electrolyte solution in the whole system (*i.e.*, in anodic and cathodic vessels and in the capillary tube), 4 m*M* NaCl. PTFE capillary of I.D. 0.4 mm, O.D. 0.6 mm. r_0 = Specific resistance; t = time. (a) Current 180 μA, cathode at the sample side, anode at the detector side; (b) current 180 μA, anode at the sample side, cathode at the detector side.

The decrease or increase in concentration at jumps of the surface heat transfer coefficient can be verified in an experiment checking the simulation described in Fig. 7. Such an experiment can be realized on a common isotachophoretic instrument using a PTFE capillary of I.D. 0.3 mm and O.D. 0.5 mm. A cathodic and anodic vessel and the capillary are filled with a 4 mol m^{-3} solution of sodium chloride and the capillary is partly immersed in a cooling water-bath. The schematic arrangement of this experiment is shown in Fig. 11. After about 3 min using a constant electric current of 200 μA, the concentration of the sodium chloride will be decreased at the site marked 5 in Fig. 11. At this site, the production of heat is higher but, owing to intensive water cooling, the temperature at this site does not exceed the boiling point of the solution. However, after removing the capillary

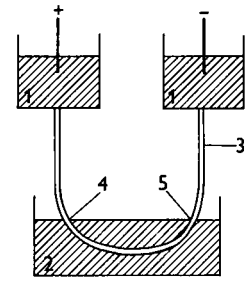

Fig. 11. Arrangement of the experimental check of the increase and decrease in concentration at jumps in the radial heat transfer. 1 = Anodic and cathodic compartments filled with electrolyte; 2 = cooling water; 3 = capillary tube; 4,5 = sites of concentration changes.

from the water-bath and maintaining the same electric current, a break in the current takes place after a few seconds.

The decrease or increase in concentration at jumps of the surface heat transfer coefficient can also be visualized if an ionic organic dye, *e.g.*, bromophenol blue, is used as an electrolyte in the electrophoretic experiment with the same arrangement as shown in Fig. 11 but with a thicker capillary tube, *e.g.*, of I.D. 0.8 mm, for better visibility. Bleaching is observed at the site marked 4 in Fig. 11 and, *vice versa*, there is a deepening of the colour at site 5. Bromophenol blue is a weak acid with $pK_A \approx 3.8$. Detailed temperature dependences of the mobility and diffusion coefficient of its anionic form or the temperature dependence of the pK_A value are not known. Nevertheless, it can be expected that the properties of the cationic and anionic constituents of the dye will differ and the dye will have an analogous migration behaviour to a solution of NaCl.

APPENDIX

Let us check whether the above-mentioned neglect of the Soret effect [13] (and the Dufour effect) [13]) plays a significant role in the described model of electromigration. Assuming a very dilute solution of a strong binary electrolyte, the thermodynamic force X_i ($i = 1, 2$) raising the mass flux of the ith ion in solution in the electric field can be written [12] according to the Onsager theory as

$$X_i = -\frac{RT}{c_i}\cdot\frac{\partial c_i}{\partial x} - \mathrm{sgn}(z_i)F\cdot\frac{\partial \phi}{\partial x} \quad (43)$$

The thermodynamic force X_3 raising the heat flux is

$$X_3 = -\frac{1}{T}\cdot\frac{\partial T}{\partial x} \quad (44)$$

Hence the fluxes J_1 and J_2 of ions 1 and 2 and flux J_3 of the heat are

$$J_1 = L_{11}X_1 + L_{12}X_2 + L_{13}X_3 \quad (45)$$

$$J_2 = L_{21}X_1 + L_{22}X_2 + L_{23}X_3 \quad (46)$$

$$J_3 = L_{31}X_1 + L_{32}X_2 + L_{33}X_3 \quad (47)$$

where L_{ij} (i, $j = 1, 2, 3$) are phenomenological Onsager coefficients. The Onsager reciprocity theorem declares $L_{ij} = L_{ji}$. In our case with very dilute solution, the interaction between ions can be neglected to a good approximation, *i.e.*, $L_{12} = L_{21} = 0$. The remaining non-diagonal coefficients L_{13}, L_{23}, L_{31} and L_{32} are responsible for the Soret and Dufour effects.

Eqns. 45 and 46 can be rewritten using eqn. 2 and the electroneutrality condition declaring $c_1 = c_2 = c$. Using further relationships between phenomenological and diffusion coefficients [13,16], the individual mass fluxes are (for the case of a uni–univalent electrolyte)

$$J_i = -D\left(\frac{\partial c}{\partial x} + sc\cdot\frac{\partial T}{\partial x}\right) + \mathrm{sgn}(z_i)\cdot\frac{u_i}{u_1+u_2}\cdot\frac{j}{F} \quad (48)$$

where $i = 1, 2$ and s is the Soret coefficient. The Soret coefficient of an electrolyte solution is strongly dependent on temperature. Its value is approximately several 10^{-3} K^{-1} for our solutions of NaCl in the temperature range 20–50°C. Knowing the value of the Soret coefficient, it is possible to calculate the term $sc\,\partial T/\partial x$ in the previously calculated results and compare it with the $\partial c/\partial x$ term. This can be done, *e.g.*, for the results shown in Fig. 5. In Fig. 12 there are plotted both terms assuming a value of the Soret coefficient of 0.005 K^{-1} and it is obvious that the amplitude of the $\partial c/\partial x$ term is much greater (about ten times) than the amplitude of the $sc\,\partial T/\partial x$ term.

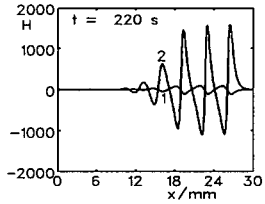

Fig. 12. Plot of $sc\,\partial T/\partial x$ and $\partial c/\partial x$ terms for the situation simulated in Fig. 5. x = Axial coordinate of the capillary tube; t = time. 1 = $sc\,\partial T/\partial x$ term; 2 = $\partial c/\partial x$ term; H = value of the terms in mol m^{-4}.

From this, it can be assumed that neglect of the Soret effect did not cause significant errors in the previous calculations. Analogously, the same would be valid for the flux of the heat and the Dufour effect.

ACKNOWLEDGEMENT

Dr. Milan Štědrý of the Faculty of Science, Charles University, Prague, is thanked for his kind assistance with the mathematical work.

REFERENCES

1 S. Hjertén, *Chromatogr. Rev.*, 9 (1967) 122.
2 M. Coxon and M.J. Binder, *J. Chromatogr.*, 101 (1974) 1.
3 J.F. Brown and J.O.N. Hinckley, *J. Chromatogr.*, 109 (1975) 218.
4 J.H. Knox and I.H. Grant, *Chromatographia*, 24 (1987) 135.
5 F. Foret, M. Deml and P. Boček, *J. Chromatogr.*, 452 (1988) 601.
6 E. Grushka, R.M. McCormick and J.J. Kirkland, *Anal. Chem.*, 61 (1989) 241.
7 A.E. Jones and E. Grushka, *J. Chromatogr.*, 466 (1989) 219.
8 W.A. Gobie and C.F. Ivory, *J. Chromatogr.*, 516 (1990) 191.
9 J.M. Davis, *J. Chromatogr.*, 517 (1990) 521.
10 L.G. Longsworth, *J. Am. Chem. Soc.*, 65 (1943) 1755.
11 W.H. Stockmayer, *Trans. N.Y. Acad. Sci.*, 13 (1951) 226.
12 K.G. Denbigh, *The Thermodynamics of the Steady State*, Methuen, London, New York, 1951.
13 R. Haase, *Thermodynamik der Irreversiblen Prozesse*, Dr. Dietrich Steinkopf, Darmstadt, 1963.
14 I. Prigogine, *Introduction to Thermodynamics of Irreversible Processes*, Interscience, New York, 1967.
15 H.S. Carslaw and J.C. Jaeger, *Conduction of Heat in Solids*, Clarendon Press, Oxford, 2nd ed., 1986.

16 T. Erdey-Grúz, *Transport Phenomena in Aqueous Solutions*, Akadémiai Kiadó, Budapest, 1974.
17 L. Onsager and R.M. Fuoss, *J. Phys. Chem.*, 36 (1932) 2689.
18 P.W. Atkins, *Physical Chemistry*, Oxford University Press, Oxford, 4th ed., 1990.
19 R.B. Bird, W.E. Stewart and E.N. Lightfoot, *Transport Phenomena*, Wiley, New York, 1960.
20 E.V. Dose and G.A. Guiochon, *Anal. Chem.*, 63 (1991) 1063.
21 A. Ralston, *A First Course in Numerical Methods*, McGraw-Hill, New York, 1965.
22 B. Gaš, M. Demjaněnko and J. Vacík, *J. Chromatogr.*, 192 (1980) 253.
23 B.E. Conway, *Electrochemical Data*, Elsevier, Amsterdam, 1952.

Journal of Chromatography, 644 (1993) 175–182
Elsevier Science Publishers B.V., Amsterdam

CHROM. 25 114

Influence of column temperature and physico-chemical properties on the electrophoretic behaviour of polyglycine peptides in free-solution capillary electrophoresis

Nong Chen*, Lei Wang and Yukui Zhang

National Chromatographic Research & Analysis Centre, Dalian Institute of Chemical Physics, Chinese Academy of Sciences, Dalian 116012 (China)

(First received October 8th, 1992; revised manuscript received March 24th, 1993)

ABSTRACT

The changes in electromigration time with column temperature for polyglycine peptides were found to be due to temperature-induced viscosity changes of water. A quantitative linear relationship between the logarithm of migration times (log t_m) and the reciprocal of column temperature ($1/T$) was derived under a constant electric field strength. The slope of the plot of log t_m *vs.* $1/T$ was directly related to the activation energy of diffusion (AED). It was also found that the effect of column temperature on migration times is much more significant under constant-voltage than under constant-current operation. Polyglycine peptides differing only in size were chosen as model molecules for the test of the mobility model. Systematic correlations between t_m and the number of glycine amino acids (n) were made. A linear relationship between t_m and $n^{0.5}$ was found for polyglycine peptides under different operating modes. It was observed that the extrapolations of the linear relationships between t_m and $n^{0.5}$ with different column temperatures at constant voltage or with different applied currents at constant temperature cross each other at the same point. The parameters m_0 and m_1 in the equation $t_m = m_0 + m_1 n^{0.5}$ were correlated with the column temperature and the operating current. The activation energy of diffusion was also obtained for the plot of log m_1 *versus* $1/T$ at constant voltage. Linear relationships between m_0 and m_1 were found for these peptides which thus result in the intersection point in the plots of t_m *vs.* $n^{0.5}$.

INTRODUCTION

Capillary electrophoresis is a high-resolution technique and free-solution capillary electrophoresis (FSCE) has been demonstrated to be a very useful and operationally simple mode for the analysis of peptides and proteins [1]. Optimization of the electrophoretic behaviour of solutes such as peptides in FSCE requires a deeper understanding of the quantitative relationships between migration parameters and the operating parameters and the intrinsic physical properties of the peptides [2,3].

The column temperature of the capillary plays a significant role in the electrophoretic behaviour of the peptides. Good temperature control is therefore very important for migration reproducibility [4–6].

The separation mechanism in FSCE has been extensively studied [7–13]. The separation mechanism is based on the differential migration of solutes in an electric field due to differences in the charge-to-size ratio of the solutes. Subtle variations in this ratio allow the resolution of peptides with minute differences in structure. Few studies have been published that deal with

* Corresponding author.

0021-9673/93/$06.00

the correlation between migration times and solute physico-chemical properties in FSCE. This originates partly from the lack of a well developed theory for the expected relationships, necessitating simplifying assumptions. It also arises from the difficulty in the estimation of the charge and size of the peptides. Nyberg *et al.* [7] reported a linear correlation between relative migration times *versus* the molecular mass to the 2/3 power divided by the calculated charge (q) for a series of peptides analysed by capillary zone electrophoresis (CZE) in phosphate buffer. Deyl *et al.* [8] also reported a similar correlation for a series of seven cyanogen bromide cleavage fragments from collagens. Grossman and coworkers [9–11] established an empirical correlation for FSCE electrophoretic mobilities in a pH 2.50 buffer with the logarithm of the quantity $q+1$ divided by the number of amino acid residues to the 0.43 power for 40 different peptides. Rickard *et al.* [12] measured electrophoretic mobilities (μ) of several protein digests and correlated the results with different charge-to-size parameters, namely $q/M^{1/3}$, $q/M^{1/2}$ and $q/M^{2/3}$, where M = molecular mass. They found the best fit for μ *vs.* $q/M^{2/3}$.

In this work, the influence of column temperature on the electromigration times of polyglycines was studied. A quantitative relationship between migration times and column temperature is presented, with which the activation energy of diffusion (AED) was derived.

Hydrophilic peptides differing in only glycine amino acids were chosen as model molecules to study the quantitative relationships between migration times and the physico-chemical properties of the peptides. These peptides have been shown to have weak retention in RP-HPLC [14,15]. Systematic correlations of migration times with physico-chemical properties of polyglycine peptides were made using different operation modes.

EXPERIMENTAL

FSCE was conducted on a Spectra-Phoresis-500 system (Spectra-Physics Analytical, Fremont, CA, USA) with a 75 cm × 50 μm I.D. fused-silica capillary column. Prior to use, the column was conditioned with 0.5 M phosphate buffer at 60°C, 50 mM buffer at 20°C and 50 mM buffer at 20°C under a voltage of 25 kV. The column was washed with the separation buffer after each separation. Analytical-reagent grade NaH_2PO_4 was used. Peptides were purchased from Serva (Heidelberg, Germany). Water was doubly distilled. Ultraviolet absorption measurement at 200 nm was used for detection.

RESULTS AND DISCUSSION

Two electrokinetic phenomena, electrophoresis and electroosmosis, occur when an external electric field is applied across an electrolyte-filled capillary column. Electrophoresis is the movement of charged particles in response to the applied field.

The velocity of a particular ion (ν_{ep}) under the influence of an applied electric field strength E is approximately

$$\nu_{ep} = \mu_{ep}E \tag{1}$$

where E ($=V/L$) is the electric field strength, V the applied potential, L the length of the capillary and μ_{ep} the electrophoretic mobility of the ion.

The electrophoretic mobility of a particle is defined as the steady-state velocity per unit field strength. The electrophoretic mobility is of considerable importance in FSCE. The simplest way to describe it is to picture ions moving through the solvent at a steady-state velocity when the electric driving force is exactly balanced by the drag force. Hence, the electrophoretic mobility for spherical particles can be generally expressed by the following equation:

$$\mu_{ep} = q/6\pi\eta a \tag{2}$$

where q is the charge of the particle's ionic cloud, a is the hydrodynamic radius of the species and η is the viscosity of the buffer.

A more accurate mathematical treatment would include a numerical factor [$f(Ka)$]; thus μ_{ep} can be expressed as

$$\mu_{ep} = \frac{q}{6\pi\eta a} f(Ka) \tag{3}$$

where K the reciprocal of the analyte double-layer thickness and $f(Ka)$ depends on Ka of the analyte in the buffer.

In columns where the local electric field strength, E, and the zeta potential are constant and homogeneous throughout the entire column, the bulk electroosmotic velocity ν_{e0} can be expressed as

$$\nu_{e0} = \mu_{eo} E \tag{4}$$

where μ_{eo} is the electroosmotic mobility of buffer, which can be written as

$$\mu_{eo} = \frac{\varepsilon \zeta_c}{\eta} \tag{5}$$

where ζ_c is the zeta potential of the inner wall of the capillary column. The ηs in eqns. 3 and 5 are considered to be identical, hence the net migration equation is given by

$$\nu_m = \frac{E}{\eta}\left[(q/6\pi a) f(Ka) + \varepsilon \zeta_c\right] \tag{6}$$

where ν_m is the net migration velocity. Hence the migration time, t_m, can be expressed as

$$t_m = \frac{L\eta}{E\left[\zeta_c \varepsilon + \dfrac{q}{6\pi a} f(Ka)\right]} \tag{7}$$

The column temperature (T) can potentially be an important factor in FSCE. Precise control of the temperature is essential for obtaining adequate precision of the migration time. Examination of eqn. 7 reveals that no term except η is temperature dependent, the changes in ε, ζ_c and $f(Ka)$ as a function of T being negligibly small. Therefore, the changes in electromigration time with column temperature in FSCE are predominantly due to the temperature-induced viscosity changes of water. Viscosity has been extensively studied in electrochemistry. The viscosity of a liquid usually has a temperature dependence that is fairly well represented by an equation of the form [16]

$$\eta = A_0 \cdot 10^{\frac{\Delta E_a}{RT}} \tag{8}$$

where ΔE_a is the activation energy of diffusion, often of the order of one third of the heat of vaporization, and A_0 is the pre-exponential factor and is a constant often called the frequency factor.

Therefore, under constant electric field strength, the quantitative correlation between migration times (t_m) and column temperature is derived as

$$t_m = A \cdot 10^{\frac{\Delta E_a}{RT}} \tag{9}$$

where A is a constant. Therefore, under a constant field strength, a linear relationship between the logarithm of migration time and the reciprocal column temperature is derived:

$$\log t_m = \log A + B/T \tag{10}$$

where A (see eqn. 9) and B are constants and can be written as

$$A = A_0 L / E\left[\varepsilon \zeta_c + \frac{q}{6\pi a} f(Ka)\right] \tag{11}$$

$$B = \Delta E_a / R \tag{12}$$

Table I gives the values of log A, B, A and ΔE_a for five polyglycines under constant voltage operation. Correlation coefficients (r) are also given.

As can be seen from Table I, excellent correlations were observed for log t_m *versus* $1/T$. The data appear to fit a straight line with nearly the same slope; for $(gly)_3$, with a slope of $0.0716 \cdot 10^4$ K,

$$E_a = R \cdot \text{slope} = (8.314\ \text{J/mol} \cdot \text{K})(0.0716 \cdot 10^4\ \text{K})$$
$$= 5.953\ \text{kJ/mol}$$

The activation energies of diffusion do not change very much with the different peptides, showing the parallel electrophoretic behaviour of migration time *versus* column temperature for these peptides. Therefore, in the temperature range investigated, parallel electrophoretic behaviour in the plots of log t_m *vs.* $1/T$ was found, which indicates that the relative migration times or electrophoretic selectivity factors do not vary with the column temperature [6].

The activation energy of diffusion obtained in this paper is of the order of one sixth of the heat of vaporization of water. The heat of vaporization for water is about 40.6 kJ/mol. Therefore, the plots of log t_m *vs.* $1/T$ under constant electric

TABLE I

LOG A, B, ACTIVATION ENERGY OF DIFFUSION (ΔE_a) AND PRE-EXPONENTIAL FACTOR (A) FOR FIVE POLYGLYCINE PEPTIDES

At constant voltage, 25 kV; column, 75 cm × 75 μm I.D., fused silica; buffer; 50 mM phosphate buffer (pH 2.5). Migration times used for regression were taken from ref. 17.

Peptide	log A	B	r	A	ΔE_a(kJ/mol)
$(Gly)_2$	−1.478	724.70	0.9989	0.0333	6.03
$(Gly)_3$	−1.397	716.00	0.9987	0.0401	5.95
$(Gly)_4$	−1.398	730.24	0.9988	0.040	6.07
$(Gly)_5$	−1.388	738.00	0.9989	0.0409	6.14
$(Gly)_6$	−1.390	747.30	0.9987	0.0407	6.21

field strength offer a method for the calculation of the activation energy of diffusion in FSCE. The pre-exponential factor has little effect on the temperature dependence of the migration time.

Under constant-current operation, if the voltage does not change significantly with column temperature, an approximately linear relationship between log t_m and $1/T$ can also be found. However, the linear correlations of log t_m *versus* $1/T$ are not better with constant-current operation. The regression results for the five peptides at constant current are as follows:

$(gly)_2$: $\log t_m = 158.94/T + 0.470$ $(r = 0.9739)$

$(gly)_3$: $\log t_m = 157.06/T + 0.531$ $(r = 0.9713)$

$(gly)_4$: $\log t_m = 158.96/T + 0.573$ $(r = 0.9712)$

$(gly)_5$: $\log t_m = 159.07/T + 0.610$ $(r = 0.9693)$

$(gly)_6$: $\log t_m = 157.12/T + 0.647$ $(r = 0.9641)$

There are at least two aspects that should be stated explicitly when examining the influence of temperature on migration times at constant applied current (I). First, at the constant I, an increase in temperature would increase the mobility by decreasing the buffer viscosity, whereas as the temperature is increased the solution resistance decreases and the voltage required to maintain a constant current would decrease, which could counteract the effect of increased mobility with increasing temperature. In contrast, at constant voltage (E = constant), an increase in temperature would increase the mobility by decreasing the viscosity, which results in a decrease in migration times. Therefore, the effect of column temperature on migration times is much more significant under constant-voltage than under constant-current operation in FSCE. Therefore, the temperature effect in FSCE is different from that in RP-HPLC [18].

Figs. 1 and 2 show the electropherograms of these peptides under constant-voltage and constant-current operation.

In order to explore the relationships between the peptides' migration and physico-chemical parameters in FSCE, peptides differing only in glycine amino acids were chosen as model mole-

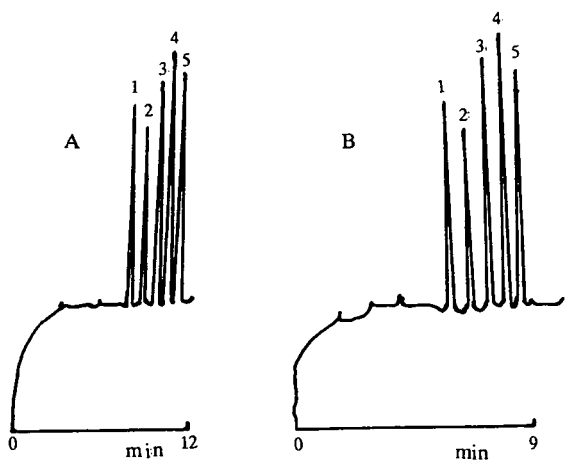

Fig. 1. Electropherograms of five hydrophilic peptides at applied column temperatures of (A) 30°C and (B) 50°C at constant voltage (25 kV). Peaks: 1 = $(gly)_2$; 2 = $(gly)_3$; 3 = $(gly)_4$; 4 = $(gly)_5$; 5 = $(gly)_6$.

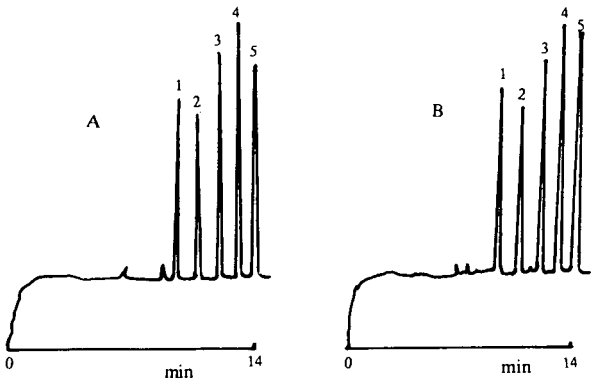

Fig. 2. Electropherograms of five peptides at the applied column temperatures of (A) 30°C and (B) 50°C at constant current (80 μA). Peaks: 1 = $(gly)_2$; 2 = $(gly)_3$; 3 = $(gly)_4$; 4 = $(gly)_5$; 5 = $(gly)_6$.

cules to study the mobility model. As the charges for these species are nearly identical, this series could be a good test for a mobility model to characterize the electrophoretic systems. They are much like homologous series in chromatography.

As the separation was performed at pH 2.5, the electroosmotic flow was negligible. The migration times were therefore not corrected for electroosmotic flow in this present study.

From eqn. 2, the electrophoretic mobility is directly related to the radius of the species. To investigate the dependence of migration times on peptide size, these peptides were treated as a classical polymer in solution. For an unperturbed random coil, the simplest model of a freely joined chain can be used. The hydrodynamic radius is given by

$$a = bn^{0.5} \tag{13}$$

where b is the apparent size of an individual monomer unit and n the number of single units in the polymer, here referring to the number of amino acid residues.

For a series of polyglycines, the net charges are equal according to the Henderson–Hasselbach equation [19]. Therefore, for the equally charged polyglycine peptides, substituting eqn. 13 into eqn. 2, the migration times have the following linear relationship with respect to n:

$$t_m = m_0 + m_1 n^{0.5} \tag{14}$$

where m_0 and m_1 are constants; m_0 is the extrapolated t_m value for $n = 0$ and the slope m_1 is

$$m_1 = 6\pi b\eta L/qE \tag{15}$$

In order to test the validity of eqn. 14, migration times of these peptides in different operating modes were plotted as functions of operating parameters in FSCE. The results are shown in Figs. 3–5 and in Tables II and III.

Table II shows the variation of the migration times of (gly)n peptides with the column temperature under constant-current operation in FSCE. Table III shows the variation of t_m of these peptides with the different applied currents at constant temperature for these peptides. The parameters m_0 and m_1 and the correlation coefficients r are also given.

As can be seen from these tables, the correlation coefficients of the linear fit all approached 1.0. Therefore, for a series of equally charged polyglycines, linear relationships between t_m and $n^{0.5}$ were obtained, and this correlation holds

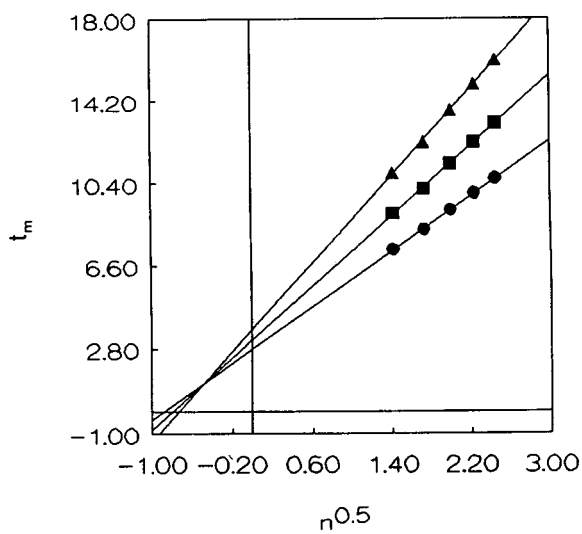

Fig. 3. Linear plots of t_m *versus* $n^{0.5}$ for a series of polyglycines at constant voltage at different column temperatures: ▲ = 15; ■ = 25; ● = 35°C. Electrophoretic conditions as in Table I. Regression results: (▲) $t_m = 3.66 + 5.05n^{0.5}$ (r = 0.9995); (■) $t_m = 3.21 + 4.05n^{0.5}$ ($r = 0.9995$); (●) t_m = $2.80 + 3.19n^{0.5}$ ($r = 0.9996$).

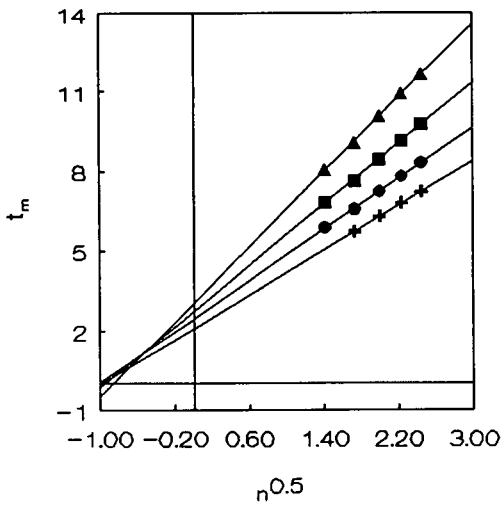

Fig. 4. Linear relationships between t_m and $n^{0.5}$ for hydrophilic peptides at constant voltage at different column temperatures: ▲ = 30; ■ = 40; ● = 50; + = 60°C. Other conditions as in Table I. Regression results: (▲) $t_m = 3.02 + 3.52n^{0.5}$ ($r = 0.9994$); (■) $t_m = 2.71 + 2.87n^{0.5}$ ($r = 0.9996$); (●) $t_m = 2.44 + 2.40n^{0.5}$ ($r = 0.9996$); (+) $t_m = 2.07 + 2.11n^{0.5}$ ($r = 0.9999$).

even with the use of different column temperatures and different applied currents (see Figs. 3–5).

Figs. 3 and 4 demonstrate a set of linear relationships between migration times and $n^{0.5}$

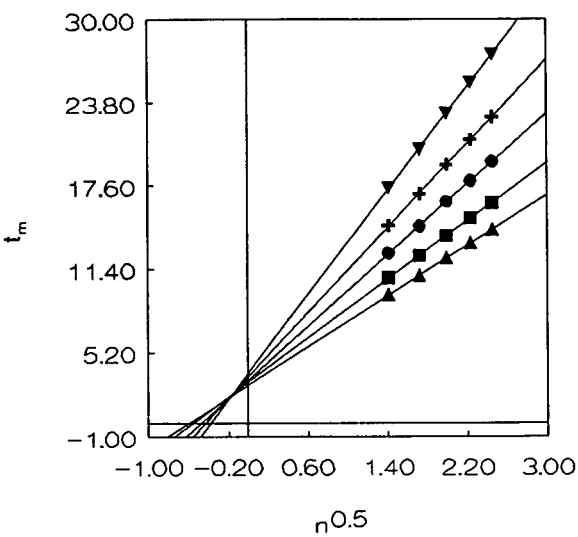

Fig. 5. Linear correlations of t_m *versus* $n^{0.5}$ for five peptides at constant temperature with different applied currents: ▲ = 100; ■ = 90; ● = 80; + = 70; ▼ = 60 μA. For electrophoretic conditions and correlation results, see Table III.

for the five polyglycines with different temperatures at constant voltage. Fig. 5 illustrates a series of straight lines for t_m *versus* $n^{0.5}$ with different applied currents at constant temperature.

As can be clearly seen, the best linear correlations were obtained when the migration times were plotted against $n^{0.5}$. The plots show good linear correlations.

The slope (m_1) at constant voltage, which mainly characterizes the viscosity of the running buffer, decreases with increasing column temperature for the peptides. Hence m_1 can also be written as

$$m_1 = A_1 \cdot 10^{\frac{\Delta E_a}{RT}} \quad (16)$$

and a linear correlation between log m_1 and $1/T$ is obtained under a constant electric field strength:

$$\log m_1 = \log A_1 + B_1/T \quad (17)$$

where $A_1 = 6\pi bLA_0/qE$ and $B_1 = \Delta E_a/R$. Therefore, the slope m_1 in the plot of t_m *vs.* $n^{0.5}$ can also be directly related to the activation energy of diffusion. A linear log m_1 *vs.* $1/T$ plot has been obtained with a slope of 826.15 K (see Fig. 6). Therefore, ΔE_a calculated from the plot of log m_1 *versus* $1/T$ is 6.87 kJ/mol, which is higher than that obtained from log t_m *vs.* $1/T$ plots.

It can be seen from Tables II and III that a non-zero intercept was found in plots of t_m *versus* $n^{0.5}$. The intercept represents extrapolated values of t_m for $n = 0$ species, and its non-zero value probably reflects the migration properties of this series of peptides at $n = 0$. Under the given operating conditions, this value is constant. From the regression results in Figs. 3 and 4, the log m_0 values are quantitatively correlated with the reciprocal of column temperature, which implies that there is a linear correlation between m_1 and m_0 under constant-voltage operation. The regression equations for log m_1 and log m_0 *versus* $1/T$ are

$$\log m_0 = 510.10/T - 1.202 \ (r = 0.9951)$$

$$\log m_1 = 826.15/T - 2.168 \ (r = 0.9973)$$

With different applied currents at constant temperature, the reciprocals of m_0 and m_1 are

TABLE II

EFFECT OF COLUMN TEMPERATURE ON MIGRATION TIMES AT CONSTANT APPLIED CURRENT AND THE PARAMETERS m_0 AND m_1 FOR FIVE PEPTIDES

Constant current, 80 μA; other conditions as in Table I.

Temperature (°C)	Migration time (min)					m_0	m_1	r
	$(Gly)_2$	$(Gly)_3$	$(Gly)_4$	$(Gly)_5$	$(Gly)_6$			
20	10.18	11.56	12.93	14.10	15.13	3.29	4.83	0.9996
25	9.92	11.23	12.54	13.65	14.63	3.37	4.59	0.9996
30	10.00	11.34	12.66	13.80	14.80	3.33	4.67	0.9996
35	9.66	10.97	12.26	13.36	14.33	3.18	4.55	0.9996
40	9.63	10.94	12.22	13.33	14.35	3.08	4.58	0.9996
50	9.17	10.42	11.64	12.68	13.63	2.99	4.33	0.9997
60	8.72	9.9	11.04	12.03	12.91	2.91	4.07	0.9997

linearly related to the applied current, which indicates that there is a linear m_0 *vs.* m_1 plot (see Fig. 7). The regression equations for $1/m_0$ and $1/m_1$ and the current are

$$1/m_1 = 0.00276I - 0.0652 \ (r = 0.9977)$$

$$1/m_0 = 00205I + 0.150 \ (r = 0.9985)$$

where I is the applied current.

The linear correlation for m_0 *vs.* m_1 indicates that the extrapolation of the t_m *vs.* $n^{0.5}$ plots for polyglycines at different temperatures at constant voltage or with different currents at constant temperature leads to a common intersection point, characterizing another feature of these peptides (see Figs. 3–5). Further elucidation to understanding this convergence point is required.

CONCLUSIONS

Logarithms of migration times in FSCE are quantitatively correlated with the reciprocal of column temperature under a constant electric field strength. The slope of the log t_m *vs.* $1/T$ plots has been directly correlated with the activation energy of diffusion. The electromigration

TABLE III

VARIATION OF THE MIGRATION TIMES WITH APPLIED CURRENT AT CONSTANT COLUMN TEMPERATURE AND COEFFICIENTS m_0 AND m_1 FOR FIVE PEPTIDES

Constant column temperature, 20°C; other conditions as in Table I.

I(μA)	Migration time (min)					m_0	m_1	r
	$(Gly)_2$	$(Gly)_3$	$(Gly)_4$	$(Gly)_5$	$(Gly)_6$			
100	9.48	10.91	12.21	13.33	14.32	2.82	4.70	0.9999
90	10.71	12.35	13.86	15.15	16.30	3.01	5.42	0.9999
80	12.56	14.56	16.39	17.96	19.39	3.16	6.62	0.9999
70	14.60	16.97	19.15	21.03	22.72	3.41	7.87	0.9999
60	17.43	20.32	22.99	25.31	27.40	3.68	9.67	0.9999

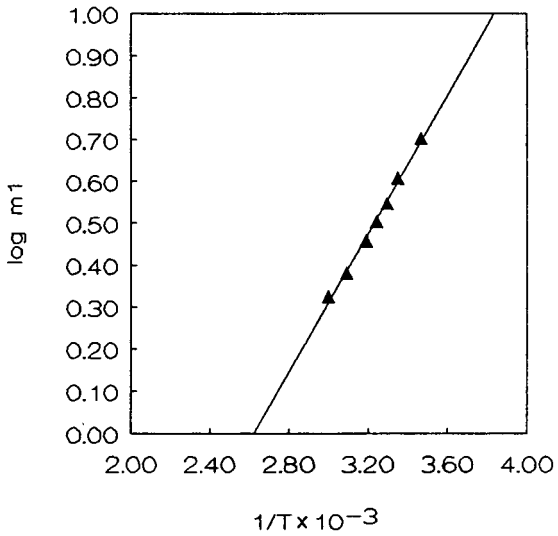

Fig. 6. Linear plot of log m_1 in the equation $t_m = m_0 + m_1 n^{0.5}$ *versus* the reciprocal of column temperature ($1/T$). For other conditions, see Table I. Parameters m_0 and m_1 were taken from Fig. 3 and 4. The regression equation is log $m_1 = (867.15/T) - 2.168$ ($r = 0.9973$).

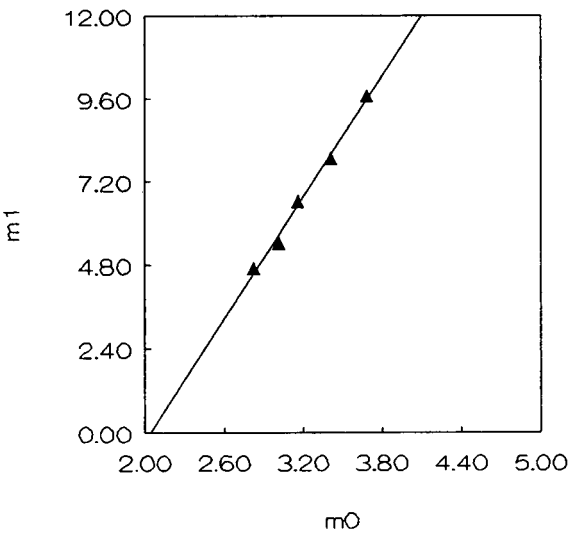

Fig. 7. Linear relationship between the parameters m_1 and m_0 in the equation $t_m = m_0 + m_1 n^{0.5}$ at constant column temperature with different applied currents. For details, see Table III. The regression equation is $m_1 = 5.85 m_0 - 11.97$ ($r = 0.9964$).

times can be correlated from the physico-chemical properties of these peptides. The proposed linear relationships between t_m and $n^{0.5}$ for five polyglycines are very useful for elucidating the migration mechanism in FSCE. The application of this knowledge can then be combined with other basic relationships to develop optimized separation methods using FSCE.

REFERENCES

1 J.N. Jorgenson and K.D. Lukacs, *Science*, 222 (1983) 266.
2 H.J. Issaq, I.Z. Atamna, G.M. Muschik and G.M. Janini, *Chromatographia*, 32 (1991) 155.
3 I.Z. Atamna, H.J. Issaq, G.H. Muschik and G.M. Janini, *J. Chromatogr.*, 588 (1991) 315.
4 R.S. Rush, A.S. Cohen and B.L. Karger, *Anal. Chem.*, 63 (1991) 1346.
5 C.W. Whang and E.S. Yeung, *Anal. Chem.* 64 (1992) 502.
6 N. Chen, L. Wang and Y.K. Zhang, *J. Liq. Chromatogr.*, in press.
7 F. Nyberg, M.D. Zhu, J.L. Liao and S. Hjerten, in C. Schafer-Nielsen (Editor), *Electrophoresis '88*, VCH, Weinheim, 1988, pp. 141–150.
8 Z. Deyl, V. Rohlicek and M. Adam, *J. Chromatogr.*, 480 (1989) 371.
9 P.D. Grossman, J.C. Colburn and H.H. Lauer, *Anal. Biochem.*, 179 (1979) 28.
10 P.D. Grossman, K.J. Wilson, G. Petrie and H.H. Lauer, *Anal. Biochem.*, 173 (1988) 265.
11 P.D. Grossman, J.C. Colburn, H.H. Lauer, R.G. Nielsen, R.M. Riggin, G.S. Sittampalam and E.C. Rickard, *Anal. Biochem.*, 179 (1989) 28.
12 E.C. Rickard, M.M. Strohl and R.G. Nielsen, *Anal. Chem.*, 61 (1989) 1186.
13 H.J. Issaq, G.M. Janini, I.Z. Atamna, G.M. Muschik and J. Lukszo, *J. Liq. Chromatogr.*, 15 (1992) 1129.
14 H.F. Zou, Y.K. Zhang and P.C. Lu, *Chin. J. Chromatogr.*, 9 (1991) 257.
15 H.F. Zou, Y.K. Zhang, L.F. Dong and P.C. Lu, *Chromatographia*, 31 (1991) 27.
16 R.S. Berry, S.A. Rice and J. Ross, *Physical Chemistry*, Wiley, New York, 1980.
17 Y.K. Zhang, N. Chen and L. Wang, *Biomed. Chromatogr.*, 7 (1993) 75.
18 N. Chen, Y.K. Zhang and P.C. Lu, *J. Chromatogr.*, 603 (1992) 35.
19 B. Skoog and A. Wichman, *Trends Anal. Chem.*, 5 (1986) 82.

Journal of Chromatography, 644 (1993) 183–187
Elsevier Science Publishers B.V., Amsterdam

CHROM. 25 215

Short Communication

Adsorption isotherm of undissociated eluent acid and its relation to the retention of system peaks in non-suppressed ion chromatography

Atushi Yamamoto*, Akinobu Matsunaga and Eiichi Mizukami

Toyama Institute of Health, 17-1, Nakataikoyama, Kosugi-machi, Toyama 939-03 (Japan)

Kazuichi Hayakawa and Motoichi Miyazaki

Faculty of Pharmaceutical Sciences, Kanazawa University, 13-1, Takara-machi, Kanazawa 920 (Japan)

(Received March 9th, 1993)

ABSTRACT

The formation of a system peak in non-suppressed ion chromatography is related to the adsorption of undissociated eluent acid onto the functionalized resin surface. To clarify the elution behaviour of system peaks, a new method for determining the isotherms from the capacity factors of system peaks using low-pH eluents free from sodium ions was developed. The isotherms for adsorption of undissociated salicylic and phthalic acids as eluents onto an IC-Anion-PW column, measured by the present method, showed two-site biLangmuir correlations. The capacity factors of system peaks calculated from the equations based on these isotherms were in good agreement with those from actual chromatograms with the acidic eluent conditions.

INTRODUCTION

In non-suppressed ion chromatography (IC), the injection of a sample may result in an extraneous peak depending on the eluent conditions [1]. This peak is called a system peak. Some attempts to eliminate systems peaks from chromatograms have been made because they distort the baseline [2,3]. In addition, selective peak enhancement analyses for the analyte whose elution is close to the system peak have also been investigated [4,5]. We have already discovered that the interaction between undissociated, neutral eluent acid and the surface of the column packing material forms the system peak [6]. This formation mechanism suggests that prediction of the retention of system peaks by an equation based on an ion-exchange model is impossible, and that the optimization of chromatographic resolution between analyte and system peaks must be made experimentally. Recently, we established a retention model of a multiple eluent system [7], but the retention volume of the system peak was indispensable for a prediction of analyte peak intensity based on this model. It is no exaggeration to say that the

* Corresponding author.

0021-9673/93/$06.00

only thing left to clarify in non-suppressed IC is the behaviour of the system peak.

Considering that the system peak is formed by the adsorption of an eluent component on the resin surface, the clarification of the isotherm may elucidate its elution behaviours. However, the existence of an ion-exchange resin functional group has made it difficult to accurately determine the adsorption isotherms by a traditional static method. In this paper, we establish a technique to determine the isotherms for adsorption of undissociated eluent acid onto low-capacity, surface-functionalized anion exchangers from the actual chromatograms and attempt to predict theoretically the behaviour of the system peak.

THEORY

In our previous publication [6] we introduced the relationship between the apparent distribution ratio of undissociated acid in the two phases ($K_d \cdot \phi$) and the capacity factor of the system peak (k'_e) with low-pH eluents free from counterions such as the sodium ion when the eluent is a monoprotic acid, EH:

$$K_d \cdot \phi = (2[H^+] + K_{ae})k'_e/2[H^+] \quad (1)$$

where K_{ae} is the dissociation constant of the eluent acid, ϕ is the phase ratio of the column and square brackets represent the concentration. The distribution ratio defined in eqn. 1 means the ratio of changed fractions between the undissociated acid adsorbed on the resin and dissolved in the eluent. This is the differential value for the adsorption isotherm of the undissociated eluent with respect to its concentration in the eluent, [EH]. Thus, the integration of the function between the two variables, [EH] and $K_d \cdot \phi$, calculated from actual chromatograms under low-pH eluent conditions, gives the adsorption isotherm. The isotherms obtained from eqn. 1 are related to the quantity of eluent acid, not to the concentration, because eqn. 1 contains the phase ratio.

When the eluent is the diprotic acid, EH_2, k'_e is determined using the following equation:

$$k'_e = d[EH_2]_s\phi/(d[EH_2]_m + d[EH^-]_m + d[E^{2-}]_m)$$

where the subscripts m and s represent the existence of bracketed species in the mobile and stationary phases, respectively. Substitution of K_d into this equation gives:

$$k'_e = d[EH_2]_m K_d \cdot \phi/(d[EH_2]_m + d[EH^-]_m + d[E^{2-}]_m) \quad (2)$$

In the acidic eluent free from sodium ion, the charge balance is indicated by:

$$[H^+] = [EH^-]_m + 2[E^{2-}]_m$$

Introduction of the first and second dissociation constants of eluent, K_{ae1} and K_{ae2}, into this equation gives the concentrations for every eluent species:

$$[E^{2-}]_m = [H^+]K_{ae2}/([H^+] + 2K_{ae2})$$

$$[EH^-]_m = [H^+]^2/([H^+] + 2K_{ae2})$$

$$[EH_2]_m = [H^+]^3/K_{ae1}([H^+] + 2K_{ae2})$$

If the hydrogen ion concentration, $[H^+]$, is much larger than K_{ae2}, the following equations are deduced:

$$d[E^{2-}]_m = 0$$

$$d[EH^-]_m = [H^+] - [H^+_x]$$

$$d[EH_2]_m = ([H^+]^2 - [H^+_x]^2)/K_{ae1}$$

where the subscript x represents the existence in the system peak zone. Substitution of these equations into eqn. 2 gives:

$$K_d \cdot \phi = (2[H^+] + K_{ae1})k'_e/2[H^+] \quad (3)$$

This equation is the same as eqn. 1, and means that, in cases of triprotic or higher protic acid eluents, the apparent distribution ratio can be calculated from eqn. 3 when $[H^+]$ is much larger than K_{ae2}.

EXPERIMENTAL

The IC system consisted of a Shimadzu (Kyoto, Japan) LC-5A pump, a Rheodyne (Cotati, CA, USA) Model 7125 injector and a Shimadzu SPD-6AV UV–visible detector. Chromatographic separation was performed on a 5 cm × 4.6 mm I.D. column packed with a low-

capacity anion exchanger (Tosoh, Tokyo, Japan, TSK gel IC-Anion-PW, 0.03 mequiv./ml) maintained at 25°C. Salicylic acid solution as a monoprotic eluent and phthalic acid solution as a diprotic one were delivered at various concentrations. k'_e was measured by injecting water and concentrated eluents.

RESULTS AND DISCUSSION

Values for k'_e measured at various concentrations of salicylate and phthalate eluents free from sodium ions and the distribution ratios, which denote the slopes of the isotherm as previously mentioned, calculated from eqns. 1 and 3, are summarized in Tables I and II, respectively. Both isotherms, the slopes of which become steep as the concentrations of the undissociated acids decrease and converge to constants at high concentrations, have the shapes expected of a Langmuir isotherm. Consequently, the relations between $K_d \cdot \phi$ and [EH] were estimated by conforming to the following Langmuir differential equation

$$K_d \cdot \phi = a \cdot b/(1 + b[EH])^2 \quad (4)$$

where a is a parameter related to maximum adsorption and b is related to heat of adsorption. Eqn. 4 means that log $(K_d \cdot \phi)$ is log $a \cdot b$ when [EH] is small enough to be negligible and converges to a line having a slope of −2 as [EH] becomes large. The values in Tables I and II are plotted as the logarithm of $K_d \cdot \phi$ *versus* the logarithm of [EH] in Fig. 1. However, neither plot showed the tendency predicted by eqn. 4. On the other hand, the solid lines in Fig. 1 are the values calculated from the following equations based on a two-site biLangmuir model.

TABLE I

EXPERIMENTAL DATA OF CAPACITY FACTOR FOR SYSTEM PEAK WITH SALICYLATE ELUENT CONCENTRATION AND DISTRIBUTION RATIO CALCULATED FROM EQN. 1

Salicylate concentration (M)	k'_e	Undissociated eluent (M)	$K_d \cdot \phi$
$1.0 \cdot 10^{-4}$	85.2	$7.20 \cdot 10^{-6}$	636
$3.0 \cdot 10^{-4}$	45.0	$5.15 \cdot 10^{-5}$	153
$5.0 \cdot 10^{-4}$	37.3	$1.20 \cdot 10^{-4}$	96.2
$1.0 \cdot 10^{-3}$	31.8	$3.51 \cdot 10^{-4}$	61.1
$1.5 \cdot 10^{-3}$	30.8	$6.30 \cdot 10^{-4}$	52.1
$2.0 \cdot 10^{-3}$	29.6	$9.39 \cdot 10^{-4}$	46.5
$3.0 \cdot 10^{-3}$	27.2	$1.61 \cdot 10^{-3}$	38.9
$5.0 \cdot 10^{-3}$	25.5	$3.08 \cdot 10^{-3}$	33.4

TABLE II

EXPERIMENTAL DATA OF CAPACITY FACTOR FOR SYSTEM PEAK WITH PHTHALATE ELUENT CONCENTRATION AND DISTRIBUTION RATIO CALCULATED FROM EQN. 3

Phthalate concentration (M)	k'_e	Undissociated eluent (M)	$K_d \cdot \phi$
$2.0 \cdot 10^{-4}$	106	$2.27 \cdot 10^{-5}$	502
$3.0 \cdot 10^{-4}$	73.4	$4.65 \cdot 10^{-5}$	268
$5.0 \cdot 10^{-4}$	47.8	$1.10 \cdot 10^{-4}$	141
$7.0 \cdot 10^{-4}$	30.8	$1.89 \cdot 10^{-4}$	78.9
$1.0 \cdot 10^{-3}$	21.4	$3.28 \cdot 10^{-4}$	43.3
$1.2 \cdot 10^{-3}$	17.2	$4.30 \cdot 10^{-4}$	33.0
$1.5 \cdot 10^{-3}$	14.4	$5.94 \cdot 10^{-4}$	24.8
$3.0 \cdot 10^{-3}$	9.0	$1.51 \cdot 10^{-3}$	13.2
$4.5 \cdot 10^{-3}$	7.8	$2.60 \cdot 10^{-3}$	9.4

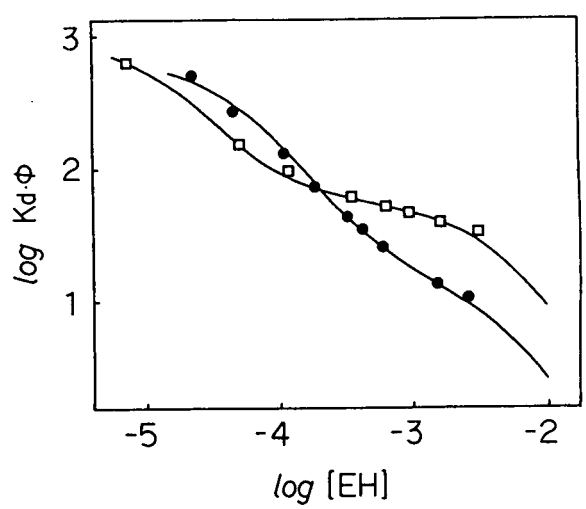

Fig. 1. Fit of differential value (solid lines) of adsorption isotherm based on biLangmuir model to calculated distribution ratio (points). ● = Phthalate eluent; □ = salicylate eluent.

They are in good agreement with the observed results:

$$\{SaH\}_s = 1010\{SaH\}_m/(1 + 44700\{SaH\}_m) + 62.0\{SaH\}_m/(1 + 161\{SaH\}_m)$$

$$\{PhH\}_s = 700\{PhH\}_m/(1 + 12500\{PhH\}_m) + 18.1\{PhH\}_m/(1 + 166\{PhH\}_m)$$

where the braces (curly brackets) represent the quantities of undissociated salicylic (SaH) and phthalic acid (PhH) eluents. The adsorption isotherms of these acids on the unfunctionalized IC-Anion-PW packing material were found to obey the Langmuir equation in the previous publication [6]. These isotherms and the second terms in the above-stated biLangmuir equations had a similar tendency, though different in their dimensions. This result suggested that the functionalization of resin produced a different, stronger adsorption site for the undissociated eluent.

By using these isotherms obtained from the present technique, the prediction of elution behaviours of a system peak was attempted. k'_e for a monoprotic eluent is calculated from the following equation:

$$k'_e = d[EH]_m K_d \cdot \phi/(d[EH]_m + d[E^-]_m) \quad (5)$$

In the acidic eluent, where $[OH^-]$ is negligible, since $[H^+] = [E^-] - [Na^+]$, $[EH]_m$ is defined by the following equation:

$$[EH]_m = (K_{ae} + 2[ET]_m - [Na^+] - (([Na^+] - K_{ae})^2 + 4[ET]_m K_{ae})^{1/2})/2$$

where [ET] is the concentration of the total eluent species. When [ET] is higher than K_{ae}, since $([Na^+] - K_{ae})^2 \ll 4[ET]K_{ae}$, the numeration in eqn. 5 is simplified to:

$$d[EH]_m \fallingdotseq [ET]_m - [ET_x]_m - K_{ae}^{1/2}([ET]_m^{1/2} - [ET_x]_m^{1/2})$$

On the other hand, since the denominator in eqn. 5 is $[ET]_m - [ET_x]_m$, eqn. 5 is rearranged by substituting these equations as follows;

$$k'_e = K_d \cdot \phi(1 - (K_{ae}/[ET]_m)^{1/2}/2) \quad (6)$$

This equation means that, in the monoprotic eluent, k'_e depends on the distribution ratio.

k'_e for the diprotic eluent is calculated from eqn. 2. From the mass and charge balances in the acidic eluent:

$$[EH_2]_m = ([H^+]^3 + [Na^+][H^+])/(K_{ae1}[H^+] + 2K_{ae1}K_{ae2})$$

$$[ET]_m = ([H^+] + [Na^+])([H^+]^2 + K_{ae1}[H^+] + K_{ae1}K_{ae2})/(K_{ae1}[H^+] + 2K_{ae1}K_{ae2})$$

Substitution of these equations into eqn. 2 gives:

$$k'_e = K_d \cdot \phi(2[H^+]^3 + (6K_{ae2} + [Na^+])[H^+]^2 + 4K_{ae2}[Na^+][H^+])/(2[H^+]^3 + (K_{ae1} + 6K_{ae2} + [Na^+])[H^+]^2 + 4K_{ae2}(K_{ae1} + [Na^+])[H^+] + K_{ae1}K_{ae2}(2K_{ae2} + [Na^+]))$$

Solving for the factors by ignoring the smaller factors, this equation is simplified to:

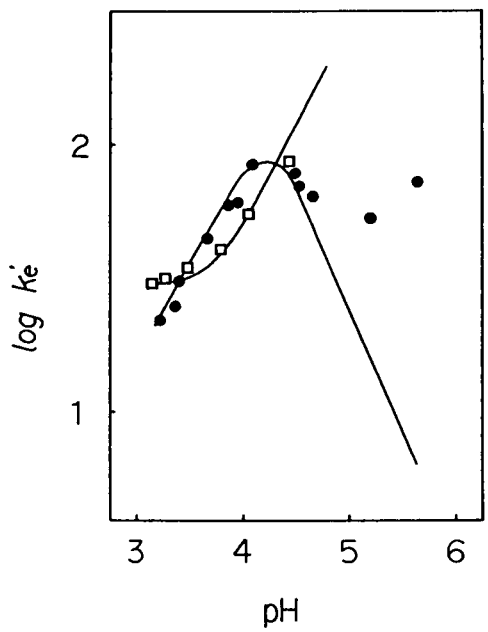

Fig. 2. Comparison between the calculated (solid lines) and experimental (points) capacity factors of system peak by changing the eluent pH. ● = 1 m*M* phthalate eluent; □ = 2 m*M* salicylate eluent.

$$k'_e = K_d \cdot \phi(2[H^+]^2 + [Na^+][H^+])/(2[H^+] + (K_{ae1} + [Na^+])[H^+] + K_{ac1}K_{ae2}[Na^+]/([H^+] + 4K_{ac2})) \quad (7)$$

This equation means that, in the diprotic eluent, k'_e is strongly affected by pH.

With 2 mM salicylate as a monoprotic acid eluent and 1 mM phthalate as a diprotic acid eluent, comparison between the actual and calculated capacity factors of system peak by changing the eluent pH is shown in Fig. 2. In the salicylate eluent, the elution behaviour of system peak was well elucidated by eqn. 6. In the phthalate eluent, changes in the eluent pH produced curious changes in k'_e. This observation (in Fig. 2) is in agreement with that by Jackson and Haddad [8]. Calculation from eqn. 7 showed a convex curve that was in close agreement with the observed values at pH values below 4.7. But the increase in k'_e observed at pH values above 4.7, when the concentration of undissociated phthalic acid is less than 10^{-5} M, cannot be explained by eqn. 7. In this pH region, the adsorption of dissociated acid such as the Donnan dialysis may be considered. For the prediction of k'_e, however, it is of little importance in this region, because the elution of system peak was very delayed and the response of the analyte peak reached a state of "standardization" in the indirect photometric detection [9].

Overall, it is possible to determine the adsorption isotherms of undissociated eluent acid onto the functionalized resin of an ion-exchange column by using k'_e in the low-pH eluent. The equations based on the isotherms thus obtained elucidate the behaviour of a system peak in non-suppressed IC with usual eluents in which counter-ions such as sodium ion exist. This result contributes much to the optimization of non-suppressed ion chromatographic separation in cooperation with our latest investigation on the prediction of the analyte capacity factor and intensity in a multiple eluent system [7].

REFERENCES

1 M. Denkart, L. Hackzell, G. Schill and E. Sjögren, *J. Chromatogr.*, 218 (1981) 31.
2 I. Yoshida, K. Hayakawa and M. Miyazaki, *Nippon Kagaku Kaishi*, (1986) 1046.
3 N. Hamada and T. Yagi, *Bunseki Kagaku*, 39 (1990) 411.
4 A. Yamamoto, A. Matsunaga, E. Mizukami, K. Hayakawa and M. Miyazaki, *Jpn. J. Toxicol. Environ. Health*, 36 (1990) 332.
5 K. Hayakawa, A. Kato, A. Yamamoto and M. Miyazaki, *Anal. Sci.*, 8 (1992) 25.
6 A. Yamamoto, A. Matsunaga, M. Ohto, E. Mizukami, K. Hayakawa and M. Miyazaki, *J. Chromatogr.*, 482 (1989) 145.
7 A. Yamamoto, K. Hayakawa, A. Matsunaga, E. Mizukami and M. Miyazaki, *J. Chromatogr.*, 627 (1992) 17.
8 P.E. Jackson and P.R. Haddad, *J. Chromatogr.*, 346 (1985) 125.
9 D.R. Jenke, *Anal. Chem.*, 56 (1984) 2468.

Journal of Chromatography, 644 (1993) 188–192
Elsevier Science Publishers B.V., Amsterdam

CHROM. 25 216

Short Communication

Preparative separation of higher fullerenes by high-performance liquid chromatography on a tetrachlorophthalimidopropyl-modified silica column

Daniel Herren

Institut für Anorganische, Analytische und Physikalische Chemie, Universität Bern, Freiestrasse 3, CH-3000 Berne 9 (Switzerland)

Carlo Thilgen

Laboratorium für Organische Chemie, ETH-Zentrum, Universitätstrasse 16, CH-8092 Zurich (Switzerland)

Gion Calzaferri*

Institut für Anorganische, Analytische und Physikalische Chemie, Universität Bern, Freiestrasse 3, CH-3000 Berne 9 (Switzerland)

François Diederich

Laboratorium für Organische Chemie, ETH-Zentrum, Universitätstrasse 16, CH-8092 Zurich (Switzerland)

(First received January 22nd, 1993; revised manuscript received April 20th, 1993)

ABSTRACT

The preparative chromatographic separation of buckminsterfullerene (C_{60}) and the larger, related carbon spheres C_{70}, C_{76}, C_{2v}- and D_3-C_{78} and C_{84} on a tetrachlorophthalimidopropyl-modified silica stationary phase was achieved and quantified. A 1-mg amount of a mixture of the higher fullerenes per injection can be separated on a 250 mm × 20 mm I.D. column using dichloromethane–hexane (33:67, v/v) as the mobile phase and 1,2-dichlorobenzene as the sample solvent.

INTRODUCTION

The discovery of a gram-scale fullerene production process in 1990 made these interesting carbon allotropes more readily available for investigation [1]. Since then, the techniques for separating and isolating C_{60} and C_{70}, a task not easy to perform on gram scale, have been constantly improved [2–6]. The separation and isolation of the higher fullerenes (C_n, $n > 70$) has proved to be even more difficult, making studies of these allotropic forms of carbon extremely tedious [2,7,8].

* Corresponding author.

0021-9673/93/$06.00

One of the most common techniques for the separation of larger amounts of fullerenes from the crude soot extract is flash chromatography on alumina using hexane–toluene (95:5, v/v) as the mobile phase. Pure C_{60}, C_{70} and a fraction containing the higher fullerenes with residual C_{70} is obtained [2,3]. A recent paper described the medium-pressure LC separation of C_{60} and C_{70}, either on normal-phase silica gel with hexane or on C_{18} reversed-phase silica gel with toluene–acetonitrile (75:25, v/v) as the eluent [4].

Different HPLC procedures have been reported for the separation/isolation of C_{60} and C_{70}. Among the stationary phases that have been used are alkyl- (C_{18}) and phenylsiloxane-based materials [9–17], Pirkle-type phases [18–20] and charge-transfer phases with residues not containing amino acid building blocks, such as 2,4-dinitroanilinopropyl- (DNAP) [21,22] and a variety of dinitrophenyl-derivatized π-acidic and some π-basic phases [20]. The eluent most commonly used is *n*-hexane, either pure or in a combination with a more polar component such as dichloromethane, diethyl ether, tetrahydrofuran or an alcohol.

A major problem always encountered is the relative insolubility of all fullerenes in the mobile phase used, a fact that severely limits the amount of material that can be processed. The best solvents for fullerenes are carbon disulphide [13,14] and benzene and alkylated or halogenated derivatives of the latter. With these solvents, on the other hand, virtually no retention is observed on any of the stationary phases mentioned above.

It is only recently that separation techniques using pure toluene as the mobile phase have been described. Gel permeation chromatography using this eluent is reported to yield a C_{60} fraction (92–95% pure), an overlapping fraction (*ca.* 1:1 C_{60}–C_{70}) and a fraction enriched in C_{70} (24% C_{60}, 76% C_{70}, with several percent of higher fullerenes). Reinjection of the fractions obtained in this way leads to purer samples, but the method is not suitable for the separation of higher fullerenes [23–25].

A recent gram-scale C_{60} purification procedure uses a gravity column packed with a mixture of Norit A carbon and silica gel [6]. This method yields pure C_{60} and a mixture of C_{60} and C_{70}. Most of the C_{70} and all the higher fullerenes, however, remain adsorbed on the stationary phase [26].

Whereas most published work refers to the

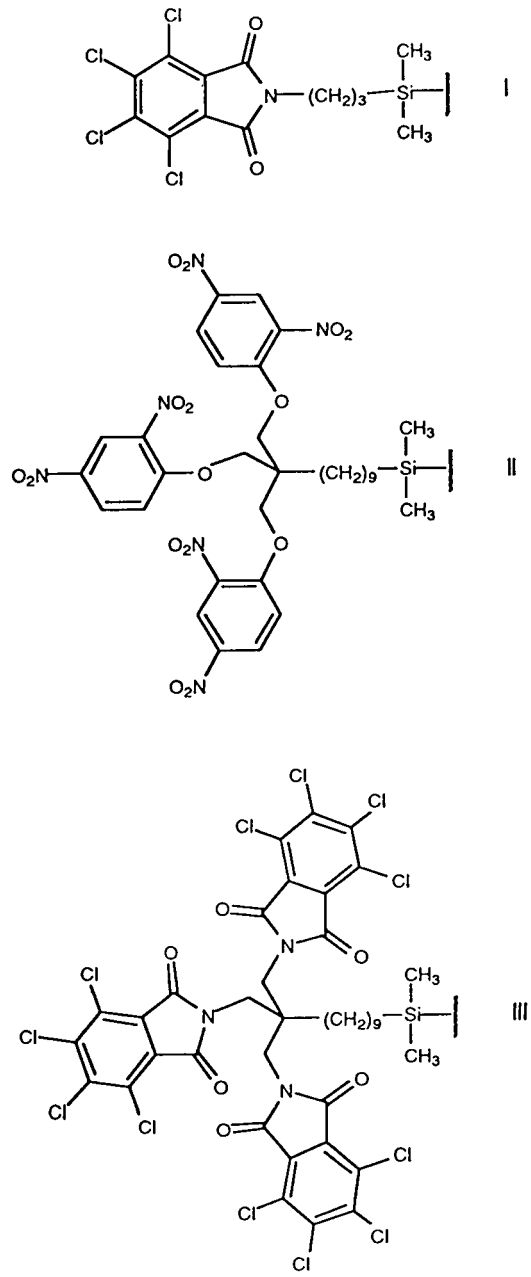

Fig. 1. Structures of stationary phases: I = tetrachlorophthalimidopropyl (TCPP) phase; II = tripodal dinitrophenyl ether phase of Welch and Pirkle [20]; III = hypothetical tripodal TCPP phase.

isolation of C_{60} and C_{70} only, a few small-scale preparative separations of higher fullerenes have been achieved by HPLC on alkylated silica [7,8,12–17]. Thus, repeated runs (2–3) on a Vydac 201 TP C_{18} phase using the unusual mixture acetonitrile–toluene (50:50, v/v) as the mobile phase yielded pure C_{76}, C_{2v}-C_{78}, D_3-C_{78} and a mixture of D_2- and D_{2d}-C_{84} [8,15–17]. An analytical separation of a different mixture of higher fullerenes on the same stationary phase with diethyl ether as the eluent has been described [10].

In this paper, we report on the efficient HPLC separation of C_{60} and especially the larger carbon spheres C_{70}, C_{76}, C_{2v}-C_{78} and D_3-C_{78} and C_{84} on a tetrachlorophthalimidopropyl (TCPP)-modified silica stationary phase (Fig. 1, I). The mobile phase used was dichloromethane–hexane and the samples were injected as 1,2-dichlorobenzene solutions.

EXPERIMENTAL

Column

Separations were performed on Shandon (Runcorn, UK) PAH-2 (5 μm) columns, 250 mm × 20 mm I.D. (preparative) and 250 mm × 4.6 mm I.D. (analytical). This stationary phase was TCPP-modified silica (Fig. 1, I).

Instrumentation

The following instruments were used: Merck–Hitachi LC 6200 HPLC pump, ERMA ERC 3511 solvent degasser, Negretti Model 190 sample injector, Kontron Uvicon LCD 725 detector (310 nm), Servograph rec 51 recorder and Hewlett-Packard HP 3396A integrator.

Fullerene production

The fullerene-containing carbon soot was produced through resistive heating of graphite under a helium atmosphere by methods described previously [1–3]. Soxhlet extraction of the soot with toluene gave an extract containing *ca.* 65% of C_{60}, 30% of C_{70} and 5% of higher-molecular-mass fullerenes consisting mainly of C_{76}, two C_{78} isomers and two C_{84} isomers [2,3,15–17]. The higher fullerene mixture was isolated by gravity chromatography on neutral alumina with hexane–toluene (95:5, v/v), yielding the fractions C_{60}, C_{70} and higher fullerenes with residual C_{70}.

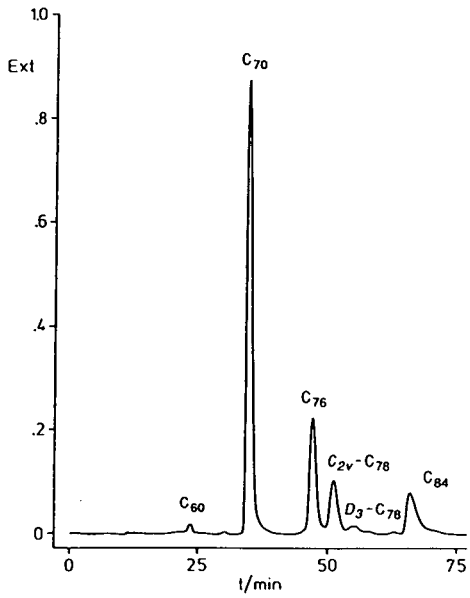

Fig. 2. Chromatogram of the separation of higher fullerenes plus C_{70} (plus traces of residual C_{60}) on a TCPP phase. Column, 250 mm × 20 mm I.D.; injection, 100 μl (1 mg) of a solution (10 mg/ml) in 1,2-dichlorobenzene; eluent, dichloromethane–hexane (33:67, v/v); flow-rate, 6.00 ml/min; temperature, ambient.

Reagents

HPLC-grade dichloromethane and hexane were obtained from Romil Chemicals (Loughborough, UK) and 1,2-dichlorobenzene (analytical reagent grade) from Merck (Darmstadt, Germany).

RESULTS

C_{60}–C_{70}

The separations were performed at ambient temperature using the preparative column and dichloromethane–hexane as the mobile phase at a flow-rate of 6 ml/min. The fullerene mixture was injected as a concentrated 1,2-dichlorobenzene solution (10 mg/ml). The capacity factors (k') and the separation factor (α) for these two fullerenes show a close dependence on the solvent mixture. With dichloromethane–hexane (33:67, v/v) as the eluent, the values were $k'(C_{60}) = 0.93$, $k'(C_{70}) = 1.88$ and $\alpha = 2.1$.

Changing the solvent to dichloromethane–hexane (5:95, v/v) gave $k'(C_{60}) = 5.11$, $k'(C_{70}) = 14.04$ and $\alpha = 2.75$. Injection of 0.5 ml of the fullerene solution (5 mg) resulted in the baseline separation of C_{60} and C_{70} with the 33:67 solvent mixture.

Higher fullerenes

The TCPP phase shows excellent selectivity for the higher fullerenes (Fig. 2). Baseline separation of C_{70}, C_{76}, C_{2v}-C_{78}, D_3-C_{78} and C_{84} was obtained with a 100-μl injection containing 1 mg of these fullerenes, using dichloromethane–hexane (33:67, v/v) as the mobile phase. The purity of the collected fractions was determined by analytical HPLC (injection of 50 μl of a 1,2-dichlorobenzene solution containing 10 mg/ml of material; percentages refer to integrated peak areas and are not exactly equivalent to mass-% because of the slightly different molar absorptivities of the different fullerenes at 310 nm): C_{70}, 100%; C_{76}, 98.5% (1.5% C_{70}); C_{2v}-C_{78}, 97.5% (1.1% C_{70}, 1.4% C_{76}); D_3-C_{78}, 45% (30% C_{70}, 15% C_{76}, 10% C_{2v}-C_{78}); C_{84}, 99.5%.

DISCUSSION

TCPP-modified silica belongs to the family of π-acidic phases which have been used for the separation of π-electron-rich polycyclic aromatic hydrocarbons (PAHs) for some time [27]. Their efficiency in separating C_{60} from C_{70} [18–22] therefore was not surprising, although there is an important difference in shape between the mostly flat PAHs and the curved fullerenes.

Recently, Welch and Pirkle [20] reported an extensive C_{60}–C_{70} separation study with ten different charge-transfer stationary phases, all of which showed retention and separation for these carbon spheres. They achieved capacity factors and separation factors even higher than those described here with a tripodal dinitrophenyl ether phase (Fig. 1, II) using dichloromethane–hexane (5:95, v/v) as the eluent (Table I). However, they did not investigate the separation of higher fullerenes.

The efficiency of the tripodal dinitrophenyl ether phase in the separation of C_{60} and C_{70} seems to be due at least in part to the cooperative effect of three π-acidic dinitrophenyl groups that adopt a cone-shaped arrangement, thus creating a "cavity" well suited for simultaneous multi-point interactions with the "buckyballs". If this assumption is correct, it would certainly be interesting to study the effect of a similar arrangement of three tetrachlorophthalimido residues in the hypothetical phase III (Fig. 1).

For PAHs, on the other hand, the TCPP phase exhibits much higher capacity factors than the phases described by Welch and Pirkle (Table I). This may be due to the enhanced planarity and active surface area of the π-acidic tetrachlorophthalimido residue compared with the dinitrophenyl group. Interestingly, the elution order of phenanthrene and anthracene is inverted on transition from the tripodal dinitrophenyl ether to the TCPP phase.

The separation of higher fullerenes on charge-transfer phases was not investigated by Welch and Pirkle, or, apparently, by other workers. In

TABLE I

CAPACITY FACTORS FOR FIVE DIFFERENT ANALYTES

Naph = Naphthalene; Anth = anthracene; Phen = phenanthrene; C_{60} and C_{70} = fullerenes. Conditions: analytical TCPP column (250 mm × 4.6 mm I.D.), eluent, dichloromethane–hexane (5:95, v/v); flow-rate, 2.00 ml/min; temperature, ambient. $\alpha_{60/70}$ = Separation factor for C_{60} and C_{70}.

Stationary phase	Analyte					$\alpha_{60/70}$
	Naph	Anth	Phen	C_{60}	C_{70}	
Tripodal DNPE [20]	0.58	1.28	1.41	6.59	20.77	3.15
TCPP	2.49	19.12	17.24	5.11	14.04	2.75

our study, we found that the TCPP phase allows the separation of the carbon spheres C_{76}, C_{2v}-C_{78}, D_3-C_{78} and C_{84} and possibly even other very minor species, with excellent resolution and peak shape. In addition to the good separation quality, the TCPP phase also provides a considerable quantitative improvement (1 mg of material per run compared with *ca.* 0.05 mg per run on a 250 mm × 20 mm I.D. preparative column [8]) so that higher fullerenes should soon become available in amounts large enough to study their exciting physical and chemical properties in greater detail.

ACKNOWLEDGEMENTS

We thank Dr. V. Meyer and R. Bühler for their contributions. This work is part of project NF 20-3404.92, financed by the Swiss National Science Foundation.

REFERENCES

1 W. Krätschmer, L.D. Lamb, K. Fostiropoulos and D.R. Huffman, *Nature*, 347 (1990) 354.
2 F. Diederich, R. Ettl, Y. Rubin, R.L. Whetten, R. Beck, M.-M. Alvarez, S. Anz, D. Sensharma, F. Wudl, K.C. Khemani and A. Koch, *Science*, 252 (1991) 548.
3 P.-M. Allemand, A. Koch, F. Wudl, Y. Rubin, F. Diederich, M.-M. Alvarez, S.J. Anz and R.L. Whetten, *J. Am. Chem. Soc.*, 113 (1991) 1050.
4 A. Mittelbach, W. Hönle, H.G. v. Schnering, J. Carlsen, R. Janiak and H. Quast, *Angew. Chem.*, 104 (1992) 1681; see also ref. 8 for the combination of C_{18} reversed phase with toluene–acetonitrile.
5 K.C. Khemani, M. Prato and F. Wudl, *J. Org. Chem.*, 57 (1992) 3254.
6 W.A. Scrivens, P.V. Bedworth and J.M. Tour, *J. Am. Chem. Soc.*, 114 (1992) 7917.
7 R. Ettl, I. Chao, F. Diederich and R.L. Whetten, *Nature*, 353 (1992) 149.
8 F. Diederich, R.L. Whetten, C. Thilgen, R. Ettl, I. Chao and M.-M. Alvarez, *Science*, 254 (1991) 1768.
9 K. Jinno, K. Yamamoto, T. Ueda, H. Nagashima, K. Itoh, J.C. Fetzer and W.R. Biggs, *J. Chromatogr.*, 594 (1992) 105.
10 R.C. Haddon, L.F. Schneemeyer, J.V. Waszcak, S.H. Glarum, R. Tycko, G. Dabbagh, A.R. Kortan, A.J. Muller, A.M. Mujsce, M.J. Rosseinsky, S.M. Zahurak, A.V. Makhija, F.A. Thiel, K. Raghavachari, E. Cockayne and V. Elser, *Nature*, 350 (1991) 46.
11 Y. Cui, T. Lee, S.V. Olesik, W. Flory and M. Mearini, *J. Chromatogr.*, 625 (1992) 131.
12 J.C. Fetzer and E.J. Gallegos, *Polycyclic Aromatic Compd.*, 2 (1992) 245.
13 K. Kikuchi, N. Nakahara, T. Wakabayashi, S. Suzuki, H. Shiromaru, Y. Miyake, K. Saito, I. Ikemoto, M. Kainosho and Y. Achiba, *Nature*, 357 (1992) 142.
14 K. Kikuchi, N. Nakahara, T. Wakabayashi, M. Honda, H. Matsumiya, T. Moriwaki, S. Suzuki, H. Shiromaru, K. Saito, K. Yamauchi, I. Ikemoto and Y. Achiba, *Chem. Phys. Lett.*, 188 (1992) 177.
15 F. Diederich and R.L. Whetten, *Acc. Chem. Res.*, 25 (1992) 119.
16 F. Diederich and Y. Rubin, *Angew. Chem.*, 104 (1992) 1123; *Angew. Chem., Int. Ed. Engl.*, 31 (1992) 1101.
17 C. Thilgen, F. Diederich and R.L. Whetten, in W.E. Billups and M.A. Ciufolini (Editors), *Buckminsterfullerenes*, VCH, New York, in press.
18 W.H. Pirkle and C.J. Welch, *J. Org. Chem.*, 56 (1991) 6973.
19 J.M. Hawkins, T.A. Lewis, S.D. Loren, A. Meyer, J.R. Heath, Y. Shibato and R.J. Saykally, *J. Org. Chem.*, 55 (1990) 6250.
20 C.J. Welch and W.H. Pirke, *J. Chromatogr.*, 609 (1992) 89.
21 D.M. Cox, S. Behal, M. Disko, S.M. Gorun, M. Greaney, C.S. Hsu, E.B. Kollin, J. Millar, J. Robbins, R.D. Sherwood and P. Tindall, *J. Am. Chem. Soc.*, 113 (1991) 2940.
22 L. Nondek and V. Kuzilek, *Chromatographia*, 33 (1992) 344.
23 M.S. Meier and J.P. Selegue, *J. Org. Chem.*, 57 (1992) 1924.
24 M.S. Meier, T.F. Guarr, J.P. Selegue and V.K. Vance, *J. Chem. Soc., Chem. Commun.*, (1993) 63.
25 A. Gügel, M. Becker, D. Hammel, L. Mindach, J. Räder, T. Simon and K. Müllen, *Angew. Chem.*, 104 (1992) 666; *Angew. Chem., Int. Ed. Engl.*, 31 (1992) 644.
26 A. Wehrsig and F. Diederich, unpublished results.
27 C.H. Lochmüller, in D.E. Leyden and W. Collins (Editors), *Silylated Surfaces*, Gordon and Breach, New York, 1980, p. 231.

Journal of Chromatography, 644 (1993) 193–197
Elsevier Science Publishers B.V., Amsterdam

CHROM. 25 220

Short Communication

Simultaneous analysis of *l*-hyoscyamine, *l*-scopolamine and *dl*-tropic acid in plant material by reversed-phase high-performance liquid chromatography

Marc-André Fliniaux*, Françoise Manceau and Annie Jacquin-Dubreuil

Laboratoire de Pharmacognosie et Phytotechnologie, Faculté de Pharmacie, 3 Rue des Louvels, 80 000 Amiens (France)

(First received February 5th, 1993; revised manuscript received April 20th, 1993)

ABSTRACT

A sensitive reversed-phase high-performance liquid chromatographic (HPLC) procedure for the analysis of the main parasympatholytic tropane alkaloids in plant material is described. It uses an acidic aqueous acetonitrile mobile phase and UV detection at 204 nm. It allows a good simultaneous separation of *l*-hyoscyamine, *l*-scopolamine and tropic acid, their acidic precursor. The detection limits are 20 ng for the alkaloids and 5 ng for tropic acid. A simple and rapid method, very convenient for HPLC analysis, is also described for the preparation of purified alkaloid extracts. The procedure was applied to the evaluation of the alkaloid content of *Datura* leaves. The results are in good correlation with those obtained with a tropic acid derivatives-specific enzyme immunoassay.

INTRODUCTION

There are numerous reports in the literature about the analysis tropane alkaloids in plant material or for pharmacological studies. Various chromatographic methods have been used: thin-layer chromatography (TLC) [1,2], and other more sensitive methods such as gas chromatography (GC) using flame ionization detection (FID) or nitrogen–phosphorus detection (NPD) [3,4], or coupled with mass spectrometry (MS) [5–7]. High-performance liquid chromatography (HPLC) has also proved to be very useful for the analysis of tropane alkaloids [6–13]. These methods generally allow a good separation and a sensitive estimation of the components of plant extracts, but the extracts have to be purified prior to injection onto the HPLC column, resulting in a long assay time for a large number of samples.

Immunoassays, radioimmunoassay (RIA) and enzyme immunoassay (EIA) have also been developed specifically for atropine [14], hyoscyamine [15], scopolamine [16] or for all the tropic acid derivatives simultaneously [17]. These methods are selective and more rapid as purification of the plant extracts is unnecessary. The one drawback is that only one alkaloid or all the tropic acid derivatives together can be estimated, depending on the kind of antibodies used.

The present paper describes a new rapid and efficient reversed-phase HPLC procedure for the determination of the main tropane alkaloids, *l*-

* Corresponding author.

0021-9673/93/$06.00

hyoscyamine and *l*-scopolamine, as well as *dl*-tropic acid, one of their biogenetic precursors, which was not analysed by GC or by HPLC as previously reported. The method has been applied to the analysis of tropane alkaloids in *Datura stramonium* L. leaves.

EXPERIMENTAL

Apparatus and chromatographic conditions

The chromatographic system consisted of a Waters Model 510 pump operated at a flow-rate of 0.8 ml/min and a Rheodyne injector with 20 μl injection volume. The UV detector was a Waters 481 Lamba-Max spectrophotometer set at 204 nm wavelength. The column was a 150 mm × 4 mm Novapack C_{18} with 4-μm packing (Waters-Millipore, Saint Quentin en Yvelines, France) maintained at room temperature.

The mobile phase was a mixture of 12.5% aqueous acetonitrile supplemented with 0.3% (v/v) phosphoric acid adjusted to pH 2.2 with triethylamine. The mobile phase was filtered through an 0.45-μm nylon-66 Millipore filter and degassed prior to use.

The data were generated using a Shimadzu C-R6A integrator, which automatically integrated peaks areas and compared them with those of authentic standards, *l*-hyoscyamine, *l*-scopolamine and tropic acid obtained from Serva Fine Biochemicals (Saint Germain en Laye, France). All chemicals used for HPLC analysis were HPLC grade.

Extraction of tropane alkaloids

Several extraction conditions were compared: leaves of *Datura stramonium* L. were freeze-dried and powdered, and samples (100 mg each) were extracted with 25 ml of either 0.2 *M* aqueous sulphuric acid, methanol–1 *M* hydrochloric acid (24:1), methanol–27% ammonium hydroxide (24:1), methanol–chloroform–27% ammonium hydroxide (10:14:1) or chloroform–27% ammonium hydroxide (24:1). In each system, the alkaloids were extracted twice under reflux for 1 h. After filtration, each crude extract was evaporated to dryness under reduced pressure.

Purification of tropane alkaloids

Three purification processes were compared:

(1) A conventional process according to Kitamura *et al.* [18]. The crude extract was treated with 3 × 10 ml of 0.1 *M* sulphuric acid. The aqueous solutions were collected, filtered and the filtrate was basified to pH 9 with 27% ammonium hydroxide, then extracted by shaking with 3 × 20 ml of chloroform. Pooled extracts were dried (sodium sulphate) and evaporated to dryness under vacuum.

(2) Purification on a self-packed silica gel column. The crude alkaloid extract was resuspended in 10 ml of water at 40°C for 15 min. A 1-ml aliquot of this suspension adjusted to pH 7 was put on an 11 cm × 0.5 cm self-packed silica gel column made with 6 ml of silica gel, particle size 30 μm, obtained from Serva (France). The silica gel was degassed for 10 min under vacuum prior to packing. The column was connected to a peristaltic pump. Elution was successively performed with 10 ml of water and 10 ml of HPLC mobile phase supplemented with methanol (20%, v/v), first degassed. This last eluate fraction was kept for alkaloid analysis.

(3) Extraction of alkaloids from the crude extract with mobile phase. The extract was directly treated with 10 ml of the HPLC mobile phase at 40°C for 15 min and filtered before chromatographic analysis. This simplified procedure could be applied to the alkaline chloroformic extract but not to the methanolic one because too many polar compounds in this last extract would be reextracted with the mobile phase, inducing possible interferences during the chromatographic analysis.

Enzyme immunoassay of tropane alkaloids

Tropane alkaloids were also analysed by a competitive indirect enzyme immunoassay (EIA) using anti *dl*-tropic acid antibodies, as previously described [17]. This method allowed the simultaneous detection of all the alkaloids derived from *dl*-tropic acid and could be performed on crude or purified alkaloids as well as directly on dry-powdered plant material.

Capillary gas chromatography

The apparatus was a Girdel Series 30 chromatograph (Delsi Instruments, Suresnes, France) fitted with a 30 m × 0.32 mm I.D. capillary SE 30 basic column (0.25 μm film) (Supelco-Serlabo, Paris, France) and a flame ionization detector. Helium was used as carrier gas at an inlet pressure of 0.8 bar. Injector and detector temperature was 250°C. Oven temperature was 230°C. The results were given by Shimadzu C-R6A integrator.

RESULTS AND DISCUSSION

The HPLC method using a Novapack C_{18} column, an acidic aqueous acetonitrile mobile phase and UV detection at 204 nm as described in the Experimental section was applied to a standard solution of tropane alkaloids, *l*-hyoscyamine and *l*-scopolamine and *dl*-tropic acid, a precursor of the alkaloids (10^{-2} mg/ml of each). It allowed a good separation of the compounds: the retention times were 5.35 min for *l*-scopolamine, 7.35 min for *dl*-tropic acid and 11.7 min for *l*-hyoscyamine, as shown in Fig. 1. Detection at 204 nm increased the sensitivity 50-fold compared with that at 254 nm used by several authors [8–10]. Under these conditions, the working range of the assays was 20 ng to 5 μg for *l*-hyoscyamine and *l*-scopolamine and 5 ng to 1 μg for *dl*-tropic acid. The injection variability did not exceed 1–2% and the variations between several analyses of a same plant powder sample did not exceed 5%.

This procedure was applied to the analysis of plant material, which necessitated extraction and purification of alkaloids prior to HPLC analysis. Conditions for these preliminary steps were studied. To check that extraction under reflux did not modify the chemical structure of alkaloids, controls were performed: internal standard alkaloids added to plant powder sample indicated that these compounds were not converted to apoalkaloids or to dimer forms, since 98% of alkaloids added were recovered as original compounds. To determine the efficiency of various solvents in the extraction of tropane alkaloids, the freeze-dried powdered leaves of

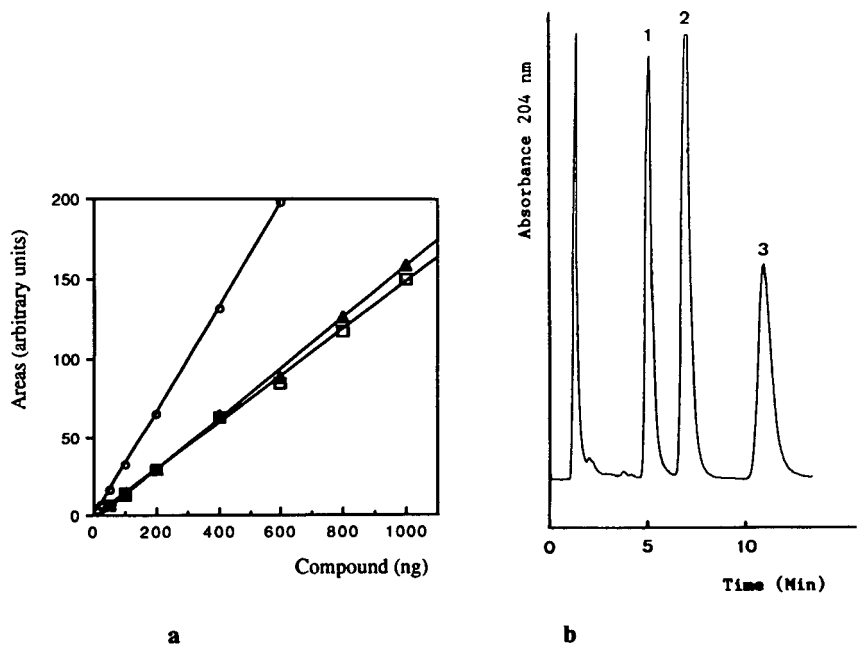

Fig. 1. HPLC analysis of a $5 \cdot 10^{-3}$ g/l standard solution of (1, □) *l*-scopolamine, (2, ○) *dl*-tropic acid and (3, ▲) *l*-hyoscyamine. (a) Calibration curves; (b) retention times: 1 = 5.35 min; 2 = 7.35 min; 3 = 11.7. Column packing: Novapack C_{18} 4 μm; mobile phase: 12.5% aqueous acetonitrile supplemented with 0.3% (v/v) phosphoric acid, pH 2.2 with triethylamine; flow-rate 0.8 ml/min; detection: UV 204 nm.

TABLE I

INFLUENCE OF THE SOLVENTS USED FOR EXTRACTION ON THE QUANTITY OF ALKALOID EXTRACTED (EXPRESSED AS mg PER g DRY MASS) FROM POWDERED LEAVES OF *DATURA STRAMONIUM*

Crude extracts and residues were analysed by ELISA. Each value represents the mean of five replicates. For details, see Experimental section.

Solvent	Alkaloids (mg per g dry mass)	
	Crude extract	Residue
Aqueous 0.1 *M* sulphuric acid	2.5 ± 0.17	0.11 ± 0.01
Methanol	2.3 ± 0.17	0.15 ± 0.01
Methanol–hydrochloric acid	2.4 ± 0.18	0.10 ± 0.01
Methanol–ammonium hydroxide	2.4 ± 0.17	0.11 ± 0.01
Methanol–chloroform–ammonium hydroxide	2.3 ± 0.17	0.10 ± 0.01
Chloroform–ammonium hydroxide	2.6 ± 0.15	0.12 ± 0.01

Datura stramonium were subjected to several extraction systems varying in pH and polarity (see Experimental section). Each extract and the corresponding residue, as well as the *Datura* powder, were submitted to EIA analysis. The alkaloid content of plant material was 2.9 ± 0.1 mg per g dry mass. The differences between the yield of alkaloids recovered with the various extraction conditions (2.3–2.6 mg/g dry mass) were not significant (Table I). The amounts of alkaloids remaining in the residues after two extraction steps were low (4–7% of the alkaloids detected in the extracts).

In order to control purification efficacy, an alkaline chloroform extract was purified by three different processes: (1) the conventional process, which used the amphoteric properties of the alkaloids [18]; (2) an elution from a silica gel column; and (3) a simple reextraction of the alkaloids from the dried crude extract with the polar HPLC mobile phase. Table II shows that the last process was quite efficient; it was also the quickest and easiest to perform. Thus, alkaloid extracts submitted to HPLC analysis were finally obtained by an alkaline chloroform extraction and a further reextraction of alkaloids from crude extract using HPLC mobile phase. Under these conditions, 50 μg per g dry mass was the detection limit of alkaloids in plant material.

One application of this HPLC procedure is the estimation of alkaloid accumulation in roots and leaves of *in vitro*-regenerated *Datura innoxia* [19]. Forty samples were analysed simultaneously by HPLC, GC and EIA. The results were compared. Mean values were 0.275 mg per g dry mass for HPLC, 0.2 mg per g dry mass for GC and 0.32 mg per g dry mass for EIA. For GC

TABLE II

COMPARISON OF EFFICIENCY OF THREE PURIFICATION PROCEDURES OF A CRUDE ALKALOID EXTRACT (PREPARED WITH ALKALINE CHLOROFORM) OF POWDERED LEAVES OF *DATURA STRAMONIUM*

Samples were analysed by HPLC. For details, see Experimental section. Each value represents the mean of four replicates.

	Conventional process	Purification on silica gel	Mobile phase extraction
Alkaloid content (mg per g dry mass)	2.6 ± 0.15	2.6 ± 0.12	2.8 ± 0.12

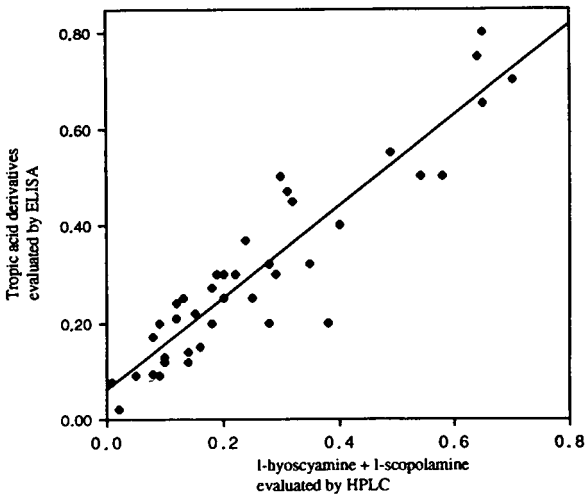

Fig. 2. Determination of the alkaloid content of *Datura innoxia* leaves by both HPLC and enzyme-linked immunosorbent assay. Comparison of the results. Units: mg/g dry mass. $y = 0.0581 + 0.9467x$; $R = 0.92$.

analysis, alkaloid extracts were necessarily prepared by the conventional process. This might partially explain the lower mean value found in this case. The results obtained with HPLC and EIA were more similar, and correlation of the results was determined and is presented in Fig. 2. The slightly higher values obtained by EIA (+16%) than by HPLC could be because tropic acid derivatives evaluated by EIA were not always only hyoscyamine and scopolamine.

CONCLUSIONS

The HPLC procedure presented in this paper is sensitive and allows a good simultaneous separation of hyoscyamine, scopolamine and one of their precursors, tropic acid. The procedure described for the preparation of the alkaloid extracts is easy to use and rapid. It has also previously been found to be efficient for the tobacco alkaloids [20], and could be of general use for the HPLC analysis of plant material containing alkaloids.

The method was applied to the evaluation of the tropane alkaloid content of *Datura* leaves and gave reliable results in good correction with those obtained by EIA. Thus the complementarity of the two methods is evident, EIA allowing a quick estimate of the total tropic acid derivatives in large series of plant samples, and HPLC giving the yield of each main tropane alkaloid in the plant material.

REFERENCES

1 A. Baerheim-Svendsen and R. Verpoorte, *Chromatography of Alkaloids, Part A: Thin-Layer Chromatography*, Elsevier, Amsterdam, 1983.
2 H. Wagner, S. Bladt and E.M. Zgainski, *Plant Drug Analysis*, Springer, Berlin, 1984.
3 A.K. Kukreja and A.K. Mathur, *Planta Med.*, 51 (1985) 93.
4 A. Martinsen, K. Hiltunen and A. Huhtikangas, *Phytochem. Anal.*, 3 (1992) 69.
5 T. Hartmann, L. Witte, F. Oprach and G. Toppel, *Planta Med.*, 52 (1986) 390.
6 H. Kamada, N. Okamura, M. Satake, H. Harada and K. Shimomura, *Plant Cell Rep.*, 5 (1986) 239.
7 P. Christen, M.F. Roberts, J.D. Phillipson and W.C. Evans, *Plant Cell Rep.*, 8 (1989) 75.
8 R. Verpoorte and A. Baerheim-Svendsen, *J. Chromatogr.*, 120 (1976) 203.
9 U. Lund and S.H. Hansen, *J. Chromatogr.*, 161 (1978) 371.
10 S. Paphassarang, J. Raynaud, R.P. Godeau and A.M. Binsard, *J. Chromatogr.*, 319 (1985) 412.
11 K.H. Plack and K.G. Wagner, *Z. Naturforsch, C: Biosci.*, 41 (1986) 391.
12 P. Leroy and A. Nicolas, *J. Pharm. Biomed. Appl.*, 5 (1987) 477.
13 Y. Mano, H. Ohkawa and Y. Yamada, *Plant Sci.*, 59 (1989) 191.
14 R.J. Wurzburger, R. Miller, H.G. Boxenbaum and S. Spector, *J. Pharmacol. Exp. Ther.*, 203 (1977) 435.
15 T. Lethola, A. Huhtikangas and R. Virtanen, *Planta Med.*, 45 (1982) 237.
16 E.W. Weiler, *Phytochemistry*, 20 (1981) 2009.
17 M.A. Fliniaux and A. Jacquin-Dubreuil, *Planta Med.*, 53 (1987) 87.
18 Y. Kitamura, H. Miura and M. Sugii, *Planta Med.*, 51 (1985) 489.
19 R. Bouami-Guennouni-Assimi, L. Cosson and A. Jacquin-Dubreuil, *Bull. Soc. Bot. Fr.*, 137 (1990) 261.
20 F. Manceau, M.A. Fliniaux and A. Jacquin-Dubreuil, *Phytochem. Anal.*, 3 (1992) 65.

Journal of Chromatography, 644 (1993) 198–201
Elsevier Science Publishers B.V., Amsterdam

CHROM. 25 121

Short Communication

Anion-exchange selectivity of cyclic phosphate oligomers

Genichiro Kura

Department of Chemistry, Fukuoka University of Education, Munakata, Akama, Fukuoka 811-41 (Japan)

(Received February 23rd, 1993)

ABSTRACT

The distribution coefficients, K_d, of inorganic cyclic phosphate oligomers, $P_nO_{3n}^{n-}$, for the Bio-Rad AG 1-X4 resin were determined in potassium chloride and tetramethylammonium chloride solutions. Considerable differences in the K_d of the same cyclic phosphate anion at the same Cl^- concentration for the potassium chloride and tetramethylammonium chloride systems were observed. The anion-exchange selectivity of the cyclic phosphate anion was discussed.

Cyclic phosphate anions, members of the group known as inorganic condensed phosphate anions and presented as $P_nO_{3n}^{n-}$, are very interesting materials from the viewpoint of electrolyte solution chemistry because of the high negative charges on their relatively compact molecules [1–3]. We have reported the separation of these cyclic oligomers by HPLC and have discussed their retention mechanism on the HPLC column. As we have described previously [4,5], the retention times of each phosphate anion can be predicted from the Cl^- concentration dependence of the distribution coefficient. The relationship between the distribution coefficient of the phosphates and the concentration of the eluting ion, Cl^-, is governed by the thermodynamic selectivity coefficient for the anion-exchange reaction. However, the thermodynamic selectivity coefficient could not be estimated since it is almost impossible at the present time to estimate the activity coefficient terms of such highly charged cyclic phosphate anions in both aqueous and exchanger phases. Therefore, the true anion-exchange behaviour of the cyclic phosphates cannot be discussed; however, in this work a qualitative explanation for the exchange reaction has been attempted by measuring the distribution coefficient in potassium chloride and tetramethylammonium chloride solutions and determining the apparent selectivity coefficient, K_{ex}.

The distribution coefficient, K_d, of cyclic phosphate oligomers for the Bio-Rad AG 1-X4 resin was determined as a function of the chloride ion concentration. Potassium and tetramethylammonium ions were used as co-ions of the chloride ion. Considerably different distribution coefficients were obtained in potassium chloride and tetramethylammonium chloride solutions at the same chloride ion concentrations. For the $P_8O_{24}^{8-}$ ion, the K_d for the tetramethylammonium chloride system was 3600 times greater than that for the potassium chloride system. K_d values were reduced by the presence of potassium ions,

0021-9673/93/$06.00

which form ion pairs with the cyclic phosphate anions. However, the slope of the log K_d *vs.* log [Cl^-] plots for both systems agreed with the structural charge of cyclic phosphate anions according to the law of mass action. The ion pair formed in potassium chloride solutions might dissociate when the phosphate anions are adsorbed into the exchanger phase. The apparent selectivity coefficient of each cyclic phosphate on the exchange resin, where the acivity coefficient term was neglected, was determined in the tetramethylammonium chloride solution. The apparent selectivity coefficient significantly depends on the equivalent fraction of Cl^- in the exchanger phase. From the apparent selectivity coefficient obtained, the anion exchange behaviour was analysed.

EXPERIMENTAL

Chemicals

Sodium salts of cyclotri- (P_{3m}) and cyclo-tetraphosphate (P_{4m}) were prepared by the usual methods [6]. Sodium cyclohexa- (P_{6m}) and cyclooctaphosphate (P_{8m}) were synthesized by the methods of Griffith and Buxton [7] and Schülke [8], respectively. All other chemicals were of analytical reagent grade and commercially available.

Determination of the distribution coefficient

Distribution coefficients for the Bio-Rad AG 1-X4 resin were measured by the usual batch method at 25°C. The phosphate contents in the solution phase were analysed spectrophotometrically with the Mo(V)–Mo(VI) reagent [3]. Since the tetramethylammonium ion contained in the test solution interfered with the colour development of the Mo(V)–Mo(VI) reagent, it was eliminated by an ion-exchange method.

Measurement of the apparent selectivity coefficient

Bio-Rad AG 1-X4 resin of Cl^- form, the exchange capacity of which was determined accurately, was converted to each phosphate form. A known amount of the resin of the phosphate form was equilibrated with a known amount of tetramethylammonium chloride solution at 25°C, and the phosphate content in the aqueous phase was determined spectrophotometrically.

RESULTS AND DISCUSSION

Suppose a solution containing the cyclic phosphate anion, P^{n-}, is agitated with the anion-exchange resin of Cl^- form (RCl), and the equilibrium is presented as:

$$nRCl + P^{n-} \rightleftharpoons R_nP + nCl^- \quad (1)$$

The thermodynamic selectivity coefficient, K_{ex}, can be written as

$$K_{ex} = \frac{(a_{P^{n-}})_r a^n_{Cl^-}}{(a_{Cl^-})^n_r a_{P^{n-}}} \quad (2)$$

where subscript r refers to the resin phase.

This equation can be rewritten as:

$$K_{ex} = \frac{[P^{n-}]_r[Cl^-]^n(f_{P^{n-}})_r f^n_{Cl^-}}{[Cl^-]^n_r[P^{n-}](f_{Cl^-})^n_r f_{P^{n-}}} = K_{ex}\frac{(f_{P^{n-}})_r f^n_{Cl^-}}{(f_{Cl^-})^n_r f_{P^{n-}}} \quad (3)$$

where

$$K_{ex} = \frac{[P^{n-}]_r[Cl^-]^n}{[Cl^-]^n_r[P^{n-}]} \quad (4)$$

and the terms f designate the activity coefficient terms of each species. The distribution coefficient of the cyclic phosphate anion, K_d, is defined as:

$$K_d = \frac{[P^{n-}]_r}{[P^{n-}]} \quad (5)$$

The dependence of log K_d of the four cyclic phosphate anions on log [Cl^-] for the potassium chloride system is shown in Fig. 1. The log K_d *vs.* log [Cl^-] plots show good linear relations and the slopes of the straight lines agreed with their anionic charge. From eqn. 4, the following relation can be derived:

$$\log K_d = -n \log [Cl^-] - n \log [Cl^-]_r + \log K_{ex} \quad (6)$$

In this equation, $[Cl^-]_r$ can be assumed to be constant since the amount of the cyclic phos-

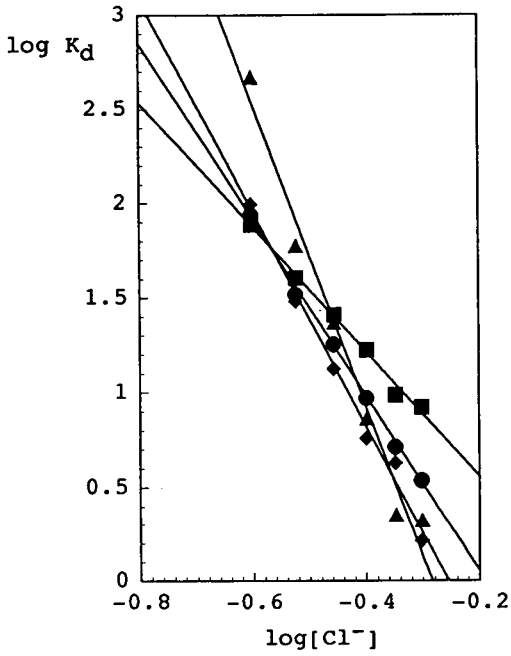

Fig. 1. Plots of log K_d *vs.* log [Cl^-] for the potassium chloride system. ■ = P_{3m}; ● = P_{4m}; ◆ = P_{6m}; ▲ = P_{8m}.

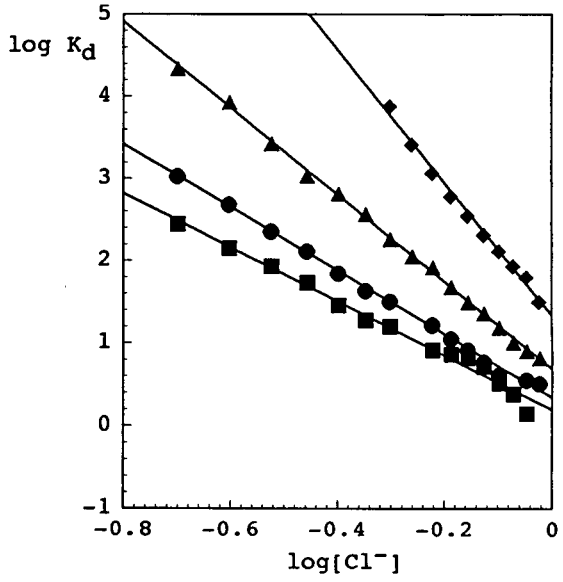

Fig. 2. Plots of log K_d *vs.* log [Cl^-] for the tetramethylammonium chloride system. ■ = P_{3m}; ● = P_{4m}; ▲ = P_{6m}; ◆ = P_{8m}.

phate anions adsorbed was very small. The linear relation between log K_d *vs.* log [Cl^-] shows that log K_{ex} is kept constant in the present experimental conditions. The agreement between the slopes of log K_d *vs.* log [Cl^-] plots and the anionic charge of cyclic phosphate anions suggests that the cyclic phosphate anions entered into the exchanger phase, leaving K^+ ions which formed ion pairs with the phosphate anions. When tetramethylammonium chloride was used as an eluting reagent instead of potassiun chloride, log K_d *vs.* log [Cl^-] plots, as shown in Fig. 2, resulted. In analogy with the case of the potassium chloride system, the plots show good linear relations and their slopes agree with their anionic charges (Table I). For each phosphate anion, the same slope values were obtained for both potassium chloride and tetramethylammonium chloride systems, however large differences in the distribution coefficients of the same cyclic phosphate at the same Cl^- concentration for the potassium chloride and tetramethylammonium chloride systems were observed. For example, for $P_8O_{24}^{8-}$ at [Cl^-] = 0.5 *M*, K_d was 2.14 in potassium chloride solution but 7610 in tetramethylammonium chloride solution. This indicates that the distribution coefficient of cyclic phosphate anions is significantly affected by the presence of the cations which interact with the anions. The difference became larger for the higher membered anions. Appreciable differences in the K_d between the potassium chloride, lithium chloride and sodium chloride systems were not observed. Smaller K_d values in the potassium chloride solution are attributed to the ion-pair formation occurring between K^+ and $P_nO_{3n}^{n-}$. The energy necessary for the dissociation of the ion pairs caused the drop in the K_d values.

The apparent selectivity coefficient, K_{ex}, where activity coefficient terms were not considered, was determined for four cyclic phosphate anions in the tetramethylammonium chloride solution. K_{ex} varied considerably with the equivalent fraction of Cl^- in the resin phase, as shown in Fig. 3. However it can be tentatively concluded that K_{ex} decreases in the order $P_8O_{24}^{8-} > P_3O_9^{3-} > P_4O_{12}^{4-} > P_6O_{18}^{6-}$. As for the major factors that influence the selectivity coefficient, Coulombic forces between cyclic phosphate anions and fixed cations in the exchanger, as well as the solvation of the cyclic phosphate anions,

TABLE I

SLOPES OF LOG K_d *VS.* LOG [Cl^-] PLOTS

	Slope			
	$P_3O_9^{3-}$	$P_4O_{12}^{4-}$	$P_6O_{18}^{6-}$	$P_8O_{24}^{8-}$
Potassium chloride	−3.3	−4.6	−5.7	−8.0
Tetramethylammonium chloride	−3.3	−4.1	−5.4	−8.0

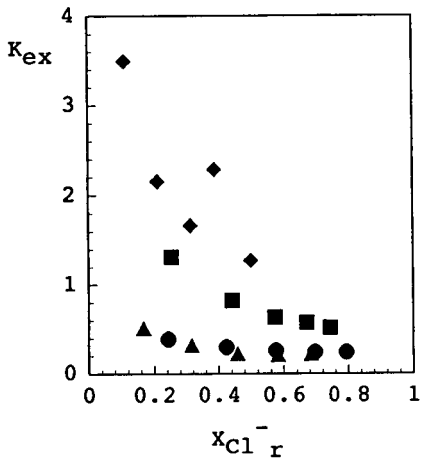

Fig. 3. Apparent selectivity coefficient, K_{ex}, for exchange between chloride and cyclic phosphate anions as a function of the equivalent fraction of chloride ions in the exchanger phase, $X_{Cl_r^-}$. ■ = P_{3m}; ● = P_{4m}; ▲ = P_{6m}; ◆ = P_{8m}.

might be considered. In this case, large Coulombic forces act as an increasing factor for K_{ex}, while the energies necessary for the desolvation act to decrease K_{ex}. From $P_8O_{24}^{8-}$ to $P_3O_9^{3-}$, Coulombic forces decrease, as do desolvation energies, and $P_6O_{18}^{6-}$ has the minimum value for K_{ex}.

REFERENCES

1 G. Kura and S. Ohashi, *J. Inorg. Nucl. Chem.*, 38 (1976) 1151.
2 G. Kura, *Polyhedron*, 5 (1986) 2097.
3 G. Kura, *J. Chromatogr.*, 447 (1988) 91.
4 Y. Baba and G. Kura, *J. Chromatogr.*, 550 (1991) 5.
5 G. Kura, E. Kitamura and Y. Baba, *J. Chromatogr.*, 628 (1993) 241.
6 G. Brauer, *Handbuch der Präparativen Anorganischen Chemie*, Ferdinant Enke, Stuttgart, 1960.
7 E.J. Griffith and R.L. Buxton, *Inorg. Chem.*, 4 (1965) 549.
8 U. Schülke, *Z. Anorg. Allg. Chem.*, 360 (1968) 231

Journal of Chromatography, 644 (1993) 202–207
Elsevier Science Publishers B.V., Amsterdam

CHROM. 25 032

Short Communication

Improved enantiomeric separation with a 2,6-di-O-pentyl-3-O-trifluoroacetylated β-cyclodextrin and OV-7 mixed stationary phase chiral capillary column

Hong Wan, Yi Wang, Qingyu Ou* and Weile Yu

Lanzhou Institute of Chemical Physics, Chinese Academy of Sciences, Lanzhou 730000 (China)

(First received November 9th, 1992; revised manuscript received March 1st, 1993)

ABSTRACT

2,6-Di-O-pentyl-3-O-trifluoroacetylated β-cyclodextrin (DP-TFA-β-CD) as a chiral stationary phase was synthesized and characterized by two-dimensional NMR spectrometry. A chiral fused-silica capillary column prepared by using a mixed stationary phase of DP-TFA-β-CD and OV-7 possesses a high column efficiency of >4100 plates/m and displays better thermal stability than a column coated with DP-TFA-β-CD alone. Enantiomers such as alcohols, diols, γ-lactones and amines could be separated in relatively short time.

INTRODUCTION

Cyclodextrin (CD) derivatives as chiral stationary phases (CSPs) for the gas chromatographic (GC) separation of enantiomers have attracted interest in recent years. Much progress has been made since Juvancz *et al.* [1] used permethylated β-CD for separating some optical isomers on glass capillary columns in 1987, and Konig and co-workers [2,3] introduced hydrophobic groups into CDs in 1988. Since then, a variety of derivatized α-, β-, and γ-cyclodextrin CSPs have been synthesized [4–10] and used in GC separations of chiral components in foods and beverages [11], essential oils [12], petroleum and coal [13]. Permethylated β-CD and dipentyl acetylated-β-CD have been used extensively. Owing to their high melting points, permethylated CDs are usually dissolved in polysiloxanes such as OV-1701 to obtain a high column efficiency [14]. Schmarr *et al.* [15] showed that the diluted cyclodextrin derivatives decreased the enantioselectivity for enantiomers. Keim *et al.* [10] demonstrated however, that in some instances, the dilution could improve the physical properties of cyclodextrin derivatives even for these viscous fluids by dissolving them in a polysiloxane liquid phase. Li *et al.* [9] demonstrated the high enantioselectivity of dipentyl trifluoroacetylated cyclodextrin for a number of enantiomers, but the thermal stability of column was below 180°C.

In this work, 2,6-di-O-pentyl-3-O-trifluoro-

* Corresponding author.

0021-9673/93/$06.00

acetylated β-CD(DP-TFA-β-CD) was synthesized and characterized by two-dimensional NMR. The enantioselectivity and thermal stability of a chiral column coated with a mixed stationary phase of DP-TFA-β-CD and conventional OV-7 were examined.

EXPERIMENTAL

Synthesis of 2,6-di-O-pentyl-3-O-trifluoroacetylated-β-CD

A 5.6-g (5-mmol) amount of dry β-CD was dissolved in 100 ml of dry dimethyl sulphoxide and 8 g (20 mmol) of pulverized NaOH and 30 ml of 1-bromopentane were added. The mixture was stirred at room temperature for 5 days, then poured into water and extracted three times with chloroform. The organic layer was washed with water until neutral and dried over Na_2SO_4. After evaporating the solvent, the product was dried at 60°C for 8 h under vacuum and further purified by gel chromatography, giving 9.3 g of 2,6-di-O-pentyl-β-CD (DP-β-CD) with a yield of 88%. Elemental analysis gave C 63.44, H 9.66; required for $(C_{16}H_{30}O_5)_7$, C, 63.54, H 10.00%.

A 4-g amount of DP-β-CD was dissolved in 80 ml dry tetrahydrofuran, a fivefold excess of trifluoroacetic anhydride was added and the mixture was refluxed for 8 h, then poured over ice to precipitate the product. The product was extracted with diisopropyl ether and washed with 5% aqueous $NaHCO_3$ and water. The organic layer was dried over Na_2SO_4 and concentrated by evaporation of the solvent. The raw product was dried at 50°C for 6 h under vacuum, purified by gel chromatography and a viscous liquid of DP-TFA-β-CD was obtained with a yield of 82%; $R_f = 0.56$ [*n*-hexane–diisopropyl ether (4:6)]. Elemental analysis gave C 49.25, H 6.64; $(C_{18}H_{29}O_6F_3)_7$ requires C 54.26, H 7.34%. $[\alpha]_D^{21} = +42.5$ (*c* 0.41, $CHCl_3$). ^{1}H NMR (400 MHz, $CDCl_3$) δ (ppm) 0.81–0.98 (m, 6H,H-5′), 1.10–1.94 (m,12H, H-2′, H-3′, H-4′), 3.30–4.48 (m,4H,H-1′), 3.30–4.48 (m, 5H, H-2, H-4, H-5,H-6), 5.01 (d,1H,$^3J = 3.4$ Hz, H-1), 5.37 (m,1H,H-3). ^{13}C-NMR (100 Hz,$CDCl_3$), δ (ppm) 13.80, 13.96 (C-5′), 22.35, 22.48 (C-4′), 24.49, 25.19, 25.75 (C-3′), 27.61, 28.36, 29.00, 29.34 (C-2′), 67.19, 68.02, 69.98, 71.69, 71.91 (C-1′), 68.92 (C-6), 71.25 (C-5), 76.69 (C-4), 76.18 (C-3), 77.72 (C-2), 98.78 (C-1), 114.48, 114.55, 114.68 (dd, C-2″, $J_{C-F} = 285.3$ Hz), 1550.03, 157.40, 157.71 (dd, C-1″, $^2J_{C-F} = 42.7$ Hz).

Preparation of chiral capillary columns

A 38 m × 0.26 mm I.D. glass capillary tube was first coated with a layer of Celite 545 by the organic gel method, then deactivated with DPTMDS–HMDS (1:2, v/v)[a] at 400°C for 12 h. The pretreated glass capillary tube was coated with a 3% solution of DP-TFA-β-CD in diisopropyl ether by a superdynamic method as described [16].

A 40 m × 0.26 mm I.D. fused-silica capillary tube was coated as above by using a 3% solution of a mixed stationary phase of DP-TFA-β-CD and OV-7 (2:1, w/w) in diisopropyl ether after it had been heated at 280°C for 2 h under a flow of nitrogen. It took only 1 h to coat the column. The finished columns showed a high column efficiency of above 4100 plates/m at 140°C using *n*-dodecane as the test solute.

Instrumentation

All chromatographic measurements were performed on a Model 1001 gas chromatograph (Shanghai Analytical Instrumentation Factory), equipped with a flame ionization detector and an HP-3390A integrator. High-purity nitrogen was used as the carrier gas at a velocity of *ca.* 25 cm/s, with a splitting ratio of 1:60.

Racemates

Most of the volatile racemates were commercial products. Some diols and amines were synthesized by Dr. Zhao Jun of this Institute. All compounds containing hydroxyl and/or amine functional groups were converted into their trifluoroacetyl derivatives before chromatographic analysis.

RESULTS AND DISCUSSION

Some peralkylated cyclodextrins have been characterized by NMR spectrometry [10,17], but

[a] DPTMDS = 1,3 - diphenyl - 1,1,3,3 - tetramethyldisilane, HMDS = hexamethyldisilane.

TABLE I

α, k_1' AND R_s VALUES FOR SOME ENANTIOMERS

Racemate	Structure	Temperature (°C)	α	k_1'	R_s
2-Bromobutane		40	1.078	2.14	1.12
2-Bromopentane		40	1.030	3.96	0.88
2-Bromoheptane	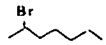	80	1.039	2.40	2.45
2-Bromooctane	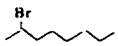	80	1.040	5.00	2.58
2-Chloroheptane	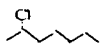	60	1.058	1.63	2.31
2-Chlorooctane	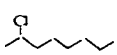	60	1.052	4.34	1.97
Epichlorhydrin		70	1.260	1.47	3.89
γ-Heptalactone		140	1.282	1.92	7.42
γ-Undecalactone	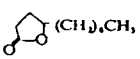	170	1.043	4.48	2.09
2-Butanol		40	1.302	0.42	4.24
2-Pentanol		40	1.290	0.88	6.85
2-Heptanol	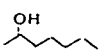	50	1.270	3.51	11.6
2-Octanol	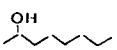	80	1.180	2.51	7.18
3-Methyl-2-Butanol		40	1.243	0.81	4.42
2-Methyl-3-Butanol		40	1.023	3.26	0.81
1,2-Propanediol		60	1.290	3.40	9.02
2,3-Butanediol		60	1.964	1.52	20.6
1,2,4-Butanetriol	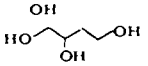	130	1.071	2.48	1.53
Methyl 2-Methylbutyrate	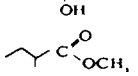	80	1.025	5.14	1.51
Ethyl 2-hydroxypropionate	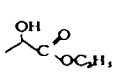	70	1.074	2.42	1.80
Methyl 2-aminobutyrate	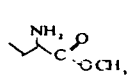	140	1.178	1.76	10.1
Methyl 2-aminoisobutyrate	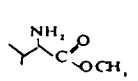	140	1.280	1.60	12.2
1-Phenylethanol		80	1.051	3.18	3.25

TABLE I *(continued)*

Racemate	Structure	Temperature (°C)	α	k_1'	R_s
1-Phenylethylamine		125	1.042	3.32	2.77
1-Phenyl-2-propylamline	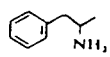	125	1.036	5.81	2.41
2,4-Pentanediol		90	1.110	1.57	4.81
2,5-Hexanediol		90	1.060	2.70	2.43
2-O-Acetylated propion aldehyde		140	1.221	1.77	8.55

no NMR or elemental analysis data have been reported for dipentylacetylated or trifluoroacetylated cyclodextrins, probably it was too difficult to obtain these derivatives in pure form. Our results with two-dimensional NMR with ^1H–^1H COSY, ^1H–^{13}C HETCOR and DEPT techniques showed that DP-β-CD was relatively pure and its ^1H and ^{13}C NMR data were consistent with published data [18]. With DP-TFA-β-CD we were puzzled at the fact that its elemental analysis data were much lower than the calculated values as no impurities were detected in DP-TFA-β-CD by NMR spectrometry. Considering that the sample had beed carefully dried before analysis, the most likely explanation would be inclusion of solvent. The enantiomeric separation data on the mixed stationary phase for some resolved compounds are given in Table I.

Figs. 1–4 illustrate some typical enantiomeric separations on a 40-m fused-silica capillary column coated with a mixed stationary phase of DP-TFA-β-CD and OV-7, with nitrogen at 24 p.s.i. as the carrier gas.

Table II gives a comparative separation of four enantiomers with different functional groups using DP-TFA-β-CD alone and a mixed stationary phase of DP-TFA-β-CD and OV-7. A better enantiomeric separation was obtained with the

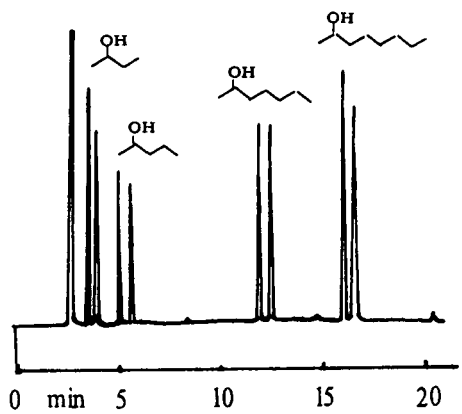

Fig. 1. Enantiomer separation of trifluoroacetylated alcohols. Column temperature, 40°C held for 4 min, then programmed to 80°C at 3°C/min.

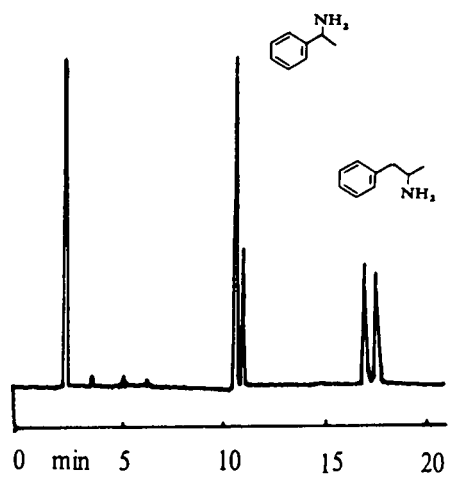

Fig. 2. Enantiomer separation of trifluoroacetylated amines. Colume temperature, 125°C.

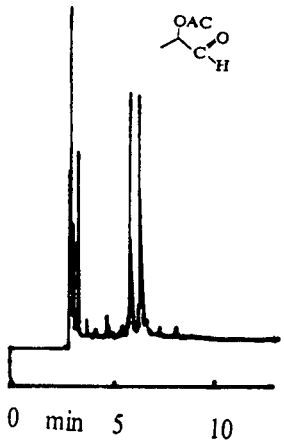

Fig. 3. Enantiomer separation of 2-O-acetylated propion aldehyde. Column temperature 150°C.

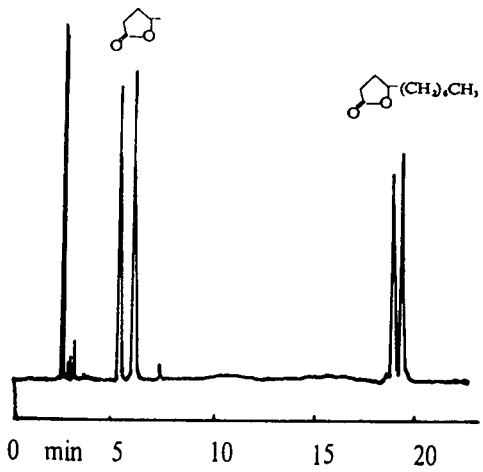

Fig. 4. Enantiomer separation of γ-lactones. Column temperature, programmed from 140 to 190°C at 2°C/min.

mixed stationary phase at lower temperature and in a shorter time, and the enantioselectivity of the DP-TFA-β-CD stationary phase was less affected when it was mixed with a small proportion of conventional polysiloxane OV-7.

Although Li *et al.* [9] found that DP-TFA-β-CD wets an untreated fused-silica capillary wall, the film was unstable above 180° and the column efficiency decreased dramatically after it had been used above 200°C. In this work, using a column coated with DP-TFA-β-CD alone, we also observed apparent droplets of stationary phase on the capillary wall after raising the column temperature to above 180°. However by using the mixed stationary phase, an easily prepared column with high efficiency can be used continuously at 210°C for 4 h without a decrease in efficiency. We have used this fused-silica capillary column for 6 months with over 2000 injections with virtually no decrease in k_1'. These

TABLE II

ENANTIOMERIC SEPARATION DATA OBTAINED ON SINGLE AND MIXED STATIONARY PHASES

Enantiomer	Column							
	DP-TFA-β-CD (38 m × 0.26 mm I.D.)				DP-TFA-β-CD + OV-7 (40 m × 0.26 mm I.D.)			
	Temperature (°C)	t_R' (min)	α	R_s	Temperature (°C)	t_R' (min)	α	R_s
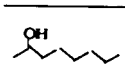	80	8.09	1.068	4.14	70	7.54	1.078	4.84
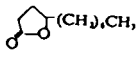	180	15.1	1.043	1.91	170	12.6	1.043	2.09
	140	8.56	1.035	1.59	130	6.32	1.038	2.66
	90	3.84	1.190	6.49	80	2.77	1.200	6.91

results demonstrate that the thermal stability of the chiral column was improved considerably by mixing a polysiloxane with a viscous liquid cyclodextrin derivative.

ACKNOWLEDGEMENT

This work was supported by the National Natural Science Foundation of China.

REFERENCES

1 Z. Juvancz, G. Alexander and J. Szejtli, *J. High Resolut. Chromatogr. Chromatogr. Commun.*, 10 (1987) 105.
2 W.A. Konig, S. Lutz and G. Wenz, *Angew. Chem., Int. Ed. Engl.*, 27 (1988) 979.
3 W.A. Konig, S. Lutz, P. Mischnick-Lubbecke, B. Brassat and G. Wenz, *J. Chromatogr.*, 447 (1988) 193.
4 W.A. Konig, S.Lutz, C. Colberg and N. Schmidt, *J. High Resolut. Chromatogr. Chromatogr. Commun.*, 11 (1988) 621.
5 W.A. Konig, R. Krebber and P. Mischnick-Lubbecke, *J. High Resolut. Chromatogr.*, 12 (1989) 732.
6 W.A. Konig, *J. High Resolut. Chromatogr.*, 12 (1989) 790.
7 D.W. Armstrong, W. Li, C.-D. Chang and J. Pitha, *Anal. Chem.*, 62 (1990) 914.
8 W.A. Konig, D. Ichtlef, T. Runge, I. Pforr and A. Krebs, *J. High Resolut. Chromatogr.*, 13 (1990) 702.
9 Y. Li, H.-L. Jin and D.W. Armstrong, *J. Chromatogr.*, 509 (1990) 303.
10 W. Keim, A. Konnes, W. Meltfzow and H. Romer, *J. High Resolut. Chromatogr.*, 14 (1990) 507.
11 A. Mosandl, U. Plener, U. Hagerauer-Hener and A. Kusterman, *J. High Resolut. Chromatogr.*, 12 (1989) 532.
12 W.A. Konig, R. Krebber, P. Evers and G. Brachn, *J. High Resolut. Chromatogr.*, 13 (1990) 328.
13 D.W. Armstrong, Y.-B. Tang and J. Zukonski, *Anal. Chem.*, 63 (1991) 2858.
14 H.-P. Nowotny, D. Schmalzing, D. Wistuba and V. Schurig, *J. High Resolut. Chromatogr. Chromatogr. Commun.*, 12 (1988) 383.
15 H.-G. Schmarr, A. Mosandl, H.-P. Neukom and K. Grob, *J. High Resolut. Chromatogr.*, 14 (1991) 207.
16 H. Wan and Q. Ou, *Fenxi Huaxue*, 20 (1992) 394.
17 G. Wenz, P. Mischnick-Lubbecke, R, Krebber, M. Richters and W. A. Konig, *J. High Resolut. Chromatogr.*, 13 (1990) 724.
18 W. Meier-Augenstein, B.V. Burger and H.S.C. Spies, *Magn. Reson. Chem.*, 29 (1991) 681.

Journal of Chromatography, 644 (1993) 208–212
Elsevier Science Publishers B.V., Amsterdam

CHROM. 25 225

Short Communication

Capillary electrophoresis with amperometric detection using a porous cellulose acetate joint

I-Chih Chen and Chen-Wen Whang*

Department of Chemistry, Tunghai University, Taichung 40704 (Taiwan)

(First received January 19th, 1993; revised manuscript received April 6th, 1993)

ABSTRACT

A system for coupling amperometric detection with capillary electrophoresis (CE) is described. The interface is formed by fracturing the capillary followed by covering the fracture with a thin layer of cellulose acetate (CA) film. The porous CA joint enables off-column amperometric detection to be performed without adverse effects from the high electrophoretic voltage. The primary advantage of this CA joint is its simple construction. The performance of the CE–amperometric detection system was evaluated with hydroquinone. A detection limit of $8 \cdot 10^{-8}$ *M* or 0.17 fmol with a theoretical plate number exceeding 90 000 was obtained. Application of the system to the separation and detection of aminophenols, catecholamines and catechol was also demonstrated.

INTRODUCTION

In the past few years, capillary electrophoresis (CE) has been shown to be a fast, powerful and efficient analytical separation technique [1]. One of the major areas of research is the development of sensitive detection systems. Owing to the small capillary dimensions encountered and the minuscule sample zone generated in CE, on-column detection methods, such as UV absorption and fluorescence detection, are the most commonly used methods. Recent advances in CE have allowed the use of other non-optical detection techniques, including electrochemistry. CE with electrochemical detection has recently been reviewed by Curry *et al.* [2] and Yik and Li [3].

Among the various electrochemical detection schemes employed in CE, amperometric detection with a microelectrode is currently one of the most sensitive detection modes. However, amperometric detection is not as easily applied to CE as the UV or fluorescence methods. This is because the electric current produced in the separation capillary upon application of a high voltage (10–30 kV) can be several orders of magnitude greater than the electrochemical currents measured at the detector. Therefore, if the detector is not isolated from the high electric field, small fluctuations in the electrophoretic current can create very high noise levels. Several methods have been developed to circumvent this problem, which include the use of a porous glass tube [4], a porous graphite tube [5], or a Nafion

* Corresponding author.

0021-9673/93/$06.00

joint [6] to couple two pieces of capillary column. The joint allows electrical connections to be made to the capillary so that the first segment of the capillary may be used for electrophoretic separation while the second segment may be used for off-column amperometric detection.

We have recently reported an alternative method for constructing a porous joint for CE [7]. The joint is formed by fracturing the capillary followed by covering the fracture with a thin layer of cellulose acetate (CA) film. Owing to its size-exclusion properties, the CA film creates a diffusion barrier which allows only small buffer ions to pass through it. Larger analyte molecules are excluded from permeating through the pores. This conductive joint has been shown to possess the advantages of high performance, long durability, inexpensiveness and easy construction. In this paper, the applicability of the porous CA joint to the amperometric detection in CE is demonstrated.

EXPERIMENTAL

Electrophoresis apparatus

A high-voltage power supply (0–40 kV, Glassman, Whitehouse Station, NJ, USA; Model PS/EH40R02.5) was used to provide the separation voltage. Fused-silica capillaries (Polymicro Technologies, Phoenix, AZ, USA) of 50 μm I.D., 360 μm O.D. and 50 cm length were used in this study.

Construction of the CA joint was similar to that described previously [7], except that the joint assembly was horizontally mounted in a plastic buffer reservoir. Briefly, a short section (*ca.* 3 mm) of polyimide coating was burned off 2.5 cm from the end of a capillary. The exposed section was cleaned with methanol and then glued to a 5 cm × 2 cm microscope slide. Using a glass-fibre cleaver, a small scratch was made on top of the uncoated silica. The capillary was then pushed up gently from below, directly under the scratch, until a fracture was produced. A small drop (*ca.* 3 μl) of 12% (w/v) CA solution (in acetone) was carefully dripped onto the fracture. Under a gentle stream of air, a thin film of CA was uniformly coated over the fracture region. The film thickness was *ca.* 80 μm, as estimated under a microscope. Subsequently, the fracture assembly was horizontally glued into a 10-ml plastic buffer reservoir, leaving 2 cm of detection capillary sticking out of the vial. A schematic diagram of the CA joint and the detector assembly is shown in Fig. 1.

Amperometric detection

The electrochemical detector was similar to that described by Knecht *et al.* [8]. Amperometric detection was performed in a two-electrode mode. A 9-μm-diameter carbon fibre (SIGRI, Meitingen, Germany) was used as the working electrode and a silver/silver chloride electrode was used as the reference electrode. The whole detector assembly was enclosed in a grounded Faraday cage to reduce noise.

Potential control between the working and reference electrodes was accomplished using a polarographic analyser (EG & G Princeton Applied Research, Princeton, NJ, USA; Model 264A). A picoammeter (Keithley Instruments, Cleveland, OH, USA; Model 485) was connected as a preamplifier at the working electrode input. Both the reference and auxiliary leads were connected to the silver/silver chloride electrode. The voltage output from the polarographic analyser was passed through a 1-s *RC* low-pass

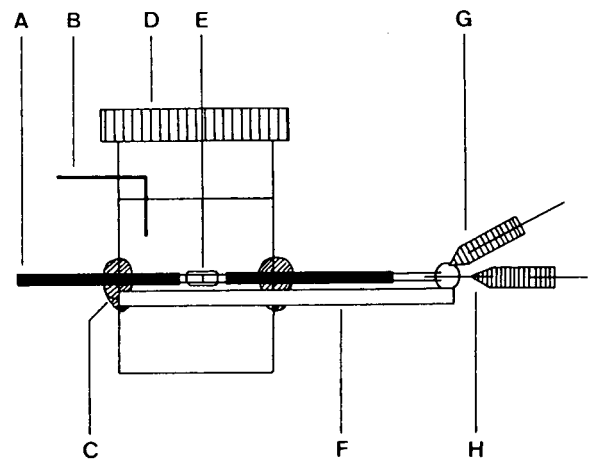

Fig. 1. Schematic diagram of CA joint and amperometric detector assembly. (A) Fused-silica capillary; (B) platinum-wire electrode; (C) epoxy glue; (D) buffer reservoir; (E) CA joint; (F) microscope slide; (G) Ag/AgCl reference electrode; (H) carbon fibre electrode.

filter and recorded on a strip-chart recorder (Pantos, Tokyo, Japan; Model U-228).

Prior to each analysis, the carbon fibre electrode was electrochemically pretreated by repetitive scanning the potential from 0.0 to +1.2 V *versus* silver/silver chloride reference at 0.1 V/s for 2 min while simultaneously flowing operating buffer past the detector. This pretreatment ensured constant electrode sensitivity.

Reagents

2-Morpholinoethane sulphonic acid (MES) buffer, hydroquinone, 2-, 3- and 4-aminophenol were obtained from Merck (Darmstadt, Germany). Dopamine, epinephrine and catechol were purchased from Sigma (St. Louis, MO, USA). All solutions were prepared in distilled, deionized water, and were filtered (0.2 μm) before use.

RESULTS AND DISCUSSION

The performance of the CE–amperometric detection system with a porous CA joint was tested with hydroquinone. Fig. 2 shows the electropherogram of $5 \cdot 10^{-7}$ *M* hydroquinone. The high efficiency achievable with this system is apparent, with the number of theoretical plates calculated from the peak half-width for hydroquinone exceeding 90 000. Linear regression analysis for concentrations ranging from $5 \cdot 10^{-7}$ *M* to $2 \cdot 10^{-4}$ *M* provided a calibration graph with a correlation coefficient of 0.997 ($n = 8$). From the electropherogram shown in Fig. 2, the detection limit ($S/N = 3$) for hydroquinone was determined to be $8 \cdot 10^{-8}$ *M*. With an injection volume of 2.1 nl (based on electroosmotic flow), the detection limit corresponds to 0.17 fmol. Relative standard deviations for the reproducibility of the migration time and the peak current for hydroquinone were 1.1% and 1.8%, respectively ($n = 6$).

Fig. 3 shows the separation and detection of three aminophenol isomers, *viz.* 4-, 3- and 2-aminophenol and hydroquinone. This was obtained in a 20 m*M* MES buffer with a pH of 5.7. At this pH, hydroquinone behaves as a neutral

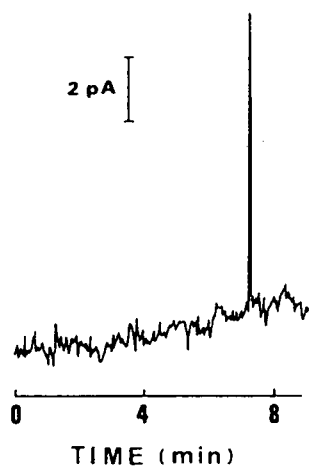

Fig. 2. Electropherogram of $5 \cdot 10^{-7}$ *M* hydroquinone. Column, 50 cm total length × 50 μm I.D. × 360 μm O.D.; 20 m*M* MES buffer (pH 4.0); separation voltage, 200 V/cm (4.0 μA); sample injection, 1 s at 10 kV; detection potential, 0.9 V *vs.* Ag/AgCl reference.

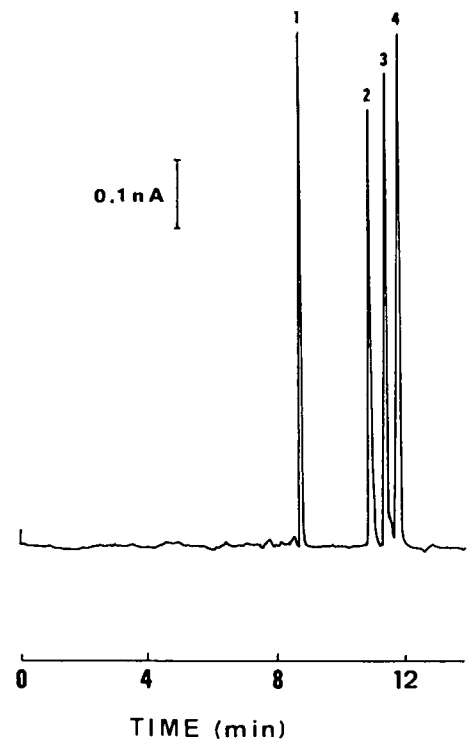

Fig. 3. Electropherogram of (1) 4-aminophenol (10 μM), (2) 3-aminophenol (12 μM), (3) 2-aminophenol (12 μM) and (4) hydroquinone (15 μM) with amperometric detection. Column, 60 cm total length; 20 m*M* MES buffer (pH 5.7); separation voltage, 250 V/cm (2.3 μA); other conditions as in Fig. 2.

marker and all three aminophenols are cations. The high efficiency obtained with this system is evident from the average number of theoretical plates, which exceeds 100 000 based on the half-width. Detection limits for the three isomers were all in the lower fmol range.

Application of this system to the separation and detection of catecholamines and catechol is shown in Fig. 4. The sample mixture contained dopamine (85 μM), epinephrine (82 μM) and catechol (27 μM). Injected amounts ranged between 170 fmol for dopamine and 54 fmol for catechol, in an injection volume of 2.0 nl. Owing to their structural proximity and similar net charge at the buffer pH (6.0), complete separation of dopamine and epinephrine was not achieved. It has been shown that a high concentration (*e.g.* 0.1 M) of borate is crucial in the CE separation of some biologically active molecules differing only by a single hydroxyl group with no change in net charge, including several catecholamines [9]. However, borate was found not to be an ideal electrolyte for amperometric detection in CE because it generated higher electrophoretic currents, which increase the detector noise. This has also been reported by Wallingford and Ewing [4] and O'Shea *et al.* [6]. In the present work, MES buffer, which has a higher resistance, was used. The high efficiency obtained with this system is evident in the catechol peak, which exhibits approximately 47 000 theoretical plates based on the half-width. The rather pronounced peak tailing found in Fig. 4 is thought to be due to electrostatic interactions between analyte and capillary wall [10]. The detection limits for dopamine, epinephrine and catechol were determined to be 12, 14 and 6 fmol, respectively.

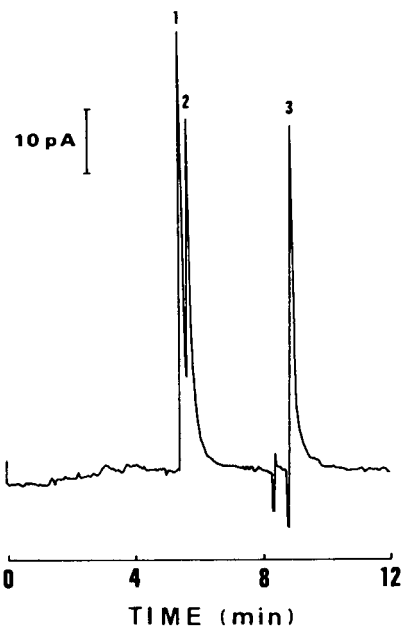

Fig. 4. Electropherogram of catecholamines and catechol with amperometric detection. 20 mM MES buffer (pH 6.0); detection potential, 0.75 V *vs.* Ag/AgCl; other conditions as in Fig. 2. Peak identities: 1 = dopamine (85 μM); 2 = epinephrine (82 μM); 3 = catechol (27 μM).

CONCLUSIONS

From the above studies we have demonstrated the feasibility of using the porous CA joint for amperometric detection in CE. In comparison with other conductive joints (*e.g.* porous glass tube, porous graphite tube or Nafion joint), the primary advantage of the CA joint is its simple design and construction. In addition, the CA joint is expected to have minimal band-broadening effect. According to other workers [4–6], the conductive joints were always constructed by threading a small section of porous glass, graphite or Nafion tube over the capillary fracture, followed by sealing both ends of the tube with epoxy glue. The inner diameter of the porous tube must be slightly larger than the outer diameter of the fused-silica capillary; therefore, a small dead volume will form around the fracture region. On the other hand, the CA membrane is tightly adhesive to the fracture region in a porous CA joint, leaving no stagnant zone formed between capillary surface and membrane. This "zero dead volume" nature partially contributes to its high performance. Since the main obstacle to the wide use of amperometric detection for CE lies in the difficulties of preparing a reliable conductive joint, we hope that the CA joint can provide an easy way for the researchers who are interested in CE–amperometric detection.

ACKNOWLEDGEMENT

Financial support from the National Science Council of Taiwan is gratefully acknowledged.

REFERENCES

1 W.G. Kuhr and C.A. Monnig, *Anal. Chem.*, 64 (1992) 389R.
2 P.D.J. Curry, S.C.E. Engstrom and A.G. Ewing, *Electroanalysis*, 3 (1991) 387.
3 Y.F. Yik and S.F.Y. Li, *Trends Anal. Chem.*, 11 (1992) 325.
4 R.A. Wallingford and A.G. Ewing, *Anal. Chem.*, 59 (1987) 1762.
5 Y.F. Yik, H.K. Lee, S.F.Y. Li and S.B. Khoo, *J. Chromatogr.*, 585 (1991) 139.
6 T.J. O'Shea, R.D. Greenhagen, S.M. Lunte, C.E. Lunte, M.R. Smyth, D.M. Radzik and N. Watanabe, *J. Chromatogr.*, 593 (1992) 305.
7 C.W. Whang and I.C. Chen, *Anal. Chem.*, 64 (1992) 2461.
8 L.A. Knecht, E.J. Guthrie and J.W. Jorgenson, *Anal. Chem.*, 56 (1984) 479.
9 J.P. Lander, R.P. Oda and M.D. Schuchard, *Anal. Chem.*, 64 (1992) 2846.
10 T.K. Towns and F.E. Regnier, *Anal. Chem.*, 64 (1992) 2473.

Journal of Chromatography, 644 (1993) 213–214
Elsevier Science Publishers B.V., Amsterdam

CHROM. 25 280

Software Review

Savant computer-based instruction series in HPLC: Troubleshooting high performance liquid chromatography (Program No. CLC-40), by D. Saunders, Savant, Fullerton, CA, price US$ 495.00. Computer requirements: IBM PC or compatible with a 286 or higher processor; at least 1 Mb of RAM, preferably more; a hard disk with 2.5 Mb of free space; color VGA adaptor and monitor; Windows 3.0 or later and mouse.

This software package is written with a program called ToolBook (Asymetrix Corporation) designed to create book-like applications of software. The author has very successfully created a computerized book that is natural and easy to use. It took me (a troubleshooting expert) about two hours to "read" the program cover to cover. The assumed target audience is technicians with limited HPLC experience. These users would benefit by spending many hours carefully reviewing the contents.

The program opens with a title page and table of contents. By using a mouse, one selects topics to view and can quickly navigate forward or backward through the program with intuitive commands (*e.g.*, clicking on the large arrows present in the upper right corner of all screens). There are eight main chapters (Introduction, Troubleshooting approach, Pressure problems, Leaks, Component malfunctions, Baseline problems, Peak problems, and Data problems) plus a Summary chapter and a set of appendices with printable tables. In addition, Chapter 9 is an expert system designed to aid fixing real problems. I chose to review the program in a linear fashion, just like I would read a book, so I paged through one screen at a time. I could have been just as successful by picking topics of interest and going directly to them. Much of the information is in text form displayed on the screen, but nearly every text box is accompanied by a clear and simple graphic to reinforce the main points. At several places there are clever tools to help reinforce common practices. My favorite tool was used to isolate high-pressure problems. An HPLC system was shown in a block diagram with the pressure displayed. By clicking on a fitting, the connection would open and the pressure would be adjusted accordingly. Thus for a blocked column, opening the column inlet fitting caused the pressure to drop dramatically, whereas opening the outlet fitting had no effect. Once I had come to my conclusion, I clicked on the "Answer" button and the proper answer was confirmed.

A short quiz was placed at the end of Chapters 3 and 6, with a final quiz at the end of the Summary. These were simple, yet they reinforced the important concepts. The multiple choice questions gave prompt feedback. A correct answer caused the display of a full explanation of the answer. An incorrect answer was accompanied by a short explanation about why the answer was incorrect.

The expert system is a simple, but effective tool to help isolate problems. The problem is described by reading a question then clicking on the appropriate response. After a few questions, the user is presented with a list of likely causes of the problem and can get help on how to fix it. While limited in scope, the expert system was easy to use and quickly came to the proper conclusions for several common problems I used for testing.

The program was very user friendly, and was designed to allow the user to jump from place to place to get more information or to review a topic. When additional information was requested, sometimes material from another chapter was displayed again, but pressing the "Back"

button returned me directly to my starting point, just as if I'd put my finger in a book to hold my place while I consulted another chapter. A variety of colors and graphics made for a pleasantly varied presentation, but not so much that it was distracting.

I have yet to meet a software program that is perfect, and this one is no exception. I found the installation routine archaic. I was required to manually copy the disks, setup the program group, and install the icon before running the program. With the broad availability of inexpensive installation software for Windows programs, I feel that this is inexcusable. One of my colleagues (who is not as computer literate as I) gave up trying to install the program. Another inconvenience is the ability to run only in standard VGA mode. This means that if you run in super VGA mode, the program will give a message that you cannot proceed. You then have to exit, go to Windows Setup, change the mode and restart. The only bug that I found was in printing. Several places when I selected the print option, my computer hung and I had to reboot, whereas other printing requests worked OK on my laser printer. My final complaint regards a backpressure calculator built into the chapter on pressure problems. One of the inputs was the solvent viscosity —I do not know many people who carry such values in their heads. There was no advice available on how to determine the viscosity. Later, while reviewing the Solvent properties appendix I discovered a list of solvent viscosities, so the information was available, but not easily referenced. A cross-reference button would eliminate this problem.

Computer requirements are consistent with today's systems: IBM compatible 286 or better with 1 Mb RAM, color VGA monitor, and 2.5 Mb of disk space. Windows 3.0 or greater and a mouse are required. My experience with ToolBook in the past indicates that a 286 will be unacceptably slow. My 33 MHz 386 ran the program quite acceptably.

Although the price of the program is considerably more than a book, its format is conducive to use by its target audience. It is an enjoyable tool to learn basic troubleshooting techniques, and the expert system helps to reinforce the problem solving thought process while quickly locating the problem source. The program is loaded with practical tips —I know that I picked up a few that were new to me. And when you master the information contained in the program, it includes a bibliography suggesting additional references to help you build your troubleshooting skills.

Amity, OR 97101 (USA) John W. Dolan

PUBLICATION SCHEDULE FOR THE 1993 SUBSCRIPTION

Journal of Chromatography and *Journal of Chromatography, Biomedical Applications*

MONTH	1992	J	F	M	A	M	J	J	
Journal of Chromatography	Vols. 623–627	628/1 628/2 629/1 629/2	630/1 + 2 631/1 + 2 632/1 + 2 633/1 + 2	634/1 634/2	635/1 635/2 636/1 636/2	637/1 637/2 638/1 638/2	639/1* 639/2 640/1 + 2	641/1 641/2 642/1 + 2 643/1 + 2 644/1	The publication schedule for further issues will be published later.
Cumulative Indexes, Vols. 601–650									
Bibliography Section				649/1			649/2		
Biomedical Applications		612/1	612/2	613/1	613/2 614/1	614/2 615/1	615/2 616/1	616/2 617/1	

INFORMATION FOR AUTHORS

(Detailed *Instructions to Authors* were published in Vol. 609, pp. 437–443. A free reprint can be obtained by application to the publisher, Elsevier Science Publishers B.V., P.O. Box 330, 1000 AH Amsterdam, Netherlands.)

Types of Contributions. The following types of papers are published in the *Journal of Chromatography* and the section on *Biomedical Applications:* Regular research papers (Full-length papers), Review articles, Short Communications and Discussions. Short Communications are usually descriptions of short investigations, or they can report minor technical improvements of previously published procedures; they reflect the same quality of research as Full-length papers, but should preferably not exceed five printed pages. Discussions (one or two pages) should explain, amplify, correct or otherwise comment substantively upon an article recently published in the journal. For Review articles, see inside front cover under Submission of Papers.

Submission. Every paper must be accompanied by a letter from the senior author, stating that he/she is submitting the paper for publication in the *Journal of Chromatography.*

Manuscripts. Manuscripts should be typed in **double spacing** on consecutively numbered pages of uniform size. The manuscript should be preceded by a sheet of manuscript paper carrying the title of the paper and the name and full postal address of the person to whom the proofs are to be sent. As a rule, papers should be divided into sections, headed by a caption (*e.g.*, Abstract, Introduction, Experimental, Results, Discussion, etc.) All illustrations, photographs, tables, etc., should be on separate sheets.

Abstract. All articles should have an abstract of 50–100 words which clearly and briefly indicates what is new, different and significant. No references should be given.

Introduction. Every paper must have a concise introduction mentioning what has been done before on the topic described, and stating clearly what is new in the paper now submitted.

Illustrations. The figures should be submitted in a form suitable for reproduction, drawn in Indian ink on drawing or tracing paper. Each illustration should have a legend, all the *legends* being typed (with double spacing) together on a *separate sheet.* If structures are given in the text, the original drawings should be supplied. Coloured illustrations are reproduced at the author's expense, the cost being determined by the number of pages and by the number of colours needed. The written permission of the author and publisher must be obtained for the use of any figure already published. Its source must be indicated in the legend.

References. References should be numbered in the order in which they are cited in the text, and listed in numerical sequence on a separate sheet at the end of the article. Please check a recent issue for the layout of the reference list. Abbreviations for the titles of journals should follow the system used by *Chemical Abstracts.* Articles not yet published should be given as "in press" (journal should be specified), "submitted for publication" (journal should be specified), "in preparation" or "personal communication".

Dispatch. Before sending the manuscript to the Editor please check that the envelope contains four copies of the paper complete with references, legends and figures. One of the sets of figures must be the originals suitable for direct reproduction. Please also ensure that permission to publish has been obtained from your institute.

Proofs. One set of proofs will be sent to the author to be carefully checked for printer's errors. Corrections must be restricted to instances in which the proof is at variance with the manuscript. "Extra corrections" will be inserted at the author's expense.

Reprints. Fifty reprints will be supplied free of charge. Additional reprints can be ordered by the authors. An order form containing price quotations will be sent to the authors together with the proofs of their article.

Biocatalysts in Organic Synthesis

by **J. Halgaš,** Comenius University, Bratislava, Czechoslovakia

Studies in Organic Chemistry, Volume 46

The fundamental problem in modern organic synthesis is the selectivity of preparative organic reactions. This book reflects the recent growth of interest in the use of biocatalysts to attain high chemo-, regio- and particularly, stereoselectivity. Enantiomerically pure compounds are required as building blocks for the synthesis of many new agrochemicals, drugs, or as bioorganic models and probes.

The first two chapters are devoted to a brief description of basic properties of various forms of biocatalysts: free and immobilized enzymes, free and immobilized microbial cells and other biopreparations, e.g., monoclonal antibodies. The third chapter deals with different levels of selectivity of biocatalyzed reactions. Attention is paid mainly to the differentiation of enantiomers, enantiotopic groups and faces. The remaining six chapters cover particular types of organic reactions and some 939 references from recent original papers are given. These include substitution reactions, eliminations and additions, synthesis and hydrolysis of esters and amides, oxidations and reductions.

Audience

Chemists specializing in the synthesis of new biologically active compounds, such as drugs, pesticides, insecticides, insect pheromones, food and cosmetic additives, etc., will find this book of immense value. The book will also be useful as a supplementary textbook for university graduate students taking courses on organic synthesis or bioorganic chemistry.

Contents: **1. Enzymes - Catalysts of Life.** Classification of enzymes. Principles of the kinetics of enzymatic reactions. Effects of organic solvents on enzymes. Effects of temperature and pH on the stability and activity of enzymes. Units of enzymatic activity. **2. The Biocatalyst Form.** Free enzymes. Immobilized enzymes. Cells of microorganisms. Immobilized cells of microorganisms. Plant and animal cells. Non-enzymatic biopreparations. **3. Biocatalysts and the Problem of Selectivity in Organic Synthesis.** Specificity of chemical action and substrate specificity of enzymes. Differentiation of enantiomers. Differentiation of enantiotopic groups. Differentiation of enantiotopic sides. **4. Substitution Reactions Using Biocatalysts.** Methylations. Halogenations. Substitution reactions in the side chain of amino acids. Substitutions on aromatic systems with the formation of a C-C bond. Substitutions at C-1 in saccharides. **5. Elimination and Addition Reactions.** Additions to the C=C bond. Additions to the C=O bond. **6. Syntheses and Hydrolyses of Esters.** Syntheses of esters. Chemo- and regioselective hydrolyses of esters. Kinetic resolutions of racemic esters, acids and alcohols. Diesters of prochiral dicarboxylic acids. Prochiral diols. **7. Synthesis and Hydrolyses of Amides.** Syntheses of amides and peptides. Hydrolyses of amides and nitriles. **8. Oxidations.** Oxidation of alcohols. Further oxidation reactions. **9. Reductions.** Reductions of aldehydes and acyclic ketones. Reductions of cyclic ketones. Reductions of di- and tricarbonyl compounds. Reductions of oxo acids, oxo esters and oxo amides. Reductions of the carbonyl group in organometallic compounds. Reductions of the C=C bond. Syntheses of α-amino acids from α-oxo acids. Reductions of the nitro group. Miscellaneous reductions. **References. Subject Index.**

1992 350 pages
Price: US $ 197.00 / Dfl. 315.00
ISBN 0-444-98698-7
Co-publication with VEDA, Bratislava and distributed in the East European Countries, China, Cuba, Mongolia, North Korea and Vietnam by SLOVART

0021-9673(19930730)644:1;1-W

711\414\145\0031